Terms and Conditions of Use of Digitised Theses from Trinity College Library Dublin

Copyright statement

All material supplied by Trinity College Library is protected by copyright (under the Copyright and Related Rights Act, 2000 as amended) and other relevant Intellectual Property Rights. By accessing and using a Digitised Thesis from Trinity College Library you acknowledge that all Intellectual Property Rights in any Works supplied are the sole and exclusive property of the copyright and/or other IPR holder. Specific copyright holders may not be explicitly identified. Use of materials from other sources within a thesis should not be construed as a claim over them.

A non-exclusive, non-transferable licence is hereby granted to those using or reproducing, in whole or in part, the material for valid purposes, providing the copyright owners are acknowledged using the normal conventions. Where specific permission to use material is required, this is identified and such permission must be sought from the copyright holder or agency cited.

Liability statement

By using a Digitised Thesis, I accept that Trinity College Dublin bears no legal responsibility for the accuracy, legality or comprehensiveness of materials contained within the thesis, and that Trinity College Dublin accepts no liability for indirect, consequential, or incidental, damages or losses arising from use of the thesis for whatever reason. Information located in a thesis may be subject to specific use constraints, details of which may not be explicitly described. It is the responsibility of potential and actual users to be aware of such constraints and to abide by them. By making use of material from a digitised thesis, you accept these copyright and disclaimer provisions. Where it is brought to the attention of Trinity College Library that there may be a breach of copyright or other restraint, it is the policy to withdraw or take down access to a thesis while the issue is being resolved.

Access Agreement

By using a Digitised Thesis from Trinity College Library you are bound by the following Terms & Conditions. Please read them carefully.

I have read and I understand the following statement: All material supplied via a Digitised Thesis from Trinity College Library is protected by copyright and other intellectual property rights, and duplication or sale of all or part of any of a thesis is not permitted, except that material may be duplicated by you for your research use or for educational purposes in electronic or print form providing the copyright owners are acknowledged using the normal conventions. You must obtain permission for any other use. Electronic or print copies may not be offered, whether for sale or otherwise to anyone. This copy has been supplied on the understanding that it is copyright material and that no quotation from the thesis may be published without proper acknowledgement.

CONFINEMENT IN
WIREBALL-REINFORCED CONCRETE MEMBERS

A Thesis Submitted to the University of Dublin for the Degree of Doctor of Philosophy in the Faculty of Engineering and System Sciences

by

Catherine Anne Ryan B.A., B.A.I.

October 2001

Department of Civil, Structural and Environmental Engineering
University of Dublin
Trinity College
Dublin

DECLARATION

The author hereby declares that this thesis, in whole or in part, has not been submitted to any other university as an exercise for a degree. Except where reference has been given in the text, it is entirely the author's own work.

The author confirms that the Library may lend or copy the thesis upon request, for academic purposes.

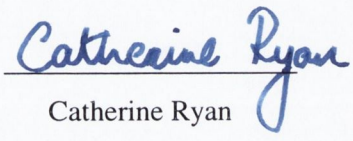

Catherine Ryan

October 2001

ACKNOWLEDGEMENTS

First, I would like to thank my supervisor Dr. Brian Broderick for his guidance and support throughout the course of my research. I would also like to acknowledge Dr. Roger West for his input into this research. Mr. Bjorn Svedberg must also be acknowledged and Mr. Magnus Jansson of BELAB for providing the wireballs reinforcement used in this project.

The friendship and technical support of Eoin Dunne, George Jones, Dave McAuley, Gerard McGranaghan and Chris O'Donovan is appreciated.

My gratitude also to Andrew Thomson for the countless hours spent helping me in the laboratory, Samuel Grave for his time and assistance, and all of the other post-graduates.

Finally, my sincere thanks goes to my family who have supported me most of all, and in every way, over the last four years.

SUMMARY

Modern codes for the earthquake-resistant design of structures rely on the dissipation of seismic energy through deformations of pre-designated plastic hinge regions. In reinforced concrete members, it is of utmost importance that these plastic hinges be confined adequately so that they possess sufficient rotational capacity. Eurocode 8, the European code for earthquake resistant design, specifies considerable quantities of transverse steel, in the form of links, in the plastic hinges where larger inelastic deformations are expected to occur.

This thesis assesses the ability of wireball reinforcement to provide confinement in reinforced concrete members, and to determine whether the combination of this novel form of reinforcement and conventional longitudinal and transverse reinforcement, increases the rotational ductility capacity of dissipative flexural members. The potential for reducing the amount of transverse steel required by earthquake design codes, through the inclusion of wireball reinforcement, is assessed.

Wireball reinforcement, or wireballs, consist of high tensile wire wrapped in three orthogonal directions to form a small open sphere, as illustrated in the figure. The diameter of the wireballs used in this research was 75mm. The wireballs used also had six 25mm rings attached, the purpose of which is to increase interlock between adjacent wireballs.

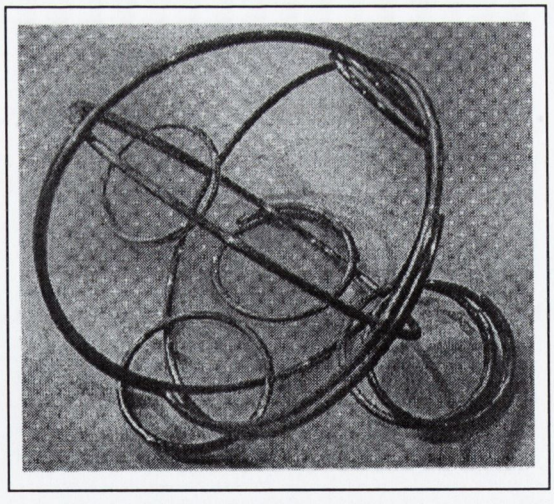

Wireball reinforcement

An experimental programme is described in which the relative performances of specimens with and without wireballs reinforcement are compared. Initial tests consider the response of specimens under monotonic compression, flexure and shear. It was concluded from the compression and flexural tests that wireballs can enhance confinement, and hence ductility, in compression and flexural members. The data also indicated that the use of wireballs, in combination with conventional reinforcement, may allow an increase in the link spacing specified by Eurocode 8,

without detrimental effect on specimen behaviour. However, it was observed that the confinement benefits of wireballs appear to diminish at closer link spacings. The results from the shear tests suggest that the addition of wireball reinforcement provides an increase in shear resistance and a consequent increase in ductility. However, the range of experimental data is insufficient for a solid conclusion on the possible shear enhancement of wireballs to be put forward.

The main part of the experimental programme consists of tests on eight beam-column specimens subject to simultaneous axial loading and lateral cyclic loading, representative of seismic response conditions. All specimens possessed the same dimensions and longitudinal steel contents, but differed with respect to the following three parameters: (i) transverse steel spacing, (ii) inclusion of wireballs and, (iii) level of axial load. Test specimens were designed with reference to the provisions of Eurocode 8. In each test the applied axial load was kept constant, while the displacement controlled lateral cyclic loading was applied with increasing amplitude.

The experimental data, in terms of numerical results and visual observations, illustrate the confinement benefits of wireballs in terms of increased ductility capability and energy dissipation capacity. The data also indicates that for loads simulating earthquake loads, and different axial load levels, the link spacing recommended by Eurocode 8 may be reduced without detrimental effect on specimen response. Visually it was observed that, the inclusion of wireballs reduced and delayed degradation of the concrete core, while reducing the amounts of link opening and distortion and longitudinal steel buckling. Quantitatively, the wireball-reinforced specimens had superior energy dissipation capacity and ductility capability that specimens with closer link spacings but no wireballs.

A numerical model is developed to predict the moment-displacement response of the beam-column specimens and their strain capacities. The objective of the model is to allow ultimate displacements, and hence, displacement ductility, of wireball-reinforced specimens to be determined numerically. The numerical model is based upon Mander's theoretical stress-strain model for confined concrete and modified to take into account the confinement enhancement effects of wireballs. The relationship between the increase in strain capacity of the wireball-reinforced specimens and the volume of wireball steel is postulated.

The predicted moment-curvature response is shown as being sensitive to link spacing, axial load level and input material characteristics. The moment-displacement response is very accurate in terms of the predicted ultimate moment but less accurate with respect to the initial stiffness. There is a good correlation between the increase in strain capacity and the volume of wireball steel.

TABLE OF CONTENTS

TITLE PAGE 1
DECLARATION 2
ACKNOWLEDGEMENTS 3
SUMMARY 4
TABLE OF CONTENTS 6
NOTATION 12

CHAPTER 1: INTRODUCTION 15

1.1 PREAMBLE 15
1.2 CONFINEMENT 15
1.3 WIREBALL REINFORCEMENT 16
1.4 CAPACITY DESIGN 17
1.5 SCOPE OF WORK 17
1.6 ORGANISATION OF THESIS 18

CHAPTER 2: LITERATURE REVIEW 20

2.1 INTRODUCTION 20
2.2 EARTHQUAKE RESISTANT DESIGN 20
2.3 DUCTILITY AND ENERGY DISSIPATION 21
2.3.1 Definition of ductility 21
2.3.2 Definition of energy dissipation 22
2.4 REINFORCED CONCRETE FOR EARTHQUAKE RESISTANCE 23
2.4.1 Introduction 24
2.4.2 Philosophy of earthquake resistant design for reinforced concrete structures 24
2.4.3 Capacity design 25
2.5 EUROCODE 8: EUROPEAN CODE FOR EARTHQUAKE RESISTANT DESIGN 27
2.5.1 Introduction 27
2.5.2 Reinforced concrete design concepts 27
2.5.3 Capacity design approach of EC8 28

2.6 CONCRETE CONFINEMENT 29
2.6.1 Introduction 29
2.6.2 Factors influencing confinement effectiveness 33
2.6.2.1 Transverse steel content 33
2.6.2.2 *Reinforcement configuration* 37
2.6.2.3 *Transverse steel yield strength* 42
2.6.2.4 *Flexural stiffness of reinforcing steel* 45
2.6.2.5 *Longitudinal steel behaviour* 46
2.6.2.6 *High strength concrete* 47
2.6.2.7 *Axial load level* 51
2.6.2.8 *Loading rate* 53
2.7 ALTERNATIVES TO STANDARD CONFINEMENT 54
2.7.1 Wire-welded fabric 54
2.7.2 Lateral prestressing 55
2.7.3 Wireball reinforcement 56
2.7.3.1 *Introduction* 56
2.7.3.2 *Wireball reinforcement* 57
2.7.3.3 *Static tests* 57
2.7.3.4 *Impact and quasi-static tests* 62
2.7.3.5 Summary 63
2.8 CONCLUSIONS 63

CHAPTER 3: DETAILS OF EXPERIMENTAL WORK AND TEST SPECIMENS 64

3.1 INTRODUCTION 64
3.2 TEST SERIES 1: STUB COLUMNS UNDER MONOTONIC COMPRESSION 64
3.2.1 Specimen description 65
3.2.2 Test set-up 66
3.3 TEST SERIES 2: SIMPLY SUPPORTED BEAMS WITH CENTRAL POINT LOAD 67
3.3.1 Specimen description 67
3.3.2 Test set-up 70

3.4 TEST SERIES 3: SIMPLY-SUPPORTED BEAMS WITH ¼ POINT LOAD 70
3.4.1 Specimen description and test set-up 70
3.5 TEST SERIES 4: BEAM-TO-COLUMN CONNECTIONS WITH LATERAL CYCLIC LOADING 72
3.5.1 Specimen description 72
3.5.2 Test set-up 74
3.5.3 Test procedure 75
3.6 TEST SERIES 5: BEAMS WITH LATERAL CYCLIC LOADING 76
3.6.1 Specimen description and test procedure 77
3.7 TEST SERIES 6: BEAM-COLUMNS WITH AXIAL COMPRESSION AND LATERAL CYCLIC LOADING 78
3.7.1 Specimen description 79
3.7.1.2 *Applied axial loads* 82
3.7.2 Test set-up 84
3.7.2.1 *P-Delta effect* 89
3.8 MATERIAL PROPERTIES AND SPECIMENS PRODUCTION 90
3.8.1 Concrete properties 90
3.8.2 Steel properties 91
3.8.3 Specimen production 92
3.9 EXPERIMENTAL EQUIPMENT & PURPOSE OF SHAKEDOWN TEST 95
3.9.1 Control of the servo-hydraulic actuator 95
3.9.3 Strain gauges 96
3.9.2 Purpose of the shakedown test 96

CHAPTER 4: INITIAL RESULTS 97

4.1 INTRODUCTION 97
4.2 TEST SERIES 1: STUB COLUMNS SUBJECT TO MONOTONIC COMPRESSION 97
4.2.1 Visual observations 97
4.2.2. Load-displacement response 98
4.2.3 Conclusions 103

4.3 TEST SERIES 2: SIMPLY-SUPPORTED BEAMS WITH CENTRAL POINT LOAD 104
4.3.1 Visual observations 104
4.3.2 Load-displacement response 104
4.3.3 Strain response 107
4.3.4 Conclusions 110
4.4 TEST SERIES 3: SIMPLY-SUPPOTED BEAMS WITH ¼ POINT LOAD 112
4.4.1 Visual observations 112
4.4.2 Load-displacement response 113
4.4.3 Conclusions 114
4.5 TEST SERIES 4: BEAM-TO-COLUMN CONNECTIONS 115
4.5.1 Visual observations 115
4.5.2 Load-displacement and moment-rotation responses 116
4.5.2.1 *Hysteresis curves* 118
4.5.2.2 *Energy dissipation* 121
4.5.2.3 *Strain response* 122
4.5.3 Conclusions 124
4.6 TEST SERIES 5: BEAMS SUBJECT TO LATERAL LOADING 125
4.6.1 Results 125
4.6.2 Conclusions 127
4.7 SUMMARY 127

CHAPTER 5: BEAM-COLUMN RESULTS 129

5.1 INTRODUCTION 129
5.2 GENERAL RESULTS 129
5.2.1 Cylinder strengths 130
5.2.2 Yield loads 130
5.2.3 Yield displacements 131
5.2.4 Initial stiffness 131
5.2.5 Yield and ultimate moment capacities 134
5.2.6 Ductility ratios 135
5.6.2.1 *Displacement ductilities* 135
5.6.2.2 Rotational ductilities 136
5.3 GENERAL OBSERVATIONS 138
5.3.1 Visual observations 138
5.3.2 Failure modes 150

5.4 LOAD-DISPLACEMENT AND MOMENT-ROTATION HYSTERESIS RESPONSE 157
5.4.1 Introduction 157
5.4.2 Load-displacement hysteresis response 158
5.4.3 Moment –rotation hysteresis response 164
5.5 COMPARISON GROUPS 168
5.5.1 Group 1 (C6.1, C6.2, C6.4) 169
5.5.2 Group 2 (C5.1, C5.2, C6.3) 173
5.5.3 Group 3 (C6.5, C6.6) 175
5.6 EFFECT OF LINK SPACING 178
5.6.1 Introduction 178
5.6.2 Ultimate displacement and link spacing 179
5.6.3 Dissipated energy and link spacing 181
5.7 CONCLUSIONS 183

CHAPTER 6: MODEL THEORY 185

6.1 INTRODUCTION 185
6.2 MATERIAL MODELS 185
6.2.1 Confined concrete in compression 186
6.2.1.1 *Lateral confinement in rectangular sections* 187
6.2.1.2 *Compressive strength of confined concrete* 190
6.2.1.3 *Ultimate concrete compression strain* 191
6.2.1.4 *Ultimate strain in beam-column specimens* 193
6.2.2 Unconfined concrete in compression 195
6.2.3 Concrete in tension 195
6.2.4 Reinforcing steel 195
6.3 MOMENT-CURVATURE RESPONSE 196
6.4 MOMENT-DISPLACEMENT RESPONSE 202
6.4.1 Basic equations 202
6.4.2 Displacement equations 204
6.5 IMPLEMENTATION OF NUMERICAL MODEL 206
6.5.1 Moment-curvature response 206
6.5.2 Moment-displacement response 208
6.5.3 Strain energy and strain in transverse steel 210
6.6 SUMMARY 211

CHAPTER 7: MODEL PREDICTIONS 212

7.1 INTRODUCTION 212
7.2 MOMENT-CURVATURE RESPONSE 212
7.3 MOMENT-DISPLACEMENT RESPONSE 219
7.3.1 Sensitivity of the predicted moment-displacement response to material characteristics 225
7.4 STRAIN AND STRAIN ENERGIES IN TRANSVERSE STEEL 227
7.4 CONCLUSIONS 233

CHAPTER 8: CONCLUSIONS 235

8.1 INTRODUCTION 235
8.2 EXPERIMENTAL STUDIES 235
8.2.1 Initial tests 235
8.2.2 Main tests 236
8.3 NUMERICAL MODEL 237
8.4 FURTHER WORK 237

REFERENCES 239

APPENDICES 244

APPENDIX A: TEST SERIES 6: STEEL STRAINS TO YIELD 244
APPENDIX B: TEST SERIES 6: CONCRETE STRAINS 248
APPENDIX C: TEST SERIES 6: BASE ELEMENT DISPLACEMENT 256
APPENDIX D: TEST SERIES 6: PREDICTED MOMENT-DISPLACEMENT RESPONSE WITHOUT 7.5 AND 10mm DISPLACEMENTS 258
APPENDIX E: TEST SERIES 6: NORMALISED STRAIN ENERGY AND STRAIN CAPACITY 262

Principal Notation

A : section area

A_{cc} : area of concrete core section enclosed by centreline of perimeter link

A_e : area of effectively confined concrete core

A_{sx} : transverse steel area in the x-direction

A_{sy} : transverse steel area in the y-direction

B : section width

b_c : core dimension to centreline of perimeter link in x-direction

b_o : minimum dimension of concrete core

D : section depth

d : depth to base (tension) steel

d' : depth to top (compression) steel

d_c : core dimension to centreline of perimeter link in y-direction

d_{bl} : longitudinal steel bar diameter

d_{bw} : transverse steel bar diameter

E_c : tangent modulus of elasticity for concrete

E_{ct} : concrete elastic modulus in tension

E_s : Young's modulus of steel

E_{spy} : post-yield stiffness of steel

F : force

F_c : concrete force

F_s : tension steel force

F_s' : compression steel force

f : stress

f_c : compressive concrete stress

f_{cc}' : compressive strength of confined concrete

f_{cu} : concrete cube strength

f_{ck} : concrete cylinder strength

f_{co}' : unconfined concrete strength

f_l : lateral confining stress

f_l' : effective lateral confining stress

f_{lx} : lateral confining stress in the x-direction

f_{ly} : lateral confining stress in the y-direction

f_t : tensile strength of concrete

f_u : steel ultimate stress

f_y : steel yield strength

f_{yh} : transverse steel yield strength

I : second moment of area

K_i : initial stiffness

k_e : confinement effectiveness factor

L : beam length or beam lever-arm

l_p : plastic hinge length

M : moment

M_p : predicted moment

M_u : ultimate moment

M_y : yield moment

N : axial load

P : applied load

s : link spacing

U : strain energy

V_{cd} : design shear resistance of a member without shear reinforcement

V_{max} : maximum applied shear force

V_L : volume of link steel

V_W : volume of wireball steel

V_{wd} : contribution of shear reinforcement to shear resistance

W : wireball

x : neutral axis depth

x, y : Cartesian co-ordinates

α : global effectiveness factor

Δ : displacement

Δ_y : yield displacement

Δ_u : ultimate displacement

ε : strain

ε_c : longitudinal compressive concrete strain

ε_{cc} : strain corresponding to confined concrete strength

ε_{co} : strain corresponding to unconfined concrete strength

ε_{cu} : ultimate strain of unconfined concrete

ε_s : steel strain

ε_t : concrete strain corresponding to tensile strength

ε_{sp} : spalling strain of concrete

ε_y : steel yield strain

ε_u : steel ultimate strain

ε_{ult} : ultimate concrete compressive strain

ϕ : curvature

μ : ductility

μ_{Δ} : displacement ductility

μ_{ψ} : rotational ductility

θ : rotation

ρ_s : transverse steel volumetric ratio

ρ_{cc} : ratio of area of longitudinal reinforcement to area of core concrete

σ : stress

ω_{wd} : minimum mechanical volumetric ratio of confining link, dependent on ductility class

CHAPTER 1

INTRODUCTION

1.1 Preamble

The main purpose of earthquake resistant design is to protect human life by avoiding structural collapse. If the members of a reinforced concrete frame are inadequately designed for shear, flexural or buckling failure, structural stability will not be maintained during earthquakes.

Confinement has been proven to greatly enhance the strength and ductility response of reinforced concrete.

The objective of this research is to consider the confinement effects of wireball reinforcement and to determine whether this unique reinforcement can enhance the earthquake resistance of reinforced concrete members.

1.2 Confinement

It is well established that through a combination of lateral confinement and axial compression, the ductility and compressive strength of concrete may be greatly improved. This is because cracks, which would have formed if the concrete was unconfined, are prevented from opening. Lateral confinement provides an inward lateral pressure, which counteracts the outward dilation of the concrete as it tries to expand laterally under the applied axial load. During inelastic load reversals, such as those occurring in an earthquake, confinement provided by transverse reinforcement has been observed to preserve the cores of structural members which if unconfined would have failed.

In practice, concrete is confined by transverse reinforcement in the form of links or spirals, wrapped around the longitudinal steel, at close spacings or pitch respectively. Circular spirals or hoops confine more effectively than rectilinear links. Circular hoops display axial hoop tension when the concrete core within them begins to dilate, and this hoop tension provides a continuous confining pressure around their circumference. Inherent of their shape, rectilinear links can only apply confinement reactions where they are restrained by longitudinal reinforcement.

Despite the lower confinement efficiency of rectilinear links with respect to hoops and spirals, their use prevails since their benefits in terms of ductility, although not strength, are significant. However, with much room for improvement, research is ongoing to determine methods of increasing the confinement effectiveness of rectilinear links. More traditional methods involve complex configurations of transverse steel through the provision of internal links and cross-ties within the standard perimeter links. This research considers a different approach – the combination of standard links with wireball reinforcement. This unique reinforcement is now discussed.

1.3 Wireball reinforcement

Wireball reinforcement, or 'wireballs', consist of 2mm diameter high tensile steel wire wrapped in three orthogonal directions to form a small open sphere. They were invented by a Swedish inventor Bjorn Svedberg in 1993. Their invention followed a survey of accidents occurring in the Swedish construction industry in the early 1990s. The survey revealed that more than half the working days were lost due to injuries arising from reinforcement steel fixing. Svedberg's objective was to remove all need of steel fixing by replacing traditional reinforcement with wireballs – the spherical reinforcement could simply be placed at random within the shuttering prior to casting of the concrete.

Early tests showed that wireballs have no significant effect on strength but that they do have an appreciable influence on concrete ductility and energy absorption capacity. It was also observed that their benefits were greater when used in combination with conventional reinforcement where they are packed tightly within the reinforcement cage. With this in mind, the potential of wireballs to increase the earthquake resistance of reinforced concrete members through enhanced confinement was considered a viable option and, hence, the motivation behind this research. The spherical shape of the wireball was regarded as having great potential for confinement. Thus, it was considered that the combination of the wireballs and standard transverse reinforcement would confine the core concrete very effectively, and perhaps that the use of wireballs would reduce the amount of standard confinement links usually required without detrimental effect on member behaviour.

1.4 Capacity design

Capacity design is the design approach commonly employed by modern earthquake design codes. The implementation of this approach implies that structures are designed to resist earthquakes

through the development of a significant inelastic response under the design seismic action, provided the magnitude of local inelastic deformations do not endanger overall structural integrity.

The yielding mode of the structure is predefined by the selection of those structural elements in which inelastic deformations and energy dissipation is allowed to occur. These elements are then detailed to possess sufficient local ductility to undergo the required inelastic deformations in a stable manner while remaining 'non-dissipative' elements are designed to remain elastic. In multistorey frames this is normally achieved by adopting the 'strong column/weak beam' approach, whereby vertical members (walls and columns) remain elastic, with the exception of the base of the bottom storey, and the ductility demands are distributed to all the beams.

To ensure the availability of sufficient levels of ductility and energy dissipation, it is essential that the pre-designated plastic hinge regions in reinforced concrete structures are confined adequately. Eurocode 8, the European code for earthquake resistant design, specifies different levels of confinement steel depending on the design seismic action. Where significant levels of inelastic deformation are relied upon, the code specifies large quantities of transverse reinforcement. It is with a view to reducing the required levels of standard confinement reinforcement, while maintaining the ductility and energy dissipation capacity, that the use of wireballs is considered in this research.

1.5 Scope and objectives of work

Despite ongoing advances in the earthquake resistant design of reinforced concrete structures, there still exists much room for improvement. A critical aspect, with respect to reinforced concrete structures, is that the pre-designated plastic hinge regions be capable of significant inelastic deformations and energy dissipation. The objective of this research is to consider the confinement potential of wireball reinforcement, used in combination with traditional rectilinear links, to:

- enhance the energy dissipation capacity and ductility capability of reinforced concrete;
- be used in partial replacement of conventional confinement links.

In order to examine the influence of wireball reinforcement on the ductility and energy dissipation capacity of reinforced concrete, an experimental programme of research was put in place. Within the first part of this programme the response of wireball-reinforced concrete members under monotonic compression, monotonic flexure and shear were considered. These tests, while forming a large part of the thesis, are considered initial tests since their purpose was to determine the

benefits of wireballs in reinforced concrete members tested under different loading arrangements. The purpose of these tests was twofold:

- to obtain an understanding of how wireball-reinforced members behave;
- to determine the optimum member type for the second part of the experimental programme where the confinement benefits of wireballs for seismic response conditions where to be examined.

Within the second part of the programme, the responses of a series of eight beam-column specimens subject to simultaneous axial loading and lateral cyclic loading, representative of seismic response conditions, were investigated. The results from these beam-columns form the substantive part of this thesis. The test specimens possessed the same overall dimensions and longitudinal steel contents but differed with respect to the following three parameters:

1. Transverse steel spacing
2. Inclusion of wireball reinforcement
3. Level of axial load

The transverse steel consisted of standard rectangular links. The applied axial load was kept constant, while the lateral displacement controlled cyclic loading was applied with increasing amplitude.

In all specimens containing wireball reinforcement, the wireballs were packed as tightly together as possible within the reinforcement cage.

Finally, a numerical model to predict the moment-displacement response and ultimate displacement capacity of the beam-column specimens is considered. The model is based upon Mander's theoretical stress-strain model for confined concrete and is adapted to include the effects of wireball reinforcement.

The presentation of this work is outlined in the following section.

1.6 Organisation of thesis

Chapter 2 presents a literature review, which introduces the concepts of ductility and energy dissipation and how they are exploited by Eurocode 8 using a capacity design approach. The bulk

of this chapter is concerned with concrete confinement and its significance, and it summarises past experimental work on factors influencing confinement effectiveness. A significant amount of this past work on the behaviour of confined concrete was on specimens tested under monotonic compression. However, in recent years, work has also been carried out to examine the response of confined concrete subject to lateral cyclic loading and axial compression in tests similar to the beam-column tests undertaken in this research. Finally, this chapter discusses some alternative methods of concrete confinement with particular emphasis on wireball reinforcement.

Chapters 3 to 5 are concerned with the experimental work undertaken in this research. Chapter 3 describes the test specimens and their production, the different experimental set-ups employed and the testing procedures involved. Chapter 4, presents and discusses the results of initial tests on the behaviour of wireball-reinforced concrete specimens subject to loading types varying from monotonic compression and bending, to some preliminary lateral cyclic loading. The results of this chapter provide the basis on which the beam-column specimen details, loading type and corresponding laboratory set-up were developed. Chapter 5, considered as the main results chapter, presents and discusses the responses of beam-column specimens subject to simultaneous axial loading and lateral cyclic loading, representative of seismic response conditions. The specimens' responses are discussed in terms of both the numerical results obtained and the visual observations made during each test. The responses of specimens with and without wireballs are compared. A comparison summary of the relative performance of the beam-column specimens is also provided in which they are ranked in terms of energy dissipation and ductility capacity.

In Chapter 6, a numerical model to predict the response of the beam-column specimens is described, while comparisons of the analytical and experimental responses are made in Chapter 7. The development of the numerical model of the test specimens allows the experimental data to be extended to the behaviour of a wider range of reinforced concrete members containing wireball reinforcement.

Finally Chapter 8 summarises the work done and presents the principal conclusions. It also suggests some further research into areas where there remains insufficient knowledge.

CHAPTER 2

LITERATURE REVIEW

2.1 Introduction

This chapter considers the earthquake resistant design of reinforced concrete. Specifically, it considers the issue of concrete confinement. Section 2.2 summarises some of the requirements for good earthquake resistance. Section 2.3 discusses two fundamental requirements of capacity design of reinforced concrete, that is ductility and energy dissipation capacity. The earthquake resistant design of reinforced concrete with respect to the capacity design approach is considered in Section 2.4, while Section 2.5 discusses how this approach is implemented in Eurocode 8. Section 2.6, which forms the largest part of this chapter, considers the issue of concrete confinement and summarises past experimental work on the factors influencing confinement effectiveness. Section 2.7 deals with some alternative confinement methods with particular emphasis on wireball reinforcement.

2.2 Earthquake resistant design

The design of structures to resist earthquakes is one of the greatest challenges facing structural engineers. Even with an ever-increasing depth of knowledge, earthquakes, lasting only a couple of minutes continue to cause destruction and devastation the world over. After many earthquakes, poorly designed reinforced concrete and steel frames collapse because basic principles are ignored and shortcuts, in terms of design and materials, are used. The converse is also true, in that tall structures, designed in adherence with basic principles have not collapsed, even in major earthquakes, and people have walked out of them alive, even when structural damage has occurred. Therefore, it is possible, through observance of earthquake resistant design codes, to prevent structural collapse during earthquakes, and more importantly, to save life. The following points (after Booth, 1994) give a broad outline of what is required for good earthquake design:

- Good initial planning: at an early stage of planning it's essential to obtain data on the soil conditions and groundwater levels at the site to estimate the site period, liquefaction potential and stability of slopes.
- Structural form: deciding between the best structural form (e.g. moment-resisting frame or shear wall) to resist an earthquake.

- Structural layout: buildings that are well tied together and have well-defined and continuous loadpaths to the foundation perform better than structures lacking such features.
- Ductile responses: a ductile response is essential to ensure against structural collapse in an extreme earthquake (this is discussed in detail in Section 2.3)
- Detailing for earthquake response: the reinforcement detailing in reinforced concrete is of utmost importance to prevent against brittle failures, such as shear and crushing, and to prevent buckling of the longitudinal steel.

2.3 Ductility and energy dissipation

Ductility and energy dissipation are two of the most important criteria in seismic design since the current design philosophies for moment-resisting frames rely upon the availability of ductility to enable energy to be dissipated through post-elastic deformations. Good energy dissipation is dependent on the availability of high levels of ductility. In terms of cyclic loading response, the area within a hysteresis loop is a measure of the energy dissipation capacity of a system. It is, therefore, important to maintain large loops on load reversal. Provision for ductility, and hence, energy dissipation, is accepted by all seismic design codes as the surest way of avoiding catastrophic collapse if an earthquake occurs.

2.3.1 Definition of ductility

With respect to static loading, if a structure is loaded to failure, it should behave in a ductile, rather than brittle, manner with ample visual warning of imminent collapse provided through large deformations at near maximum load carrying capacity. For earthquake loading, a ductile structure is one than can maintain its stability under repeated cyclic deflections considerably greater than its yield deflection. The importance of ductility was summarised by Booth (1994) in the following points:

- Ductility provides 'robustness', the ability of a structure to withstand unforeseen local accidents without collapse.
- A ductile structure gives ample warning of imminent collapse through large deformations prior to collapse.
- Provision of ductility enables moment distribution in indeterminate structures near ultimate conditions.
- Seismic design depends upon adequate ductility being available to enable large distortions to be accommodated, and energy to be absorbed and then dissipated, during an earthquake.

Ductility is a non-dimensional factor equal to the ratio of ultimate deformation to yield deformation. For this project, two kinds of ductility are relevant, as defined below:

Curvature Ductility: This is the ratio of ultimate curvature (φ_u) to yield curvature (φ_y). It is referred to as 'section ductility' because it is dependent on material type, section shape and section properties. Curvature ductility can be determined from a moment-curvature curve.

Displacement Ductility: This is the ratio of ultimate displacement (Δ_u) to yield displacement (Δ_y). Displacement ductility is the 'member' or 'structural' ductility since it is related to a whole structural member or system. It is represented in the load-displacement curve.

2.3.2 Definition of energy dissipation

The effects of inelastic behaviour on the response of a structure to severe earthquake motions may be seen with reference to a single degree of freedom oscillator as shown in Figure 2.1. For an elastic response, the oscillator has a load deflection response as shown in Figure 2.1(a) where point *b* is the maximum response. The shaded area *abc* under the curve is the potential energy stored at maximum deflection. When the mass returns to its zero position this potential energy is converted to kinetic energy. If the oscillator is not strong enough to carry the full elastic response load a plastic hinge develops and a curve like that shown in Figure 2.1(b) results. When the plastic hinge develops the deflection response follows line *de* with point *e*, representing the maximum response. The potential energy stored is represented by the shaded area *adef*. However, unlike the elastic response, only a small proportion of this energy is converted to kinetic energy (area *egf*) while a large amount of energy (area *adeg*) is dissipated by the plastic hinge, in the form of heat and other irrecoverable types of energy, as the system undergoes damage. In other words, in elastic structures all the potential energy stored in a cycle is returned in the form of velocity energy to the next cycle, whereas in elastic-plastic structures some of the stored energy is dissipated before entry into the next cycle.

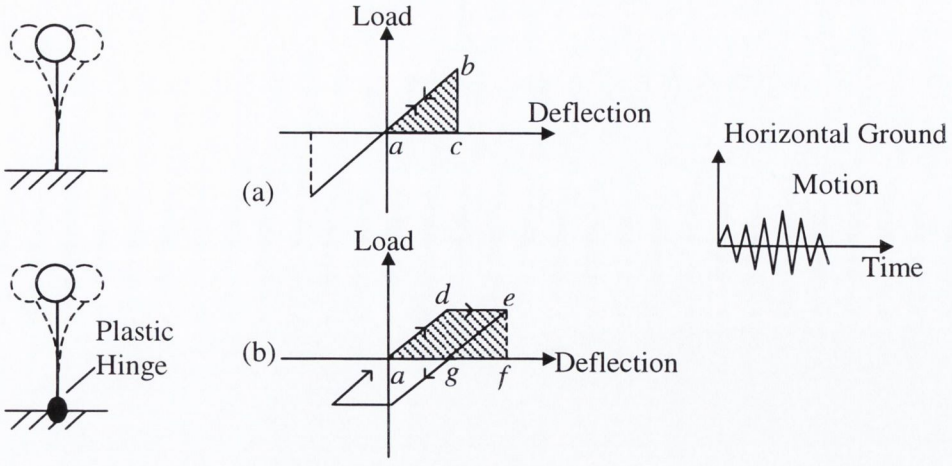

Figure 2.1: Response of single degree of freedom oscillator to earthquake motions, (a) elastic response, (b) elasto-plastic response, (after Park *et al.*, 1975)

2.4 Reinforced concrete for earthquake resistance

Reinforced concrete is a highly non-linear material, with two constituents having very different properties. As a material, it suffers many drawbacks as regards earthquake resistance. It has an unfavourably large mass-to-strength ratio, (compared with steel), since earthquake loads arise from inertia effects, which are proportional to mass. Moreover, reinforced concrete displays low levels of ductility in compression unless confined adequately. However, despite the disadvantages of reinforced concrete it also has many advantages in earthquake resistant design (Booth, 1994):

- Properly detailed reinforced concrete structures can possess excellent ductility in bending, equalling that of structural steel.
- Well confined reinforced concrete can possess good ductility in compression with a lower tendency for buckling failure compared with an equivalent steel structure.
- In-situ concrete construction provides a monolithic structure that contributes to the overall continuity of the structure, leading to well defined loadpaths and, hence, provides increased earthquake resistance.
- In many countries concrete is the building material of choice, the technology is familiar, some of the materials are available locally, while the finished structure can possess good thermal and acoustic insulation and fireproof properties.

2.4.1 Introduction

For many years, building codes have recommended seismic design forces much less than the inertia forces that would be induced if the structures responded elastically to severe earthquakes. Despite this, it is well known that these structures, when properly designed and detailed, have survived major earthquakes. Their survival is attributed to the ability of ductile structures to dissipate seismic energy through the development of inelastic deformations at critical regions of the members. The following sections introduce the concept of "capacity design", where structures are designed to resist earthquakes through inelastic deformations in selected members and how this approach has been adopted by Eurocode 8.

2.4.2 Philosophy of earthquake resistance design for reinforced concrete structures

Although technically feasible, it is uneconomical to design a structure to withstand its design seismic action, (i.e. ground motion), elastically and without damage. For a structure to remain elastic under its design seismic action, it may have to be designed for lateral forces with magnitudes up to 50% or more of its weight (CEB, 1997). This is also entirely unnecessary as the earthquake action is a dynamic action, representing for a structure a certain total energy input and a demand to tolerate a certain level of displacement and deformation, but not a demand to withstand specific forces. Therefore, the current philosophy of seismic design codes allows the development of a significant inelastic response under the design seismic action, provided the magnitude of inelastic deformations does not endanger the integrity of the individual members, and of the structure as a whole. The strategy is to accept that the structure may yield, but to ensure that the post-yield response is ductile rather than brittle. A ductile structure resists an extreme earthquake not through strength alone, but by allowing plastic deformations to absorb and dissipate the kinetic energy induced by the ground shaking. Figure 2.2 illustrates the difference in forces, for the same level of deformation, that arise in ductile and elastic systems. It is clear that the development of plasticity in the ductile system limits the amount of force acting on the system.

The occurrence of post-elastic strains in a structure during an earthquake implies some degree of damage at the yielding regions. The criteria for the levels of seismic design force set by many codes for ductile structures are that structures should be able to resist moderate earthquakes without structural damage, and be able to resist severe earthquakes without collapse but with some damage. These criteria mean that a structure should behave elastically during a moderate earthquake, but during a severe earthquake, the structure may undergo post-elastic deformations and damage should occur. However, while the possibility of damage, and consequent economic loss, is acceptable during such a severe earthquake, the structural deformations should not be such as to endanger life.

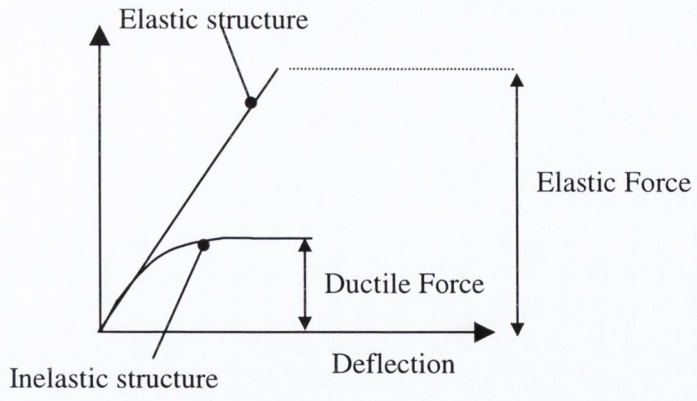

Figure 2.2: Forces in ductile and elastic systems (after Booth, 1994)

While earthquake resistant design is based on the ability of a structure and its members to undergo displacement, a simple and reliable method of design based on displacement demand has yet to be fully developed. Structures are still designed to ensure earthquake resistance on a force-based rather than a displacement-based system. Thus, structural members are proportioned for internal forces computed from a linear elastic analysis of the structural response to specific lateral design forces. These design forces are obtained from a design acceleration spectrum which is obtained by factoring down the elastic spectral accelerations by a "behaviour factor", q (EC8, 1998) or a "force reduction factor", R (ACI, 1992). An important factor in earthquake resistant design is that all members be detailed such that they can reliably, and safely, sustain the local ductility demands associated with the q-value being used.

2.4.3 Capacity design

The concept of "capacity design" was developed in New Zealand in the 1970s (Hakuto *et al.*, 2000), and since then it has been adopted in many other seismic regions. It is a procedure for imposing on a structure a desired hierarchy of member strengths to ensure the development of the most appropriate plastic mechanism in the event of a severe earthquake. Capacity design ensures a predictable structural response with inelastic deformations occurring only in suitably detailed locations, while all other locations are provided with sufficient strength to ensure that the chosen energy dissipation mechanism is maintained. In building structures, this is normally achieved if the vertical members (wall and columns) remain elastic, with the exception of the base bottom storey, and the ductility demands are distributed to all the beams. That is, a strong column/weak beam design approach, rather than a weak column/strong beam, is advocated (Figure 2.3). In other words, the vertical members are over-designed, while the ductility of the flexural members is enhanced. Comparison of the two sway-mechanisms (a) and (b) of Figure 2.3 shows that column sway, or "weak storey" suffers from a number of disadvantages. In this mechanism the plastic

hinges arise in the columns and are concentrated at relatively few points so that each hinge must dissipate a large amount of energy - implying severe strength degradation of the column, and lessening its capacity to support gravity loads. Failure of a column can be catastrophic as it may result in loss of support to floors above, whereas beam failure involves damage of a much less limited area. Moreover, column failure is more likely to be governed by concrete strain than steel strain, because of the gravity-induced axial stresses. This is because columns experience compressive axial loads which require the columns to have larger neutral axis depths than beams, which in turn means that the flexural capacity of the column is more dependent on the contribution of the concrete compressive stress distribution (Mander *et al.*, 1988). Hence, the available rotational capacity is generally less (and brittleness greater) for this mechanism than for mechanism (a), unless elaborate measures are used to provide the necessary ductility. However, some plastic hinging of columns will be inevitable during a very large earthquake. At the bases of columns in multistorey frames, plastic hinging cannot generally be avoided and may actually be relied upon for energy dissipation (Park, 1992). Thus, the potential plastic hinge regions in columns should be properly detailed for ductile behaviour.

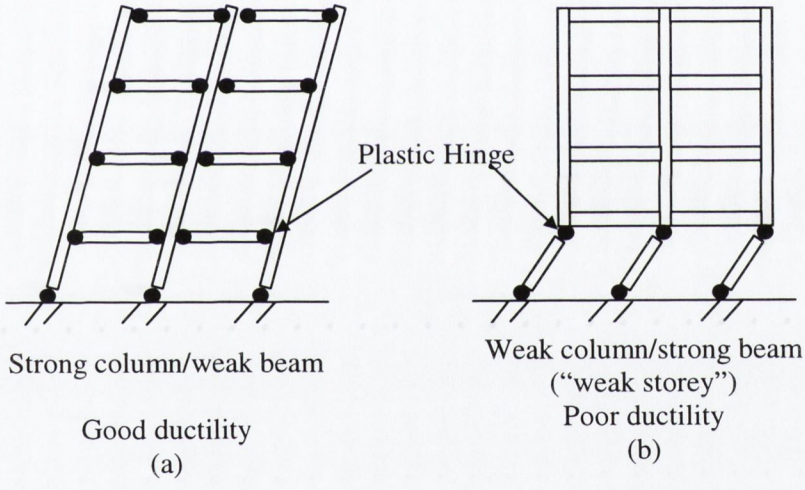

Figure 2.3: Multistorey frames: (a) strong column/weak beam, (b) weak column/strong beam (after Booth, 1994)

Although based on a relatively straightforward philosophy, the application of capacity design is often complex and is made more complex when higher ductility capacities are required. However, the fact that design forces are almost inversely proportional to ductility is thought sufficient incentive for increasing the ductility supply (Comité Euro-International du Béton, 1998). The advantages of limiting the magnitude of the lateral forces are manifold. Foundation structures are lighter, the forces transmitted to the soil are lower, which reduces the likelihood of permanent deformation, and the maximum response accelerations of the structure are smaller, which protects any equipment mounted to the structure that might be sensitive to acceleration. Finally, ductility is

seen as the "most effective defence against unanticipated and unfavourable characteristics of ground shaking" (Comité Euro-International du Béton, 1998).

Most modern design codes specify different combinations of strength and ductility. Four world regions, each with codes dealing with capacity design can be identified: Europe, America, Japan and New Zealand (EC8, 1998, ACI, 1992, AIJ, 1990, NZ, 1995). The aim of these codes is "to control the behaviour of a structure acted upon by a ground motion of very variable and unpredictable characteristics, intense enough to bring the structure close to, but not beyond, the exhaustion of its inelastic capacity" (Comité Euro-International du Béton, 1998). Each code is based on a capacity design approach where reliance is placed on the availability of ductility, over-design of the vertical members, and the avoidance of premature failure to ensure adequate dissipative measures.

2.5 Eurocode 8: European code for earthquake resistant design

2.5.1 Introduction

Eurocode 8 is the European code for earthquake resistant design. The aim of EC8 is that, in the event of an earthquake, human lives are protected, damage is limited and structures important for civil protection (e.g. hospitals) remain operational. There are two fundamental requirements of the code (EC8, 1998):

- No collapse requirement (Ultimate Limit State): Structures are designed and constructed such that they withstand the design seismic action without local or general collapse, thus retaining structural integrity and residual load bearing capacity after the earthquake.
- Damage limitation requirement (Serviceability Limit State): Structures are designed and constructed to withstand a seismic action having a larger probability of occurrence than the design seismic action, without damage and the associated limitations of use, where the costs are disproportionately high relative to the costs of the structure itself.

2.5.2 Reinforced concrete design concepts

The design of reinforced concrete for earthquake resistance by Eurocode 8 is based upon the capacity design approach. The following points summarise the design concepts of the code with respect to reinforced concrete (EC8, 1998):

- Earthquake resistant concrete buildings should be designed to have adequate energy dissipation capacities without substantial reduction of their overall resistance against horizontal and vertical loading. Adequate resistance of all structural elements should be provided under the seismic combination of actions, and non-linear deformations in the critical regions should provide the required level of structural ductility.
- An overall ductile behaviour is ensured if the ductility demand is spread over a large number of elements and locations per element. Therefore, ductile modes of failure should precede brittle modes with sufficient reliability.
- With regard to the required hysteretic dissipation capacity, the draft European Prestandard (Eurocode 8, 1998) defined three ductility classes DCL, DCM and DCH for concrete structures (Section 2.5.3). However, the DCH class has been effectively removed in the final version. In spite of this, the original DCH definition is included within this literature review.
- In order to provide the appropriate ductilities for each ductility class, specific provisions for each class have to be satisfied.
- Corresponding to the different levels of available ductility, different values of the behaviour factor q are used in each class.

2.5.3 Capacity design approach of EC8

As mentioned in the previous section, the draft EC8 distinguished three ductility classes such that design could be carried out using one of three different balances between the strength and ductility of a structure; the higher the ductility, the lower the design forces, and hence, the lower the required structural strength. The three levels, labelled as DCH, DCM, and DCL are as follows (EC8, 1998):

DCH (Ductility class high): corresponds to structures for which the design, dimensioning and detailing provisions are such as to ensure, in response to the seismic excitation, the development of chosen stable mechanisms associated with large dissipation of hysteretic energy.
DCM (Ductility class medium): corresponds to structures designed, dimensioned and detailed according to specific earthquake resistant provisions, enabling the structure to enter well into the inelastic range under repeated reversed loading, without suffering brittle failures.
DCL (Ductility class low): corresponds to structures designed and dimensioned according to Eurocode 2 (1998), supplemented by rules enhancing available ductility.

Ductility demand and capacity design provisions increase with the required ductility level, and the recommended detailing procedure for ductility becomes increasingly complex when higher ductility is sought from the structural system. Taking DCH as a reference, DCM corresponds to

designing for 75% of the DCH q-factor, and DCL corresponds to designing for 50% of the DCH factor. For DCL the capacity design provisions are quite minimal. The flexibility of EC8, with respect to the three ductility classes, is a necessity for countries with large differences in seismicity and construction practice. For example, DCL may be more appropriate in low seismicity regions where there is little emphasis and tradition in earthquake resistant design and construction. The three ductility levels are intended to provide equivalent levels of seismic protection at the ultimate limit state. Fardis (1995) studied the effect of designing the same building to each ductility class. The results showed that frames designed for the three ductility classes result in approximately the same total quantities of steel and concrete, so whereas in one case a lot of steel is required for strength but not so much for ductility, in another case the opposite will be true.

2.6 Concrete confinement

2.6.1 Introduction

Confinement is a means of imparting ductility to concrete and is of utmost importance in reinforced concrete design because a satisfactory response of reinforced concrete structures is based on the ability of sections to carry the imposed load coupled with a certain level of ductility. While plain concrete under uniaxial compression behaves in a brittle manner, the deformability of concrete improves with confinement. Confined concrete can sustain higher strain at peak load, and may show little strength decay thereafter. After inelastic load reversals, such as those occurring in earthquakes, confinement, in the form of transverse reinforcement, has been observed to preserve in the cores of structural members what would have otherwise been crushed.

Plain concrete subject to longitudinal compression is in a uniaxial state of stress. The compressive loading generates longitudinal strains that give rise to transverse tensile strains, which result in dilation and vertical cracking of the concrete. As the concrete reaches its ultimate strength, both the transverse and longitudinal strains reach their limiting value and the concrete fails. However, it is well known that if there is a combination of lateral confinement and axial compression, then the ultimate strength and deformability (ductility) of concrete can be greatly enhanced.

As early as 1903 Considère (Richart *et al.*, 1929) had concluded from tests on laterally confined concrete, that lateral restraint (confinement) can significantly increase the strength of concrete. He stated that the strength of laterally confined concrete is the sum of the uniaxial compressive strength of concrete plus an added strength, which is a function of the lateral confinement. During the 1920s, Richart *et al.* (1928) addressed the question of the relation between the added strength of

confined concrete and its confinement. An extensive programme was put in place to study both hydraulically and spirally confined concrete cylinders. In the case of the hydraulically confined specimens, a liquid pressure was applied to the sides of the specimens while an axial load was applied on top. Both types of specimens exhibited large deformations and high ultimate strengths. The following empirical relationship was deduced,

$$f_{cc} = f_c' + 4.1 f_l \tag{2.1}$$

where f_{cc} is the confined axial stress, f_c' is the uniaxial compressive strength of concrete, and f_l is the confining lateral stress applied to the concrete.

The increase in strength and ductility with confinement is due to the lateral confinement counteracting the concrete's tendency to expand laterally, due to internal cracking, just prior to failure. For stress levels up to 70% of the cylinder strength of concrete, Poisson's ratio usually falls in the range 0.15 to 0.2, however, for stresses higher than this, Poisson's ratio increases. As the concrete expands, it pushes out against the confining reinforcement, which in turn applies a restraining force against the expanding concrete. The stress-strain curves for confined and unconfined concrete are similar up to the cylinder strength, but at higher strains, confined concrete displays enhanced strength and greater strain capacity. It is this greater strain capacity, or 'ductility', that is exploited in seismic design. Figure 2.4 presents the stress-strain curves obtained by Richart et *al.* (1928) for a series of concrete cylinders confined by a range of lateral fluid pressures.

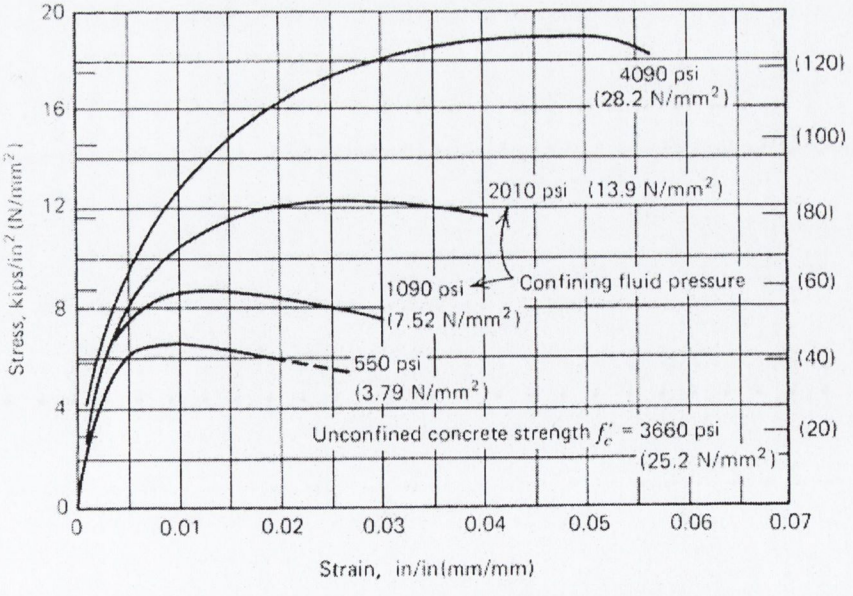

Figure 2.4: Axial stress-strain curves from triaxial compression tests on concrete cylinders (Richart *et al.*, 1928)

Concrete Confinement by Transverse Steel

In practice, concrete is confined by transverse reinforcement in the form of links or spirals at close spacings or pitch respectively. This type of confinement is called 'passive confinement' because it is only as the stress within the concrete approaches its uniaxial strength, and the transverse strains become high enough for internal cracking to occur, that the confinement becomes effective. As the concrete dilates and bears out against the transverse reinforcement, the transverse reinforcement reacts by imposing a confining inward force on the concrete. Tests by many investigators, including Richart *et al.*, proved that concrete confined by circular spirals has strength approaching that of concrete confined by lateral fluid pressure.

Circular spirals and hoops confine more effectively than rectilinear links. Figure 2.5 below shows a circular and square section confined by circular hoops and square links respectively (Booth, 1994). The shaded areas represent the confined concrete. Circular hoops, because of their shape, are in axial hoop tension, and therefore, provide a continuous confining pressure around their circumference, at large transverse strains this approximates fluid confinement. In the plane of a circular hoop, all the concrete within the hoop is confined; however, this is not the case for the square link. Inherent of their shape, rectilinear links, can only apply confining reactions near their corners since the flexural stiffness of the transverse steel between the corners is insufficient to restrain the expansion of the concrete along the whole bar length. The pressure of the concrete against the link causes its sides to bend outwards (internal arching) leaving a considerable portion of the concrete cross-section unconfined. This internal arching means that the concrete is confined effectively only at the corners and central region of the section. The confining reaction from rectilinear links comes from the longitudinal bars at the positions where they are restrained by the links. However, despite the superior confinement effectiveness of circular spirals and hoops, the use of rectilinear transverse steel prevails because of their advantages in design, detailing and fabrication, and the fact that their benefits in terms of ductility, while not as good as those gained with circular spirals, are still significant.

Apart from confining compressed concrete, transverse steel has two other vital functions; restraining the longitudinal steel against buckling and acting as shear reinforcement. These three functions tend to compliment each other, in that the provision of confinement steel usually serves to restrain the main bars, and the confining forces developed in the transverse steel also provide shear resistance.

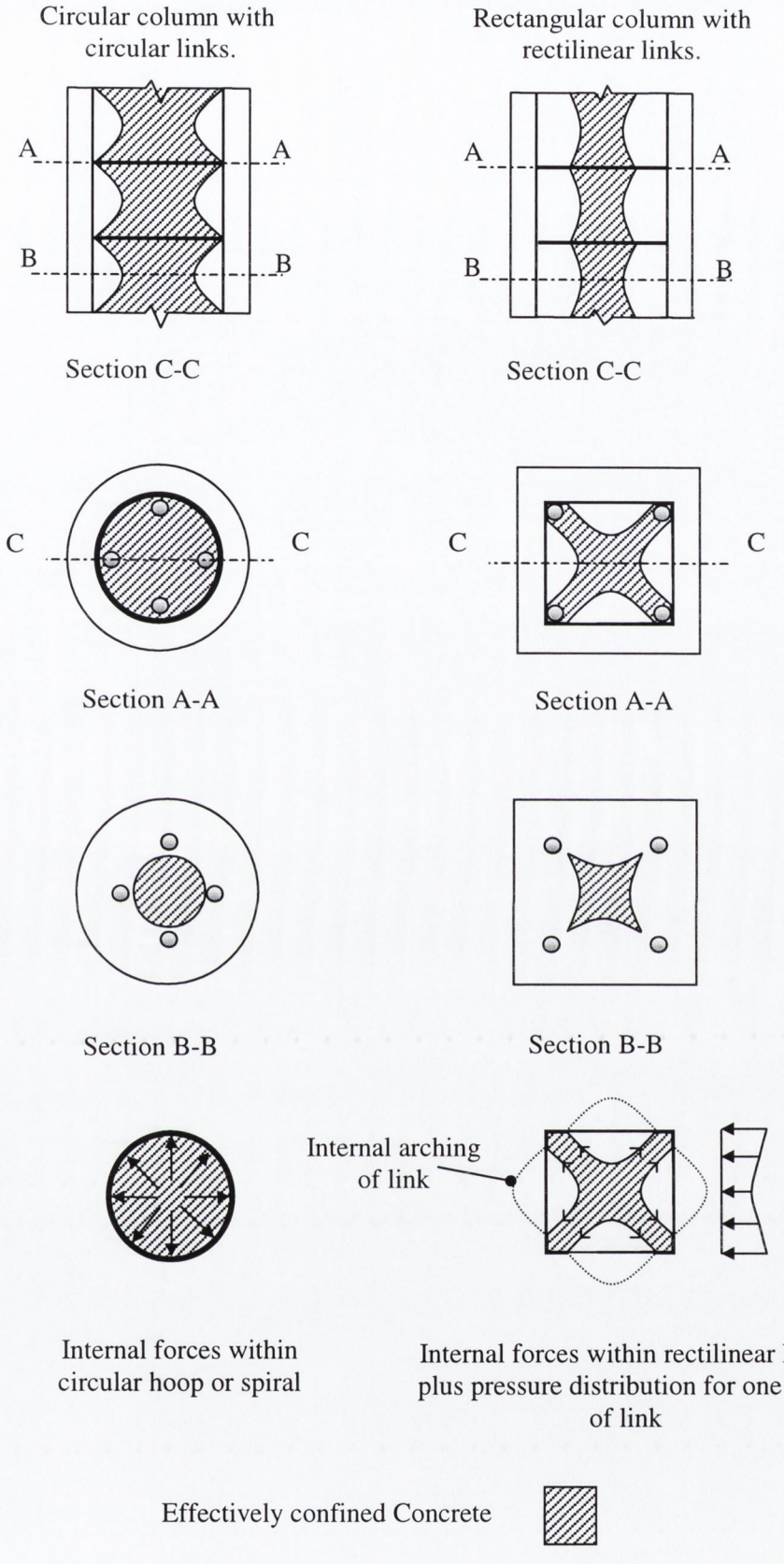

Figure 2.5: Circular and rectilinear sections confined by circular and rectilinear links respectively - areas of effectively confined concrete and internal forces (after Booth, 1994)

2.6.2 Factors influencing confinement effectiveness

Confinement by lateral reinforcement has little effect on the stress-strain curve of concrete, until the uniaxial strength is approached. However, beyond the uniaxial strength the shape of the stress-strain curve is a function of many variables, these are summarised below and treated individually in the proceeding sections:

- The ratio of the volume of transverse steel to the volume of the concrete core
- The spacing of the transverse steel with respect to the dimensions of the concrete core
- Reinforcement configuration
- Yield strength of the transverse steel
- Flexural stiffness of the transverse and longitudinal steel
- Longitudinal steel behaviour
- Concrete strength, especially with respect to high strength concrete
- Axial load level
- Rate of loading

2.6.2.1 Transverse steel content

The most influential parameter in determining confinement effectiveness is the amount of transverse confinement steel provided. The amount of confinement steel may be considered in terms of (a) the volumetric ratio (ratio of the volume of transverse steel to the volume of the concrete core) and (b) the transverse steel spacing. Although the two parameters are closely linked, it is important to distinguish between them. A high transverse steel volumetric ratio does not necessarily imply a very close link spacing since it depends not only on the transverse steel spacing but on the diameter of the transverse steel. An increase in the volumetric ratio means an increase in the amount of confinement reinforcement, which translates into an equivalent increase in passive confinement pressures, implying strength and ductility enhancements. The link spacing affects the confinement pressure distribution, where a decrease in link spacing means an increase in the efficiency of confinement pressure, which potentially reduces the need for high volumetric ratios. Figure 2.6 illustrates how a closer link spacing leads to more effective confinement – concrete is confined by arching of the concrete between links, therefore, if the links are too far apart a large volume of concrete cannot be confined and will spall off.

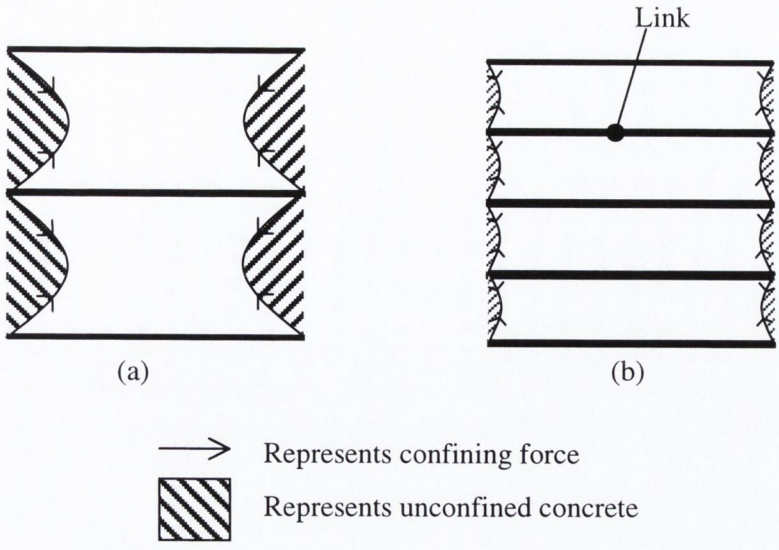

Figure 2.6: The effect of link spacing on concrete confinement, (a) large link spacing (b) small link spacing, (after Park *et al.*, 1975)

The work of Considére and Richart *et al.* (Section 2.6), at the beginning of the 20th century, demonstrated that strength and ductility of concrete could be significantly improved with confinement. With respect to the capacity design approach introduced in the early 1970s, and now the current earthquake design philosophy, the issue of ductility has become increasingly important. With this in mind, much research has been done to determine the effect of the amount of transverse confining steel on the ductility of concrete; there is general agreement among investigators that the presence of closely spaced links, or spirals, greatly enhances ductility.

Initial research was on columns subject to monotonic axial compression. Both Burdette *et al.* (1971) and Sheikh *et al.* (1980) concluded, from tests on short columns, that the presence of closely spaced links results in an appreciable increase in column ductility. Sheikh et *al.* determined that transverse steel volumetric ratio and transverse steel spacing are both important parameters in determining the behaviour of confined concrete. Figure 2.7 presents the stress-strain curves of columns with (a) different volumetric ratios and (b) different link spacings.

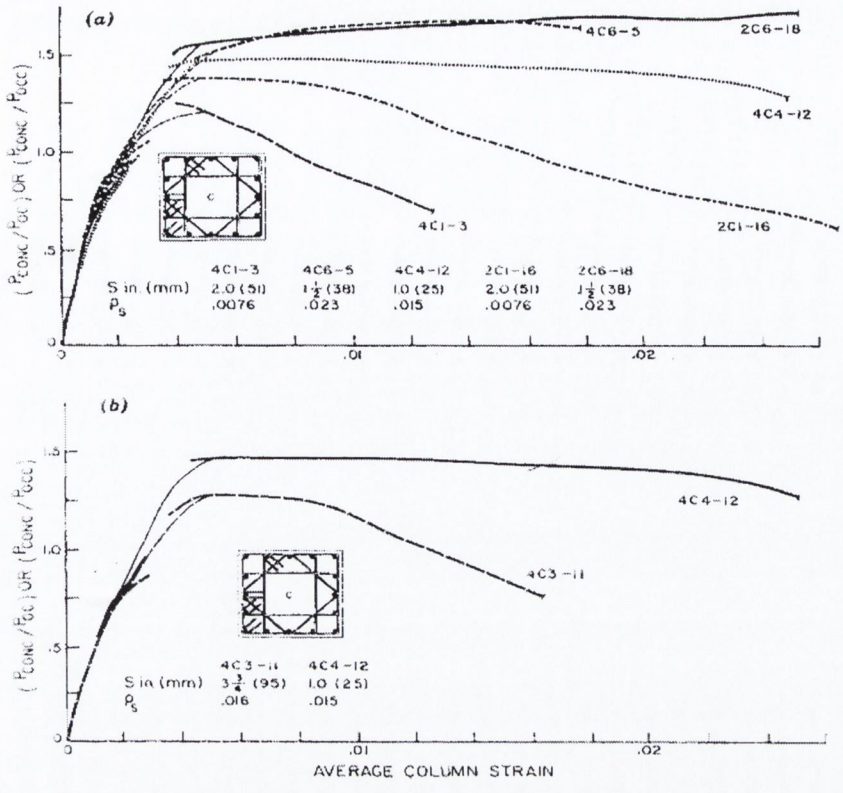

P_{conc} = load carried by concrete
P_{oc} = theoretical capacity of column concrete
P_{occ} = theoretical capacity of column core concrete
s = link spacing
ρ_s = lateral steel volumetric ratio

Figure 2.7: Effect of: (a) transverse steel volumetric ratio, (b) link spacing (Sheikh *et al.*, 1980)

Mander *et al.* (1988) concentrically loaded 31 full-size concrete columns, of circular, square, or rectangular wall cross sections, with transverse steel volumetric ratios (ρ_s) in the range of 0.006 to 0.025. Even for the lightly confined columns (ρ_s = 0.006) there was a greatly extended falling branch on the stress-strain curve, as well as substantial enhancement of compressive strength, compared with unconfined concrete. For more heavily confined columns, (ρ_s = 0.020) the results were similar but more dramatic. They concluded that the most significant parameter affecting the shape of the stress-strain curve of confined concrete, for all cross-sections, was the quantity of confining reinforcement. Increasing the volumetric ratio led to increases in peak stress, the strain at peak stress, the fracture strain of the confinement steel, and a decrease in the slope of the falling branch of the stress-strain curve. To determine the effects of transverse steel spacing, with respect to volumetric ratio, two columns with the same volumetric ratio, but two different spiral pitches, of 93mm and 36mm respectively, were tested. While the larger pitch resulted in a slightly less satisfactory falling branch than the smaller pitch, the influence was small, and neither the peak stress nor the corresponding strain, were influenced significantly. Therefore, unlike Sheikh *et al.*

(1980), the transverse steel spacing did not appear to be as influential as the transverse steel volumetric ratio.

Skeikh *et al.* (1993) tested short spirally reinforced columns to examine the effect of link spacing with respect to different transverse steel volumetric ratios. In specimens with the amount of spiral steel required by the ACI code (ρ_s = 0.0011) an increase in the s/D_c ratio (spiral pitch to spiral diameter) led to significant improvement in concrete behaviour, especially ductility. In specimens with lower ρ_s values, a change in s/D_c ratio did not significantly alter behaviour since the ρ_s value was too low for any substantial improvement in concrete properties due to confinement to occur. For specimens with large ρ_s values (>0.0017), the confinement provided by the steel was so effective that changes in s/D_c ratio could not affect the concrete behaviour significantly since the existing confinement was already completely efficient.

Razvi *et al.* (1996) compared the stress-strain relationships of fifteen large-scale columns confined by circular and rectilinear transverse reinforcement of different volumetric ratios and spacings. Their results showed that the detrimental effect of increasing link spacing may be offset by an increase in the volumetric ratio, and conversely that, columns with closely spaced links do not require high volumetric ratios of lateral reinforcement for effective confinement. However, these conclusions are limited since when the link spacing becomes excessively high, increases in the volumetric ratio lose their effectiveness.

Sheikh *et al.* (1994), Bayrak *et al.* (1998) and Légeron *et al.* (2000) all studied the effects of confinement in columns subject to axial compressive loads and lateral cyclic loading. Sheikh et *al.* considered high strength concrete columns and found that improvements in ductility and energy dissipation capacities appeared to be proportional to the increase in the transverse steel content. Bayrak et *al.* tested normal, high and ultra strength concrete columns, and observed improved ductility and energy dissipation capacities with increase in the amount of transverse steel content for all concrete strengths considered. Légeron *et al.* presented work on the effects of axial load and volumetric ratio on the cyclic behaviour of columns. For three levels of axial load (15, 25 and 40% of the column compressive capacity) higher volumetric ratios of lateral steel led to an ability to sustain larger inelastic cyclic displacements. They concluded that, while axial load is an important parameter, the volumetric ratio of confinement steel is the main parameter in controlling the column response. Figure 2.8 presents the moment-curvature hysteresis envelope curves of two column pairs, subject to axial load levels of 25% and 40% respectively, but different volumetric ratios within each pair.

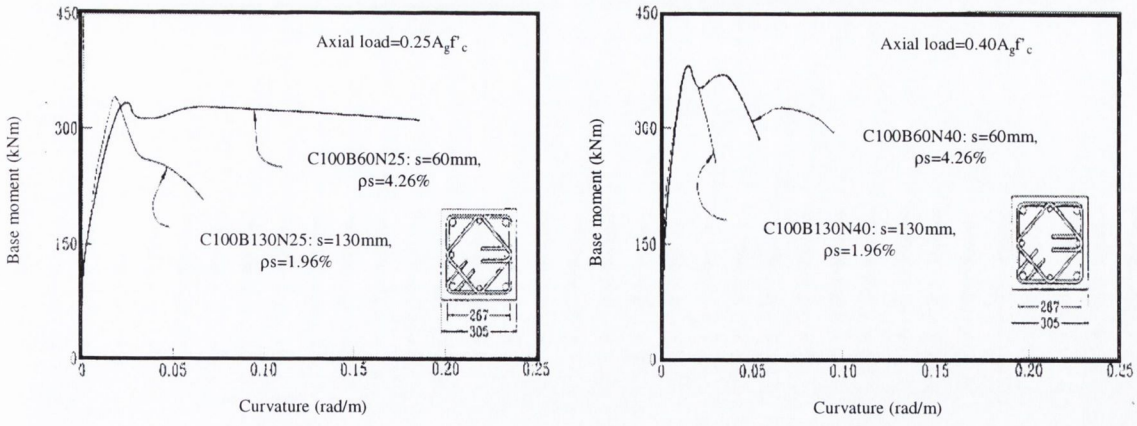

(a) (b)

Figure 2.8: Influence of transverse steel volumetric ratio for columns subjected to axial load levels of: (a) 25% and (b) 40% (Légeron *et al.*, 2000)

2.6.2.2 Reinforcement configuration

A key aspect of confinement effectiveness is the chosen transverse and longitudinal steel configuration. A lot of research has been carried out to study the effects of different link configurations, in terms of intermediate ("internal") links, support to longitudinal steel, the use of cross-ties, and the hook angles of the lateral steel.

Link configurations determine the effectively confined concrete area. The efficiency of a chosen configuration depends on the lateral restraint it offers to the longitudinal steel, rather than on the configuration shape (Sheikh *et al.*, 1980). For the confinement benefits of longitudinal steel to be utilised, it is essential that it be supported laterally. Cross-ties offer a sound option to intermediate links, provided they engage the longitudinal steel rather than the perimeter link. Care must be taken with the anchorage of cross-ties, especially for seismic design. Within the following section, a number of different configurations are discussed, and these are presented in Table 2.1.

Reinforcement Configuration Type	**Diagram**	**Description**
I Cusson *et al.* (1994) Razvi *et al.* (1996)	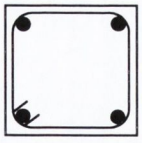	• Single perimeter link. • 4 longitudinal bars, all supported.
II Moehle *et al.* (1985) Bayrak *et al.* (1988)		• Single perimeter link. • 6 longitudinal bars, unsupported intermediary bars.
III Moehle *et al.* (1985) Sheikh *et al.* (1980) Bayrak *et al.* (1988) Cusson *et al.* (1994)		• Perimeter link plus internal diamond shaped link. • 6 longitudinal bars, all supported.
IV Sheikh *et al.* (1980)		• Perimeter link plus internal octagonal link. • 12 longitudinal bars, all supported.
V Sheikh *et al.* (1980) Cusson *et al.* (1994) Razvi *et al.* (1996) Mo *et al.* (2000)	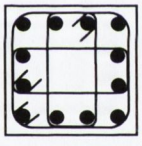	• Perimeter hoop plus 2 internal rectangular links. • 12 longitudinal bars, all supported.
VI Sheikh *et al.* (1980)	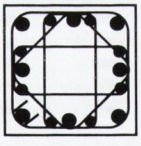	• Perimeter link plus 2 internal rectangular links and diamond shaped link. • 16 longitudinal bars, all supported.
VII Moehle *et al.* (1985)	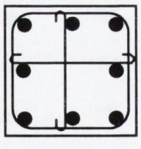	• Perimeter link plus 2 cross-ties (with 180° hooks that engage the link). • 6 longitudinal bars, all supported.
VIII Moehle *et al.* (1985)	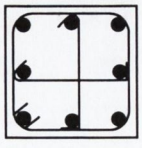	• Perimeter link with 2 cross-ties (with 90°& 135° hooks that engage the longitudinal steel). • 8 longitudinal bars, all supported.

Table 2.1: Steel configuration types

Reinforcement Configuration Type	Diagram	Description
IX Razvi *et al.* (1996)	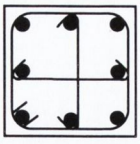	• Perimeter link with 2 cross-ties (with 135° hook that engage the longitudinal steel). • 8 longitudinal bars, all supported.
X Mo *et al.* (2000)	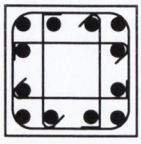	• Perimeter link with 4 cross-ties that engage the longitudinal steel. The cross-ties have 90° and 135° hooks. • 12 longitudinal bars, all supported.
XI Mo *et al.* (2000)	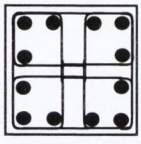	• Four C-Shaped links. • 12 longitudinal bars, all supported.

Table 2.1: continued

Two important aspects of confinement efficiency in rectangular sections are the complexity of the transverse steel configuration, and how much support the chosen configuration offers to the longitudinal steel. Sheikh *et al.* (1980) performed a series of tests on short columns tested under monotonic compression. The confinement efficiency of four different configurations were compared; Types III, IV, V and VI respectively. All of the link steel was fully anchored with 135° bends extending a minimum of 14 link diameters into the confined core. Specimens with configuration Type III (the simplest steel configuration) showed the least enhancement in concrete strength and ductility, while specimens with configuration Type VI (the most complex configuration) showed the largest gains in strength and ductility. Figure 2.9 presents the strength gain and increase ductility of the confined concrete core in columns, with almost equal amounts of longitudinal and transverse steel and approximately equal link spacing. It was also determined, from the similar behaviour of specimens with the same longitudinal steel distributions but, configurations IV and V respectively, that it is not the configuration shape that governs behaviour, rather whether the chosen configuration provides support to the longitudinal steel.

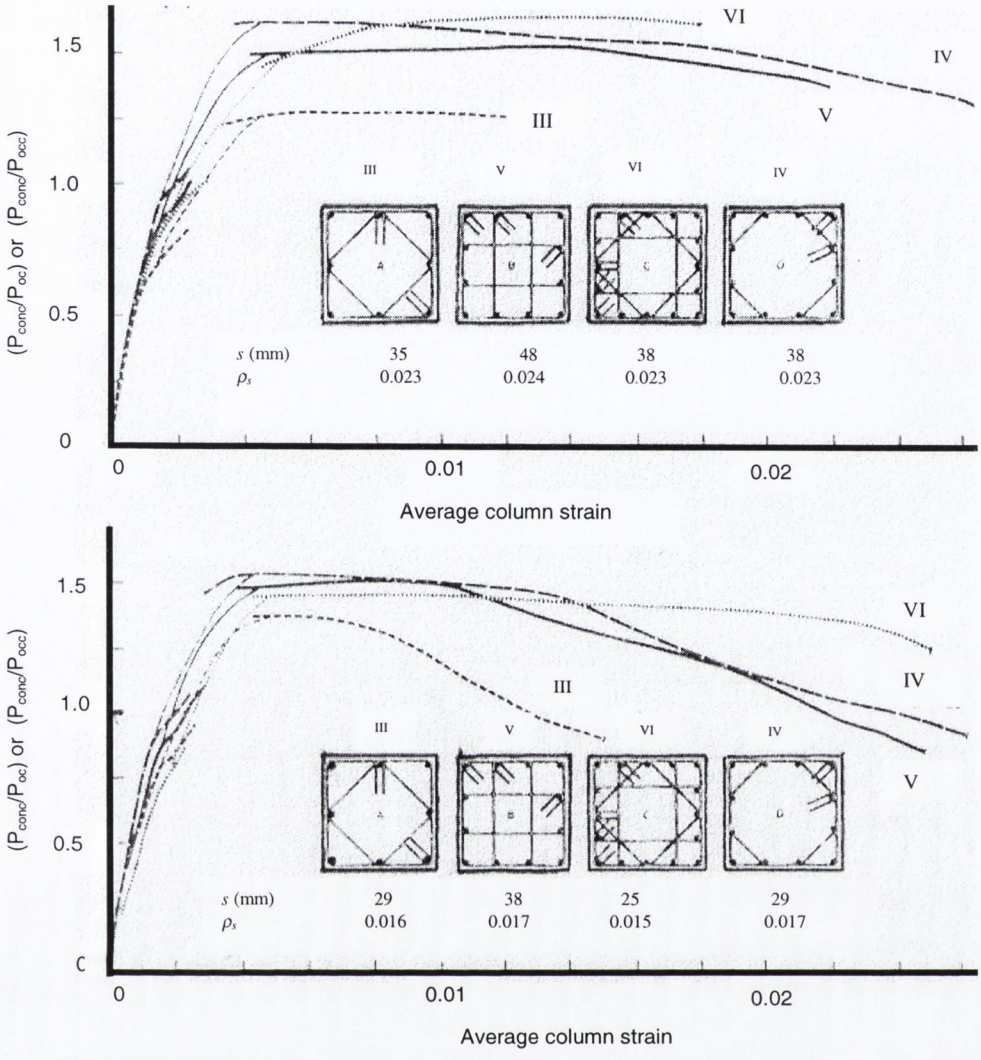

P_{conc} = load carried by concrete
P_{oc} = theoretical capacity of column
P_{occ} = theoretical capacity of column core concrete
ρ_s = ratio of volume of lateral steel to volume of core

Figure 2.9: Effect of steel configuration (a) ρ_s = 0.0023-0.0024, (b) ρ_s = 0.015-0.017, (Sheikh *et al.*, 1980)

Cusson *et al.* (1994) performed similar tests to Sheikh *et al.* but on large-scale high strength concrete columns. They considered the confinement effectiveness of the same configurations types with the exception of Type VI, which was replaced by the simpler configuration of Type I. All of the links were anchored with 135° bends extending 75mm into the concrete core. All of the configurations, with the exception of Type I, were very effective in enhancing strength and ductility. An interesting result was that the Type III configuration was just as effective at enhancing strength and ductility as Types IV and V, despite containing less longitudinal steel.

Bayrak *et al.* (1998) tested columns under a combination of constant axial load and reversed cyclic displacements. They compared the response of two link configurations - Type II and Type III. The

columns with support to all of the longitudinal bars (Type III) were considerably more ductile, and had a substantially larger energy dissipation capacity, than columns with no support offered to the intermediate longitudinal bars (Type II). For example, in two columns, identical except for their link configuration, the column with configuration Type III had an energy dissipation capacity of 4.4 times that of the column with configuration Type II, and a curvature ductility factor 43% larger.

Razvi *et al.* (1996) tested high strength columns under monotonic compression to determine the effectiveness of cross-ties. The response of columns reinforced with configurations Types I, V and IX were investigated. All of the links and cross-ties were anchored by 135° bends extending into the core. The column with Type I configuration (single perimeter link) displayed a very brittle response with failure at 0.25% strain. In contrast, the other two arrangements (with either internal links or cross-ties) displayed little strength decay at 0.75% strain level. These two specimens had very similar responses, but the specimen with intermediate links, rather than cross-ties, showed the most gradual loss in strength. Hence, they concluded that the use of cross-ties is certainly beneficial and their benefits may approach those of internal links.

Moehle *et al.* (1985) compared the behaviour of two confinement details using cross-ties as permitted by the Uniform Building Code (UBC, 1982) and the American Concrete Institute (ACI, 1983). The arrangement recommended by UBC is Type VII, where cross-ties, with 180° hooks, engage only the perimeter link steel. In many situations, placement of this form of cross-tie is considered inconvenient. As an alternative, the ACI Codes recommends cross-ties that engage the longitudinal steel (Type VIII) and have a 135° hook at one end and a 90° hook at the other end of the cross-tie. Confinement configurations Types II and III were also considered within this experimental programme, where columns were tested under monotonic compressive loading. Of the four configurations, Type III proved the most effective. However, Types VII and VIII performed only marginally worse than Type III, implying that cross-ties are almost as effective as intermediate links. In fact, it was observed that the lower confinement effectiveness observed for the columns with cross-ties relative to columns with intermediate links may have been due in part to differences in transverse steel ratios. Of the different cross-ties considered, it was concluded that the 135° and 90° hooks led to slightly less ductile performance than the 180° hook, however, the difference in confinement effectiveness was considered negligible. As expected, the 90° hook eventually pulled out of the concrete leading to a partial loss of the cross-tie effectiveness. Stress concentrations arose in the perimeter links, where they were engaged by the cross-ties, leading to link fracture at that location. Therefore, it was recommended that this detail be avoided and that the longitudinal steel be engaged instead. In conclusion, it was warned that for seismic loading the confinement effectiveness of all the above configurations will decrease with progressive degradation of the hook anchorage, in particular the 90° hook.

Mo *et al.* (2000) considered the seismic response of a new configuration of "C-shaped" links (Type XI). Nine columns, subjected to a constant axial load and cyclic lateral load, were tested to compare the performance of the new configuration to that of more standard configurations (Types V and X). The proposed configuration consisted of four C-shaped ties with 40mm lap splice, as based on the ACI Code compression lap splice requirement. The displacement ductilities and dissipated energies of three specimens, identical except for their lateral steel configurations, are summarised in Table 2.2. These results show that the new configuration performed as well as the other configurations in terms of displacement ductility, and was slightly superior with respect to energy dissipation capacity. Therefore, it was concluded that the C-shaped ties offer a good alternative to standard configurations. Also, the 40mm lap splice of the C-shaped ties was seen to work sufficiently. Of the standard confined specimens, the specimen with cross-ties performed marginally worse in terms of energy dissipation.

Configuration Type	**Displacement Ductility**	**Energy Dissipation Capacity (kNmm)**
V	5.82	431643.0
X	5.74	525245.4
XI	5.49	596957.6

Table 2.2: Displacement ductilities and energy dissipation capacities (Mo *et al.*, 2000)

2.6.2.3 Transverse steel yield strength

The yield strength of confinement steel determines the upper limit of the confining pressure applied to the concrete core - the higher the yield strength the higher the confinement pressure applied to the core and, hence, the higher the confinement efficiency. This could prove advantageous in situations where large amounts of confinement steel are required, such as in high strength columns under large axial loads. Another possible advantage of high-grade steel is that it may allow a reduction of the required lateral steel volumetric ratio, without detrimental effect on member behaviour, while at the same time lessening the detailing complexity. However, it has been found (Cusson *et al.*, 1994)) that the use of high-grade steel for confinement in columns is effective only if the yield strength of the steel is achieved; this is only possible through effective confinement. As an aside, research by Lin *et al.* (2001) considered the use of high-flowability high-performance concrete (HPC) where there is steel congestion due to the large amounts of confinement required for earthquake resistance. Steel congestion often results in poor concrete quality in members where the steel cage is so dense as to prevent the concrete from completely filling the reinforcement cage. An alternative solution to mitigate the problem of poor concrete quality in densely reinforced

regions, is the use of high performance concrete, which has high slump and flowability while also having sufficient strength.

The New Zealand design codes permit a reduction in the required amount of transverse steel for higher strength steel. That is, the required amount of transverse steel is inversely proportional to the yield strength of that steel. Zahn *et al.* (1986) investigated this by testing six spirally reinforced concrete columns under concentric loading. They found that the volumetric ratio of confining reinforcement can be decreased with increasing steel yield strength without resulting in a reduction in the compressive strength of the confined concrete, and that the ductility of the confined concrete, although reduced, will remain high.

Cusson *et al.* (1994) compared pairs of high strength, rectilinearly confined columns with different transverse steel yield strengths and confinement configurations. The stress in the transverse steel was measured at the maximum strength of the confined concrete, and it was observed that it was only in well confined specimens that the yield strength was developed at peak strength. Negligible improvements in specimen behaviour were observed in specimens with high yield lateral steel where the recorded steel stress was well below its yield value. On the other hand, in well confined columns where the transverse steel was able to reach its yield strength at peak strength of confined concrete, there were significant increases in strength, and especially, ductility of the specimens.

Razvi *et al.* (1996) compared the response of companion columns with different grades of transverse reinforcement. In two rectangular columns with the same detailing, but two different steel grades (570N/mm^2 and 1000N/mm^2) the stress-strain responses, (Figure 2.10), indicated improved ductility in concrete confined with higher grade steel. Two circular columns with different steel grades (400N/mm^2 and 1000N/mm^2) and different transverse steel volumetric ratios, but designed to provide similar confinement pressures (as indicated by the product of the volumetric lateral steel ratio by the transverse steel yield strength) were also tested. The results showed that the detrimental effects of reducing the volumetric ratio could be offset by a proportional increase in the steel grade. However, additional data on other columns indicate that this observation is limited to columns with efficient arrangements of reinforcement.

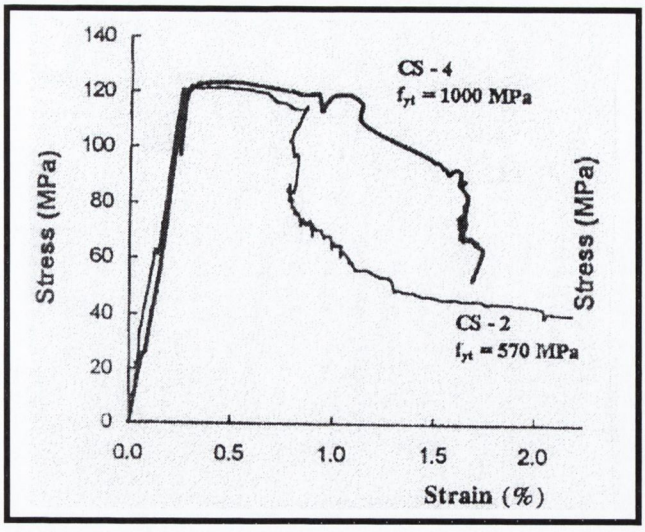

Figure 2.10: Effect of transverse steel yield strength, (Razvi *et al.*, 1996)

Paultre *et al.* (2001) investigated the influence of transverse steel yield strength by comparing the responses of eight full-scale columns subject to combined axial load and cyclic flexure. Their objectives were - (i) to evaluate the potential of high yield steel to confine HSC, with the aim of lessening the amount of required confinement steel, and (ii) to assess the efficiency of the confinement index $\rho_s f_{yh}/f_c'$ in predicting the ductility of confined HSC columns, where:

ρ_s = volumetric ratio of confinement steel
f_{yh} = yield strength of confinement steel (N/mm^2)
f_c' = concrete strength (N/mm^2)

They found that for HSC columns the amount of transverse steel can be decreased with increase in the yield strength of the transverse steel. For example, comparison of two specimens, identical except that one had 30% less confinement steel, showed that the two specimens behaved very similarly. This was achieved by using high yield confinement steel in the specimen with the lower confinement steel content.

With respect to the confinement index, column ductility was observed to increase with increase in the confinement index. For example, four specimens subject to the same axial load level and having the same concrete strength, but confinement indexes of 0.079, 0.179, 0.181 and 0.248 respectively, the displacement ductilities increased from 2.9 to 4.6 to 7.6 to 8.0. However, examination of factors such as the normalised dissipated energy (as defined by Equation 2.3, Section 2.6.2.6) indicated that the correlation between the confinement index and dissipated energy was far from perfect. Figure 2.11 presents the load-displacement hysteresis response of two specimens which had approximately the same confinement index (0.179 and 0.181 respectively), however the specimens displayed very different load-displacement responses. Specimen

C100BH80N40 exhibited a stable ductile behaviour to a ductility of about 5 while C100B60N40 behaved in a fragile manner with an ultimate displacement of about half that reached by the corresponding specimen.

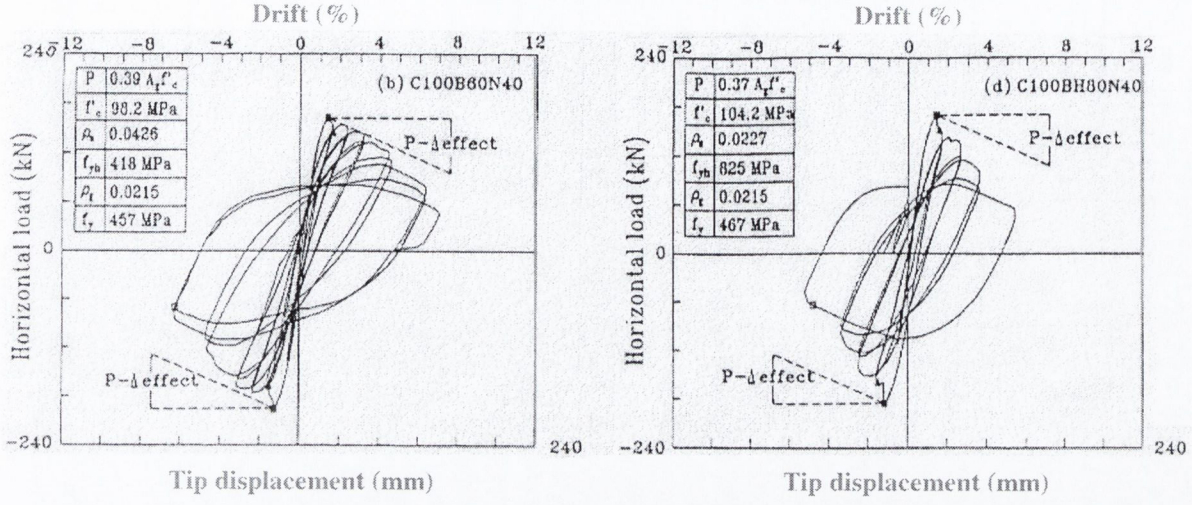

Figure 2.11: Lateral load versus tip displacement for specimens with the same confinement index but different behaviour (Paultre *et al.*, 2001)

2.6.2.4 Flexural stiffness of reinforcing steel

The flexural stiffness of reinforcing bars depends on their diameter and span. Lower flexural stiffness of the transverse steel may lead to lateral confinement only by edge forces acting along the diagonals of the concrete core section, whereas high flexural rigidity results in more uniform lateral confinement of the entire concrete core (Park *et al.*, 1975). Figure 2.12 illustrates a reinforced concrete section, showing where concrete is unconfined due to inadequate flexural stiffness of the transverse and longitudinal steel.

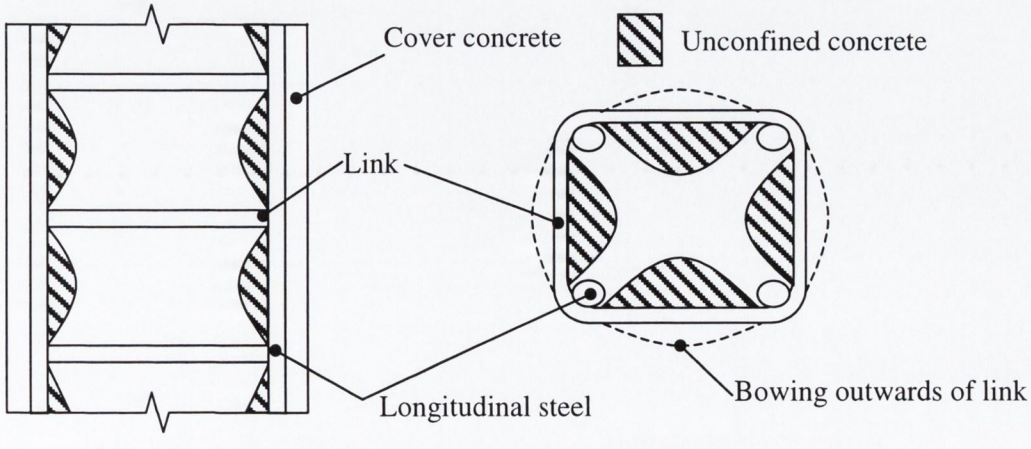

Figure 2.12: Effectively confined concrete (after Park *et al.*, 1975)

Naturally, a larger bar diameter leads to more effective confinement than a small bar diameter. Transverse bars of small diameters act merely as ties between the longitudinal bars, bowing outwards as the concrete expands, rather than resisting its expansion. A shortening of the transverse steel span also increases its flexural stiffness. It is for this reason that reinforcement configurations with well distributed longitudinal steel and/or cross-ties (Section 2.6.2.2) are advocated since they lessen the unsupported span of the transverse steel, hence, increasing its flexural rigidity. Burdette *et al.* (1971) considered the effect of welding "crossing-bars" to the links (where "crossing-bars" are similar to cross-ties, except that they are welded to the lateral steel) in order to vary their flexural rigidity. The increase in flexural rigidity due to the presence of cross-bars led to column ductilities, and strengths, significantly above those attained in columns with just links. The issue of flexural rigidity also applies to the longitudinal steel. Larger diameter longitudinal steel bars and shorter unrestrained spans (i.e. smaller spacing of the lateral steel) prevent the longitudinal steel from buckling, increasing its capacity to confine the concrete. In Eurocode 8 (EC8, 1998) equations for beams and columns, the longitudinal reinforcement bar diameter is included as one of the limiting factors when calculating the required transverse steel spacing.

2.6.2.5 Longitudinal steel behaviour

For effective capacity design, a reliable estimate of the ductility available in reinforced concrete members must be available. In other words, either a complete range of statistical information on the stress-strain characteristics of the steel and concrete, or accurate models to predict their material behaviour must be on hand. For concrete, a thorough knowledge of its confinement is required, as will be discussed in Chapter 6. As regards the steel, its yield and ultimate strengths, strain hardening characteristics, and the effects of strain rate must be given due consideration. For instance, the actual yield strength of reinforcing steel commonly exceeds the nominal yield value used in design calculations. Further, within plastic hinge regions, during an extreme earthquake the longitudinal steel may reach strains 20 times, or more, that of its yield strain. Increases in steel strength leads to increases in flexural strength of plastic hinges. This is a matter of concern in capacity design because the increases in shear forces, which accompany such increases in flexural strength, may lead to brittle failure. Also, associated increases in column bending moments could result in the formation of undesirable column plastic hinges (Park, 1992).

As an example of the work done on the effect of reinforcing steel characteristics on the flexural capacity of reinforced concrete sections, Andriono *et al.* (1986) carried out an extensive statistical study on five years production of reinforcement steel in New Zealand. Using material test results in moment-curvature analysis of reinforced concrete beams, they confirmed that the flexural over-strength at plastic hinges should be taken as $1.25M_i$, where M_i is the ideal flexural strength of the

section calculated using the lower characteristic yield strength of steel. The lower characteristic yield strength is that value below which not more than 5% of the results fall on a normal distribution and is considered the appropriate value in New Zealand for the determination of steel areas in strength design of members. The 25% increase in M_i takes into account the probability of the actual steel yield strength being greater than the nominal yield strength and the increase above yield strength due to strain hardening.

Furakawa *et al.* (1996) demonstrated, by a mathematical model and tests on reinforced concrete cantilever beams, that if high strength longitudinal steel is used in a plastic hinge regions subject to large plastic rotations, this can lead to the tensile fracture of the longitudinal steel. They considered the steel behaviour in terms of its yield strength ratio, which is defined as the ratio of ultimate strength to yield strength. Of particular concern was the effect of a high yield strength ratio on the ductility of plastic hinges in reinforced concrete structures for earthquake resistance. They concluded that the use of reinforcing bar with a high yield strength ratio may jeopardise the ductile behaviour of plastic hinges, due to concentration of strain within the hinge regions, which leads to rupture of the reinforcing steel. Therefore, to avoid rupture of reinforcing bars, it is recommended to avoid the use of longitudinal steel with high yield strength ratios in plastic hinges where large plastic rotation is expected.

2.6.2.6 High strength concrete

Over the last two decades, the technology of high strength concrete (HSC) has greatly improved such that is now readily available for various applications such as bridges, offshore platforms and multi-storey buildings (Légeron *et al.*, 2000). Its high compressive strength, durability, greater modulus of elasticity and substantial savings resulting from section reduction, are all appealing properties of HSC. However, despite its advantages, and its acceptance into the construction industry, many aspects of the material remain questionable. One of these aspects is the more limited inelastic deformability of HSC earthquake columns relative to those of normal strength concrete (NSC) columns, and the fact that when loaded in compression HSC columns display "early spalling", (Cusson *et al.*, 1994, Razvi *et al.*, 1996). It is well known that concrete deformability decreases with increase in concrete strength (Figure 2.13). This raises serious concerns regarding the suitability of HSC for seismic regions where the ductility of structural components is relied upon for the dissipation of earthquake-induced energy. Some concrete design codes even limit the maximum strength that can be used for seismic designs. For example, the New Zealand Code (NZS, 1995) limits concrete compressive strength to 100N/mm^2 for ordinary structures relative to 70N/mm^2 for ductile structures.

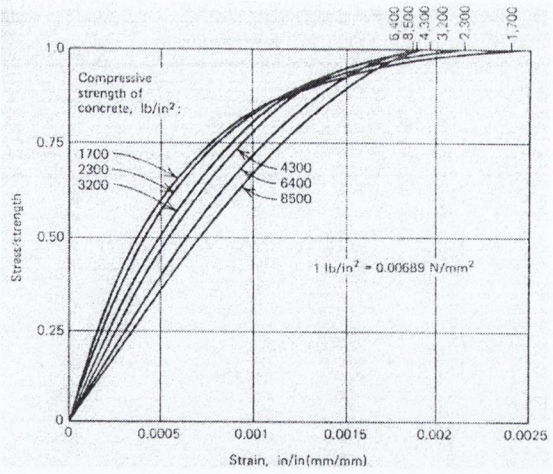

Figure 2.13: Relationship between stress to strength ratio and strain for concrete of different strengths (Park et *al.*, 1975)

With the introduction of HSC lower storey columns in multi-storey buildings, it is essential that the behaviour of these members is well understood so that they may be confined correctly. Published data on the performance of HSC laterally confined columns are scarce relative to those on NSC confined columns. Tests have shown that HSC exhibits less lateral expansion under axial compression than NSC due to a higher modulus of elasticity and lower internal microcracking. Consequently, the confining reinforcement comes into play later in the response, and the efficiency of the passive confinement of HSC is reduced relative to that of NSC. Despite this, it has been observed that the ductility of HSC columns can be improved by lateral confinement, although to a lesser degree than NSC columns. (In should be noted that the definition of HSC varies and strength values range from greater than 42N/mm^2 to greater than 60N/mm^2).

Yong *et al.* (1988) tested to failure a series of rectilinearly confined high strength concrete columns subject to monotonically increasing axial load. Concrete strengths ranged from 83.6 to 93.5N/mm^2. A general improvement in the behaviour of HSC columns with confinement was observed, although this was less significant than that observed in NSC columns. They found that for effective rectilinearly confined HSC columns, the link spacing should be less than the lateral dimension of the specimen, and not less than eight longitudinal bars should be distributed along the perimeter.

Cusson *et al.* (1994) also performed monotonic compression tests on HSC rectilinearly confined columns with strengths of 60, 80, 100 and 120N/mm^2. They observed that the behaviour of HSC columns was characterised by early and sudden spalling of the cover, resulting in losses of axial capacity before any lateral confinement could come into effect. However, after the cover had completely spalled off, important gains in strength and ductility were recorded in the well-confined specimens. It was observed that, despite the lower confinement efficiency of HSC compared to lower strength concrete, large gains in strength and ductility of HSC columns are possible with

adequate detailing of longitudinal and transverse reinforcement. Strength improvements of 50 to 100% and, ductilities 10 to 20 times greater than that of unconfined concrete were achieved. However, it was observed that increasing concrete compressive strength leads to significant decreases in the scope for strength and ductility enhancement through concrete confinement, and it was also suggested, that, with the early spalling, only the core concrete area be taken account of when calculating compressive strength.

Razvi *et al.* (1996) performed similar tests to Cusson *et al.*, testing columns confined with spirals or rectangular ties. They concluded that reinforced columns with 124N/mm^2 concrete may be successfully confined to develop substantial inelastic deformabilities, but they also observed premature spalling of the concrete prior to the attainment of concrete crushing strength.

Research has also been carried out on the confinement requirements of HSC columns subject to combined compressive axial loading and lateral cyclic loading. Sheikh *et al.* (1994) and Bayrak *et al.* (1998) tested HSC columns under a combination of high axial load and lateral cyclic loading, and compared the HSC response to that of NSC. In both cases, it was concluded that it is possible for well-confined HSC columns to behave in a ductile manner under high axial loads. As with lower strength columns, it was found that improvements in ductility and energy dissipation in HSC columns were directly proportional to increases in transverse steel content, but less than proportional in terms of moment capacity.

Ahn *et al.* (2000) and, Légeron *et al.* (2000) considered the ACI Codes and their lack of provision for confinement detailing of HSC columns. They investigated whether the code formulations for determining the amount of transverse steel for ensuring ductility in NSC columns were also adequate for HSC columns. Ahn *et al.* found that, while the load-resisting capacity of RC columns improved with increase in concrete strength, there was unstable hysteretic behaviour owing to the brittle nature of HSC. They concluded that high-strength reinforced concrete columns must be designed carefully with respect to ductility. Légeron *et al.* concluded that for low axial load levels, HSC columns can behave in a very ductile manner, even when confined with less reinforcement that recommended by the ACI Code for NSC columns. Specifically, for HSC columns subject to axial loads less than, or equal, to 15% of the gross axial-load capacity, only 50% of the code-required steel for NSC columns is needed. However, for high axial load levels, it was found that more confinement than is recommended for NSC columns is required for HSC columns.

Paultre *et al.* (2001) presented data on the behaviour of eight HSC columns subjected to combined axial load and reversed cyclic flexure. Three target strengths of concrete were considered - 80, 100 and 120N/mm^2 respectively. They concluded that the ductility of HSC columns is dependent on concrete strength. Figure 2.14 presents the lateral load versus displacement response of three

specimens with increasing concrete strength (78.7, 98.2, and 102.9N/mm^2). All three specimens were subject to the same axial load level and had identical geometry and amounts of confinement steel. It is clear from the figure that, with increase in concrete strength the capacity to sustain large inelastic displacement decreases sharply. The displacement ductilities drop from 10.2 to 5.2 to 4.7 when the concrete strength increases from 78.7 to 98.2 to 109.2N/mm^2. The same influence was also observed in the values of normalised energy dissipation (E_N) which dropped from 66.9 to 33.8 to 26.2 with respective increases in concrete strength. The normalised energy dissipation was defined as follows (Paultre *et al.*, 2001):

$$E_N = \frac{1}{H'_{\max} \Delta_{yI}} \sum_{i=1}^{n} E_i \qquad (2.3)$$

where:

E_N = Normalised dissipated energy

H' = applied horizontal load (H) plus the equivalent horizontal load due to the P-delta effect (kN)

Δ_{yI} = Idealised yield displacement (mm)

Ei = energy dissipation for cycle i (Joules)

n = number of cycles

Finally, to address the problem of early spalling in HSC columns, Paultre *et al.* (1996), and Foster *et al.* (2001) showed that, by adding steel fibres to the concrete mixture, cover spalling can be effectively prevented. Foster *et al.* tested HSC concrete columns containing 2% steel fibres subject to either concentric or eccentric compression. During testing, the cover remained intact throughout the tests, well beyond peak load, due to the inclusion of fibres. The results indicate that fibre-reinforced columns were greatly superior to columns without fibres, particularly with respect to post-failure ductility.

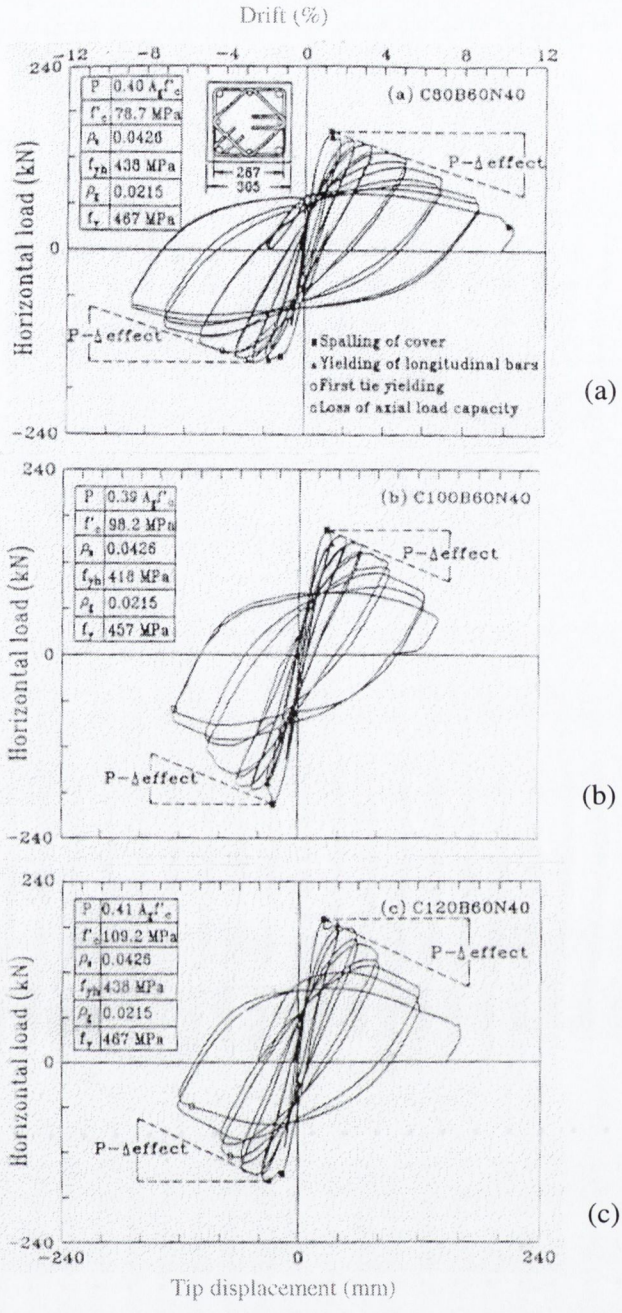

Figure 2.14: Lateral load versus tip displacement for specimens with increasing concrete strength, (a) 78.7N/mm^2, (b) 98.2N/mm^2, (c) 109.2N/mm^2, (Paultre *et al.*, 2001)

2.6.2.7 Axial load level

Experimental results show that axial loads have beneficial influences on the moment-resistance of reinforced concrete columns (Bayrak *et al.*, 1998, Ahn *et al.,* 1999), but negative effects on their inelastic cyclic behaviour. For columns subject to lateral cyclic loading, an increase in axial load decreases column deformability and ductility, while accelerating strength and stiffness degradation with every cycle. All recent research (Watson *et al.*, 1994) highlights the need for codes to consider carefully the influence of axial load when computing the required amount of confinement.

A considerable amount of work has been carried out with respect to the ACI Code confinement provisions for columns subject to lateral cyclic loading and axial load. Tests on columns by Watson *et al.* (1994) indicated that the current ACI Code equations for ductility are conservative for columns with low axial loads, but less conservative for columns with higher axial loads. Bayrak *et al.* (1998) compared the response of columns subject to cyclic lateral loads and different levels of axial load. They found that specimens with higher axial loads had increased strength but reduced ductility and greater stiffness degradation. Figure 2.15 compares the moment-curvature responses of two columns with the same reinforcement details but subject to axial load levels of 36% and 50% the column compressive capacities, respectively.

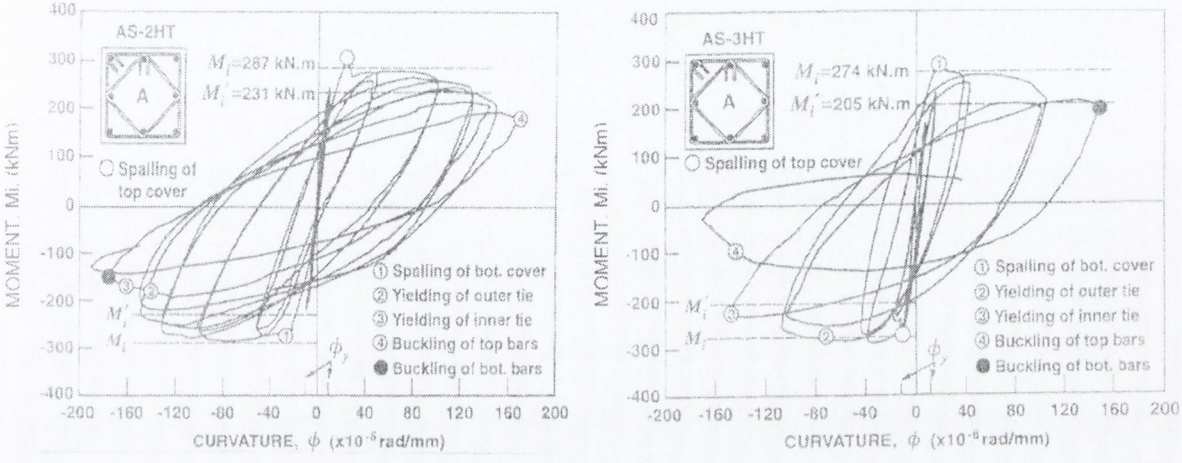

(a) (b)

Figure 2.15: Moment-curvature response for different axial load levels: (a) 36% and (b) 50%, (Bayrak *et al.*, 1998)

In similar tests by Ahn *et al.* (1999), a remarkable decrease in column ductility with increased axial load was observed. Their results showed that for identical columns, the amount of lateral reinforcement required for a high axial load ratio is 45% more than for a low axial load ratio, if the same ductility is to be achieved. (A high axial load ratio is defined as greater than 40% the gross-section capacity.) Légeron *et al.* (2000) tested HSC columns with lateral cyclic loading and three axial load levels; 15%, 25% and 40% the gross section capacity. These three levels represented a ductile, balanced and fragile failure respectively. They determined that for each axial load, the presence of axial load had a beneficial influence on the column moment resisting capacity but a negative effect on the inelastic cyclic behaviour. The column subject to the lower axial load level was able to sustain reasonable inelastic load increases. However, with increased axial load, the columns displayed insufficient levels of ductility and energy dissipation for seismic applications.

2.6.2.8 Loading rate

Since the mechanical properties of all materials are strain-rate dependent, the behaviour of structural elements under dynamic loading conditions cannot be predicted accurately unless the time-dependent properties of materials are taken account of. Loading rates can range from the static case of $10^{-5}s^{-1}$, through an intermediate range ($\cong 10^{-1}$ to $10s^{-1}$) requiring consideration of inertia forces, to yet higher levels ($>\cong 10s^{-1}$) that encompass either impact or explosive loading, (Figure 2.16).

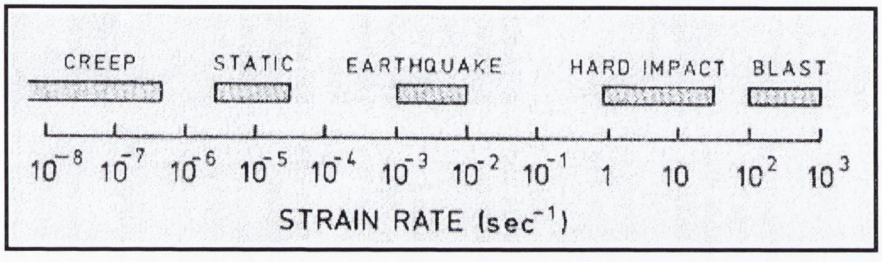

Figure 2.16: Magnitude of strain rates expected for different loading cases (Bischoff *et al.*, 1991)

The behaviour of concrete under static loads can be quite different to its behaviour under dynamic loads. As loading rate increases, compressive strength, modulus of elasticity, and the slope of the descending portion of the stress-strain curve of concrete, also increase (Fu *et al.*, 1991). For concrete structures subjected to earthquake and impact type loading, evaluation of both the inertial and the resisting forces depends upon the concrete and steel properties. During severe earthquakes high strain rates are imposed on a structure. Bertero (Booth, 1994) predicted that for a very rigid structure with a short fundamental period of 0.1s the rate of strain at critical regions may be as high as $2.5s^{-1}$.

Early research by Abrams, Jones and Richart and Glanville (Bischoff *et al.*, 1991) investigated the relation between strain rate and the compressive strength of concrete. The general conclusion was that an increase in loading rate is accompanied by an increase in compressive strength. In subsequent tests, by Watstein (Bischoff *et al.*, 1991), on concrete cylinders under monotonic loading at strain rates between 1×10^{-6} and $10s^{-1}$ it was found that at the highest strain rate, the average concrete strength increased by over 80% above that obtained in quasi-static tests typical of normal testing rates (1×10^{-6}). Atchley and Furr (Bischoff *et al.*, 1991)) observed increases of 25-38% in strength, while Hughes and Gregory (Bischoff *et al.*, 1991) recorded a 90% increase in strength for concrete impacted by means of a drop-hammer apparatus.

Results of all tests certainly indicate an increase in the compressive strength of concrete under dynamic conditions. However, there is wide scatter of the experimental findings on the magnitude of the strength increase, and its variation with rate of loading. These discrepancies exist mainly because the behaviour of concrete is strongly affected by many variables such as the static strength, water/cement ratio, aggregate type, curing conditions, age of testing and geometry of the specimen. For example, many researchers have observed that at higher rates of loading of stronger concretes, (that is those with a higher uniaxial static compression strength), exhibit a smaller percentage gain in compressive strength than in weaker concretes (Bischoff *et al.*, 1991).

2.7 Alternatives to standard confinement

2.7.1 Wire-welded fabric

An alternative to conventional steel links for confinement is welded-wire fabric (WWF). The advantages of WWF are that it is prefabricated and simple to place, hence, incurring fewer labour costs during construction. The first study in recent years for use in WWF concrete columns was by Razvi *et al.* (1989). They tested 34 small columns, reinforced with conventional links, but with the column cores also wrapped in WWF, under concentric compression. The intention was to use WWF as a supplement to the confinement already offered by the links. The results were favourable but they concluded that practical difficulties arose in placing the WWF in the columns, especially when 135° hooks were used.

Mau *et al.* (1998) considered a different approach to the use of WWF as a confinement material. They placed the WWF panels at uniform spacing to form a parallel stack within the column. The WWF panels were soldered to 1.6mm wires at each corner (Figure 2.17). The corner wires were of such small diameter that their contribution to longitudinal strength was negligible. The columns were tested under concentric axial compression and different longitudinal spacings and grid sizes of WWF panels were considered.

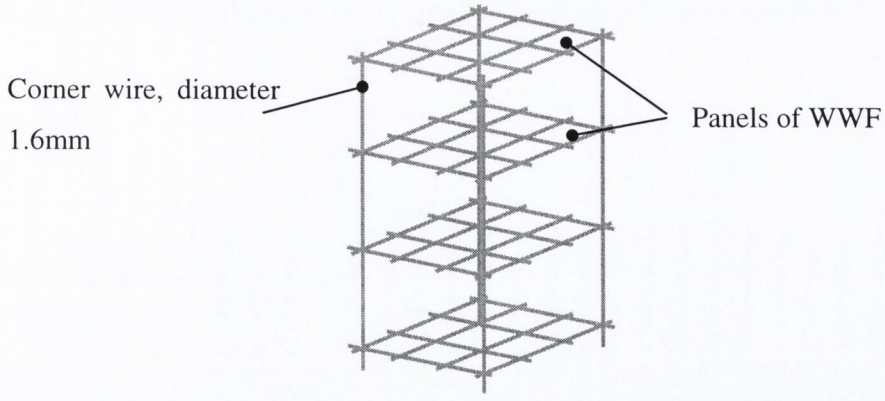

Figure 2.17: Wire-welded fabric (after Mau *et al.*, 1998)

In all specimens, failure occurred in their middle regions where all the wires across that surface fractured. As the specimen load-capacity decreased, sounds of fracture were heard, so it was thought that the wires broke gradually. They concluded the following from their tests that:

- WWF concrete composite behaves more like a homogenous material than a structure reinforced with two discrete components
- WWF reinforcement does provide confinement, hence increasing concrete strength and ductility
- The dominant factor affecting strength enhancement is the longitudinal spacing of the WWF panels rather than its volumetric ratio

2.7.2 Lateral prestressing

Cheong *et al.* (1991) studied a method of confining concrete stub columns utilising an arrangement of orthogonal, de-bonded, high-tensile steel bolts. This method of confinement requires a series of ducts to be pre-formed in the columns for subsequent insertion of the bolts (Figure 2.18). The bolts act in direct tension, in reaction to the lateral expansion of the concrete, applying confining forces at discrete points, thus creating a confinement of varying intensity throughout the concrete. An additional feature of this form of confinement is that the bolts may be tensioned to generate an active confinement stress in addition to the passive confinement stress already offered.

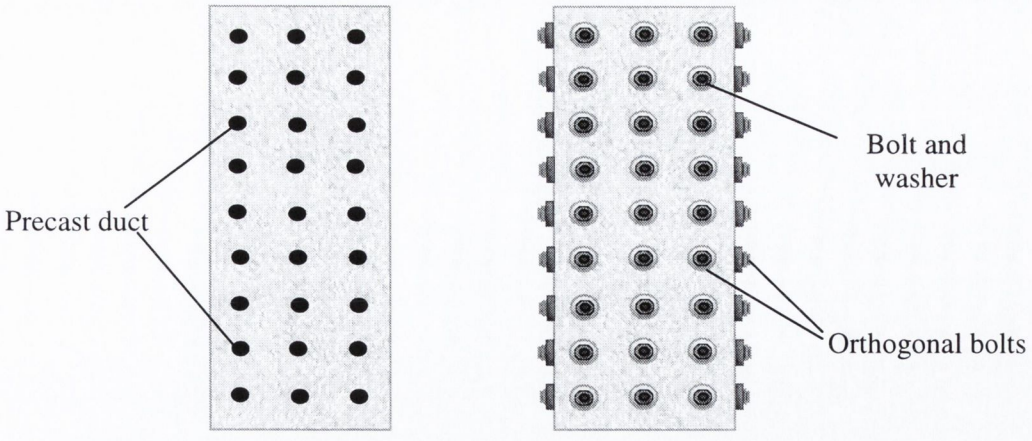

Figure 2.18: Laterally prestressed column (after Cheong *et al.*, 1991)

Columns were loaded monotonically to maximum load. The influence of prestress, for bolt tensions of 0, 125 and 220N/mm^2 levels, respectively, and the effect of grouting the annular cavities around the bolts were investigated.

Notwithstanding the non-uniformity of the confinement offered, the bolt-reinforced columns, regardless of prestressing, were observed to exhibit substantial strength and ductility gains over companion columns of plain concrete. The chief benefits of prestressing were the enhancement of the cracking load, and therefore, a delay in the deviation from linear behaviour. Bigger improvements in cracking load were obtained with increased prestress, although the relationship was non-linear. While prestressing increased the column strength only marginally, it had a significant effect on the longitudinal strains reached at maximum strength. In prestressed grouted columns the strains reached at maximum strength were 20% lower than those reached in the unprestressed columns. The annular cavities had the effect of greatly diminishing the concrete bearing area at the level of the bolts, leading to premature cracking due to stress concentrations around the ducts. It was found that grouting significantly mitigated this deficiency, and consequently strengths 30-70% higher than in the ungrouted columns were achieved in the grouted columns.

2.7.3 Wireball reinforcement

2.7.3.1 Introduction

A study of accidents in the construction industry in Sweden, conducted in the early 1990s, revealed that more than half of the working days lost were due to injuries arising from fixing reinforcing steel. In light of this, a Swedish engineer, Bjorn Svedberg, proposed a new method of reinforcing

concrete involving spherical reinforcement, or "wireballs", which would not require fixing – they could simply be placed at random within the shuttering prior to casting of the concrete. This section discusses wireball reinforcement and past research on the response of wireball reinforced concrete to static, quasi-static and impact loading.

2.7.3.2 Wireball reinforcement

Wireball reinforcement, or 'wireballs', as the reinforcement is referred to throughout this thesis, was invented in 1993. The original wireball was fabricated by wrapping a single strand of 1.2mm diameter high tensile steel in three orthogonal directions to form a small open sphere. Early tests highlighted a lack of continuity between adjacent wireballs, so they were modified through the attachment of six 25mm diameter rings. The purpose of these rings was to provide increased interlock between adjacent wireballs within the concrete member. The wireballs used in the tests presented in this thesis consisted of 2mm high tensile steel open spheres, 75mm in diameter, with six 25mm rings attached. Figure 2.19 illustrates 75mm diameter wireballs, with and without additional rings attached.

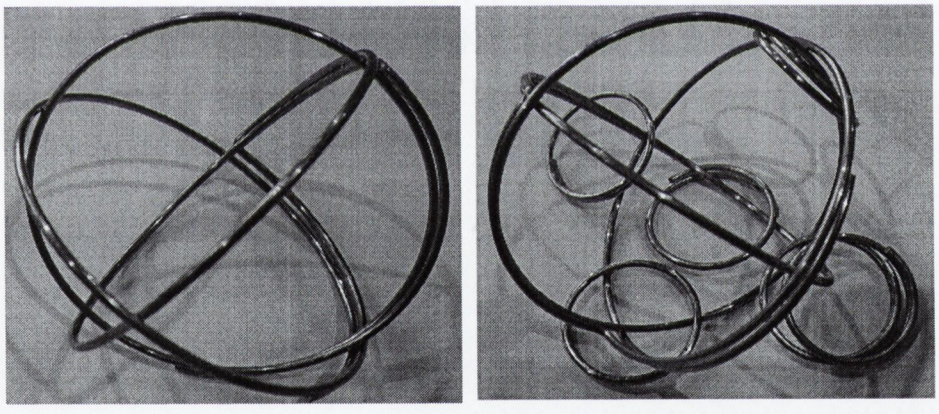

Figure 2.19: 75mm diameter wireball with and without 25mm rings attached

2.7.3.3 Static tests

Beams

The first tests on wireball reinforced concrete were by Jansson (1994) in Sweden and consisted of three separate test series in which simply-supported beams were loaded in flexure. The objectives were to determine whether the addition of wireballs to concrete was beneficial, and how they should be placed within the concrete to maximise their effectiveness.

Table 2.3 summarises the beams tested in terms of reinforcement (wireballs or steel fibres) and whether they were concrete or mortar beams. The steel fibre reinforced beam was superior to the other beams, in terms of strength, but especially, in terms of ductility. Of the wireball reinforced beams the beam with densely packed wireballs displayed the best ductility. Wireball density appeared to have little impact on strength.

The second test series consisted of two beams; one with a single layer of densely packed wireballs at its base and the other with two layers of densely packed wireballs at its base. The third series compared the behaviour of two beams densely packed with different diameter wireballs (50mm or 80mm diameters) where both wireball sizes had six 25mm rings attached. Figures 2.21 and 2.22 present the load-displacement responses of both test series. In both cases, the number of wireball layers or the wireball size did not affect beam strength. However, the use of two layers of wireballs, rather than one, and the use of larger sized wireballs, led to a more ductile response.

Specimen	Reinforcement type	Concrete/Mortar	Reinforcement density (kg/m^3)
1	Wireballs	Mortar	Densely hand-packed
2	Wireballs	Concrete	60
3	Wireballs	Concrete	78
4	Dramix ZC 60/80 steel fibres	Concrete	78

Table 2.3: Static tests on wireball-reinforced beams, reinforcement details

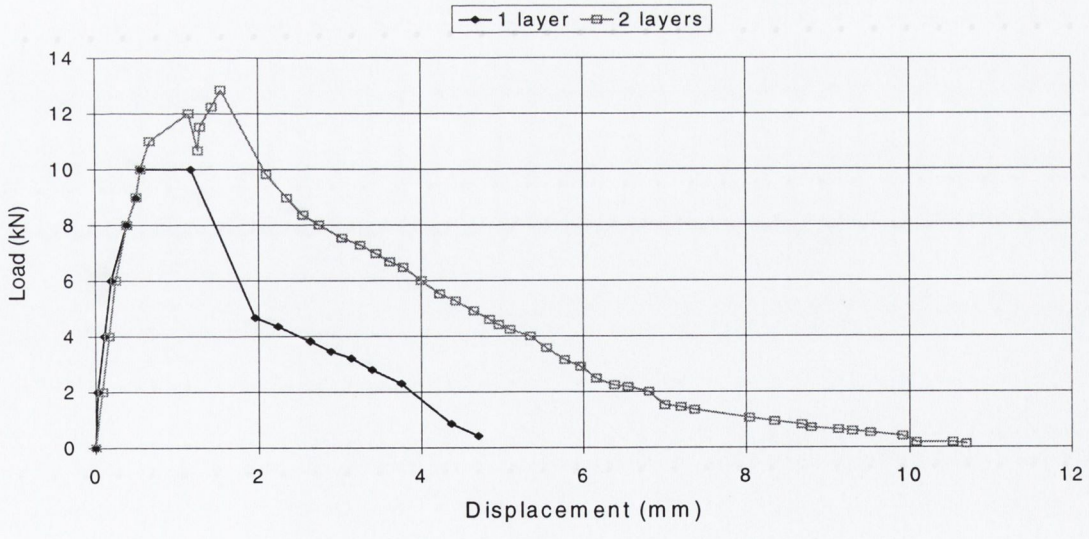

Figure 2.20: One and two layers of wireballs (Jansson, 1994)

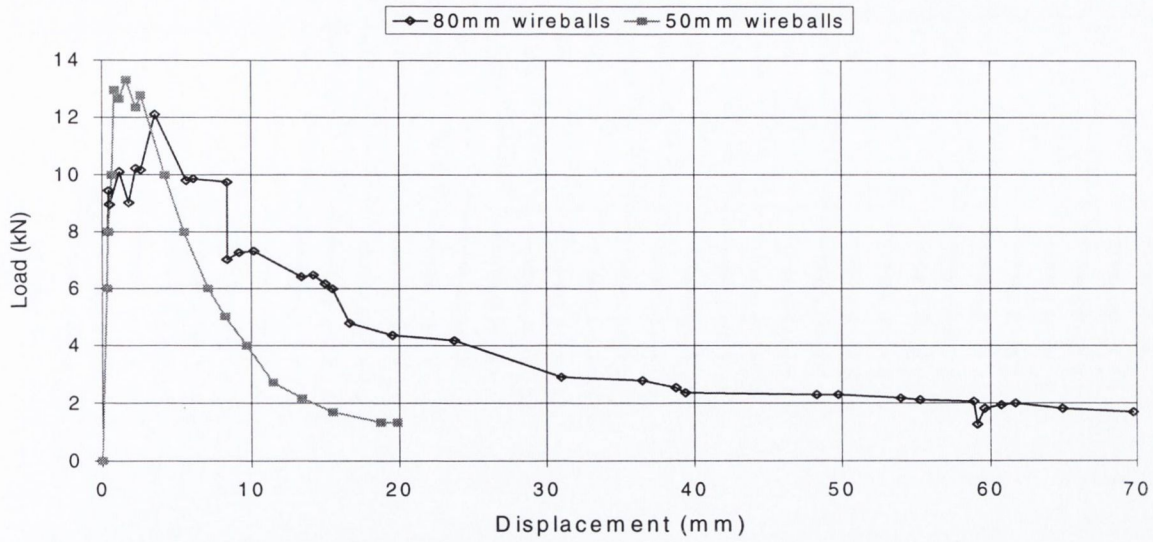

Figure 2.21: Different wireball sizes (Jansson, 1994)

Cubes

Levins (1994) tested cubes in compression, to compare the behaviour of plain and wireball reinforced concrete. Four test series, with different combinations of 100mm and 150mm cubes, plain or reinforced, were carried out. Table 2.4 summarises each test series by cube size and number of plain and reinforced cubes. Where the wireballs had rings attached, this is indicated by the letter "R". Two different wireball configurations were considered; a single wireball at the cube centre or a "4-1-4" arrangement with a single wireball at the centre and four wireballs forming the top and bottom layers.

Test Series	Wireball configuration	150mm cubes		100mm cubes	
		Plain	With wireballs	Plain	With wireballs
1	1	3	4	3	4
2	1	-	-	3	6
3	4-1-4	3	6	-	-
4	4-1-4	4	5R	-	-

Table 2.4: Static tests on cubes, details of wireball configuration and number of cubes in each test series

The wireballs had no quantifiable effect on cube strengths. However, they did have a significant effect on the failure modes and hence, ductilities, of the cubes. Where the plain cubes failed explosively, with their sides bursting out leaving two pyramids with their apexes meeting at the cube centre, the wireball reinforced cubes failed gradually. In cubes reinforced with a single wireball, a substantial cylindrical core remained intact that was still capable of carrying load. The cubes packed with wireballs remained mostly intact with only the cover to the wireballs spalling.

Figure 2.22 presents the load-displacement responses of the cubes of Test Series 4, illustrating the greater ductility of the wireball reinforced cubes relative to the plain cubes.

Further tests on wireball reinforced cubes, by O'Connor (1996), verified Levins results. Again, wireball reinforced cubes were observed to display significant increases in ductility, but not strength, over plain cubes.

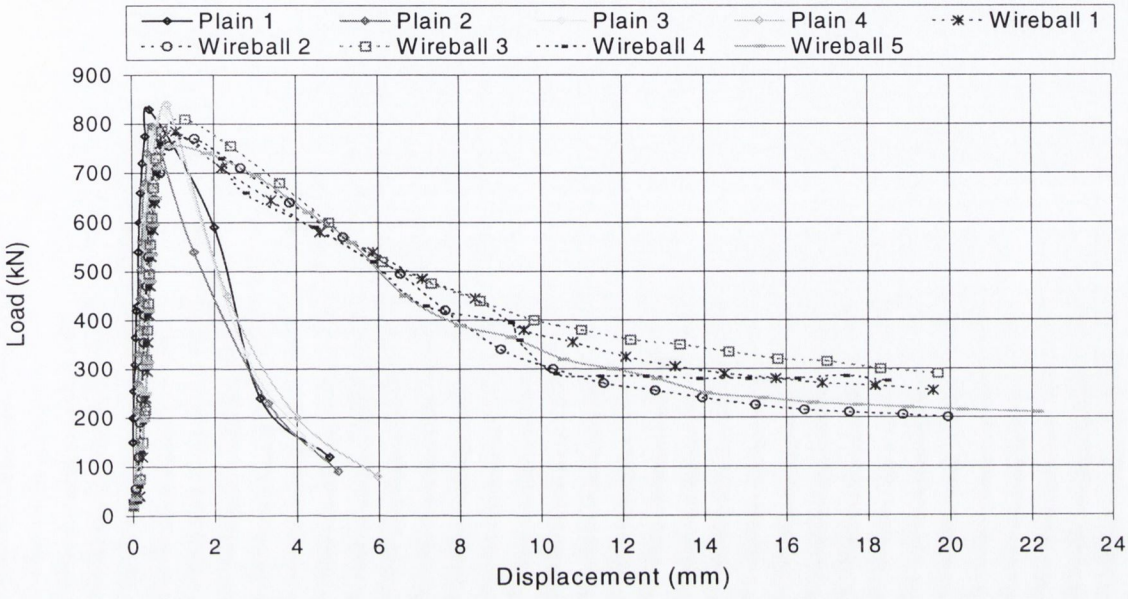

Figure 2.22: Load-displacement response of plain and wireball reinforced cubes (Levins, 1994)

Stub columns

Levins (1994) also carried out a series of tests on wireball reinforced stub columns (150mm × 150mm × 450mm). They were tested monotonically to failure. Wireballs were packed in a 4-1-4 arrangement throughout the length of the column. Despite considerable spalling and distortion, the binding nature of the wireballs (Figure 2.23) led to substantial increases in ductility over that achieved in plain specimens. Figure 2.23 compares the load-displacement response of two stub columns, with and without wireballs.

O'Connor (1996) compared the load-displacement response of wireball reinforced and fibre reinforced stub columns. Figure 2.24 presents a typical load-displacement response. The steel fibres worked similarly to the wireballs, preventing brittle failure and enhancing ductility. However, the wireball-reinforced columns displayed much larger ductilities than the fibre-reinforced columns.

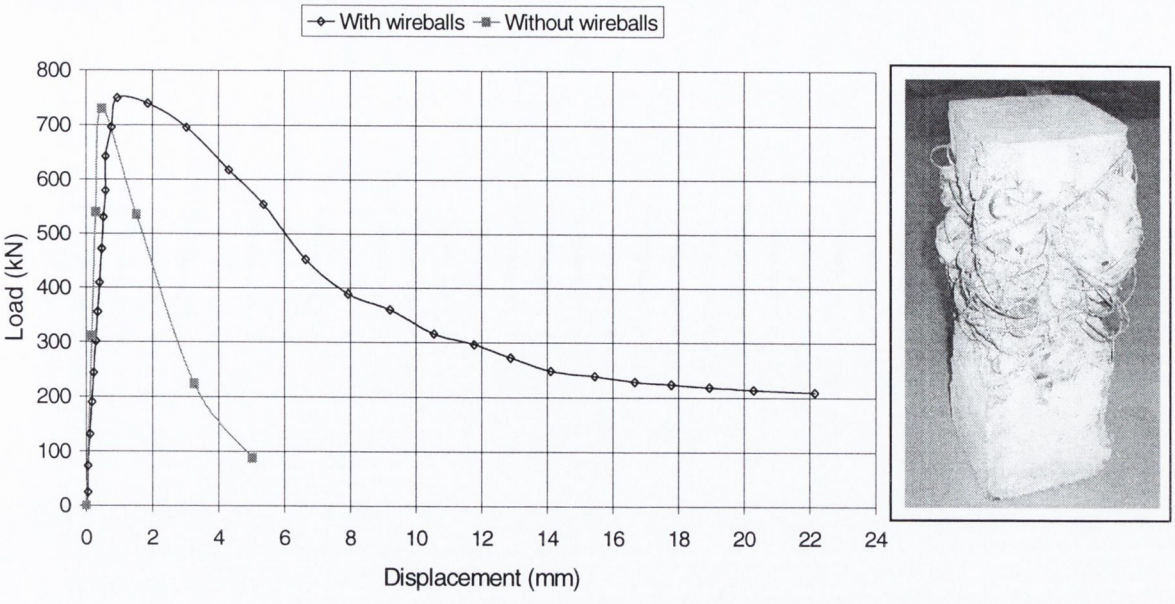

Figure 2.23: Load-displacement response of wireball reinforced stub column (West *et al.*, 1997)

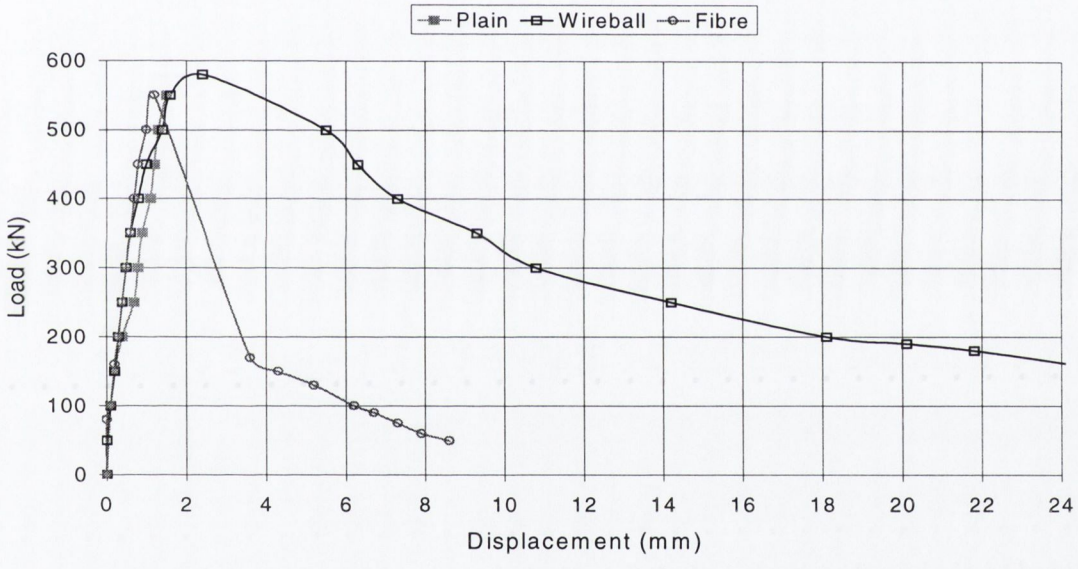

Figure 2.24: Load-displacement response of wireball and fibre reinforced stub columns O'Connor (1996)

Short columns

A series of 2m long concrete columns (150mm square) reinforced with wireballs (with rings), both with and without conventional reinforcement, were tested by O'Rourke (1995). Under compressive axial load, the specimens without longitudinal steel failed by buckling, whereby the wireballs at the four corners acted with those wireballs above and below them, effectively forming four separate columns, each well confined within its own right by wireballs. The columns as a whole clearly had insufficient lateral binding (provided here by the rings, but normally by links) to

prevent buckling of each 'column'. However, when wireballs were used as a supplement to conventional column steel, the column capacity was enhanced as the confinement, provided by the wireballs, in the column core was excellent.

2.7.3.4 Impact and quasi-static tests

Di Cioccio (1997) compared the behaviour of wireball reinforced concrete under impact loading to that of fibre reinforced and plain concrete. A series of 150mm cubes were impacted by a 76.7kg steel billet dropped from heights of 1.3m and 2.3m producing impact velocities of 5.05m/s and 6.72m/s. The wireballs were observed to increase the concrete's energy absorption capacities. Cubes containing wireballs absorbed 80% more energy than plain cubes and 40% more energy than fibre reinforced cubes. It was also reported that, while both wireballs and steel fibres prevented the cubes from shattering into fragments, wireball reinforced cubes sustained much less damage than fibre reinforced cubes.

Whelan (1998) examined the energy absorption response of stub columns (450mm × 150mm × 150mm) under quasi-static loading. The response of wireball reinforced columns was compared to that of plain, conventionally reinforced and fibre-reinforced columns. Two different wireballs types were used, Type 1 with a 70mm diameter and six 80mm rings, and Type 2 with a 50mm diameter and six 25mm rings. Table 2.5 summarises the percentage increase in energy absorption capacity for the different reinforcement types for a loading rate of 36 tonnes/min. The wireball reinforced specimens, regardless of wireball size, were superior to all the other specimens. It was stated that, while the wireball reinforced specimens did not significantly outperform the conventionally reinforced specimens, substantial improvements in the failure modes of the wireball reinforced specimens were observed. Failure of the conventionally reinforced specimens did not occur as early as in the fibre reinforced and plain specimens, but when it occurred it was still very sudden, whereas the wireball reinforced specimens failed gradually with ample visual warning (early cracking and bulging) prior to failure.

Reinforcement Type	**Percentage increase in energy absorption capacity (%)**
Plain	-
Fibre	35
Conventional	75
Wireball Type 1	80
Wireball Type 2	94

Table 2.5: Energy absorption capacities (Whelan, 1998)

2.7.3.5 Summary

It was determined from static tests on beams, cubes, stub and short columns that wireballs have no significant effect on concrete strength, but that they do have an appreciable influence on concrete ductility. With respect to the compressive tests on cubes and stub columns, the presence of wireballs promoted gradual failure as they held the concrete together. However, in the case of the short columns, the interlocking properties of the wireballs were insufficient unless used in combination with conventional reinforcement; they then greatly enhanced confinement. The results of the quasi-static and impact tests indicated significant increases in energy absorption capacities in wireball reinforced specimens with respect to fibre reinforced and conventionally reinforced specimens. For quasi-static loading, the presence of wireballs made failure more gradual, while for impact loading their presence prevented specimens from shattering into fragments. In all of these tests, it was important that the wireballs were packed tightly within the formwork if their benefits were to be realised

2.8 Conclusions

The prevailing philosophy in the earthquake-resistant design of reinforced concrete structures is that structures resist seismic action by undergoing displacements well into the inelastic range. In the 'capacity design approach', structures are designed to develop plastic hinges in pre-designated locations. It is essential that these plastic hinge regions be detailed carefully to ensure sufficient ductility and energy dissipation capacity. In reinforced concrete, this is achieved through careful confinement of the hinge regions by lateral reinforcement. Traditionally, confinement is provided in the form of steel links. The confinement efficiency depends on numerous factors, many of which have been described in this chapter, and all of which should be taken into account in design. In recent years, alternative confinement methods have been considered, such as the use of wire-welded fabric and pre-stressed bolts. The use of wireball reinforcement, which has already been seen to improve the ductility of concrete, is addressed in this thesis.

CHAPTER 3

DETAILS OF EXPERIMENTAL WORK

3.1 Introduction

The purpose of this chapter is to describe the test specimens, experimental set-ups and testing procedures within this research. Table 3.1 summarises the different types of tests performed in terms of specimen and loading type, given in order of test completion. The succeeding sections treat each test series in detail with respect to specimen details and test description. The penultimate section, Section 3.8 considers the material properties of the concrete and steel used throughout the tests, while also describing the specimen production process. Finally, Section 3.9 details any remaining untreated material that is considered of value.

Test Series	Specimen Type	Load Type
1	Stub column	Monotonic axial compression - force control
2	Simply-supported beam	Monotonic bending, mid-point load – displacement control
3	Simply-supported beam	Monotonic bending, ¼ point loads - force control
4	Beam-to-column connection	Lateral cyclic loading - displacement control
5	Beam	Lateral cyclic loading - displacement control
6	Beam-column	Lateral cyclic loading and constant axial compression - displacement control

Table 3.1: Test series type

3.2 Test Series 1: Stub columns under monotonic compression

The objectives of these tests was to determine whether the inclusion of wireballs is beneficial to the stress-strain behaviour of compressed concrete, with particular emphasis on their contribution to ductility. With the exception of some plain specimens, transverse reinforcement was according to the requirements of the three draft EC8 ductility classes (EC8, 1998) to determine whether wireballs can be used in partial replacement of confinement links.

3.2.1 Specimen description

The stub columns were 450mm long with a 150mm × 150mm cross-section. Figure 3.1 is a stub column cross-section. Four T16 bars provided the longitudinal reinforcement and the transverse steel consisted of 120mm square R6 links. The links were bent by hand and had 135° hooks, with an anchorage of 10 times the bar diameter, as recommended by EC8. The link spacings of the specimens were determined from Equations 3.1 to 3.3 below; these equations define the EC8 link spacings required for columns for the three ductility classes DCL, DCM and DCH (as defined in Eurocode 8, 1994). The concrete cover was 15mm which corresponds to the minimum cover recommended by Eurocode 2 (1991). The concrete had a nominal strength of 25N/mm^2, the details of the concrete mix are provided in Section 3.8.1.

$$DCH\ (column):\ s = min\{b_o/4;\ 100mm;\ 5d_{bl}\} \quad (3.1)$$

$$DCM\ (column):\ s = min\{b_o/3;\ 150mm;\ 7d_{bl}\} \quad (3.2)$$

$$DCL\ (column):\ s = min\{b_o/2;\ 200mm;\ 9d_{bl}\} \quad (3.3)$$

where:

b_o = minimum dimension of concrete core (mm) = 120mm

d_{bl} = diameter of longitudinal bars (mm) = 16mm

s = link spacing (mm)

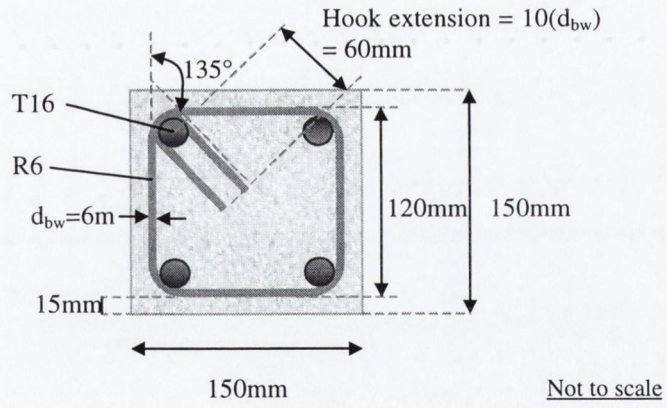

Figure 3.1: Cross-section details of stub column specimens (Test Series 1)

The stub columns were divided into seven groups, within each of which there were up to four specimens, each with different reinforcement details. Table 3.2 details the specimens contained within each group. Each specimen is identified by the letters "SC", to indicate a "stub column" specimen, a number that indicates which group the specimen belongs to, followed by the appropriate reinforcement code as given in Table 3.3 below.

Group	Specimens
1	SC/1.1/DCH, SC/1.2/DCL
2	SC/2.1/P
3	SC/3.1/DCL, SC/3.2/DCH
4	SC/4.1/DCM, SC/4.2/DCM, SC/4.3/DCM/W
5	SC/5.1/P, SC/5.2/P/W
6	SC/6.1/DCL, SC/6.2/DCL/W, SC/6.3/DCL(75%)/W, SC/6.4/DCL(50%)/W
7	SC/7.1/DCL, SC/7.2/DCL/W, SC/7.3/DCL(75%)/W, SC/7.4/DCL(50%)/W

Table 3.2: Stub column test programme (Test Series 1)

Code	Specimen Reinforcement	Link Spacing (mm)
DCH	DCH column transverse reinforcement	30
DCM	DCM column transverse reinforcement	40
DCL	DCL column transverse reinforcement	60
DCL(75%)	75% of DCL column transverse reinforcement	75
DCL(50%)	50% of DCL column transverse reinforcement	90
W	Contains wireballs	N/A
P	No reinforcement (Plain concrete)	N/A

Table 3.3: Stub column reinforcement codes (Test Series 1)

3.2.2 Test set-up

The stub column specimens were tested under monotonic compression at a constant rate (BS1881, 1983) up to and beyond failure. The test machine used was a Losenhausen Testing Machine with a 3000kN capacity and the ability to apply post-yield loads. A photograph and diagram of the test set-up are presented in Figure 3.2. A single LVDT was attached to the top machine platen to measure the axial deformation of the specimen as it was compressed. A 1000kN capacity load cell was placed beneath the specimen to measure load. A steel plate (25mm thick) was placed between the specimen and the load cell to provide a base for the specimen to sit on. The LVDT and load cell were connected to a System5000 Data Acquisition Unit.

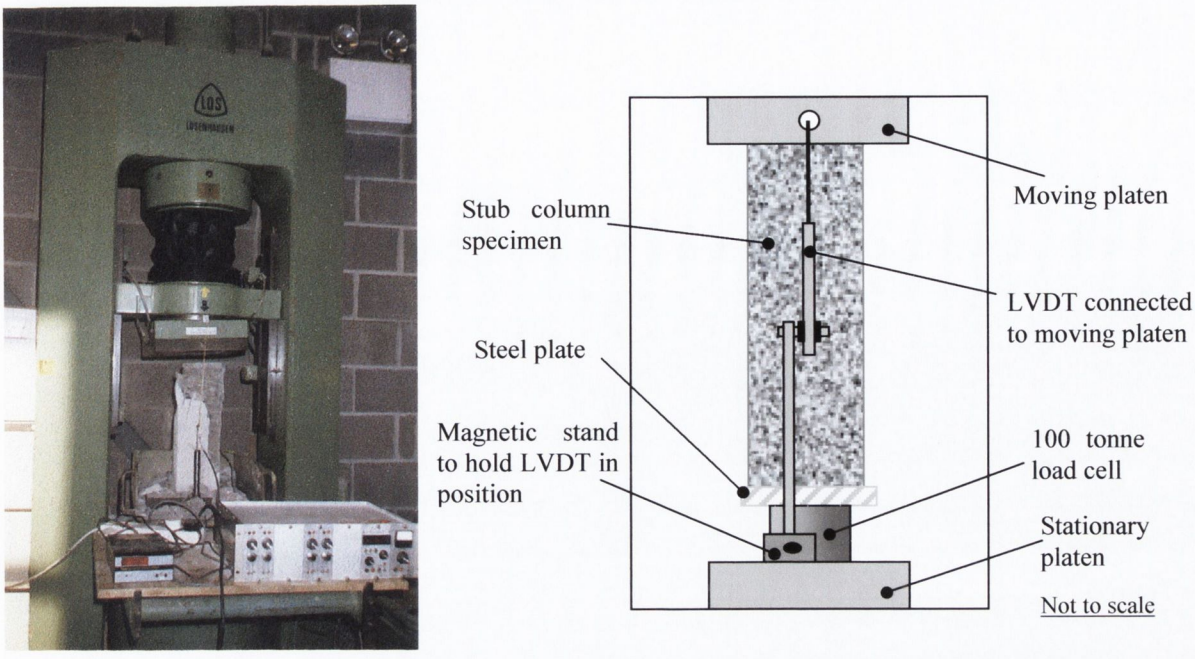

Figure 3.2: Stub column test set-up (Test Series 1)

3.3 Test Series 2: Simply-supported beams with a central point load

The results of the stub column tests showed that the inclusion of wireballs is beneficial to reinforced concrete in compression and that, through their inclusion, the amount of standard confinement, for a required ductility level, may be decreased without detrimental effect on specimen behaviour. The stub column results are discussed in Section 4.2. The next step was to determine whether wireballs could be beneficial to reinforced concrete in flexure, where only a limited part of the member cross-section is in compression.

3.3.1 Specimen description

The beam specimen dimensions and details are provided in Figure 3.3. The beams were 1.7m long, with a test span of 1.5m, and a cross-section of 200mm × 200mm. Cover of 25mm was provided to the longitudinal steel. The links were T12 steel and 150mm × 150mm. Unlike in the stub columns, the links had 90° hooks (Shape Code 61, BS 4466:1989) rather than 135° hooks recommended by EC8.

The beams were under-reinforced to ensure that they would fail in flexure. The longitudinal base steel consisted of 3T12 bars. The top steel content was kept to a minimum, consisting of two R6 bars. The presence of top steel reduces the compressive strain of the top concrete. Since the aim

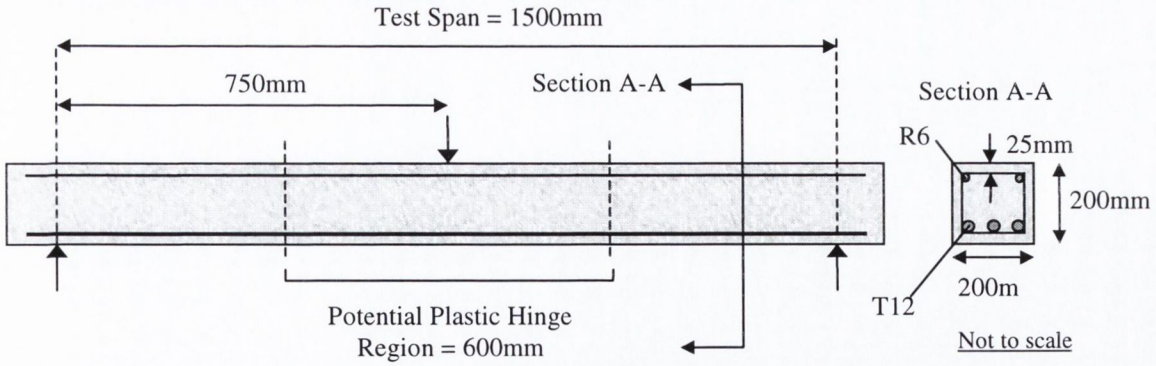

Figure 3.3: Beam specimens (Test Series 2)

was to check whether wireballs could delay concrete crushing in the plastic hinge region, minimal quantities of top steel were required. In other words, the beam is considered as a singly-reinforced section.

Table 3.4 provides details of the link spacings used in the beams, and identifies whether or not they contained wireballs. In the first column of Table 3.4, the beams' nomenclature is also provided. The first section of the nomenclature provides the beam number (for example, B2), this is followed by the link spacing used within the potential plastic hinge region of the beam (for example, 80), and finally, if the specimen contained wireballs, this is indicated by the letter "W".

Beam ID	Link Spacing (mm)	Wireballs (Y/N)
B1/80	80	N
B2/80/W	80	Y
B3/100	100	N
B4/100/W	100	Y
B5/120/W	120	Y

Table 3.4: Beam specimen details (Test Series 2)

Outside of the potential plastic hinge region, in all of the beams, a link spacing of 100mm was employed to provide adequate shear resistance. Within the potential plastic region the link spacings were 80mm, 100mm or 120mm. A spacing of 100mm was chosen as it is the recommended maximum spacing by EC8 for DCL conditions where, in this case, the EC2 stipulations for shear govern; the relevant equations are detailed later in Equations 3.5 to 3.7 of Section 3.5.1. A spacing of 80mm was chosen as an intermediate value between the 100mm DCL recommended spacing and the spacing of 50mm recommended for DCM conditions. The recommended DCM link spacing was determined from Equation 3.8, Section 3.5.1. A 120mm link

spacing was chosen to determine whether a beam containing wireballs could behave as well as a beam with a smaller (100mm) link spacing but no wireballs. Equations 3.4a to 3.4c, with Figure 3.4, show how the plastic hinge length was estimated, where L is the test span, l_p is the plastic hinge length and M_y and M_u are the yield and ultimate moments respectively. The plastic hinge region was estimated as 500mm but just in case this was an under-estimation a potential plastic hinge region of 600mm was adopted and the strain gauges placed at intervals within this 600mm region.

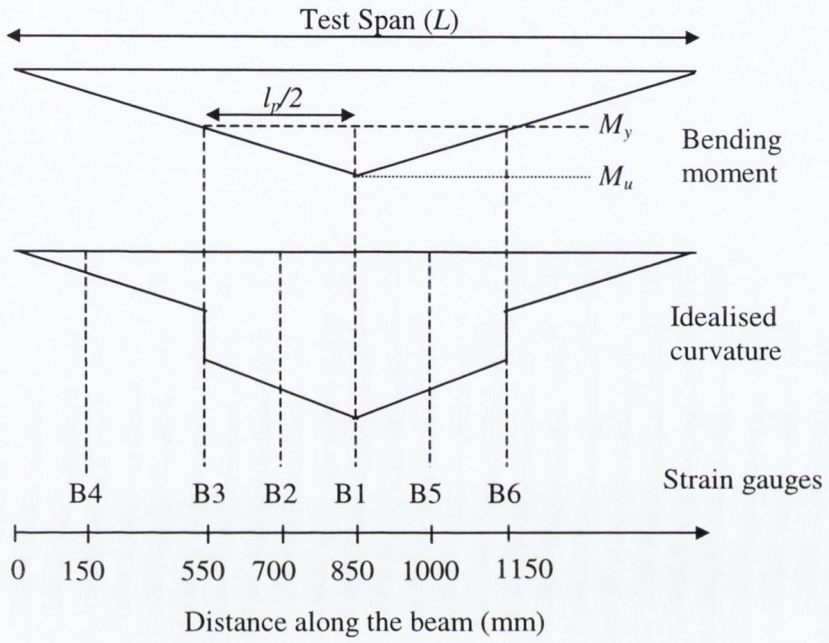

Figure 3.4: Potential plastic hinge region (Test Series 2)

$$\textit{By similar triangles: } \frac{l_p/2}{M_u - M_y} = \frac{L/2}{M_u} \tag{3.4a}$$

$$\textit{Assuming that: } M_u = 1.5M_y \tag{3.4b}$$

$$l_p = L/3 = 1500/3 = 500mm \tag{3.4c}$$

The middle bottom steel bar in all specimens was strain gauged at the locations illustrated in Figure 3.4 in which the gauges are identified as B1-B6. The positions of the strain gauges were based upon the predicted plastic hinge length. Five gauges were placed at equal intervals within the estimated potential plastic hinge region and one gauge was placed close to the end of the beam, where the strains were expected to be small.

3.3.2 Test set-up

The beams were simply-supported and subject to a monotonic mid-point load. A 100 tonne capacity actuator applied the load to the beam. The hydraulic pressure to the actuator was supplied by an Amsler pressure supply. The beams were loaded to failure. The actuator load cell allowed the load to be measured while the actuator's internal LVDT provided displacement measurements, both of these were logged by a Datascan 7221 Measurement Processor. Strain gauge measurements were logged to the System 5000 Data Acquisition System. The beams were set up within the 7m by 5m 300 tonne capacity, laboratory testing frame. The simple-supports had rounded edges to prevent them cutting into the concrete. Figure 3.5 illustrates the test set-up.

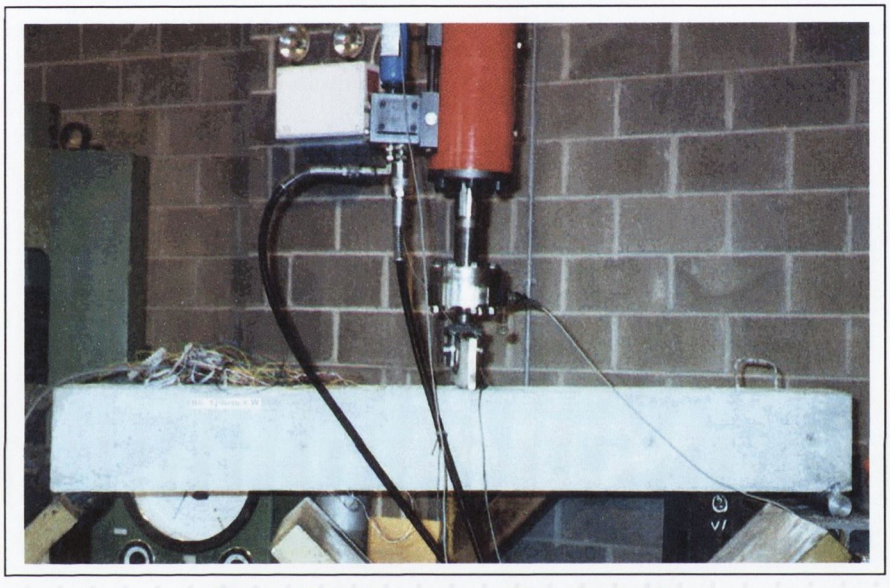

Figure 3.5: Test set-up (Test Series 2)

3.4 Test Series 3: Simply-supported beams with ¼ point loading

This test series considered beams designed to fail in shear to investigate the effect of wireballs on shear strength.

3.4.1 Specimen description and test set-up

The specimens within this test series were similar to those of Test Series 2 described in Section 3.3.1. However, they employed a different link spacing of 150mm along the complete span. Two of the specimens contained wireballs while the other two did not. The specimen details are summarised in Table 3.5. They were tested in monotonic compression under a ¼-point loading arrangement as illustrated in Figure 3.6. This loading arrangement was chosen such that the beams would fail in shear. The value of the shear span (375mm) to depth ratio (169mm) is 2.2 which

Beam ID	Link spacing (mm)	Wireballs (Y/N)
S1/150	150	N
S2/150	150	N
S3/150/W	150	Y
S4/150/W	150	Y

Table 3.5: Test Series 3 specimen details

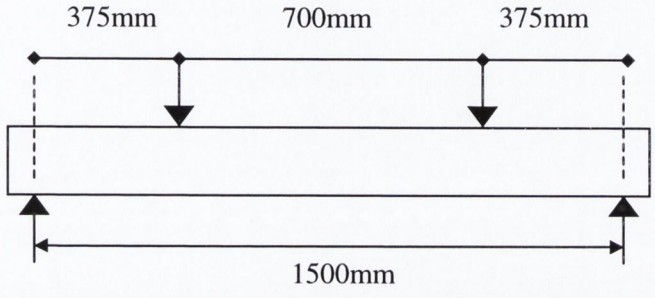

Figure 3.6: ¼ Point loading arrangement (Test Series 3)

according to O'Brien *et al.* (1995) gives rise to shear failure where cracks develop between the support and the applied load.

The test set-up is shown in Figure 3.7. The load was applied to the beams by means of a 100 tonne hydraulic jack connected to an Amsler pressure supply. The jack pushed upwards against a heavy steel beam running over the test beam and held above the floor by two large cylindrical steel sections. The steel beam was anchored to the floor by two high strength threaded McAlloy bars, running through the cylindrical sections, extending through the 1m deep laboratory floor and bolted underneath it, hence, creating a reaction frame system. Therefore, when the jack pushed up against the steel beam, an equal force acted down into the test beam. A load cell, placed beneath the jack, and an LVDT at the beam centre, enabled load and displacement measurements. Both load cell and LVDT were connected to a System 5000 Data Acquisition System.

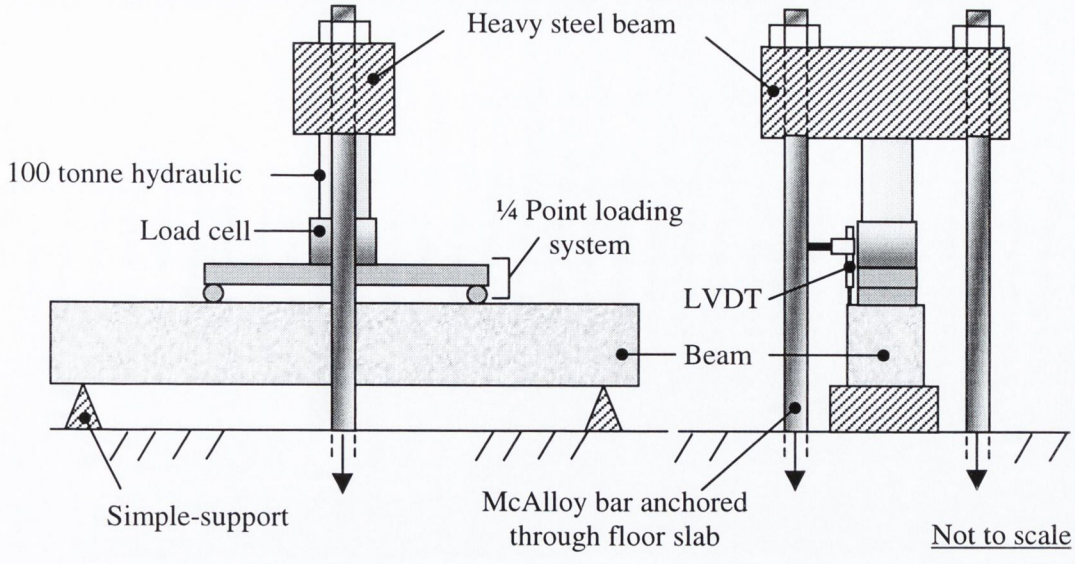

Figure 3.7: Test set-up (Test Series 3)

3.5 Test Series 4: Beam-to-column connections with lateral cyclic loading

The results of Test Series 3 (see Section 4.4) suggest that wireballs may contribute to reinforced concrete shear strength. With this is mind, beam-to-column connections with substandard reinforcement detailing (in which the longitudinal bars are bent out of, rather than into, the connection area) such that shear failure would occur, were tested. Other researchers have found that this detail leads to shear failure of the connection area (Hakuto *et al.*, 2000 and Scott, 1992).

3.5.1 Specimen description

The beam-to-column specimens are illustrated in Figure 3.8. The beam and column each had a cross-section of 200mm × 200mm and both were 1.0m long. Both beam and column had 170mm × 170mm T10 links (Shape Code 61, BS4466: 1989). The beam had four T12 longitudinal bars bending out of the beam-column connection, hence, forming the base longitudinal steel of the column. Another T12 bar spanned the total length of the column base, providing longitudinal steel in the connection area were there was none provided by the bends of the beam bars. Two T12 bars formed the top column steel. The cover was 15mm and the design concrete strength was 25N/mm^2, as detailed in Section 3.8.1.

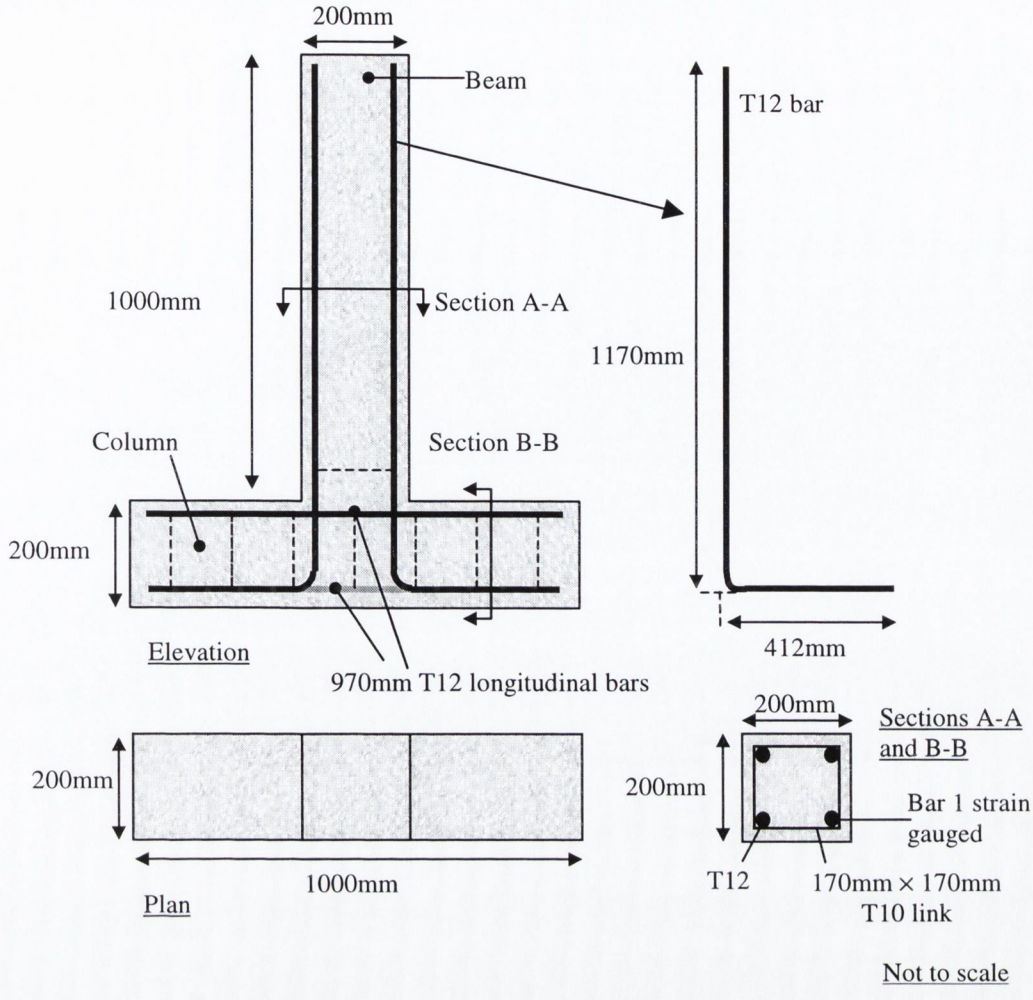

Figure 3.8: Specimen details (Test Series 4)

The column was designed for DCM conditions, and to fail within the maximum actuator load of 100kN. For DCM, the shear capacity (V_{cd}) of the unreinforced section within the critical regions is taken as 40% of that calculated by EC2. The column link spacing was 110m, as calculated using Equations 3.5 to 3.7.

$$V_{cd} = (\tau_{rd})(k)(1.2 + 40\rho_L) + (0.15)(\rho_{cp})(b_w)(d) \tag{3.5}$$

$$V_{wd} = V_{\max} - V_{cd} \tag{3.6}$$

$$V_{wd} = (A_{sw}/s)(0.9)(d)(f_{ywd}) \tag{3.7}$$

where:

V_{cd} = Design shear resistance of the member without shear reinforcement (N)

V_{wd} = Contribution of shear reinforcement to shear resistance (N)

V_{max} =Maximum applied shear force (N)

τ_{rd} = Basic design shear strength (N/mm^2)

k = Greater of (1.6-d) and 1, where d is in metres

d = Effective depth (mm)

b_w = Web breadth, in this case the breadth of the section (mm)

ρ_L = Lesser of the longitudinal tension reinforcement ratio and 0.02

ρ_{cp} = N/A_g, where N is the factored design axial force and A_g is the gross cross-sectional area (N/mm^2)

The link spacing in the beams differed from specimen to specimen. As recommended by EC8, the first link was always 50mm above the beam-column interface surface. Table 3.6 provides the beam reinforcement details of the four specimens in terms of their link spacing and wireball content.

Specimen ID	Link Spacing (mm)	Wireball Reinforcement (Y/N)
CB1.1/85/W	85	Y
CB1.2/145/W	145	Y
CB1.3/145	145	N
CB1.4/50	50	N

Table 3.6: Beam reinforcement details (Test Series 4)

The 50mm and 85mm link spacings are the DCM beam requirements for local ductility and prevention of longitudinal buckling respectively, as detailed in Equation 3.8 below. The link spacing of 145mm, is the DCL requirement, where the recommended link spacing is that required for shear resistance.

$$DCM\ (beam): s = min\ \{h_w/4;\ 24d_{bw};\ 200mm;\ 7d_{bL}\} \tag{3.8}$$

where:

h_w = beam depth (mm)

d_{bw} = diameter of links (mm)

d_{bL} = diameter of longitudinal steel (mm)

s = link spacing (mm)

3.5.2 Test set-up

Figure 3.9 is a diagram of the test set-up. A lateral load is applied to the column by means of a 10 tonne actuator connected to the beam by a steel collar. The distance between the applied lateral load and the interface surface of the beam with the column is 845mm. Further details of the test set-up and control programmes used to run the actuator are provided in Sections 3.7.2 and 3.9.1

respectively. In each specimen, the longitudinal bar labelled "Bar 1" in Figure 3.8 was strain gauged along its length at 50mm below the beam-column interface and 50mm, 200mm and 400mm above the interface. The first beam link just above the beam-column interface, was strain gauged on two sides, the sides beside and opposite the actuator.

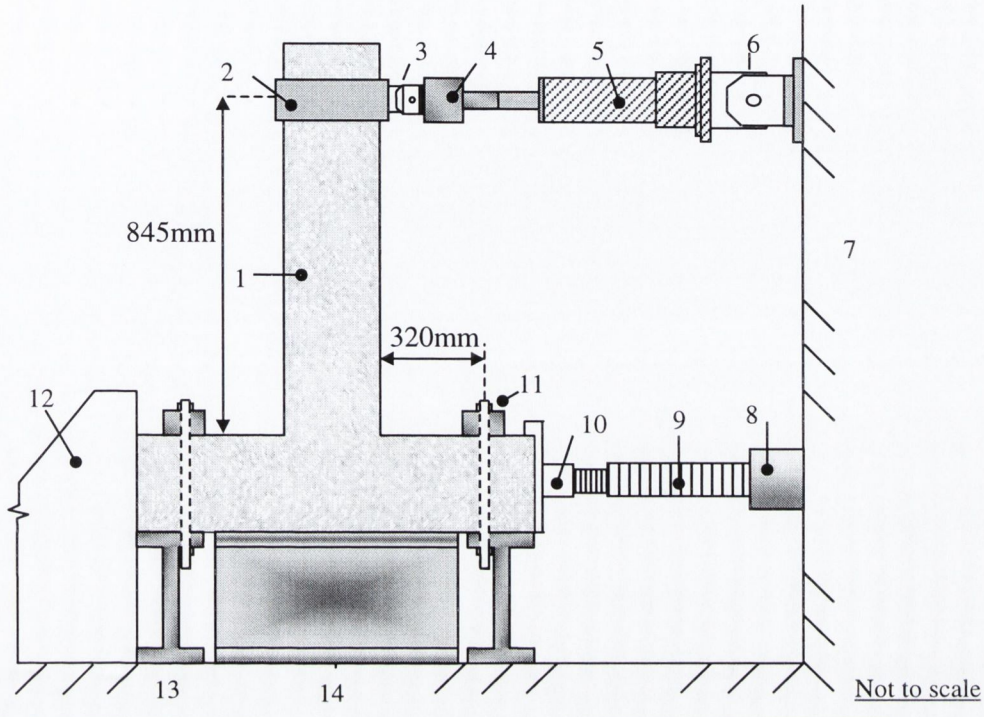

1: Specimen, **2:** Collar, **3:** Hinge connection **4:** Actuator load cell, **5:** Actuator, **6:** Hinge connection, **7:** Reaction frame, **8:** Load cell, **9:** Jack, **10:** Plate & spigot, **11:** Plate & bolt, **12:** Reaction block, **13:** I-Section, **14:** I-Section

Figure 3.9: Test set-up (Test Series 4)

3.5.3 Test procedure

The specimens were subject to cyclic lateral loading applied at a lever-arm of 845mm from the beam-column interface. A shakedown test was performed prior to each test, the purpose of which is discussed in Section 3.9.3. The shakedown test and test displacement histories are illustrated in Figures 3.10 and 3.11 respectively. Both the shakedown and test displacement histories were based upon a predicted yield displacement of 4.25mm, which was calculated from the following standard equation for the tip displacement of a cantilever due to a point load applied at its free end:

$$\Delta_y = \frac{P_y L^3}{3EI} \tag{3.9}$$

where:

Δ_y = yield displacement (mm)

P_y = yield load (N)

L = test span (mm)

E = modulus of elasticity (N/mm^2)

I = second moment of area (mm^4)

In the shakedown test, the maximum applied displacement was half this predicted yield value. The first two cycles of the actual test were within the elastic range, at ½ and 1 times the predicted yield displacement. These elastic cycles were followed by two cycles of 1.5 and 2 times the predicted yield displacement. After this, cycles of 4, 6, 8, 10 and 12 times the predicted yield displacement were cycled through, three times each.

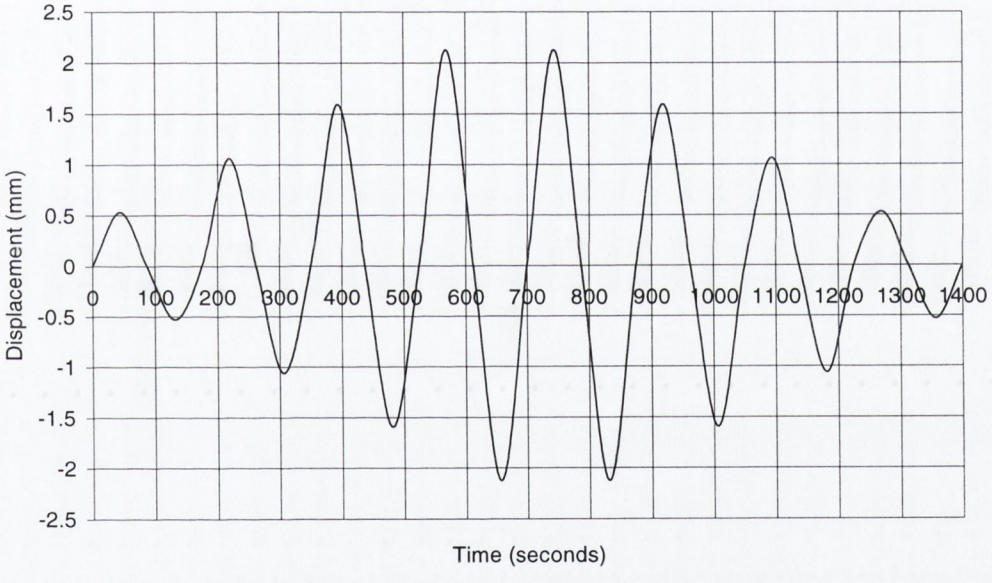

Figure 3.10: Beam-to-column connections shakedown displacement history (Test Series 4)

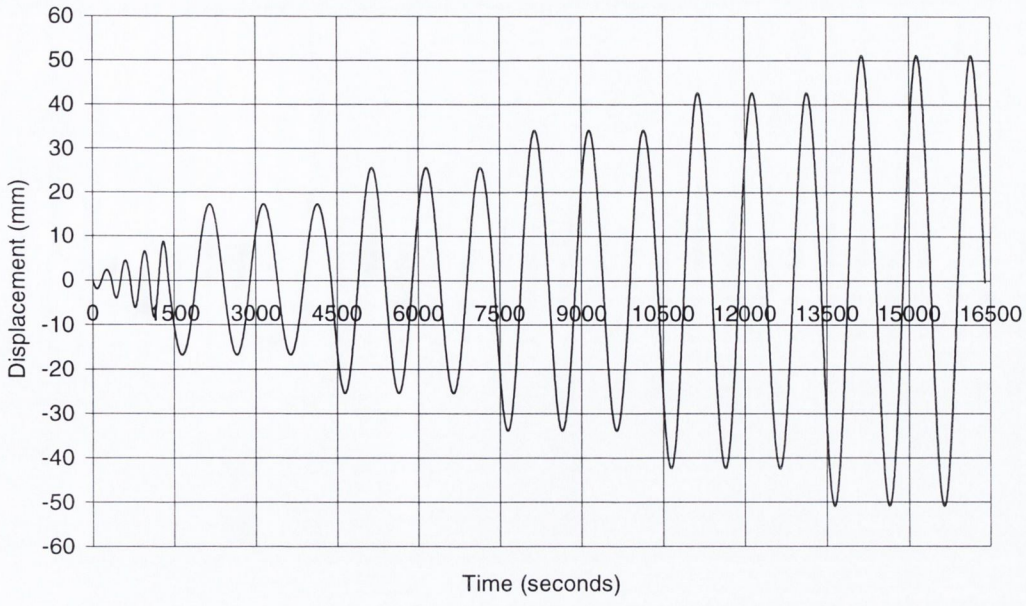

Figure 3.11: Beam-to-column connections test displacement history (Test Series 4)

3.6 Test Series 5: Beams with lateral cyclic loading

The purpose of this test series was to determine the appropriate specimen size and longitudinal reinforcement content to ensure satisfactory testing of the confinement effects of wireballs in specimens subject to lateral cyclic loading. Test Series 2 endeavoured to assess the confinement contribution of wireballs to reinforced concrete in flexure. However, the tests were limited, in hindsight it was observed that the beams were too under-reinforced (see Section 4.3.4) for the wireballs contribution to be tested sufficiently. With the restrictions of the laboratory equipment, it was difficult to determine the correct balance between specimen size and reinforcement detailing to obtain the desired specimen failure mode to fully examine the confinement effectiveness of wireballs. Therefore, this test series was an essential step towards determining the optimum specimen size and detailing, for the available laboratory equipment, to achieve the optimum failure mode, which would ensure sufficient assessment of the confinement effectiveness of wireballs in specimens subject to lateral cyclic loading.

3.6.1 Specimen description and test procedure

There were two specimens, which were beam-columns. They had the same dimensions as the beam-column specimens of the final test series (Test Series 6) as illustrated in Figure 3.13. Specimen C2 was detailed in the same manner as the beam-column specimens of Test Series 6 (Section 3.7.1), with a link spacing of 145mm (for a DCL beam). Specimen C1 was detailed the same as specimens C1.1 to C1.4 (Test Series 4) with a 145mm link spacing. However, where the

beam longitudinal steel had been bent out of the beam-column connections of C1.1 to C1.4, the steel in specimen C1 was bent into the beam-column connection, as illustrated in Figure 3.12. The beam longitudinal steel used in C1 came from the same batch as that used to detail the beams of specimens C1.1 to C1.4, such that the beam longitudinal steel extended approximately 225mm outside of the connection area into the column (Figure 3.12). In addition to the extension of the beam's longitudinal steel into the column, four T12 bars also provided the column longitudinal steel. The transverse steel consisted of T10 links, 270mm × 220mm, at 100mm spacing, with 90° hooks (BS Shape Code 61). The beam's transverse reinforcement extended into the beam-column connection such that, in addition to the column transverse steel, there were two links on the horizontal plane in the connection area.

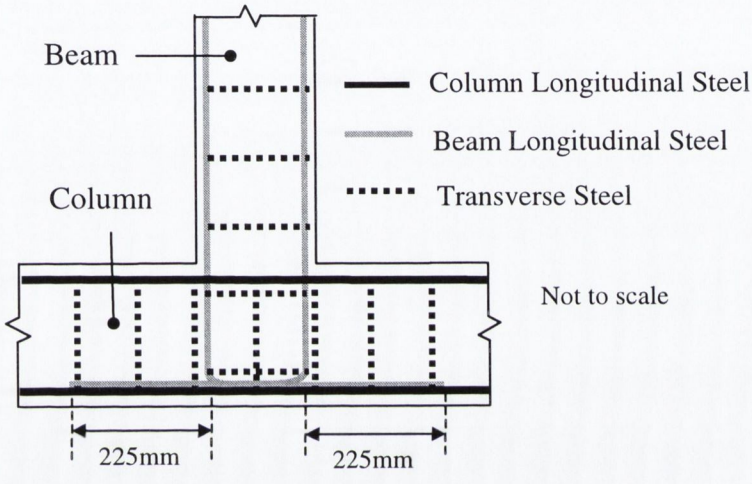

Figure 3.12: Joint detail of specimen C1 (Test Series 5)

Both of these specimens were tested in the same manner as those of Test Series 4. In this case, however, the lever-arm between the point of application of lateral load and the beam-column interface was 745mm. This was smaller than in Test Series 4, due to the increase in column depth from 200mm to 300mm. The displacement history imposed on C1 was the same as that of Test Series 4, (Figures 3.10 and 3.11), while the displacement history imposed on C2 was the same as that of Test Series 6, (Figures 3.19 and 3.20).

3.7 Test Series 6: Beam-columns with axial compression and lateral cyclic loading

The objectives of Test Series 6 were:

(i) To examine the confinement benefits of wireballs in reinforced concrete members with a combination of axial compression and lateral cyclic loading representative of earthquake loading.

(ii) To assess thoroughly, which Test Series 2 had failed to do, the confinement effects of wireballs in reinforced concrete failing in flexure.

The specimens were detailed for the lowest ductility class (DCL) of Eurocode 8. Different link spacings were used in the specimens to determine whether the use of wireballs in combination with standard confinement steel could decrease the code-required level of conventional confinement, without detrimental effect on specimen behaviour.

3.7.1 Specimen description

The test specimens were beam-columns connected to a base element representative of a footing or a foundation, or, in the case of a beam, representative of a column. Figure 3.13 illustrates the specimen dimensions and detailing. The beam-column was 900mm long, 200mm × 200mm in cross-section, with 15mm of cover and reinforced with 170mm × 170mm T10 links with 90° hooks (Shape Code 61 BS4466). These links did not comply with EC8 standards, where closed links with 135° bent-in hooks are specified. The first beam-column link was always placed 50mm above the interface surface of the beam-column (where it joins the base element) since EC8 recommends that for beams the first link should be placed not more than 50mm from the end cross-section. Details of link spacing further along the specimens' lengths are provided in the next section. Four T20 bars provided the longitudinal reinforcement in the beam-column, these bars being bent into the connection area. The bending details of the longitudinal bar (Shape Code 37 BS4466) are provided in Figure 3.13.

The base element was 1000mm long, 250mm in breadth, 300mm deep and with 15mm cover. It had T10 links 220 × 270mm (Shape Code 61 BS4466). The design strength of the concrete was 30N/mm^2 and the mix details are provided in Section 3.8.1.

The transverse reinforcement configuration of a single rectilinear link with 90° hooks is well known (Cusson *et al.*, 1994) as a weak configuration with respect to ductility enhancement. This weak transverse steel configuration was chosen to ensure that the specimens without wireball reinforcement would fail under the applied displacements. This was a necessary step because the optimum specimen size and detailing to determine the benefits of wireball reinforcement was dependent on the available laboratory equipment.

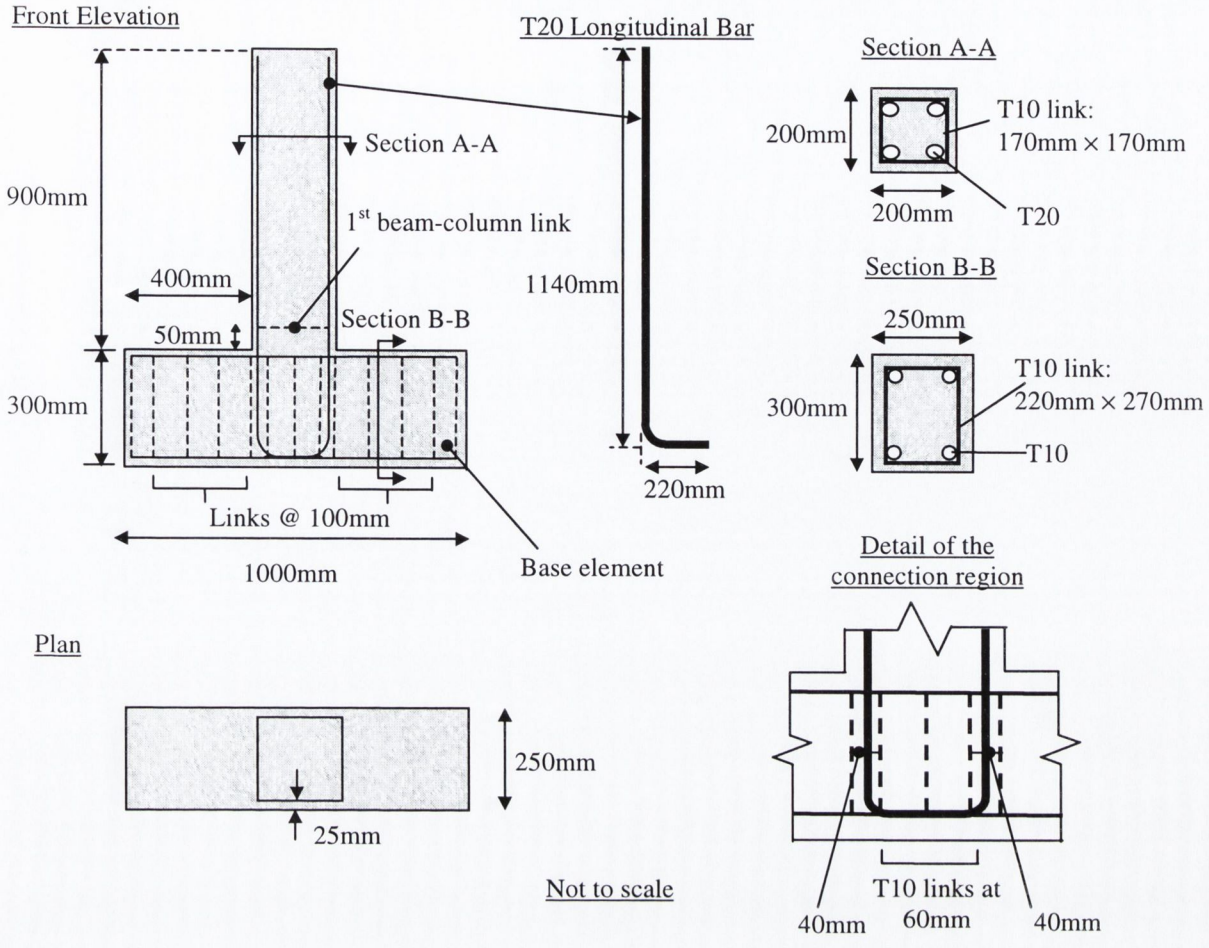

Figure 3.13: Beam-column dimensions and detailing (Test Series 6)

Beam-column link spacing and wireball reinforcement

As stated above, in all specimens the first beam-column link was always 50mm above the interface surface where the beam-column meets the base element. However, beyond this point the link spacings of the specimens differed. Table 3.7 details the link spacing used in each the specimen. Beyond the first link, these spacings apply throughout the full length of the beam-columns. Table 3.7 also details which specimens contained wireball reinforcement, as indicated by the letter "W" and the levels of axial load (see Section 3.7.1.2) that were applied to the specimens.

A spacing of 105mm is the minimum recommended by EC8 for a DCL column with an axial load of 30% of the cross-section capacity. A spacing of 145mm is that recommended for a DCL beam subject to lateral loading only. The spacings 125mm, 175mm and 200mm are 20%, 67% and 90% greater than the 105mm spacing. Equations 3.10 to 3.12 are the EC8 rules for determining the

Specimen	Link spacing (mm)	Wireball reinforcement (W)	Nominal axial load (%)
C6.1(105,30)	105	-	30
C6.2(125,W,30)	125	W	30
C6.4(125,W,40)	125	W	40
C5.2(145,30)	145	-	30
C5.1(145,W,30)	145	W	30
C6.3(145,W,40)	145	W	40
C6.6(175,30)	175	-	30
C6.5(200,W,30)	200	W	30

Table 3.7: Link spacings, wireball reinforcement and axial loads (Test Series 6)

volume of confinement links required for local ductility in an axially loaded specimen. For a rectangular column:

$$(\alpha)(\omega_{wd}) \geq (k_o)(\mu_{1/r})(v_d)(\varepsilon_{sy,d})(0.35\frac{A_c}{A_o} + 0.15) - 10\varepsilon_{cu} \tag{3.10}$$

$$\omega_{wd} = \left(\frac{volume\ \ of\ \ confining\ \ links}{volume\ \ of\ \ concrete\ \ core}\right) \cdot \left(\frac{f_{yd}}{f_{cd}}\right) \tag{3.11}$$

$$\alpha = \alpha_n \cdot \alpha_s \tag{3.12}$$

$$\alpha_n = 1 - \sum {b_i}^2 / 6A_0 \tag{3.12a}$$

$$\alpha_s = (1 - s/2b_0)^2 \tag{3.12b}$$

where:

ω_{wd} = minimum mechanical volumetric ratio of confining links to the volume of the concrete core, dependent on the ductility class

$\mu_{1/r}$ = required value of CCDF, ratio of post-failure curvature to yield curvature, (≥5 for DCL, ≥ 9 for DCM and ≥ 13 for DCH)

v_d = normalised design axial force, $v_d = N_{sd}/(A_c \times f_{cd})$

N_{sd} = design value of acting axial force (N)

A_c = gross cross-sectional area of concrete = 40,000mm^2

f_{yd} = design yield strength of transverse steel = 420N/mm^2

f_{cd} = design concrete compressive strength = 30 N/mm^2

$\varepsilon_{sy,d}$ = design value of tension steel strain at yield = 0.002

A_0 = cross-sectional core area of concrete = 25600mm^2

ε_{cu} = nominal ultimate strain of unconfined concrete = 0.0035

k_o = coefficient dependent on the ductility class (65 for DCL, 60 for DCM and 55 for DCH)

α = global effectiveness of the confinement

b_i = distance between consecutive longitudinal bars = 130 mm

b_0 = minimum dimension of concrete core = 160 mm

3.7.1.2 Applied axial loads

Within the test series, six specimens were subject to axial loads equal to 30% of their compressive capacity, while two specimens were subject to axial loads equal to 40% of their compressive capacity. Figure 3.14 is the theoretical interaction diagram for the specimens. The predicted ultimate moment capacities for each axial load level were calculated from Equations 3.13 and 3.14, using a cylinder strength of 30N/mm^2, an assumed steel strength of 460N/mm^2 and a factor of safety of unity. The cylinder strength of 30N/mm^2 was obtained by multiplying the average of the control cubes' strengths by 0.8 (Neville, 1995).

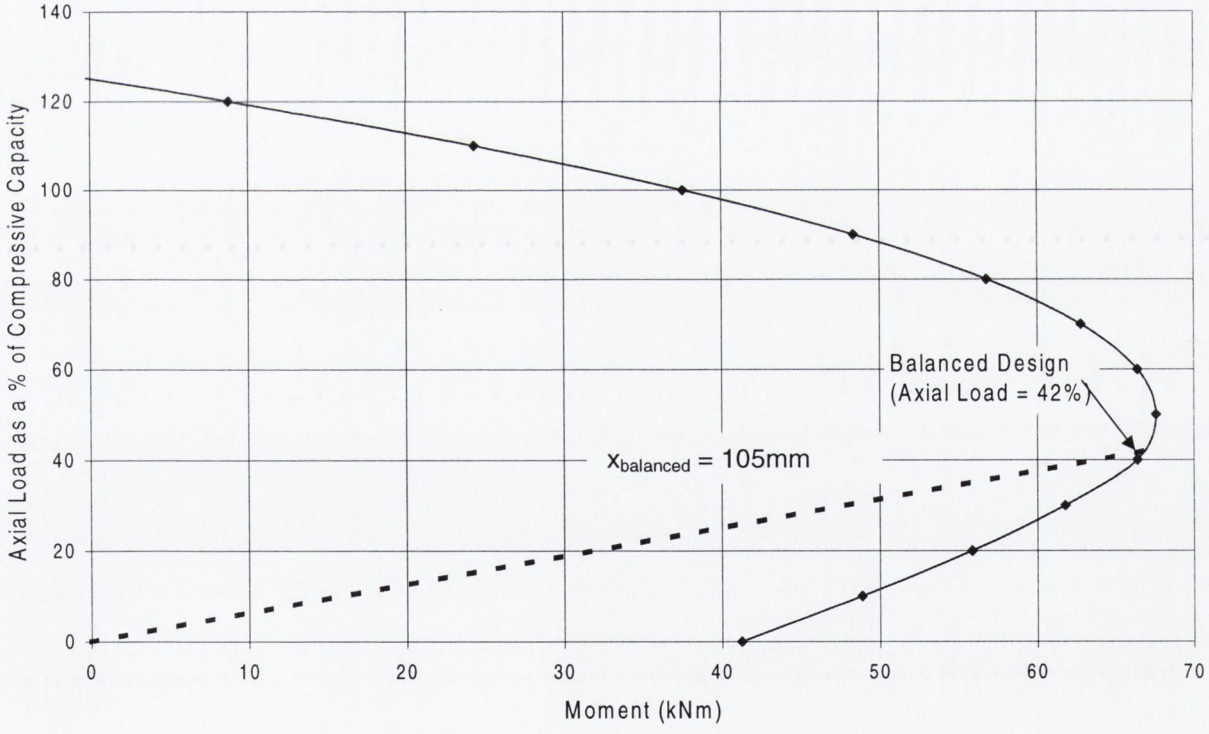

Figure 3.14: Theoretical interaction diagram (Test Series 6)

Theoretical moment calculation:

The predicted ultimate moment capacities for each axial load level were calculated as follows:

Consider the member of Figure 3.15 which is subjected to a compressive axial force N (acting at its centre) and a moment M. The member is reinforced top and bottom as illustrated in Figure 3.15. The location of the neutral axis depends on the relative magnitude of the compressive axial force N and the moment M. In broad terms two design cases may be distinguished (O'Brien *et al.*, 1995) as follows:

1. The neutral axis lies between the rows of reinforcement such that the reinforcement is in tension at one side of the neutral axis and in compression on the other side.
2. The neutral axis lies outside the section and the entire section is in compression.

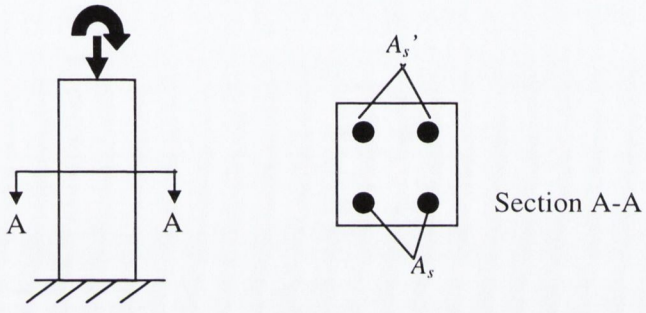

Figure 3.15: Combined axial force and bending of a reinforced concrete member

According to O'Brien *et al.* (1995) equilibrium of all axial forces gives:

$$N = F_c + f_s' A_s' + f_s A_s \tag{3.13}$$

where f_s' and f_s are both considered positive when compressive and f_s is negative when tensile (i.e. when the neutral axis lies between the layers of reinforcement). By taking moments about the centre line of the specimen the moment is given by the following (O'Brien *et al.*, 1995):

$$M_p = F_c(D/2-0.4x)+F'_s(D/2-d')-F_s(d-D/2) \tag{3.14}$$

where:

F_c = force in the compressed concrete (N)

f_s' = stress in the top steel (N/mm^2)

f_s = stress in the base steel (N/mm^2)

A_s' = area of top steel (mm^2)

A_s = area of base steel (mm^2)

F'_s= force in the top steel (N)

F_s = force in the base steel (N)

N = Axial load (N)

M_p = Theoretical ultimate moment (Nmm)

D = Total depth of the section (mm)

d = depth to base steel (mm)

d' = depth to the top steel (mm)

x = distance to the neutral axis (mm)

The interaction diagram shows that balanced failure occurs when the applied axial load is 42% of the compressive capacity of the column. For axial loads above this point, the section is over-reinforced and will fail in a brittle manner as the concrete crushes before the steel yields. For axial loads below 42%, the section is under-reinforced and will fail in a ductile manner with the steel yielding prior to concrete crushing. Axial loads greater than that required for balanced failure are considered very high. The two axial load levels employed in these tests were 30% and 40%. The 30% level was chosen as an intermediate level of axial load where a ductile failure was guaranteed. The 40% level was chosen to reflect a higher level of axial load where a ductile failure is still expected but where the concrete will crush at lower displacements than in tests with only 30% axial load levels.

3.7.2 Test set-up

Figures 3.16 and 3.17 illustrate the test set-up used in Test Series 6. The lateral load was applied to the specimen by means of a 10 tonne actuator attached to the specimen by a steel collar. The lever-arm distance, from the point of application of lateral load to the beam-column interface, was 745mm. A test control program, written in the graphical programming language LabView (Section 3.9.1), provided the actuator command displacement and enabled acquisition of the load-displacement results. There were 1000 movements of the actuator per cycle and 4 per second implying that each cycle took 250 seconds and therefore the frequency was 1/250, or $0.004sec^{-1}$, which was considered a quasi-static rate of loading.

Axial loads were applied by means of a 100 tonne jack sitting centrally on top of the specimens and bearing up against a rectangular channel section through which two McAlloy bars run. The load jack was placed into a seating which slotted over the specimen top. This seating provided lateral restraint to the jack. The McAlloy bars, bolted through the channel section and running down both sides of the specimen, were connected to the laboratory test frame by means of a mechanism that

allowed the axial load system to rotate with lateral movement of the specimen. The force of the 100 tonne jack pushing up against the channel section created a reaction force, which acted down into the specimen.

Figure 3.18(a) illustrates the rotation mechanism in detail. It consists of two 25mm thick steel plates which a McAlloy bar run through. The top plate is welded to the laboratory frame and has a slotted hole to allow lateral movement of the McAlloy bar. The base plate is bolted to the McAlloy bar so that the semi-circular bar welded to it bears against the top plate while allowing movement of the McAlloy bars with lateral loading of the specimen as illustrated in Figure 3.18(b).

The test specimen was seated on I-Sections welded to the laboratory test frame (Figure 3.16). The base element of the specimen was secured to the I-Sections by means of two 70mm thick by 100mm wide plates running over the base element and bolted through the I-Sections. The base element was further prevented from movement by a 10 tonne loading jack bearing against one end of the specimen while the other end of the specimen was flush with a reaction block rigidly attached to the test frame. A 30mm thick steel plate, 200mm × 300mm in area, was placed between the jack and the specimen. This had a spigot in its centre over which the ram of the jack slotted.

An internal load cell monitored the 10 tonne actuator load while an external load cell monitored the load applied by the 10 tonne jack. A load cell to monitor the axial load level was not included since its presence would have increased the complexity and height and hence decreased the stability of the set-up. Instead, the pressure applied to the jack was monitored throughout the test and maintained at a constant level. Hydraulic pressure supply for the actuator and the 100 tonne jack were provided by two 10,000 psi capacity Amsler Pressure supply units.

An external LVDT on the actuator was used to verify the actuator's internal LVDT displacement readings. LVDTs were also placed on the specimen at one half and one quarter the lever-arm length, unfortunately the displacement range on these LVDTs was quite small (approximately 60mm) so the acquired data was limited. A LVDT mounted to the base section enabled monitoring of any movement that might occur there. These LVDTs were connected to a System 5000 Data Acquisition Unit and their readings logged.

A shakedown test was applied before each test. No axial load was applied during the shakedown test. Figure 3.19 presents the control displacement history for the shakedown test, in which the maximum applied displacement was 3mm.

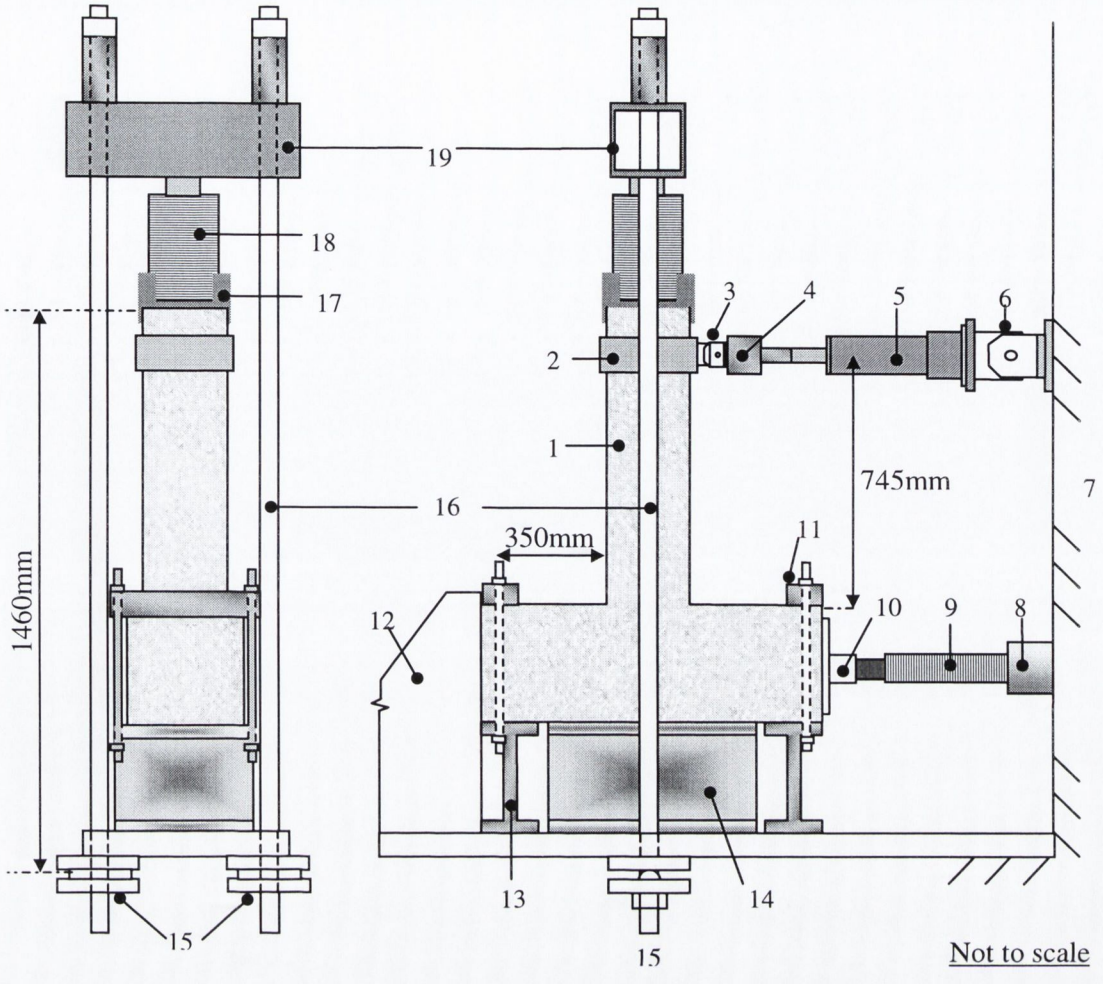

1: Specimen, **2:** Collar, **3:** Hinge connection **4:** Actuator load cell, **5:** Actuator, **6:** Hinge connection, **7:** Reaction frame, **8:** Load cell, **9:** Jack, **10:** Plate & spigot, **11:** Plate & bolt, **12:** Reaction block, **13:** I-Section, **14:** I-Section, **15:** Rotation mechanism, **16:** McAlloy bars, **17:** Seating for 100 tonne jack, **18:** 100 tonne jack, **19:** Rectangular channel section

Figure 3.16: Test set-up (Test Series 6)

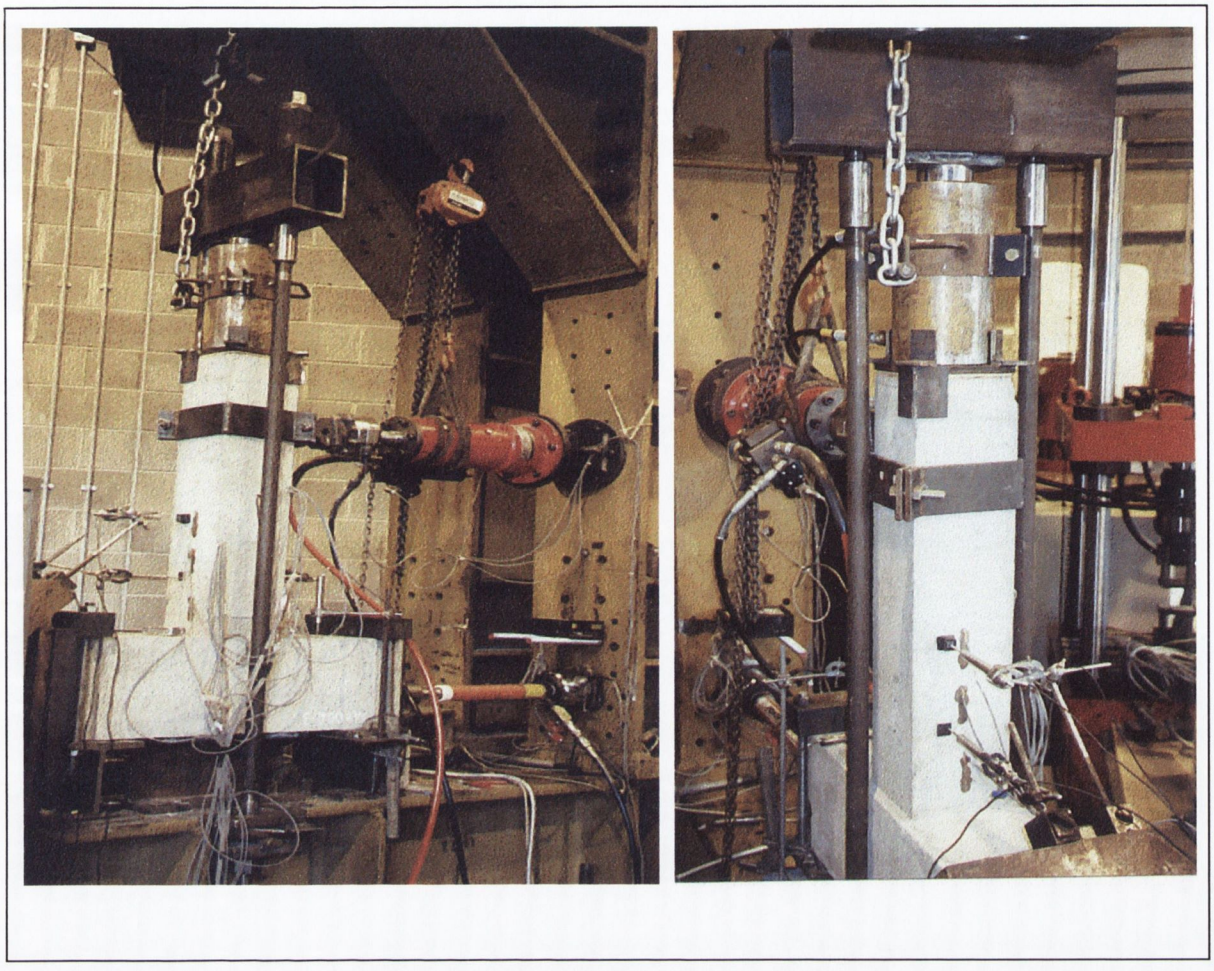

Figure 3.17: Photographs of test set-up (Test Series 6)

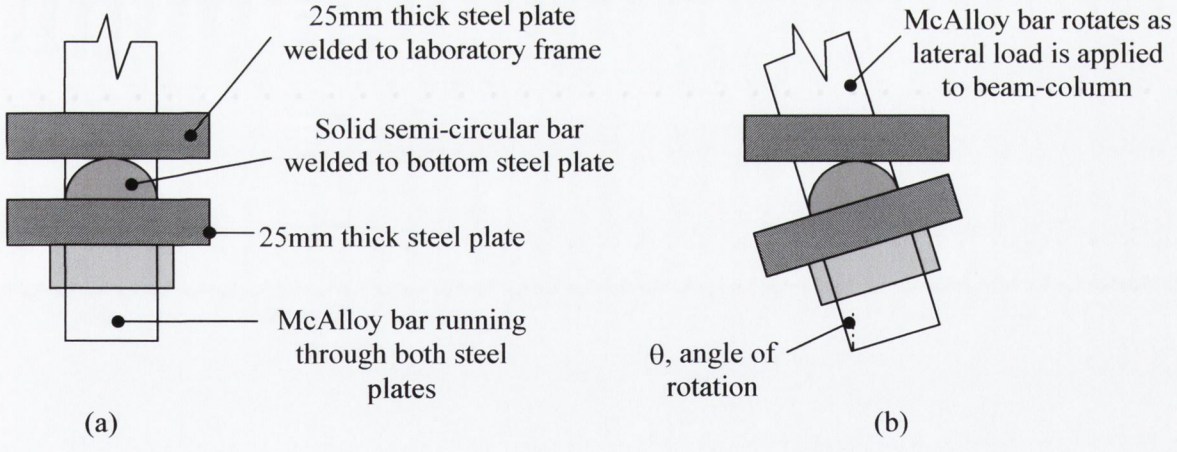

Figure 3.18: Rotation mechanism for axial load application (Test Series 6)

Each full test began with the application of the axial load, followed by imposition of lateral displacements. The displacement history imposed on the specimens is illustrated in Figure 3.20. The first four cycles were at displacements of ¼, ½, ¾ and 1 times the predicted yield displacement (10mm) respectively. Thereafter, all other displacement cycles (20, 30, 40, 50mm) were repeated three times. Both the shakedown and test displacement histories were in accordance with ECCS (1986) recommendations.

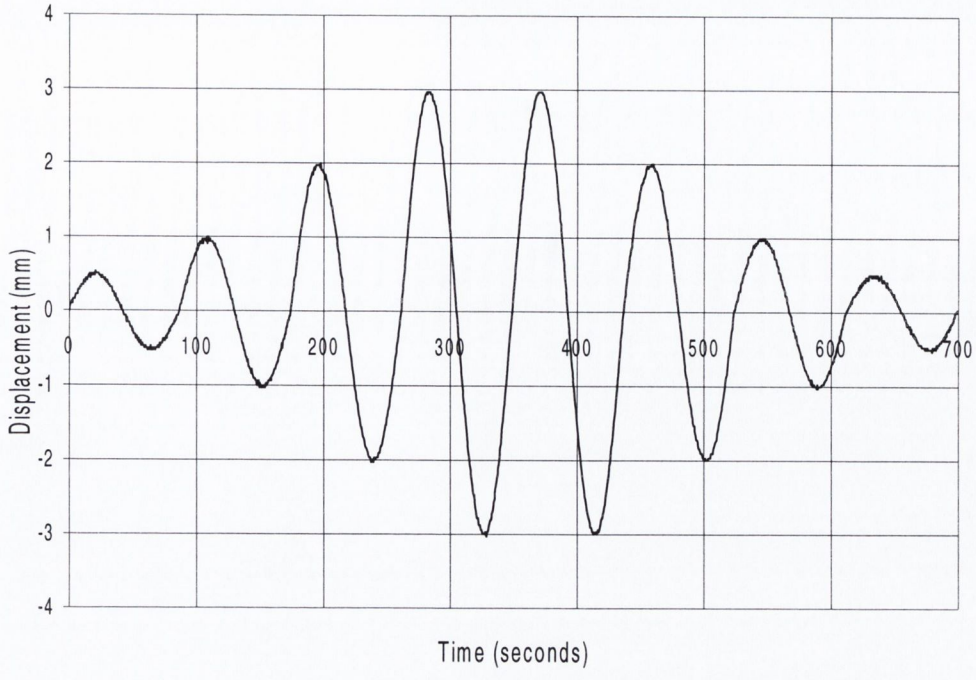

Figure 3.19: Shakedown test displacement history (Test Series 6)

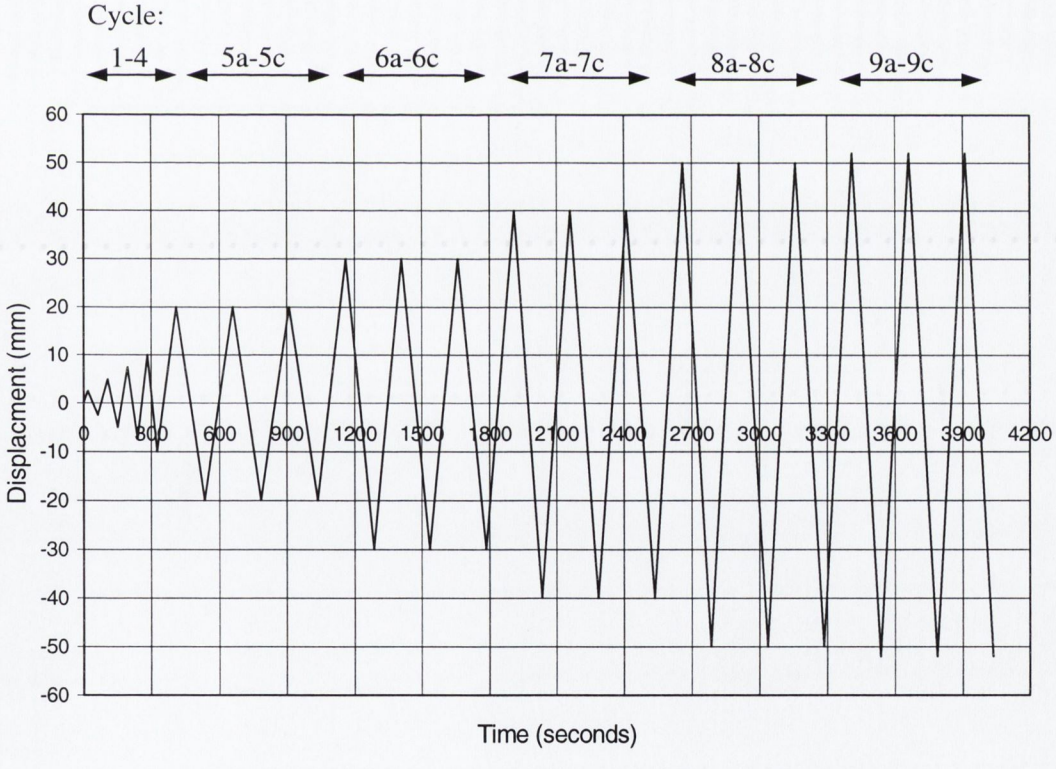

Figure 3.20: Test displacement history (Test Series 6)

3.7.2.1 P-Delta effect

An additional moment due to P-Delta effects was imposed on the specimens due to an eccentricity between the line of the axial force and the longitudinal axis of the beam-column as the specimens displaced laterally. This was because the specimens rotated about a point some distance above the rotation point of the axial load apparatus. Therefore, specimens were subject to:

- A moment due to the applied lateral load
- A moment due to a component of the axial load acting eccentrically (by a distance δ as shown in Figure 3.21) to the specimens' central axis, or a 'P-Delta moment'

It is important that the P-Delta moment is included when considering the moment applied to the specimens since it was part of the applied and measured moment. Equations 3.15 to 3.17, with reference to Figure 3.21, detail the calculations involved in determining the total moment imposed upon the specimens.

$$\theta = tan^{-1}(\Delta/1460) \tag{3.15a}$$

$$\alpha = tan^{-1}(\Delta/900) \tag{3.15b}$$

$$\gamma = \alpha - \theta \tag{3.15c}$$

$$P_h = Pcos(90-\gamma) \tag{3.16}$$

$$M = (F)\times(0.745)+(P_h)\times(0.9) \tag{3.17}$$

where:

θ = rotation angle of axial load apparatus

α = rotation angle of central axis of the specimen

γ = angle between the specimen central axis and the McAlloy Bar

P = applied axial load (kN)

P_h = component of P causing P-Delta moment (kN)

Δ = applied lateral displacement (mm)

F = applied lateral load (kN)

M = moment (kNm)

δ in Figure 3.21 = off-set of the axial load with respect to point of rotation of specimen (mm) = $\Delta(560/1460)$

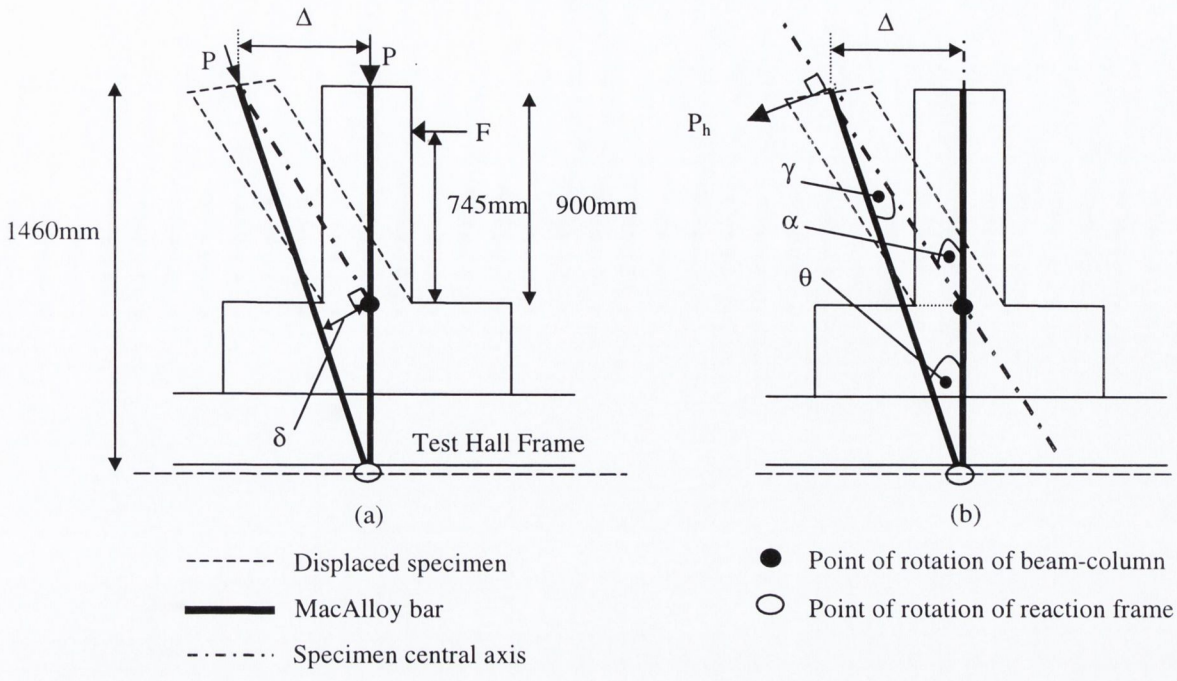

Figure 3.21: P-Delta Effect: (a) Specimen loads and displacements (b) Relevant angles

3.8 Material properties and specimen production

3.8.1 Concrete properties

Two different concrete mixes were used in the tests, their characteristics, in terms of specified 28-day compressive cube strength (f_{cu}), slump, water-cement ratio and maximum aggregate size, are provided in Table 3.8 and their material quantities are given in Table 3.9. In both mixes, the cement was grade 42.5 Normal Portland Cement, the coarse aggregate was pit run uncrushed gravel and the fine aggregate was naturally occurring washed sand with 52% passing through a 600 micron BS test sieve. The B.R.E. report *Design of normal concrete mixes* (Teychenne, 1988) was used as a guide to mix design.

Mix Property	Mix 1	Mix 2
f_{cu} (N/mm^2)	25	30
Slump (mm)	60-180	60-180
Water-cement ratio	0.52	0.55
Max. aggregate size (mm)	20	10

Table 3.8: Concrete mix characteristics

Material	Mix 1 (kg/m^3)	Mix 2 (kg/m^3)
Water	195	225
Cement	375	409
Fine Aggregate	536	587
20mm coarse Aggregate	830	None
10mm coarse Aggregate	420	1090

Table 3.9: Material quantities for concrete mixes

The concrete strengths obtained for each test are not detailed here, but in the results chapters (Chapters 4 and 5) where they are tabulated with the other test results for each test series.

3.8.2 Steel properties

Tensile tests were performed (with reference to BS EN 10 002-1: 1990) on samples of the steel used in the test series. Table 3.10 presents the average results for each bar diameter with respect to yield force (f_y), yield stress (σ_y), yield strain (ε_s), Young's Modulus (E_s), ultimate force (f_u), extension at failure and ultimate strain (ε_u). All samples were tested to failure in a Denison universal testing machine (500kN capacity). Each sample was strain gauged at its midsection to enable the elastic properties of the steel to be determined. Beyond yield, in every sample, the strain gauge became detached implying that only the ultimate load and not the ultimate strain could be recorded directly. However, using the initial and final lengths of the samples, an ultimate strain value is attainable. It is important to note that, with respect to the ultimate strain calculations, the extension for the full bar length rather than specific gauge length at the midsection of the bar is used. Therefore, it is likely that the ultimate strains are underestimated. With respect to the yield and ultimate stresses, these values are approximate since the initial bar area, rather than the reduced bar area, is used in the calculations.

Bar size mm	f_y kN	σ_y N/mm^2	ε_y	E_s N/mm^2	f_u kN	σ_u N/mm^2	Extension at failure mm	ε_u
20	113	360	0.00180	200000	195	620	23	0.0765
16	69	343	0.00175	195000	117	582	22	0.0733
12	38	336	0.00175	192000	70	619	18	0.0600
10	27	344	0.00175	193000	48	612	18	0.0600

Table 3.10: Steel reinforcement material properties

3.8.3 Specimen production

The first stage in specimen production was the fabrication of the reinforcement cages, examples of which are illustrated in Figure 3.22 and 3.24. Before the reinforcement cages were placed in the formwork, spacers were attached to ensure the desired cover to the steel was achieved. For each specimen type, formwork had to be constructed. In all cases the specimen formwork was fabricated from 12mm thick formwork-plywood and designed such that the cast specimens could be placed upon the vibration table for compaction. The stub columns were poured vertically while the beams were poured with their longitudinal axis lying horizontal. All of the T-shaped specimens (i.e. the beam-to-column connection specimens and the beam-column specimens) were poured on the flat.

Figure 3.23 shows some beam-to-column specimens, before and after pouring, while Figure 3.24 shows each stage of manufacture of simply-supported beam specimens. The base of the formwork for the beam-to-column connection and beam-column specimens was a single sheet of plywood for added stability upon the vibration table. A large laboratory mixer, with a capacity of $0.9m^3$, was used to make all the concrete. In the case of the T-shaped sections, two mixes were necessary since the volume of one specimen was greater than the mixer capacity. The insides of the formwork (including the control cubes) were cleaned thoroughly to remove any loose particles before a de-moulding agent was applied to ensure easy de-moulding.

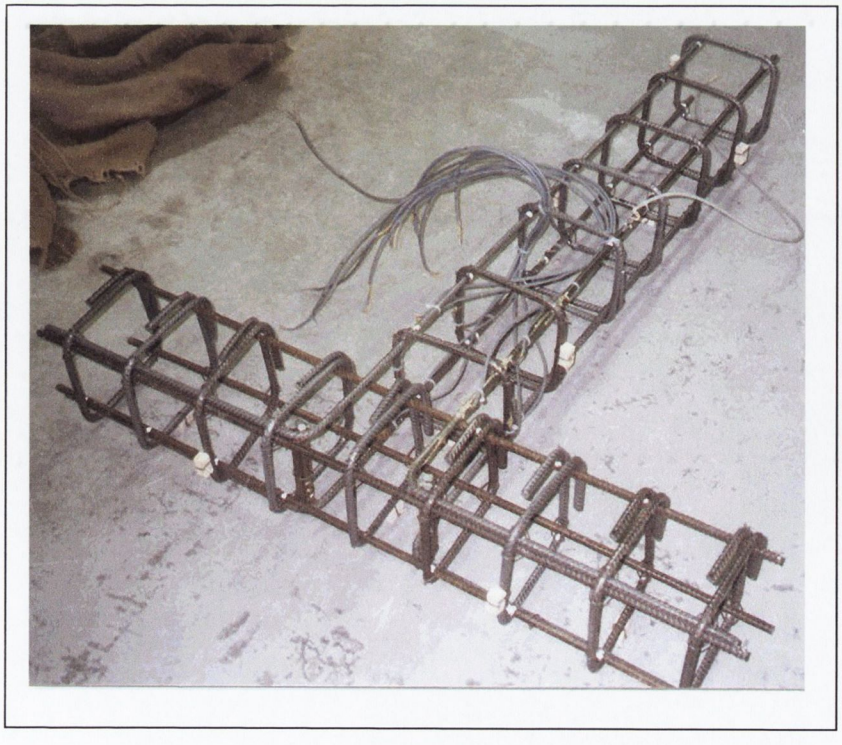

Figure 3.22: Example of steel cage used in Test Series 5

Casting Process:

- In reinforced specimens, the steel cages were placed carefully within the formwork. Where specimens contained wireballs these were packed within the steel cage as closely together as possible, but at random. Where wireballs were only required in a limited part of the specimen, a mesh of tying wire was tied to the reinforcement cage at the required position to prevent movement of wireballs out of position. Figure 3.23 shows wireballs packed within a reinforcement cage used in Test Series 5.
- The coarse and fine aggregate and cement were mixed thoroughly for three minutes. The water was added and the concrete was mixed for a further three minutes. The concrete was allowed to sit for 10 minutes before performing a slump test.
- With the vibrating table turned on, the concrete was added gradually. The compaction process was slightly slower in the wireball-reinforced specimens since the presence of the wireballs made compaction more difficult to achieve, especially in specimens using the 20mm aggregate mix. For each mix, control cubes were cast (BS1881: Part 108: 1983). They were filled in two separate layers with vibration between each additional layer.
- Two hours after casting, the specimens and their accompanying control cubes were covered in wet hessian and polythene for 24 hours before de-moulding.
- Upon de-moulding the specimens were re-covered with wet hessian and polythene until the date of testing, usually 28 days from the casting date.
- All the control cubes were placed in a curing tank at approximately 20°C where they remained until the date of testing. The cubes were tested according to BS1881: Part 116.

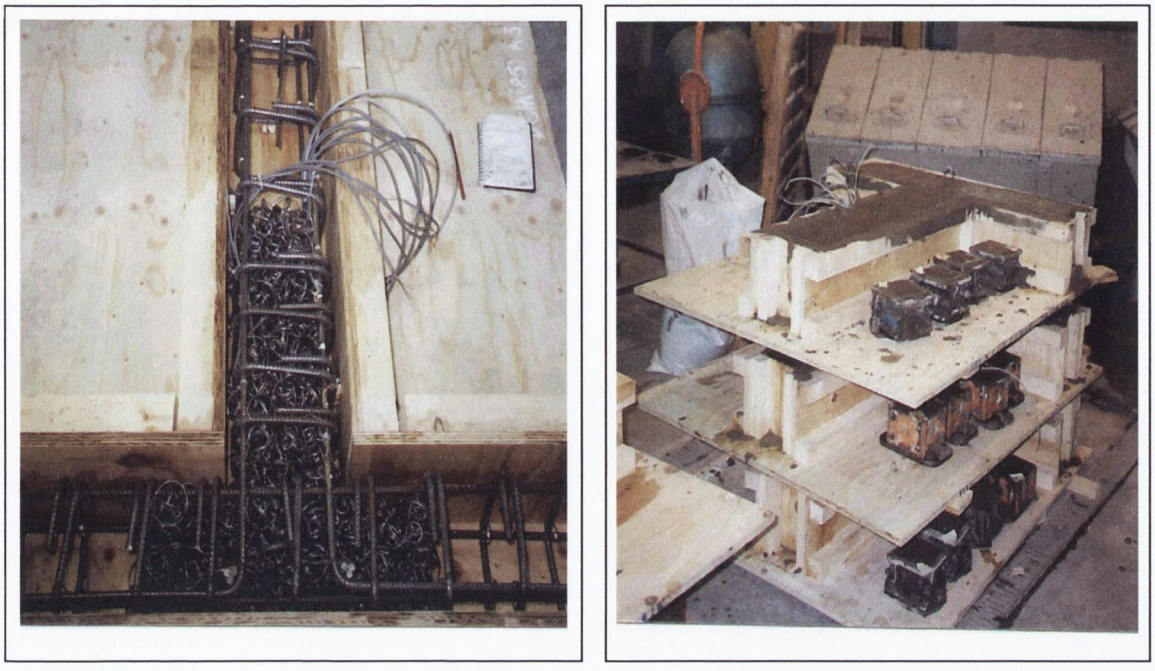

(a) (b)

Figure 3.23: (a) Wireballs packed within reinforcement cage, (b) Specimens just after pouring

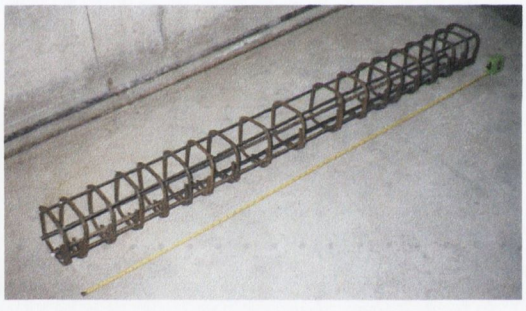

(a)

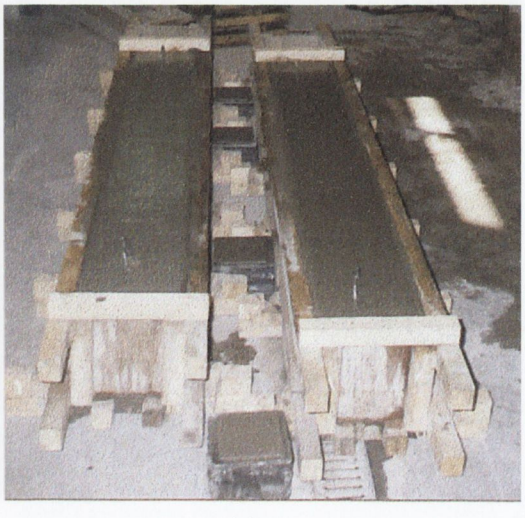

(c)

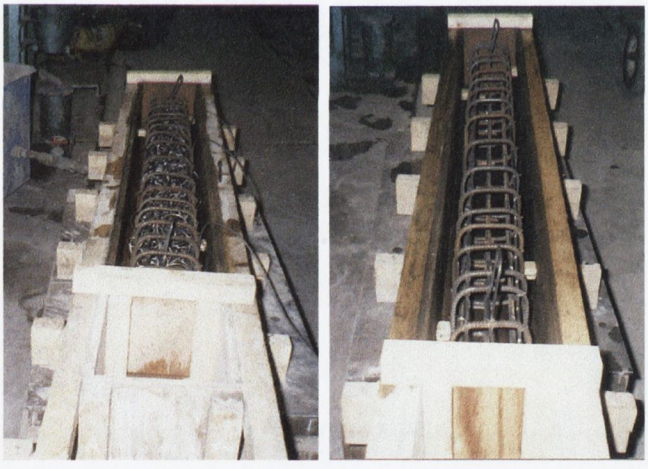

(b)

Figure 3.24: Manufacturing process of simply-supported beams from (a) reinforcement cage to (b) placement of cage and wireballs within the formwork (c) pouring of the beams and control cubes

3.9 Experimental equipment and purpose of the shakedown

3.9.1 Control of the servo-hydraulic actuator

In all tests employing a servo-hydraulic actuator, the actuator was controlled though loading programs developed by *Thomson* (2001). They were written in LabView, a graphical programming language specially developed to meet the requirements of engineers and scientists operating data acquisition equipment. The programs were designed to impose cyclic displacement waveforms as well as being capable of scanning the response of multiple strain gauges, load cells and LVDTs.

The Labview programmes were designed to control the displacements of any of the servo-hydraulic actuators present in the structural laboratories. These actuators consist of a hydraulic ram, together with an internal displacement transducer, load cell, servo-valve and command console. The command console allows an actuator to be controlled in one of three ways:

- *BALANCE* mode allows the manual control of the load or displacement. It enables the user to set the actuator to its "zero", or centre position, and enables a pre-load or an initial displacement to be imposed.
- *DISP* mode allows displacement control of the actuator using the internal displacement transducer.
- *LOAD* mode allows load control of the actuator via the internal load cell.

When used as a stand-alone unit the actuator command unit has a built-in signal generator that creates waveforms of different frequencies, amplitudes and type. These waveforms are then sent to the actuator, which is set to either *DISP* or *LOAD* control. To integrate a computer system into this set-up, the signal generator is removed and replaced with the output cable of a signal-conditioning unit. A voltage signal is sent from the computer's data acquisition card - DAQcard (National Instruments card type PCI-MIO-16E-1) - through the signal-conditioning unit, to the actuator command console. The DAQcard facilitates communication between the control software and the actuator command console. It was designed specially for use in the LabView programming environment and consists of both digital and analogue input-output channels for use in different situations. The analogue capabilities of the card are used to control the actuator by sending a voltage to the command module of the actuator. This voltage tells the actuator what distance and direction to move in. The signals passed to and from the DAQcard are filtered through the signal-conditioning unit consisting of a chassis, a module and terminal blocks. The terminal blocks allow signals from different measurement devices to be fed into the modules. Different types of terminal blocks and modules are used for different measuring devices.

3.9.2 Strain gauges

Certain specimens were strain gauged. The concrete gauges used were PL-60-11, PL-90-11 or PL-120-11 ERS gauges with 2.09, 2.11 and 2.12 gauge factors respectively. Before they were adhered to the concrete, the concrete surface was lightly wire-brushed to remove any dust that might interfere with the bonding process. Strain gauges on the reinforcing steel were 350 Ohm ERS gauges 5mm in length. Since the bars were ribbed, the steel had to be milled down slightly with an angle grinder to create a flat surface for placement of the strain gauges on the steel. For both concrete and steel, the gauges were adhered using type 454 adhesive. The gauges on the steel were covered with a moisture-proofing agent (N1), to protect them from the concrete as it was poured.

3.9.3 Purpose of the shakedown test

The purpose of a shakedown test is to impose small amplitude cyclic displacements (much less than the predicted yield displacement) to ensure that all experimental equipment is working correctly and that the data acquisition systems are logging correctly. The shakedown test also removes any initial restraining forces arising from the installation of the specimen within the laboratory frame.

CHAPTER 4

INITIAL RESULTS: WIREBALL-REINFORCED MEMBERS UNDER VARIOUS LOADING CONDITIONS

4.1 Introduction

Table 3.1 detailed the types of tests performed within the body of this research. The purpose of the initial tests was to study the effects of wireball reinforcement in different loading situations with the eventual aim of testing their confinement enhancing properties for earthquake resistance. This chapter discusses the experimental results of those tests, with the exception of Test Series 6, which is considered separately in the Chapter 5. Section 4.2 considers the results of the stub columns tested under monotonic compression while Section 4.3 and Section 4.4 look at the results from the simply-supported beams subject to monotonic bending with central and ¼ point loading arrangements. Section 4.5 considers the response of beam-to-column connections under lateral cyclic loading, while Section 4.6 deals with the results from beams subject to lateral cyclic loading.

4.2 Test Series 1: Stub columns subject to monotonic compression

4.2.1 Visual observations

The conventionally reinforced stub columns failed in a similar manner with cover spall occurring at the mid-regions of the specimens and spreading upwards in most specimens. In the majority of specimens, the bottom half of the specimen remained intact. Spalling initiated from vertical cracks at the corners of the specimens and spread inwards towards the centres of each face. The amount of cover spall was sufficient to reveal the links and longitudinal steel. The links remained free of distortion, the longitudinal steel was not buckled, and the cores of all the specimens remained intact. However, in these early tests, the load was usually taken off the specimens with the occurrence of significant cover spall, where the reinforcement cage was revealed. If the load had been applied for longer, it is probable that the longitudinal steel would have buckled, and the links would have become distorted. The stub columns depicted in Figure 4.1 are typical in appearance to the majority of stub columns after testing. A minority of the conventionally reinforced specimens failed through cover spall from the bottom section rather than the top section. The plain specimens and specimens reinforced solely with wireballs failed through the development of a large shear crack running through their middle sections at 45° so that the specimens were split in two.

Figure 4.1: Typical failure of conventionally reinforced stub columns with and without wireballs

4.2.2 Load-displacement response

The stub column details, experimental set-ups, and experimental programmes are described in Chapter 3. Table 4.1 details the stub column results in terms of cylinder strength (f_{ck}), initial stiffness (K_i), yield, ultimate and predicted loads (P_y, P_u and P_p respectively) and displacement ductility ratios (μ_Δ, defined as the ratio of ultimate to yield displacement). The predicted force (P_p) was calculated by multiplying the concrete cylinder strengths by the section area (150mm × 150mm). Yield load was defined as the last load value prior to significant non-linear behaviour, while the ultimate strength corresponds to the peak load value. The yield displacement was defined by the intersection of a secant, running through zero and 75% of the ultimate load, and a line parallel to the displacement axis and running through the point of ultimate strength (Figure 4.2). This method to define the yield displacement is considered reasonable for reinforced concrete since it takes into account stiffness reduction that might occur near the elastic limit. This definition was used rather than defining the yield displacement as that displacement occurring at the first departure from linearity since the latter definition can underestimate yield displacement substantially for reinforced concrete, where early cracking occurs, and may lead to a large over-estimation in displacement ductility. The ultimate displacement is that occurring when the resistance had decreased to 85% its peak value, thereby taking into account post-ultimate behaviour. If the load had been applied to the specimens long enough for buckling of the longitudinal or transverse steel to occur then the displacement at which buckling occurred could have been used as the ultimate displacement.

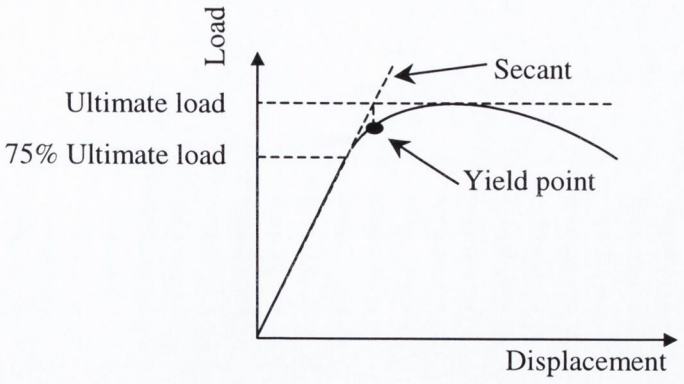

Figure 4.2: Definition of yield by Secant Method

Specimen	f_{ck} N/mm^2	K_i N/mm	P_y kN	P_u kN	P_p kN	P_u/P_y	P_u/P_p	μ_Δ
SC/1.1/DCH	20	0.34	394	500	450	1.27	1.11	3.4
SC/1.2/DCL	20	0.22	324	430	450	1.33	0.96	1.9
SC/2.1/P	25	0.15	100	114	563	1.14	0.20	1.5
SC/3.1/DCL	24	0.21	394	423	540	1.07	0.78	1.7
SC/3.2/DCH	24	0.27	387	463	540	1.20	0.86	3.6
SC/4.1/DCL/W	21	0.24	369	485	473	1.31	1.03	3.1
SC/4.2/DCM	21	0.25	374	488	473	1.30	1.03	2.9
SC/4.3/DCM/W	21	0.25	378	496	473	1.31	1.05	2.8
SC/5.1/P	20	0.15	169	213	450	1.26	0.47	1.3
SC/5.2/P/W	20	0.18	266	327	450	1.23	0.73	2.0
SC/6.1/DCL	20	0.26	342	422	450	1.23	0.94	2.7
SC/6.2/DCL/W	20	0.27	347	451	450	1.30	1.00	3.5
SC/6.3/DCL(75%)/W	20	0.23	306	394	450	1.29	0.88	2.9
SC6.4/DCL(50%)/W	20	0.55	332	378	450	1.14	0.84	1.2
SC/7.1/DCL	18	0.18	332	382	405	1.13	0.94	1.9
SC/7.2/DCL/W	18	0.21	338	428	405	1.27	1.06	2.5
SC/7.3/DCL(75%)/W	18	0.22	328	414	405	1.26	1.02	3.8
SC/7.4/DCL(50%)/W	18	0.15	334	378	405	1.13	0.93	2.0

Table 4.1: Stub column results

The cylinder strengths were determined by multiplying the cube strengths by a factor of 0.8 (Neville, 1995). The cylinder strengths range between 18N/mm^2 and 25N/mm^2, while the initial stiffness values range between 0.15N/mm and 0.34N/mm. For the most part, the specimens

containing standard transverse and longitudinal reinforcement display higher initial stiffnesses than the plain specimens and those specimens containing only wireball reinforcement. Specimen SC/2.1/P has the lowest yield load of 100kN, while specimens SC/1.1/DCH and SC/3.1/DCL have the highest yield loads of 394kN. The ultimate forces vary from 500kN for SC/1.1/DCH to 114kN for SC/2.1/P.

With the exception of SC/3.1/DCL, the ultimate load values of all the specimens are at least 10% greater than the yield loads. The specimen's load carrying capacities indicate that the inclusion of wireballs may enhance specimen strength. In the plain specimens, the increase in strength with wireballs is significant, specimen SC/5.2/P/W being 54% stronger than its counterpart specimen SC/5.1/P. This is not consolidated by previous research - plain and wireball reinforced columns in previous tests had the same strengths (Section 2.7.3.3). Comparison of specimen pairs with the same levels of conventional reinforcement, with and without wireballs, also shows that the wireball reinforced specimens are somewhat stronger that the specimens with wireballs. For instance, specimen SC/4.3/DCM/W is slightly stronger that specimen SC/4.2/DCM. In Group 7, both specimens SC/7.2/DCL/W and SC/7.3/DCL(75%)/W are stronger than specimen SC/7.1/DCL, however, specimen SC/7.4/DCL(50%)/W is slightly less strong than specimen SC/7.1/DCL. In Group 6, which contained the same specimen types as Group 7, the same trends do not exist since only one of the wireball reinforced specimens (SC/6.2/DCL/W) is stronger than specimen SC/6.1/DCL which contained no wireballs. Therefore, while there is some evidence to suggest that wireballs enhance strength the results are inconclusive and the range of data limited.

Finally, the ratios of ultimate loads to the predicted loads show that in the majority of cases the ultimate forces were within 10% of the predicted value as would be expected. However, in other cases the ultimate loads were only 20% to 70% that predicted, but this was usually in the case of plain or just wireball reinforced specimens.

The results are encouraging in terms of the potential of wireballs to enhance ductility. Table 4.2 ranks the specimens in terms of their displacement ductilities, a ranking of 1 indicating the highest displacement ductility, and a ranking of 6 indicating the lowest displacement ductility. The table also details the level of ductility corresponding to each ranking.

The lower ranking specimens ($\mu<2$), with the exception of SC/6.4/DCL(50%)/W, are either plain or DCL specimens. Despite having no links or a relatively large link spacing, both specimens SC/5.2/P/W and SC7.4/DCL(50%)/W achieve higher displacement ductility levels than all of the DCL specimens (with no wireballs), with the exception of specimen SC/6.1/DCL. Significantly, the DCM and DCH specimens are no more ductile than specimens with considerably larger link spacing but containing wireballs. For example, specimens SC/6.2/DCL/W and

SC/7.3/DCL(75%)/W, with link spacings of 60mm and 75mm, respectively, are as ductile as SC/3.2/DCH with the closer link spacing of 30mm.

Displacement Ductility μ	**Specimens**	**Ranking**
$\mu \geq 3.5$	SC/3.2/DCH, SC/6.2/DCL/W, SC/7.3/DCL(75%)/W	1
$3 \leq \mu < 3.5$	SC/1.1/DCH, SC/4.1/DCL/W	2
$2.5 \leq \mu < 3$	SC/4.2/DCM, SC/4.3/DCM/W, SC/6.1/DCL, SC/6.3/DCL(75%)/W, SC/7.2/DCL/W	3
$2 \leq \mu < 2.5$	SC/5.2/P/W, SC/7.4/DCL(50%)/W	4
$1.5 \leq \mu < 2$	SC/1.2/DCL, SC/2.1/P, SC/3.1/DCL, SC/7.1/DCL	5
$1 < \mu \leq 1.5$	SC/5.1/P, SC/6.4/DCL(50%)/W	6

Table 4.2: Stub columns ranked in order of decreasing displacement ductilities.

The results suggest that the inclusion of wireballs offers potential reductions in the amount of conventional links for a ductility class while still achieving the required ductility. Figure 4.3 presents the load-displacement response for six specimens. Four are reinforced for DCL conditions, two with wireballs and two without, and two are reinforced for DCM conditions, with and without wireballs.

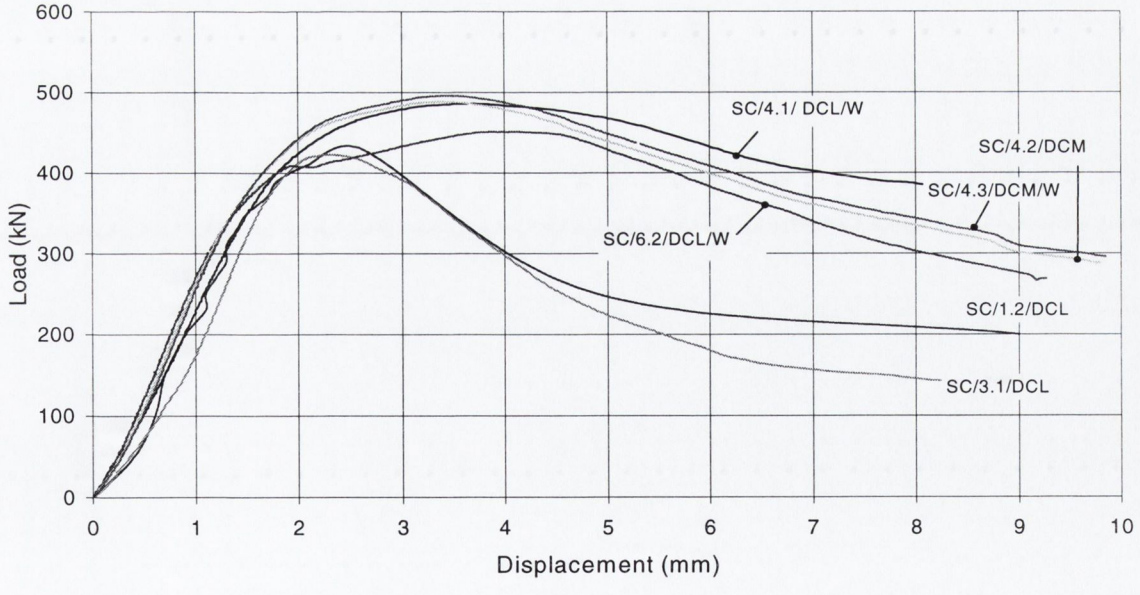

Figure 4.3: Load-displacement response of stub columns with various link spacings and wireball contents

Comparison of the four specimens with DCL link spacings illustrates the greater load-carrying capacity of the wireball reinforced specimens. It is also clear from the plot that the wireball reinforced DCL specimens perform as well as both DCM specimens with and without wireballs. However, the almost identical results of specimens SC/4.2/DCM and SC/4.3/DCM/W suggest that the confinement benefits offered by wireballs are limited to specimens with DCL link spacings. With this is mind, Groups 6 and 7 were designed to determine how much the recommended DCL spacing of 60mm could be increased, through the use of wireballs, without detrimental effect on specimen behaviour. Both groups were the same in terms of the type of specimens they contained (Section 3.2.1). Figures 4.4 and 4.5 present the load-displacement responses of Groups 6 and 7 respectively.

Of the Group 6 specimens, specimen SC/6.1/DCL/W maintains its load carrying capacity, beyond ultimate load, best. Specimens SC/6.1/DCL and SC/6.3/DCL(75%)/W behave very similarly to each other while specimen SC/6.4/DCL(50%)/W behaves in a very brittle manner. The plot for Group 7 is similar to that of Group 6 except that specimen SC/7.4/DCL(50%)/W with the largest link spacing behaves almost as well as the other wireball reinforced specimens, while outperforming the specimen without wireballs. The results of both test series indicate that the DCL link spacing may be reduced (by 75% at least, and perhaps by 50%) without detrimental effect on specimen behaviour. However, the brittle behaviour of specimen SC/6.4/DCL(50%)/W may indicate that there is a maximum limit on the link spacing, even with wireballs, beyond which the specimen will fail suddenly.

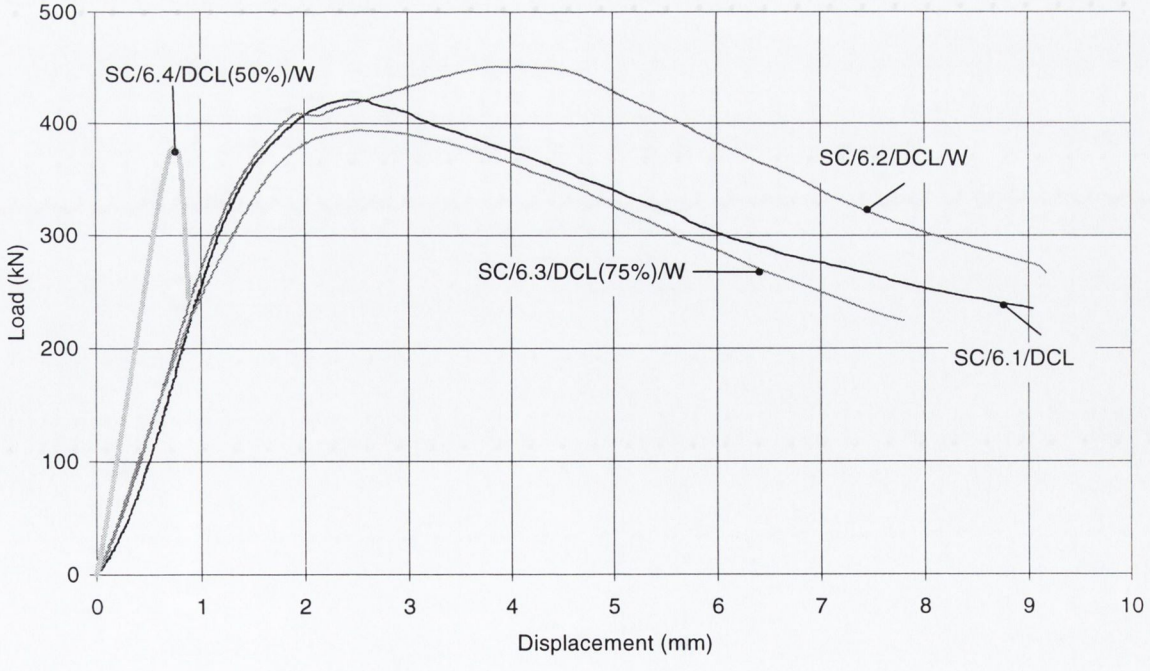

Figure 4.4: Load-displacement response Group 6 stub columns

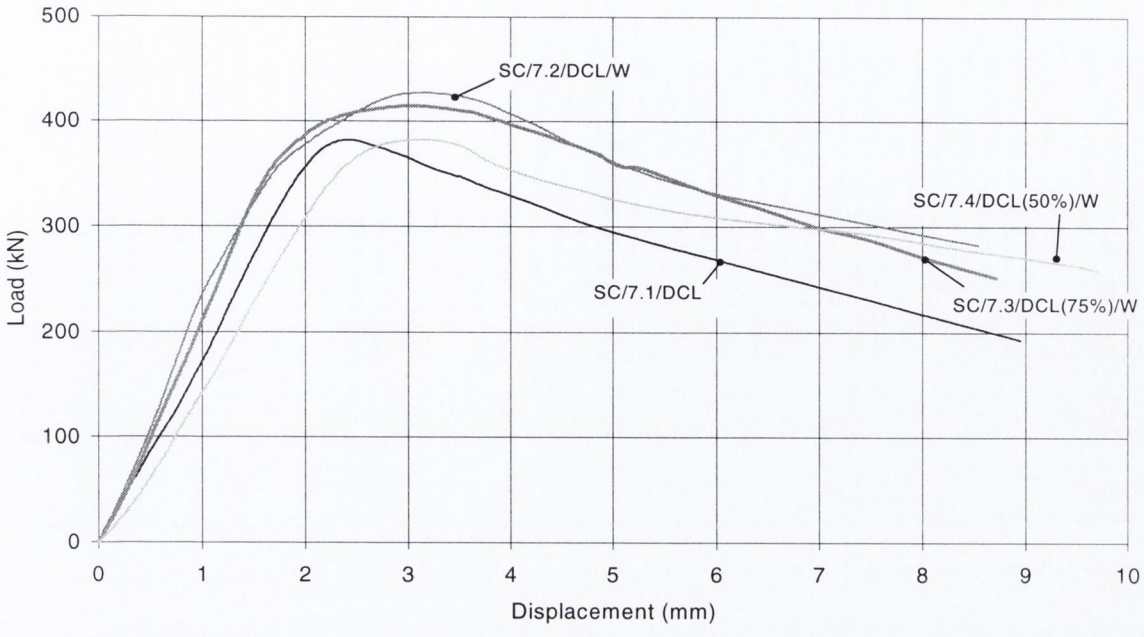

Figure 4.5: Load-displacement response Group 7 stub columns

4.2.3 Conclusions

The main conclusion drawn from the tests on stub columns is that there is potential for wireballs to enhance the ductility of conventionally reinforced specimens. However, it would seem that the possible benefits of wireballs depend upon the level of conventional transverse reinforcement. This is indicated by the almost identical behaviour of the two specimens with EC8 DCM link spacing, one containing wireballs and one with no wireballs. In contrast to this, in specimens with the larger DCL spacing, the inclusion of wireballs enhances ductility, to the extent that the specimens perform as well as the DCM detailed specimens.

The results of the final two test series also suggest that the use of wireballs, in combination with conventional reinforcement, may allow a reduction in the level of transverse reinforcement required by EC8, without any detrimental effect on specimen behaviour. However, the results show that there may be a limit on how much the link spacing may be reduced before a brittle failure may ensue.

4.3 Test Series 2: Simply-supported beams with central point loading

4.3.1 Visual observations

Five beams were tested within this test series as described in Section 3.3. All of the beams behaved in a very similar fashion failing through flexure at their midpoints. The first cracks developed on the base of the beams, at their midpoint, and spread onto the two side faces as vertical (flexural) cracks. With increased loading, further flexural cracks developed around the mid-points of all of the beams, providing visual evidence of the formation of a plastic hinge. With plastic elongation of the steel, the crack widths increased. Some crushing of the concrete on the top face of the beam occurred at the point of load application. Figure 4.6 illustrates the typical failure mode.

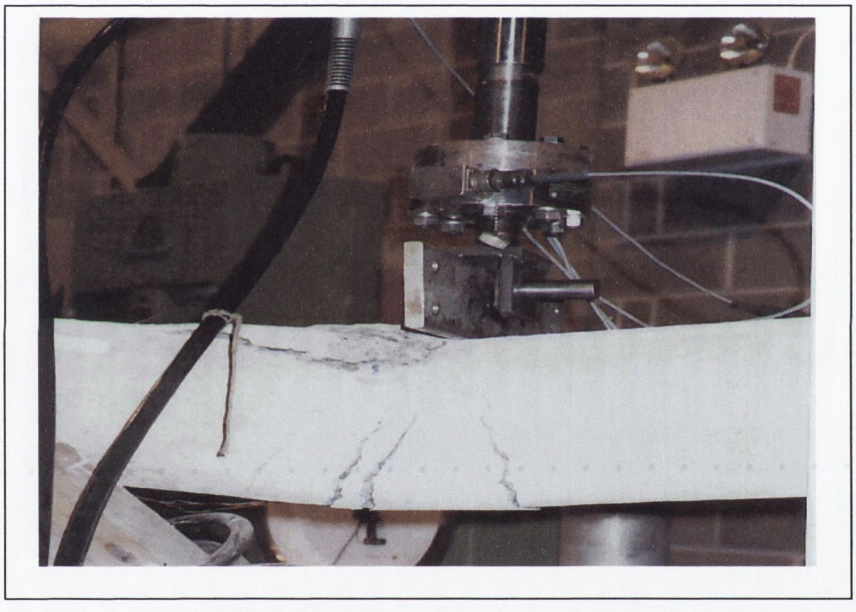

Figure 4.6: Typical beam failure in Test Series 2

4.3.2 Load-displacement response

The results of the tests are provided in Table 4.3, in terms of cylinder strength (f_{ck}), initial stiffness (K_i), yield and ultimate displacements (Δ_y and Δ_{ult} respectively), yield, ultimate and predicted loads (P_y, P_{ult} and P_p respectively) and displacement ductility (μ_Δ). As before, the cylinder strengths were determined by multiplying the cube strengths by a factor of 0.8.

Specimen	f_{ck} N/mm^2	K_i N/mm	P_y kN	Δ_y mm	P_{ult} kN	P_p kN	Δ_{ult} mm	μ_Δ	P_{ult}/P_p
B1/80	40	6.8	43.9	6.6	72.4	66.3	75	11.4	1.09
B2/80/W	34	5.1	36.9	6.6	71.7	65.6	104	15.8	1.09
B3/100	34	7.0	56.9	8.4	68.0	65.6	65	7.7	1.04
B4/100/W	40	5.4	42.0	8.3	67.1	66.3	100	12.0	1.01
B5/120/W	26	5.7	48.0	8.4	67.8	64.1	74	8.8	1.06

Table 4.3: Simply-supported beam with central point load, results

With the exception of B5/120/W, all the beam concrete strengths lie between 34 and 40N/mm^2. B5/120/W has a lower strength of 26N/mm^2 but this does not affect its ultimate strength relative to that of the other specimens. The beam stiffnesses range from 5.1N/mm to 7.0N/mm. All of the beams reached similar ultimate strengths (P_{ult}) of between 67.1kN and 72.4kN. Ratios of ultimate loads to predicted loads show that the predicted values slightly under-estimate the beam strengths, there being a maximum under-estimation of 9%.

The yield points of the beams were determined by considering the strain results of the three central strain gauges of the middle base longitudinal steel bar. The average value of load at which the gauge readings went beyond yield was taken as the yield load, while the value of displacement corresponding to this load was taken as the yield displacement. The use of the 75% Secant Method (as described in Section 4.2.2), that takes into account stiffness reduction of reinforced concrete near the elastic limit to determine the yield point was considered. However, after inspection of the load-displacement curves of the beams, this was not employed since the load-displacement curves showed only minimal amounts of stiffness degradation before the ultimate loads are reached. The ultimate displacement is that occurring when the resistance had decreased to 85% its peak value and the displacement ductility is defined as the ratio of ultimate to yield displacement.

With respect to their load-displacement characteristics, the specimens are considered in two groups. Figure 4.7 presents the load-displacement curves of the beams of Group 1 - B1/80, B2/80/W and B4/100/W. It is clear from Figure 4.7, and the results of Table 4.3, that the three beams behaved quite similarly.

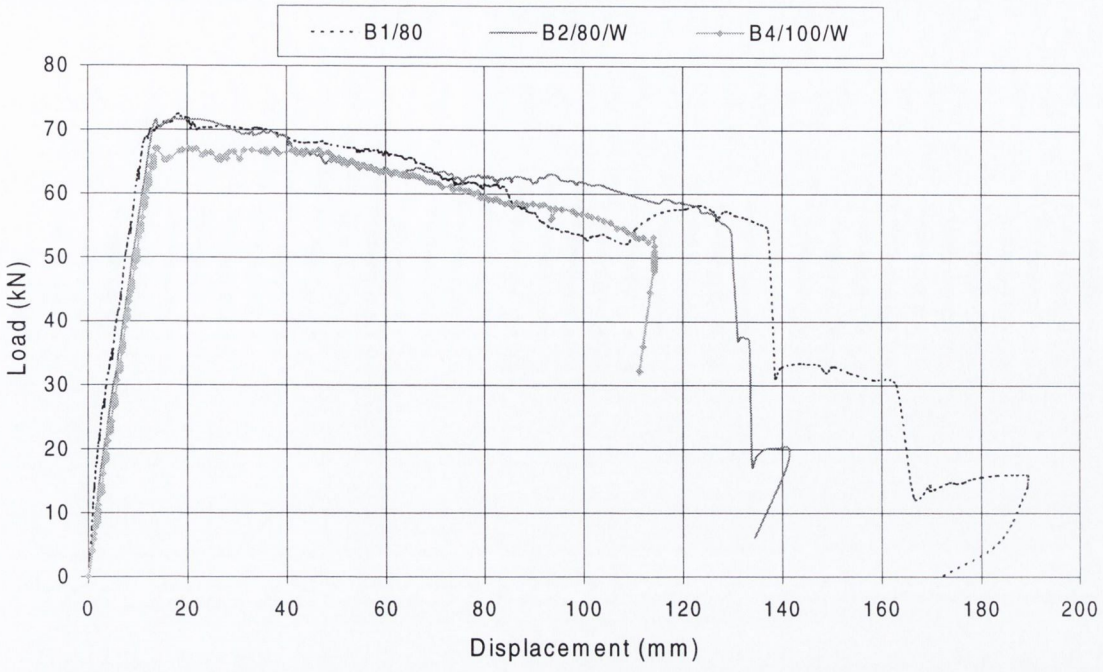

Figure 4.7: Load-displacement response of specimens B1/80, B2/80/W and B4/100/W

The beams all display the same behaviour up to their ultimate load points. Beyond their ultimate loads, the beams continue to behave quite similarly, with approximately the same losses in resistance. However, while the differences in the resistance losses are small, it is interesting to note that of the three beams B2/80/W maintains the superior load-carrying capacity. This superior capacity is reflected in its displacement ductility factor, which is 39% and 32% greater than the displacement ductilities of specimens B1 and B4 respectively. The greater displacement ductility of specimen B2 is due to its combination of closely spaced links and wireballs. It is also noteworthy that B4/100/W has a slightly higher displacement ductility factor than B1/80 despite having a larger link spacing. Therefore, while the distinctions between the beam behaviours are slight, they are such that they provide positive, if not conclusive, indications of the ductility enhancing properties of wireballs.

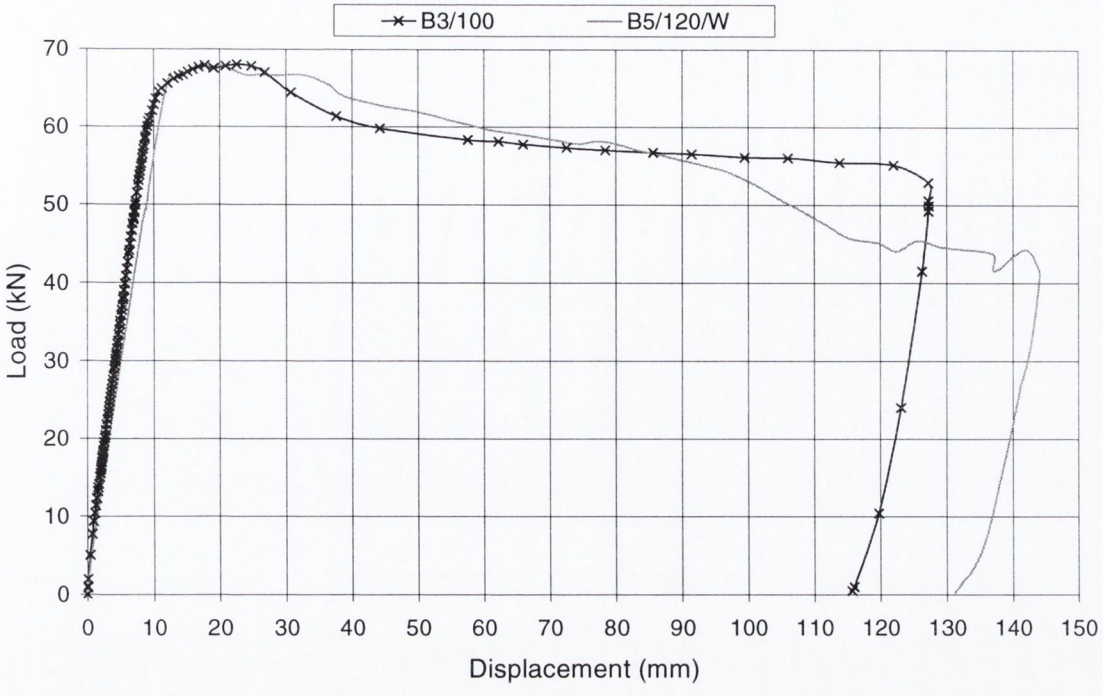

Figure 4.8: Load-displacement response of specimens B3/100 and B5/120/W

Figure 4.8 is the load-displacement response of specimens B3/100 and B5/120/W. B3 achieved a displacement ductility factor of 7.7, while B5 achieved a slightly higher ductility of 8.8 - these being the lowest displacement ductilities of the five beams tested. The load-displacement responses of the two beams are more or less the same up to their ultimate load. However, beyond this point the beams behave slightly differently. Initially, B5 displays the superior load carrying capacity, but by displacements of 80mm, its load carrying capacity begins to decrease whereas B3 continues to carry load with little reduction in its capacity. For the definition of displacement ductility used, B5 has the superior capacity, although, if the ultimate displacement had been defined for a larger drop in load capacity, B3 may have been slightly superior. Notwithstanding this, both beams behaved quite similarly, and both collapsed at displacements of approximately 130-140mm. The comparable behaviour of the two beams is another positive indication of the benefits of wireballs since B5 had a larger link spacing than B3 and yet performed more or less as well due the inclusion of wireballs.

4.3.3 Strain response

The middle base bars of each beam were strain gauged along their length (Section 3.3.1) allowing the longitudinal strain profile of the beams to be recorded at different load levels. This provides information on the development of plastic hinges with loading. Figures 4.9 to 4.11 present these strain profiles for loads of 50%, 75% and 100% of the ultimate load.

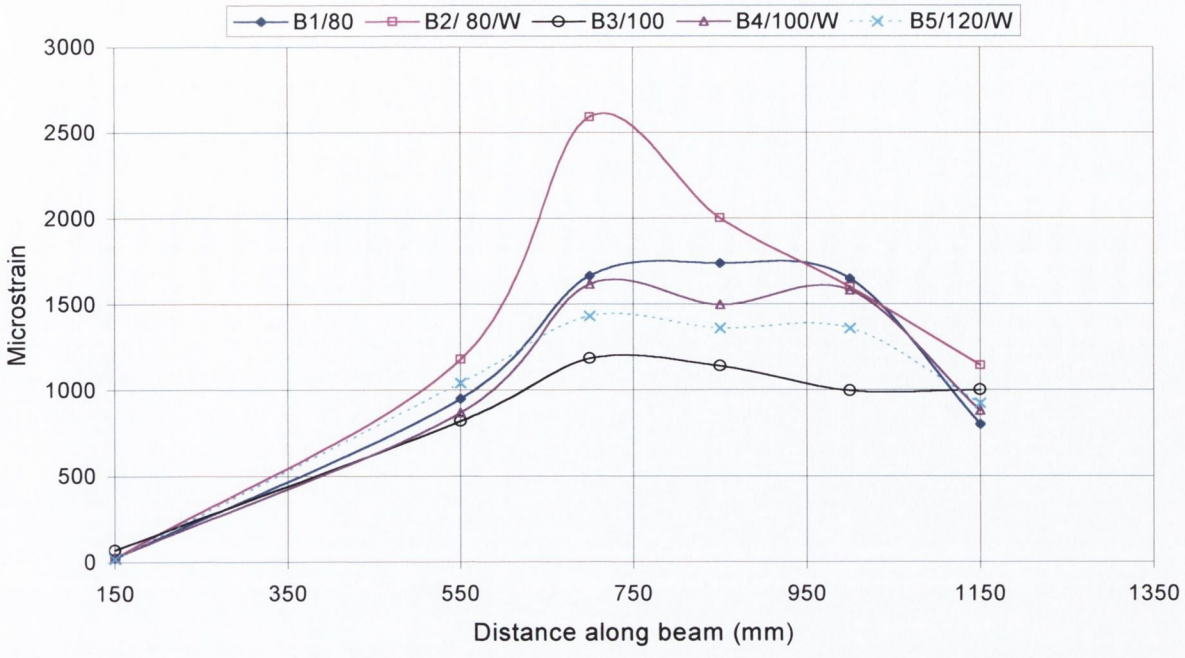

Figure 4.9: Longitudinal strain profile at 50% ultimate load (Test Series 2)

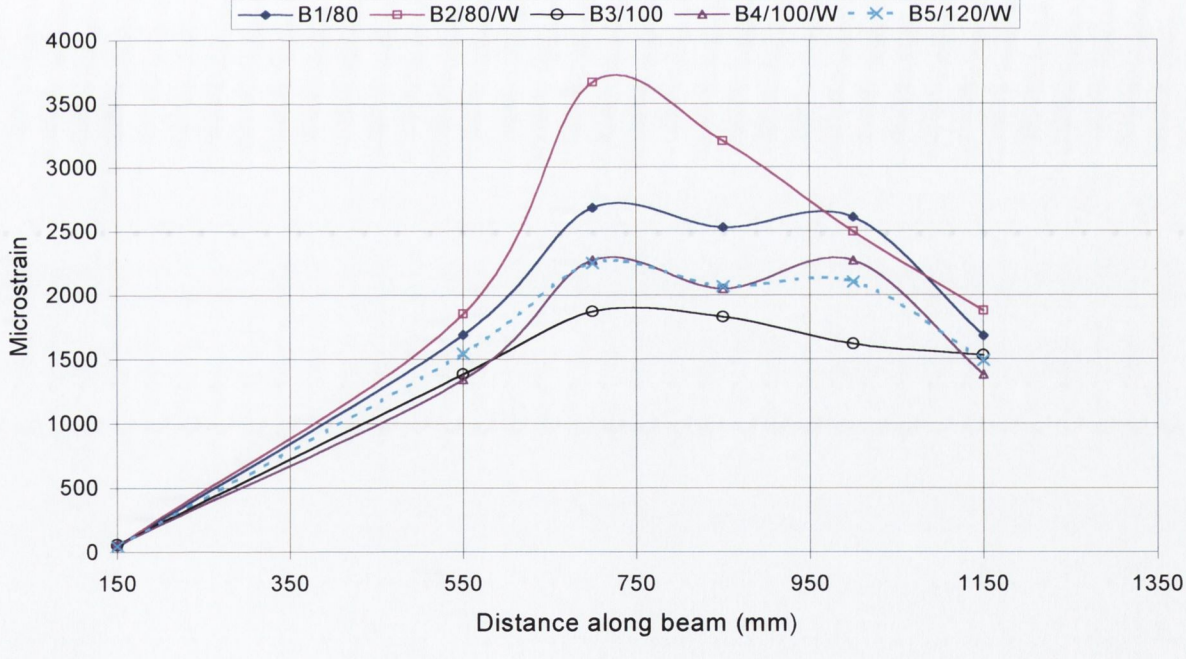

Figure 4.10: Longitudinal strain profile at 75% ultimate load (Test Series 2)

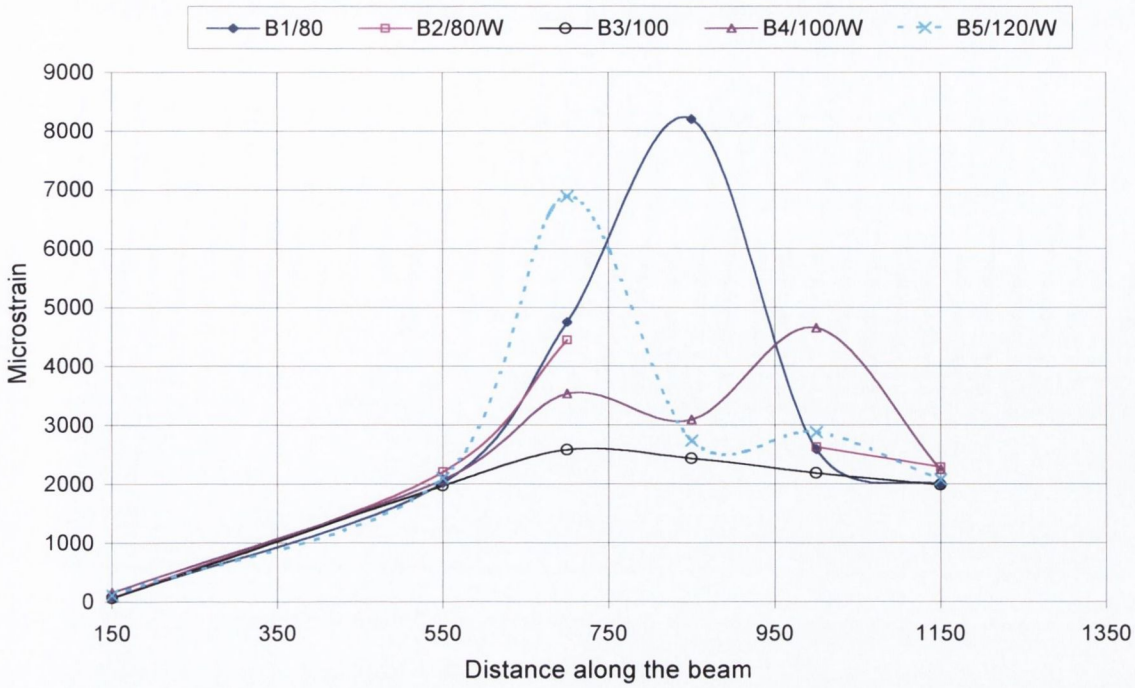

Figure 4.11: Longitudinal strain profile at 100% ultimate load (Test Series 2)

By 50% of the ultimate load, the only beam to have developed a plastic hinge region is B2/80/W. Visually the beam was observed to fail through flexural cracks forming at the centre of the beam, and these cracks widened as the steel underwent plastic elongation. The strain profiles along the beams show that in all of the beams, the strains are noticeably higher around the central region. Even in the four beams that have not reached yield, the regions of potential plasticity are easily identifiable by "plateau" regions of strain. Within these regions the strain is constant and approaches yield level whereas elsewhere along the beams strains remain quite low. On reaching loads of 75% the ultimate load, all of the beams, except B3/100, have developed plastic hinge regions extending about 200mm either side of the beam centre. Obviously, all of the beams develop a plastic hinge region by ultimate load, as illustrated in Figure 4.11. At ultimate load, the strain gauge at 850mm in specimen B2/80/W had stopped reading. The majority of the strain gauges failed to provide accurate readings beyond ultimate load.

Table 4.4 summarises the approximate plastic hinge lengths of the beams, obtained from strain readings at 50%, 75% and 100% ultimate load levels. With the exception of B3/100, all of the beams had developed plastic hinge regions, spreading 400-550mm about the midpoint, at 75% of ultimate load level. By ultimate load these plastic hinges had lengthened to 600 to 685mm about the centre. Notably, B3/100, which had not developed a plastic hinge at 75% of peak load, eventually developed a hinge region of similar proportions to the other beams. However, from Figure 4.11, it is evident that its strain values within this region were lower than in any of the other beams.

In summary, the ultimate plastic hinge lengths of all the beams were of similar lengths, approximately 600-685mm. However, it is clear from Table 4.5 that the beams with closer link spacing plus wireballs had slightly longer plastic hinge lengths than the other specimens for the three load levels considered. This may suggest that smaller link spacings in combination with wireballs promotes development of larger plastic hinge regions and less localised failure.

Beam	**Plastic hinge length at 50% ultimate load level (mm)**	**Plastic hinge length at 75% ultimate load level (mm)**	**Plastic hinge length at ultimate load (mm)**
B1/80	0	500	600
B2/80/W	210	547	685
B3/100	0	0	600
B4/100/W	0	403	636
B5/120/W	0	397	620

Table 4.4: Plastic hinge lengths in beams of Test Series 2

4.3.4 Conclusions

The results of these tests give positive indications that wireballs can enhance the ductility of reinforced concrete, and justify further testing to provide more conclusive evidence of the benefits of wireballs.

Despite these positive indications, the response data are somewhat limited. The specimens were designed to fail in flexure with the development of a substantial plastic hinge. The aim was to determine whether, with increased compressive strains, the wireballs would provide effective concrete confinement. Unfortunately, the manner in which the beams failed did not allow a satisfactory assessment.

Ductile failure implies that failure occurs through the formation of flexural cracks. With increased loading, the width of these cracks increases as the steel undergoes plastic elongation, and large increases in strain also occur in the extreme compressive fibre of the concrete. With this increase in strain, the distribution of stress in the concrete becomes distinctly non-linear and there is an increase in the mean stress in the compressive block (Figure 4.12). An increase in compressive stress implies that the neutral axis depth must decrease to ensure equilibrium of the internal forces. The design value recommended by EC2 for the strain, in the extreme compression fibre, at which the ultimate strength of a specimen is reached is 0.0035. Any increase in strain beyond this level and crushing of the compression region is assumed to commence. For the wireballs to be given a

real chance to prove their confinement effectiveness, the compressive strains in the specimens would have had to be higher than they were. This would have occurred if the section had been designed such that its failure would have been less under-reinforced and more approaching that for balanced failure. Beams are defined as balanced if their neutral axis depth to section depth ratio (*x/d* ratio) is equal to 0.603 (O'Brien *et al.*, 1995). Any beam with a ratio less than this is under-reinforced. Equations 4.1 and 4.2 and Figure 4.13 detail where the *x/d* ratio of 0.603 for balanced failure derives from.

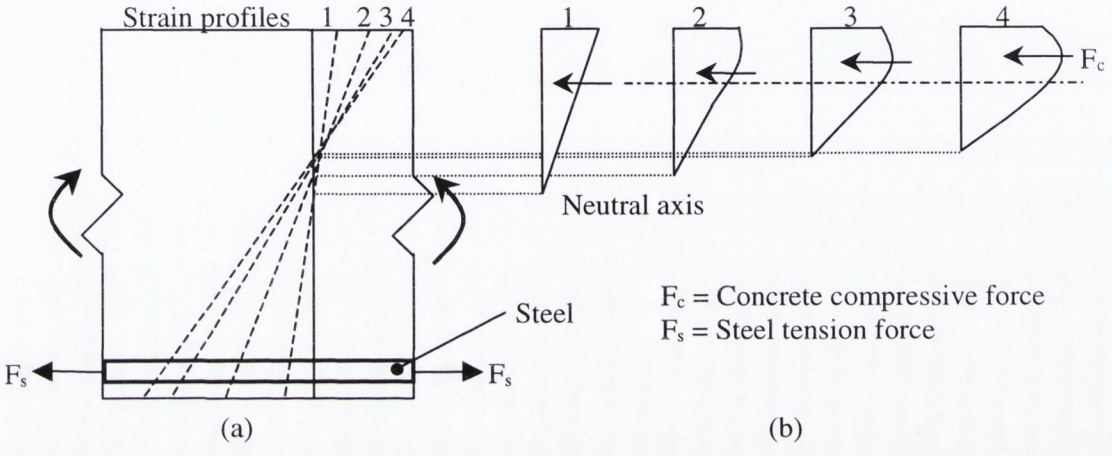

Figure 4.12: Compressed concrete section as the bending moment is increased up to ultimate flexural strength (a) Beam element with strain profiles (b) Stress profiles

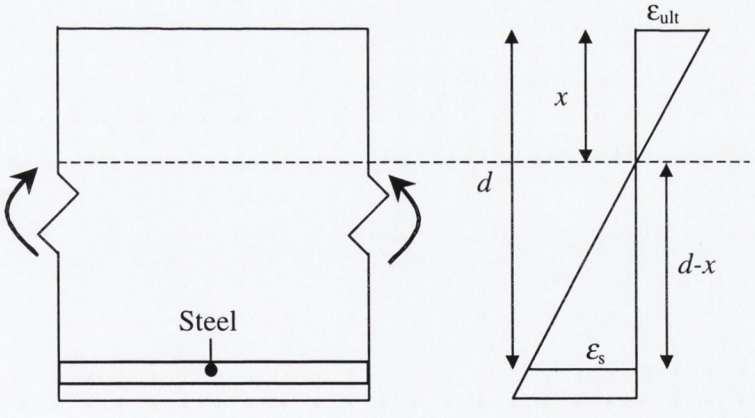

Figure 4.13: Strain profile at ultimate strength

$$\frac{\varepsilon_{ult}}{x} = \frac{f_y / E_s}{d - x} \tag{4.1}$$

$$\frac{0.0035}{x} = \frac{460/200000}{d - x} \text{ from which } x \text{ is determined} \tag{4.2}$$

where:

ε_{ult} = ultimate concrete compressive strain (EC2 value of 0.0035)

x = neutral axis depth (mm)

d = depth to steel (mm)

f_y = assumed steel yield strength of 460N/mm^2

E_s = assumed steel Young's Modulus of 200,000N/mm^2

For the chosen beam section, the *x/d* ratio was calculated as 0.15, for a concrete strength of 40N/mm^2 (as in the case of the majority of the beams). The ratio was calculated by considering the beam as a singly reinforced section. If the beam *x/d* ratio had been closer to 0.603, for balanced failure, conditions would have been more conducive for the wireballs' effectiveness to be tested, because the compressive strains in the concrete, through the beam depth, would have been closer to crushing strain. This could have been achieved by (i) increasing the cover to the bottom steel (ii) decreasing the concrete strength and (iii) increasing the bottom steel content. Increasing the cover would mean a decrease in the depth, *d*, to the steel, while a decrease in concrete strength or an increase in base steel content, would increase the neutral axis depth and hence, the compressive strains.

4.4 Test Series 3: Simply-supported beams with to ¼ point loading

4.4.1 Visual observations

This test series contained four beams, two containing wireballs and two containing no wireballs. The two beams without wireballs failed in shear through the development of 45° shear cracks running between the supports and the points of loading. On the other hand, the beams with wireballs failed in flexure with vertical cracks forming at the base of the beams. In S3/150/W these cracks formed slightly to one side of the centre but in S4/150/W they formed at the beam centre. Some shear cracks also developed at the supports of the wireball reinforced beams but these were smaller than the flexural cracks and much less severe than in the previous two beams without wireballs. Figure 4.14 illustrates one of the beams that failed in shear while Figure 4.15 shows flexural cracks that occurred in specimen S4/150/W.

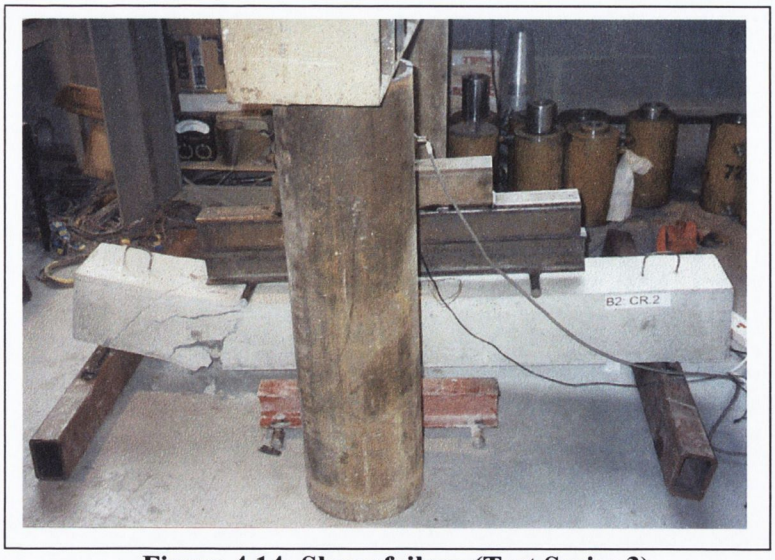

Figure 4.14: Shear failure (Test Series 3)

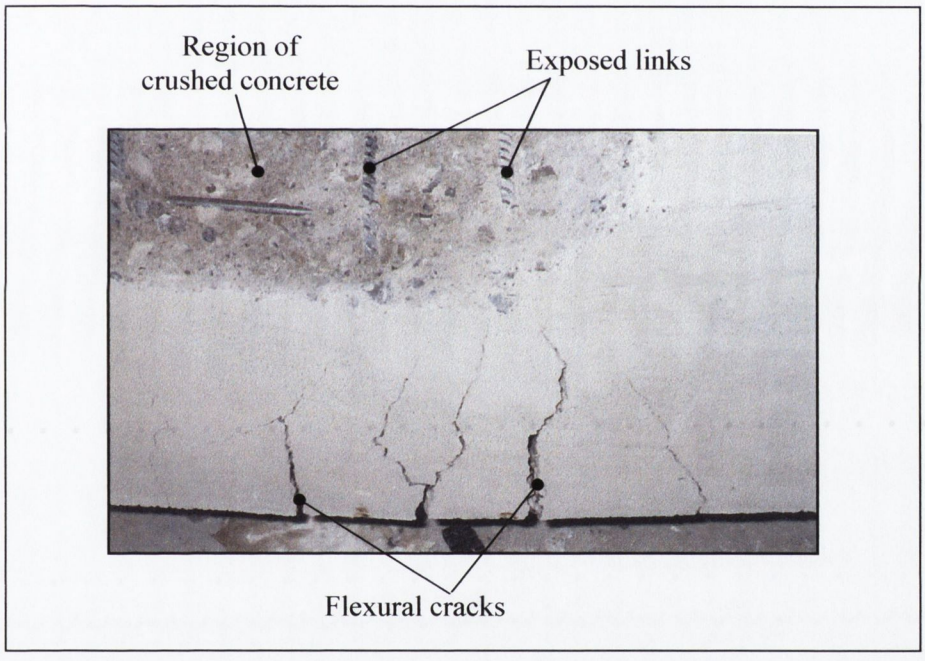

Figure 4.15: Flexural failure (Test Series 3)

4.4.2 Load-displacement response

The specimens were tested in monotonic compression under a ¼ point loading arrangement as detailed in Section 3.4. The results are tabulated in Table 4.5 below where the quantities are as defined in Section 4.3.2.

In terms of cylinder strength, initial stiffness and yield displacements the beams were alike, although S4/150/W was somewhat less stiff, and had a larger yield displacement than the other

beams. There are significant differences between the yield loads of the pairs of beams and these are reflected in the peak loads. Both of the wireball reinforced beams are considerably stronger than the specimens without wireballs. From the ratios of ultimate to predicted strength, it is clear that while the predicted strength was very accurate in the case of the lower strength specimens, it under-predicted the strengths of the wireball reinforced specimens by 20-27%. These results indicate the potential of wireballs to increase shear strength.

Specimen	f_{ck} N/mm^2	K_i N/mm	P_y kN	Δ_y mm	P_{ult} kN	P_p kN	Δ_{ult} mm	μ_Δ	P_{ult}/P_p
S1/150	16.8	14.3	113.5	8.2	119.0	121.3	20.33	2.5	0.98
S2/150	15.2	15.3	114.8	8.7	125.7	119.3	18.33	2.1	1.05
S3/150/W	16.0	15.0	133.2	8.6	145.7	121.3	51.0	5.9	1.20
S4/150/W	16.8	11.7	144.2	12.0	150.9	119.3	50.6	4.2	1.27

Table 4.5: Simply-supported beams, subject to ¼ point loading, results

Figure 4.16 presents the load-displacement response of the four beams. There are distinct differences between the behaviour of beams with and without wireballs; the wireball reinforced beams are stronger and considerably more ductile than the beams with no wireballs. The ultimate displacements in Table 4.5 are just prior to beam failure. In the case of the wireball reinforced beams the ultimate displacements are more than twice those attained in the beams without wireballs. The distinct differences between load-displacement plots and displacement ductility values of beams relate well to the modes of failure that were observed during testing.

4.4.3 Conclusions

The beams within this test series had a low shear span to depth ratio such that a shear failure was expected. The aim of the tests was to determine whether the inclusion of wireballs would affect the failure mode and promote flexural rather than shear failure. The wireball reinforced specimens did indeed fail in flexure, whereas the other beams failed in shear. Overall, the wireball reinforced specimens were stronger and considerably more ductile.

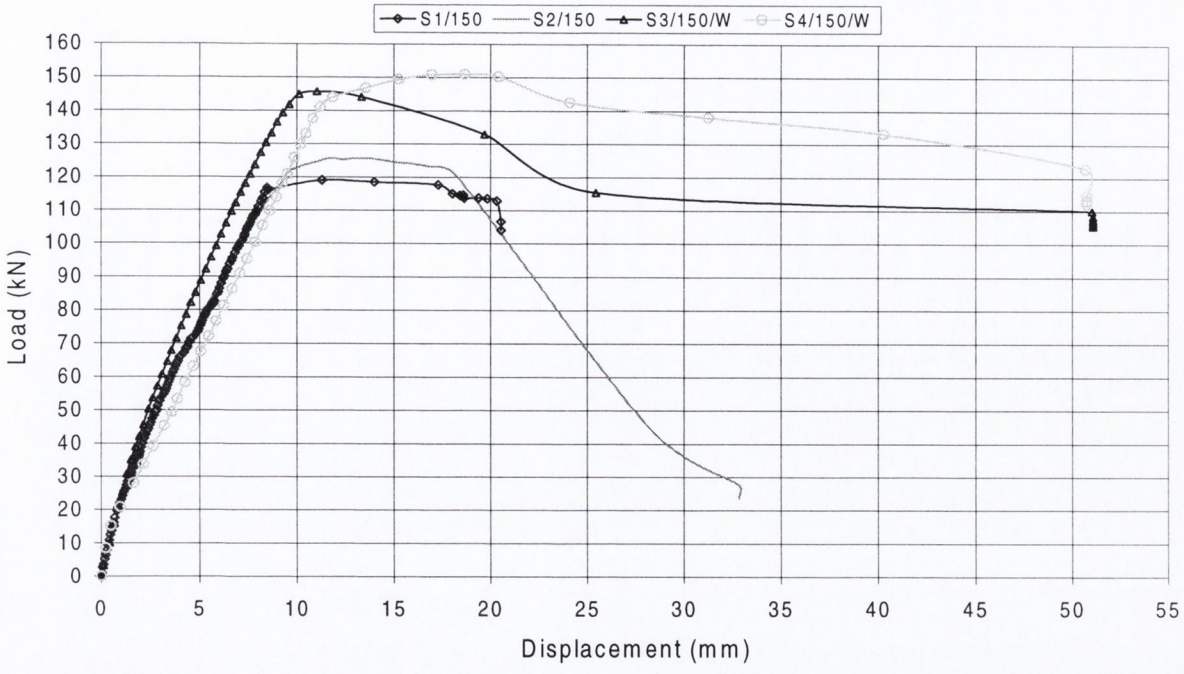

Figure 4.16: Load-displacement response for beams of Test Series 3

4.5 Test Series 4: Beam-to-column connections

The objectives of these tests were twofold. The results of Test Series 3 indicated that wireballs may increase shear strength and promote flexural failure. Therefore, the first objective of these tests was to investigate further the shear strength benefits of wireballs, because the connections were designed to fail in shear due to their substandard reinforcement detail. This test series was the first to have cyclic loading. Hence, the second objective of the tests was to determine appropriate specimen size, reinforcement detailing, and experimental set-up to allow thorough testing of wireball reinforced specimens under lateral cyclic loading within the restrictions imposed by the available laboratory equipment.

4.5.1 Visual observations

Four specimens were tested within this test series, as described in Section 3.5. All of the specimens failed in a similar manner. They each developed a localised plastic hinge at the beam-column joint interface and, in three of the four specimens, final failure was due to rupture of one or two of the longitudinal steel bars. None of these bars ruptured in specimen C1.2/145/W, and the specimen did not fail. By the end of each test, cracking at the joint interface was significant with deep cracks extending into the specimen cores such that the beams and columns were almost completely separated.

Figure 4.17 illustrates the specimens after failure. Damage elsewhere in the specimens was limited, as is clear from Figures 4.17(a) and 4.17(c). In the joint region, a criss-cross pattern of shear cracks developed in all of the specimens. However, with the exception of specimen C1.3/145 (Figure 4.17(d)), this cracking was not severe enough to initiate cover spall of the concrete. In specimen C1.3/145 the cover concrete did spall from the joint region, exposing the transverse steel. In the beams, hairline cracks developed at the beam corners, usually forming at the position of a link.

After the tests, the cover concrete of the lower beam sections was removed by means of a Kango hammer to allow inspection of the core concrete. This was observed to be completely intact in all the beams, except at the joint interface (Figure 4.17(b)). It was also observed that the links were free from distortion of any kind, while damage to the longitudinal steel was restricted to the interface area where the steel had elongated, and in some cases fractured.

4.5.2 Load-displacement and moment-displacement responses

Table 4.6 details the results of the four tests. The results for each property are the average of the positive and negative sides of the hysteresis curves. There is little distinction between the results of the specimens. The concrete cylinder strengths (calculated by multiplying the cube strengths by a factor of 0.8) range from 40.8 to 46.1N/mm^2, while the initial stiffness values lie between 2.0N/mm and 3.4N/mm. The yield displacements ranged from 10.5mm to 12.1mm. The lowest yield moment was 12.5kNm (C1.2/145/W) and the highest yield moment was 14.1kNm (C1.1/85/W). With respect to Figure 4.2, the yield point was defined, using the Secant Method, by dropping a vertical line onto the hysteresis curve from the intersection point of a secant, running through the origin and 75% of the ultimate strength, and the horizontal line running through the ultimate load.

The ultimate displacement is defined as either the displacement at which first fracture of a longitudinal bar occurred, or the displacement when the resistance had decreased by 15% below ultimate. The ultimate moment is the maximum observed moment. There is a difference of 3.8kNm between the strongest specimen (C1.2) and the weakest specimen (C1.3). However, the ultimate displacements of the specimens are more or less the same, as are the displacement ductility ratios. The ratios of ultimate moment to predicted moment show that the predicted moments were very accurate in the specimens without wireballs but much less accurate in specimens with wireballs where the ultimate moments were under-predicted by 20-30%.

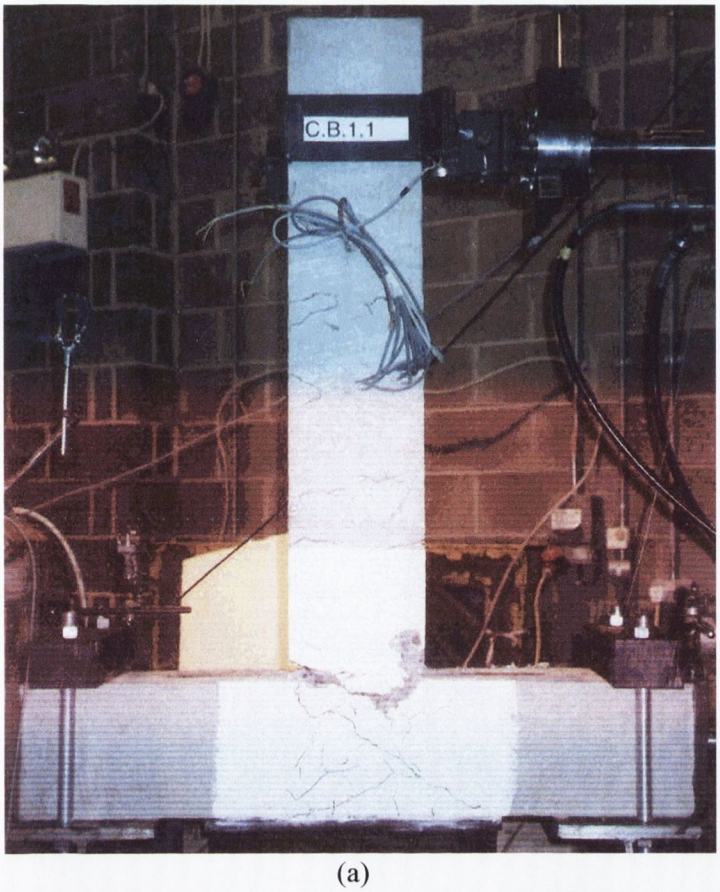

(a)

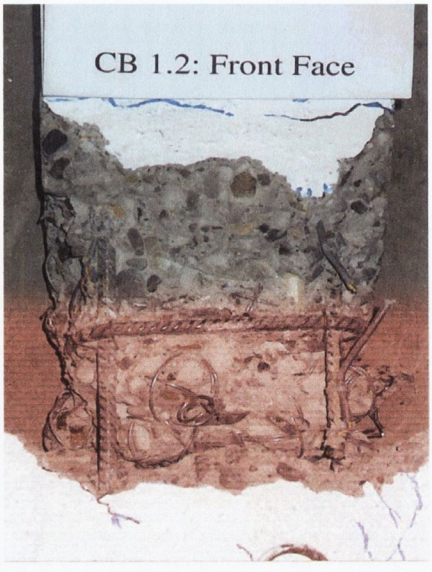

(b)

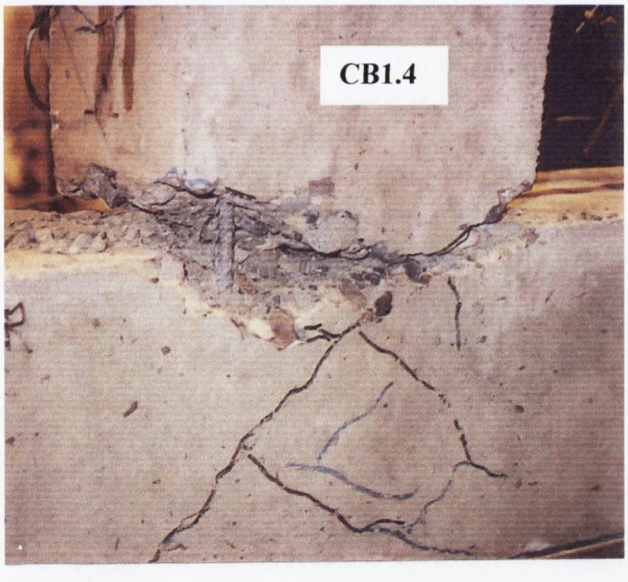

(c)

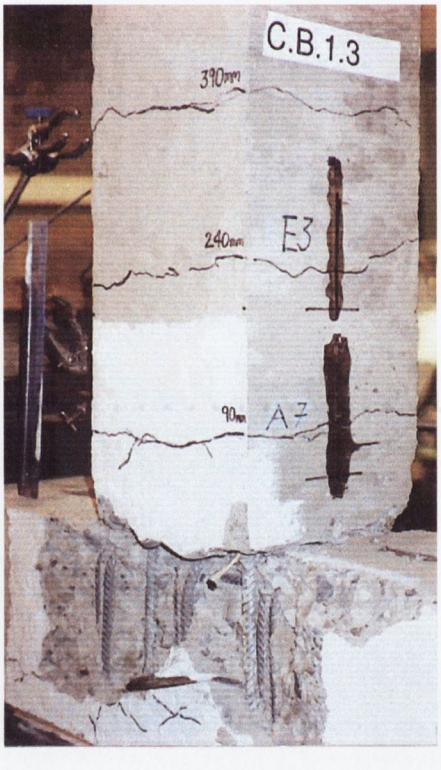

(d)

Figure 4.17: (a) C1.1 (or "CB1.1") localised failure at beam-column interface (b) Detail of base beam section of C1.2 (or "CB1.2") after cover was removed (c) C1.4 (or "CB1.4") detail of beam-column interface (d) C1.3 or ("CB1.3") Cover spall of column

Specimen	f_{ck} N/mm^2	K_i N/mm	Δ_y mm	M_y kNm	Δ_u mm	M_u kNm	M_p kNm	M_u/M_p	μ_Δ
C1.1/85/W	46.1	2.5	10.7	14.1	37.2	16.7	13.9	1.2	3.5
C1.2/145/W	40.8	3.4	12.1	12.5	38.1	18.0	13.8	1.3	3.2
C1.3/145	46.1	2.0	10.5	13.1	38.4	14.2	13.9	1.0	3.6
C1.4/50	46.0	2.4	11.2	13.1	37.7	15.1	13.9	1.1	3.4

Table 4.6 Beam-column connection results

4.5.2.1 Hysteresis curves:

Figures 4.18 to 4.21 present the load-displacement hysteresis responses of the four specimens. All four specimens behaved in a stable manner and their hysteresis curves are very similar. The hysteresis loops are pinched; during early displacements in each loop there is little increase in load with increasing displacement, such that the loops display a delayed peak stiffness rather than an initial peak stiffness. This behaviour is a direct consequence of the specimens' failure modes, which were governed by a localised plastic hinge at the beam-column interface. This meant a significant crack developed at the beam-column interface and the steel elongated locally at this point, while the rest of the specimen remained more or less intact. Over the initial portions of the hysteresis loops, the load is carried by the steel alone since a localised crack formed at the joint at an early stage in the test. This is because, when the steel yields in tension, cracks form in the tension zone which, because of plastic elongation of the steel, cannot close when the load returns to zero. When the direction of load reverses, the steel has to yield in compression before the tension cracks can close and allow some of the compressive force to be transferred to the concrete. In other words, over large portions of loading, the concrete does not contribute to resistance, however, it does perform a vital function in preventing the longitudinal steel from buckling. When the load is being resisted by the steel alone the flexural stiffness is reduced, it increases when the cracks close and the concrete begins to carry compression, hence the delayed peak stiffness.

In three of the four specimens, fracture of one or two of the longitudinal bars occurred, resulting in the sudden losses in load capacity as evident in the curves. None of the longitudinal steel fractured in specimen C1.3, but during the final cycles its hysteresis loops became progressively convex, since the steel alone resisted load, such that only at very large displacements did the beam resist a significant load. A consequence of this behaviour is that the tensile steel underwent large deformations as the interface-crack tried to close. It is likely that, while the steel in C1.3 did not fracture, it was close to doing so when the maximum actuator displacement was reached.

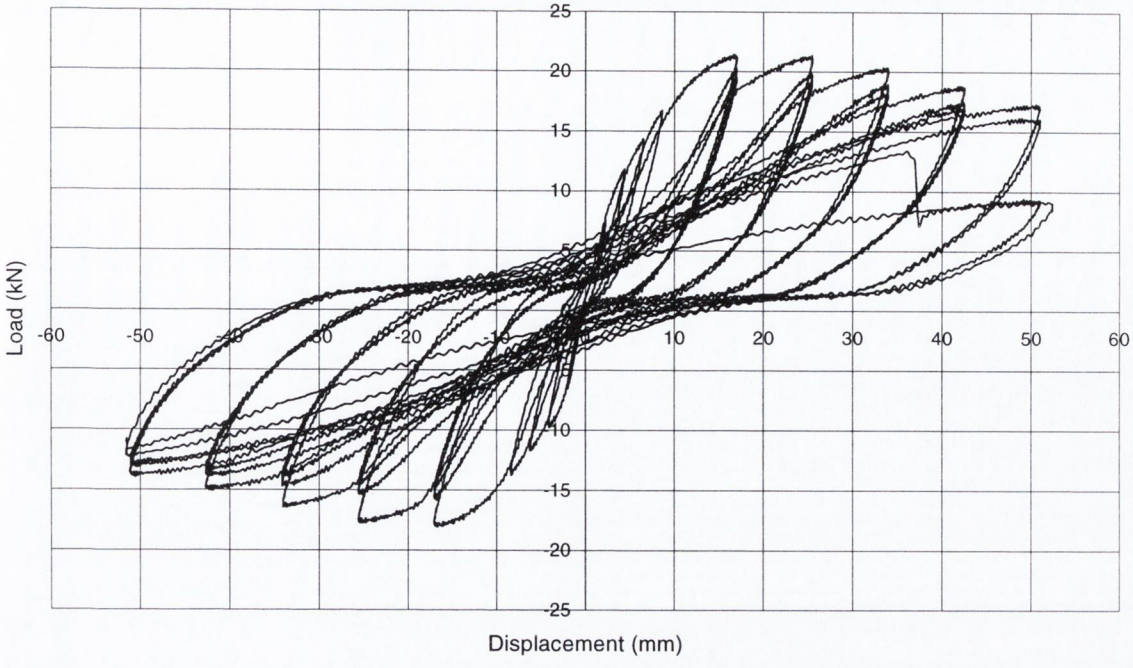

Figure 4.18: C1.1/85/W Load-displacement hysteresis response

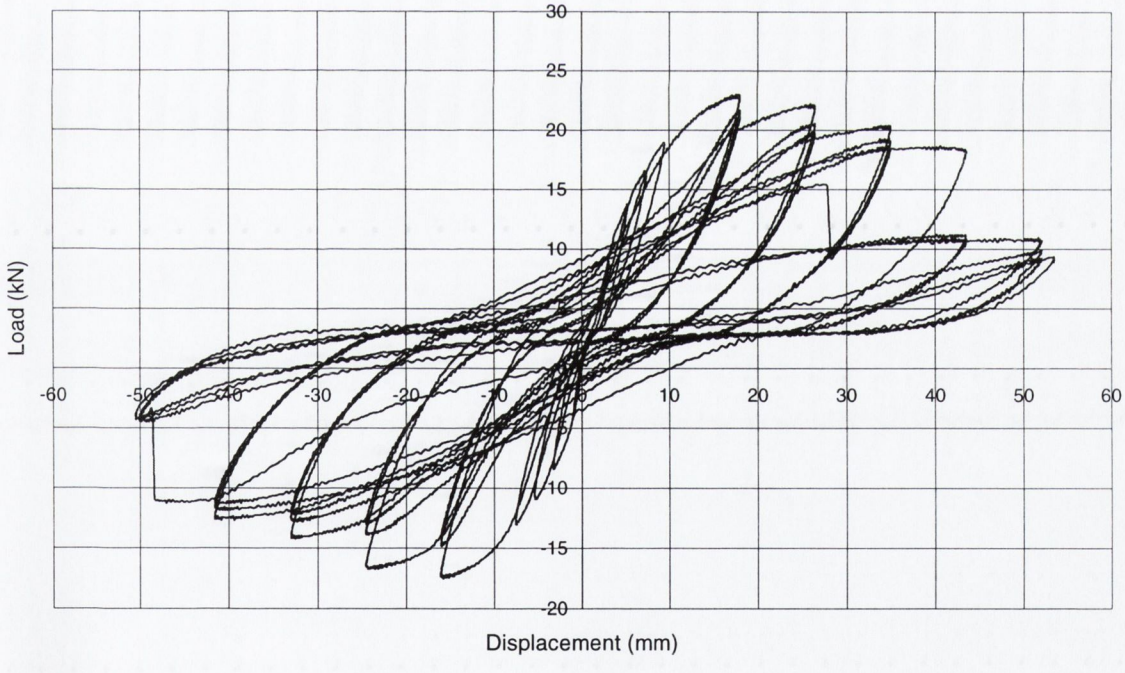

Figure 4.19: C1.2/145/W Load-displacement hysteresis response

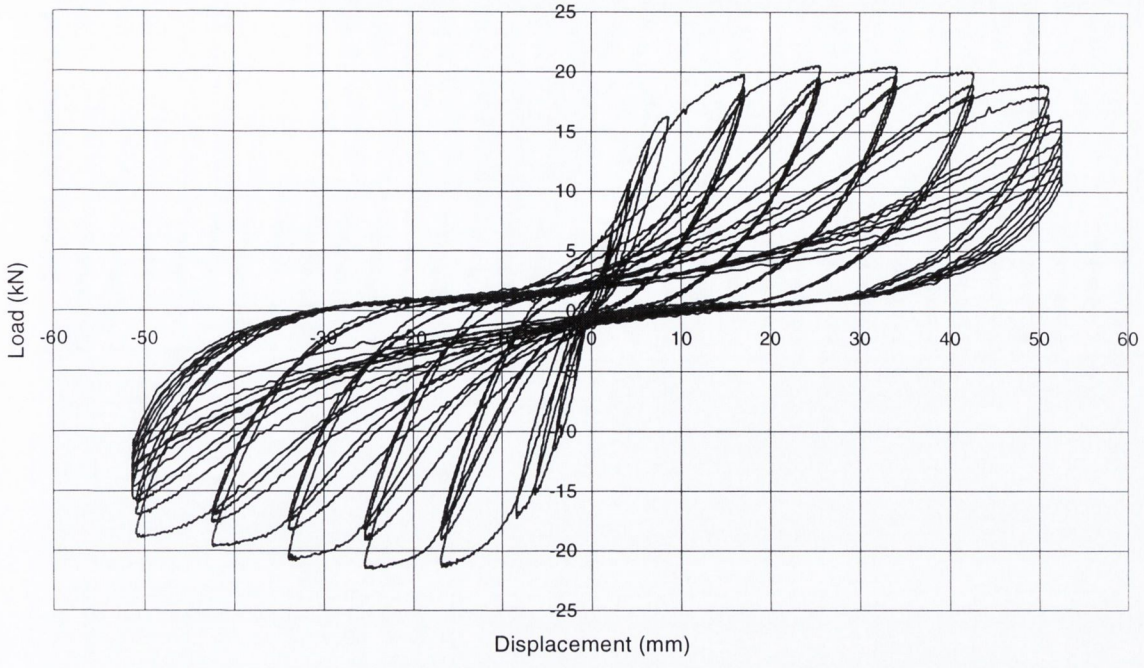

Figure 4.20: C1.3/145 Load-displacement hysteresis response

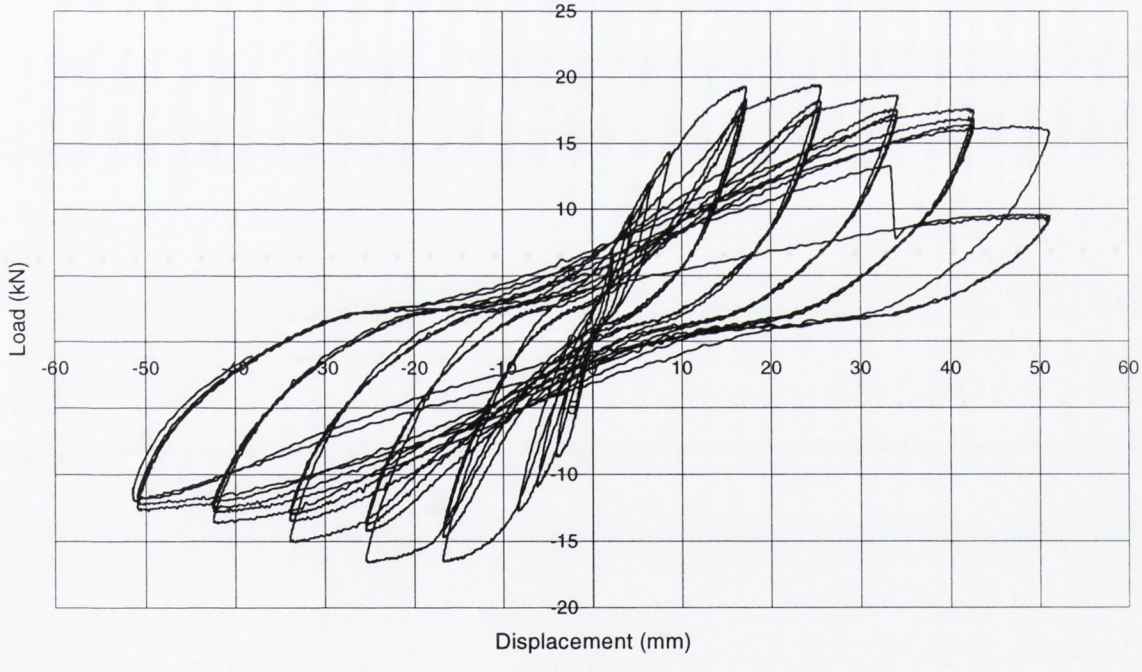

Figure 4.21: C1.4/50 Load-displacement hysteresis response

4.5.2.2 Energy dissipation

Figure 4.22 shows the average energy dissipated in each cycle by each specimen, where the dissipated energy equals the area within a hysteresis loop, and the average dissipated energy refers to the average of the energy dissipated during positive and negative force cycles. Up to and including cycle 5c, the dissipated energy levels of the specimens are very similar. During group cycle 6 the plots diverge a little, with specimen C1.2/145/W dissipating the most energy and specimen C1.3/145 dissipating the least. This divergence continues during group cycle 7. Specimen C1.2/145/W reaches its peak at cycle 8a, after which, with the exception of a small increase in cycle 9a, it loses capacity to dissipate energy. This loss in energy dissipation capacity is due to fracture of two of its longitudinal bars, one in group cycle 8 and the other in group cycle 9. All of the other specimens reach their peak in cycle 9a, beyond which a steady decrease in their energy dissipation capacities occurs. The lower capacity of C1.3 reflects the more convex shape of its hysteresis loops.

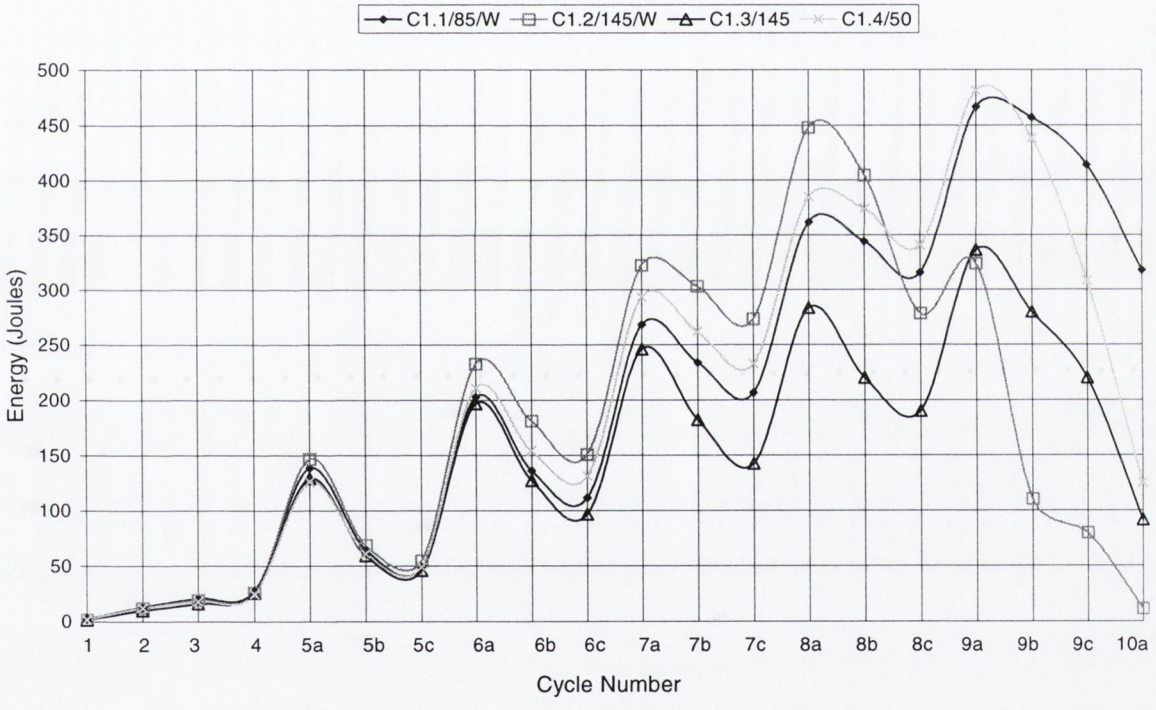

Figure 4.22: Test Series 4: Energy dissipation with respect to cycle

The energy dissipation results are inconclusive as regards the benefits of wireballs. Figure 4.23 shows the average (of positive and negative force cycles) total energy dissipated by each of four specimens. Specimen C1.1/85/W with the highest energy dissipation capacity contained wireballs but the difference between its capacity and that of specimen C1.4/50, without wireballs, is negligible. A more positive indication of the benefits of wireballs is that specimen C1.3/145, without wireballs, had the smallest energy dissipation capacity. Despite this, the results give no clear evidence that wireballs enhanced the behaviour of these specimens.

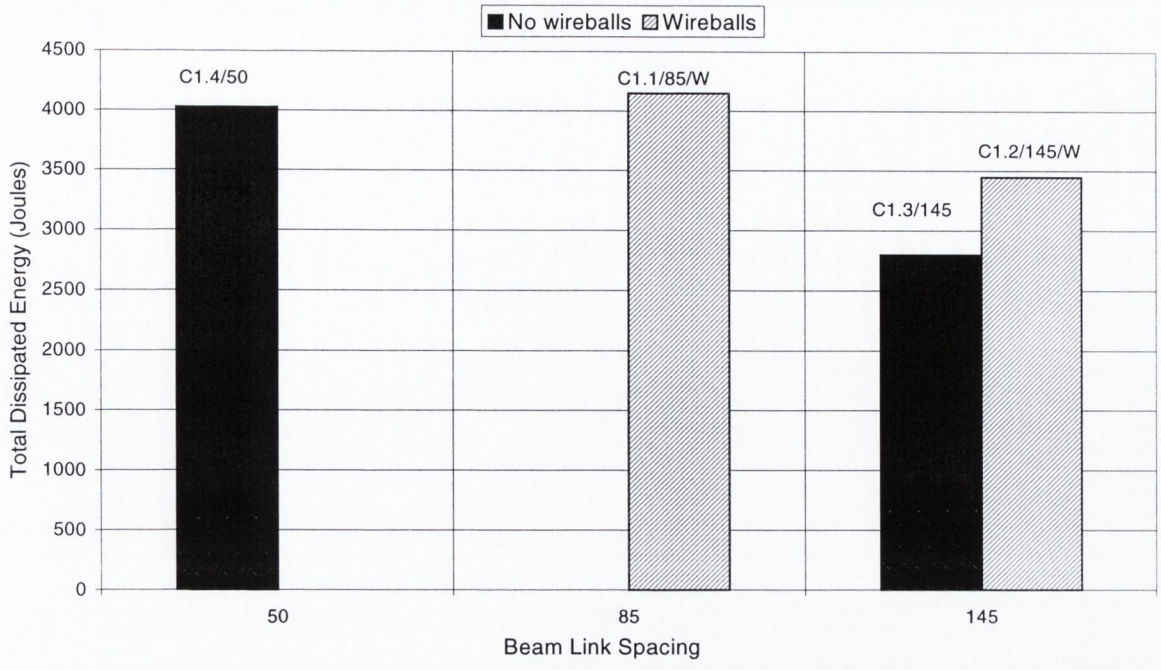

Figure 4.23: Test Series 4: Average total energy dissipation

4.5.2.3 Strain response

As described in Section 3.5.2, Bar 1 of each specimen was strain gauged along its length, and the first link above the beam-column interface was strain gauged at two locations. Unfortunately, the recorded data were not very accurate. Possible reasons for this lie in the method in which the steel bars were strain gauged. The gauges were adhered to the steel bars and then coated with a moisture proofing agent. Connection wires soldered to the gauge passed through the concrete to the exterior of the beam, where they were linked to the logging system. The presence of the moisture proofing agent lessens the degree of bond between the steel and concrete while the wire running through the concrete to the specimen exterior could exert a pull on the gauge and possibly tear it from the steel if the surrounding concrete was undergoing damage. However, the strain results in some of the specimens do illustrate how the strain concentrated around the beam-column interface. Figures 4.24 and 4.25 present plots of strain versus scan reading for specimens C1.1 and C1.3, where two scan readings were recorded every second. In the legends of these plots, a negative distance corresponds to a strain gauge position below the beam-column interface, that is within the joint region, whereas a positive distance corresponds to a point above the beam-column interface, in the beam. It is clear from both plots that higher strains occurred just below the joint interface rather than elsewhere along the beam.

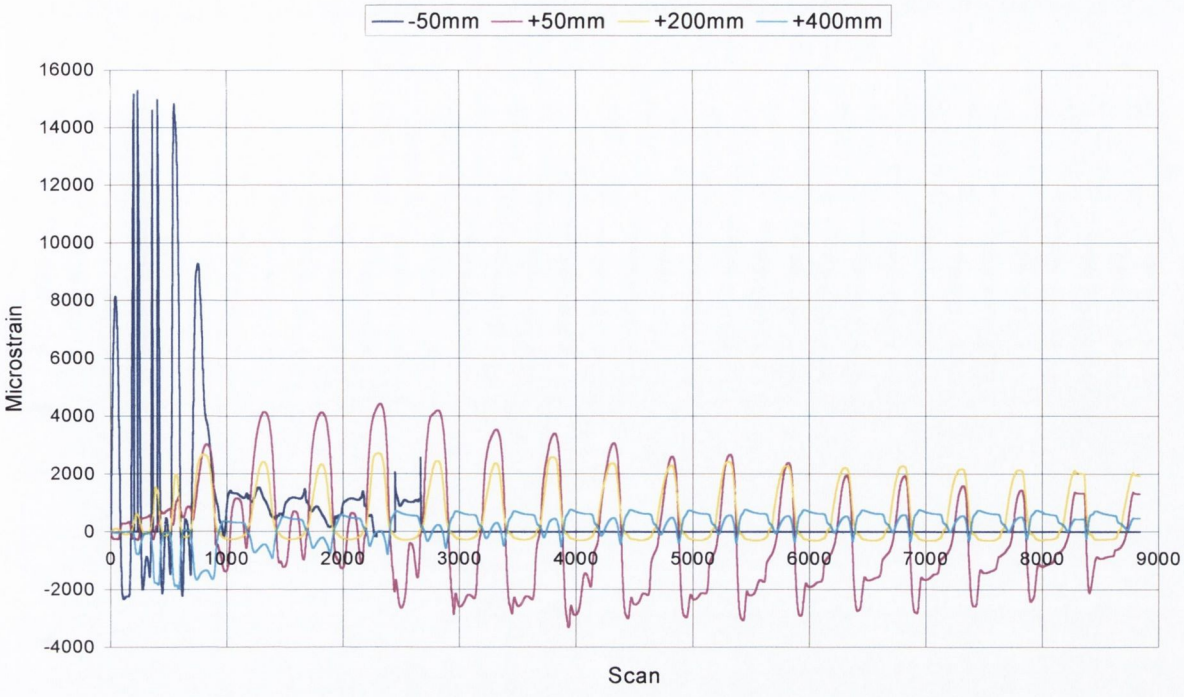

Figure 4.24: C1.1/85/W Bar 1 strains

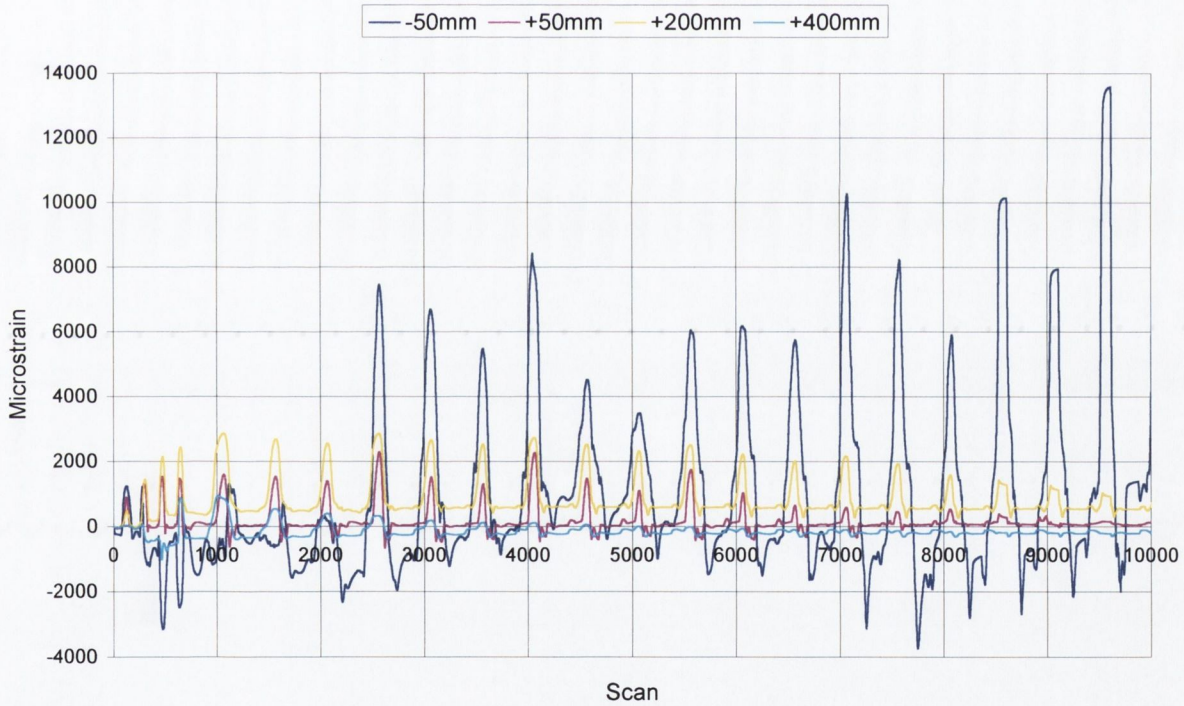

Figure 4.25: C1.3/145 Bar 1 strains

Figures 4.26 and 4.27 are strain plots, with respect to scan, for the first beam link in specimens C1.1 and C1.4. In each specimen strain was measured on two sides of the link – the side nearest the actuator and the side furthest the actuator. It was previously noted that the beams remained mostly intact throughout the tests, except at the beam-column interface, and that on removal of the cover, the links were observed to be undistorted. The very low strain levels recorded in the links

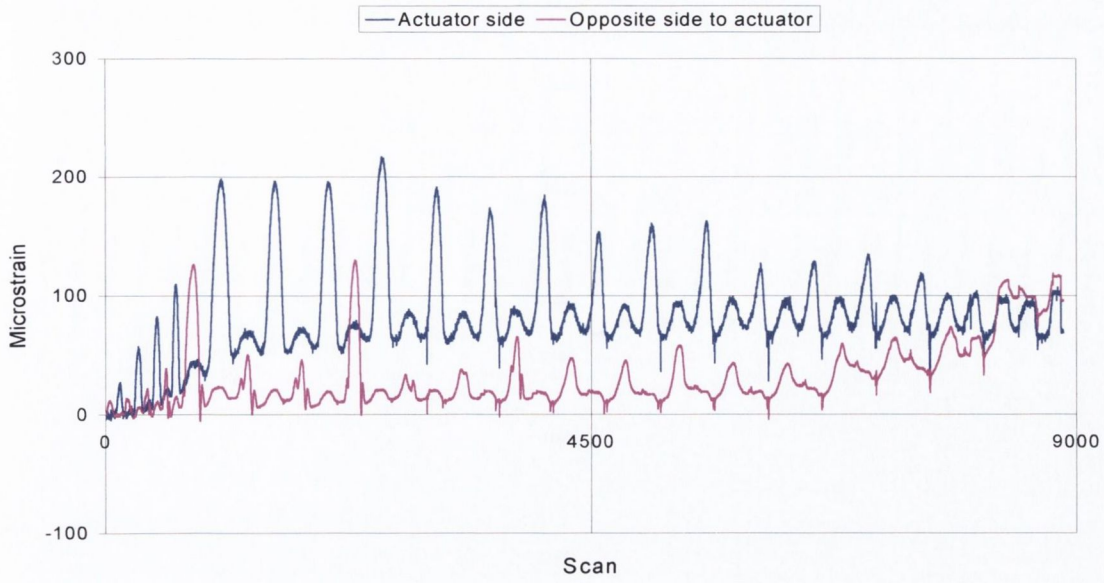

Figure 4.26: C1.1/85/W Strain in the first link up from the beam-column interface

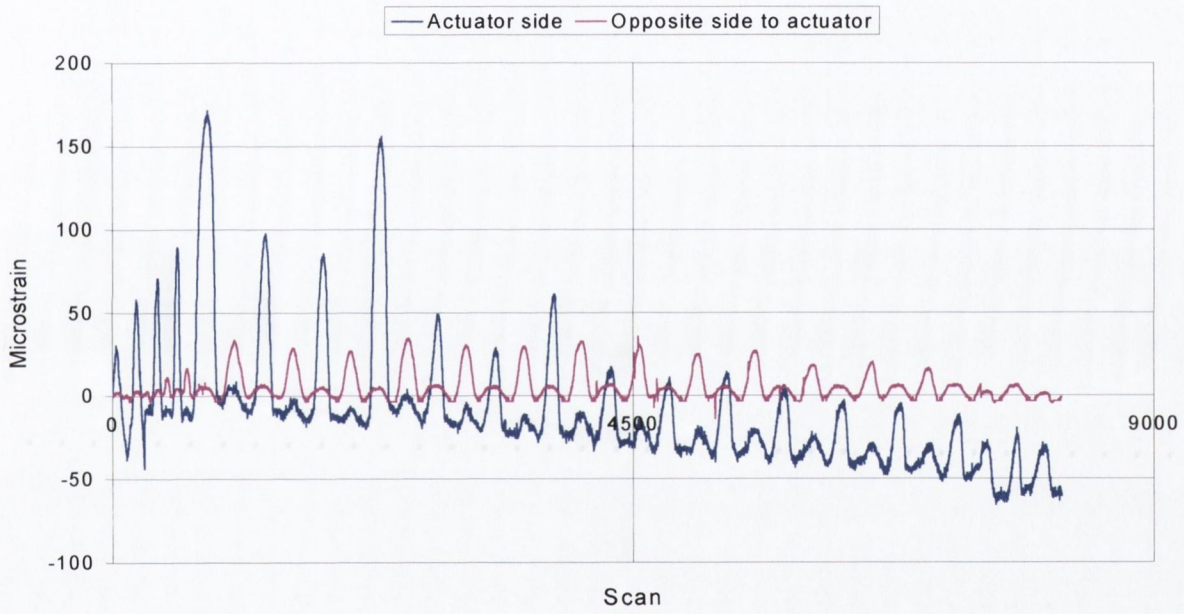

Figure: 4.27: C1.4/50 Strain in the first link up from the beam-column interface

during testing confirm this observation. In Figure 4.27 the baseline of the strain measured on the actuator side of the link displays some negative drift. However, the fact that the baseline drift is so clear accentuates the very low levels of strain that occurred throughout the test.

4.5.3 Conclusions

The four specimens of this test series behaved similarly irrespective of whether or not they were wireball reinforced. Their displacement ductilities and hysteresis curves were almost identical. The somewhat greater energy dissipation capacity of the wireball-reinforced specimens may link

wireballs with increased energy dissipation capacity, but with respect to these results, it is a tentative link. The failure mode of the specimens was not favourable to testing the confinement effectiveness of the wireballs, since once the interface crack had formed it was the steel alone, rather than the steel *and* concrete, that was providing load resistance. As the concrete strains never reached high values, wireballs could not play an effective confinement role. It was stated already, that one objective of these tests was to investigate further the shear enhancement properties of wireballs. However, where the failure mode of the specimens was not conducive to testing their confinement effectiveness, it was not conducive to testing their shear enhancement potential either.

4.6 Test Series 5: Beams subject to lateral loading

Two beams with the same dimensions but different longitudinal steel contents were tested within this test series. The two test specimens are described in Section 3.6. The purpose of these tests was to provide guidance on the most suitable specimen design and test set-up in which to assess the confinement properties of wireballs, taking into account the available laboratory equipment. More specifically, the aim was to determine the best combination of specimen and loading to ensure the formation of a substantial plastic hinge region. Therefore, the objective of these tests was not to examine the effects of wireball reinforcement, nor are the results from the two specimens comparable. Nonetheless, the results and observations of the tests are included to illustrate, briefly, an important step in the design of the final test series.

4.6.1 Results

Both test specimens failed through the formation and growth of a local crack at the beam-column interface. Table 4.7 details the specimen results in terms of cylinder strengths, yield displacements and yield, ultimate and predicted moments.

Again, it is important to note that, since specimen C2 contained almost three times the amount of longitudinal steel as C1, and was subject to a different displacement history, the results are not directly comparable. Despite this, it is interesting to note that for both specimens the predicted moments were both greater, (12% and 28% respectively), than the experimental moments.

Specimen	f_{ck} N/mm^2	Δ_y mm	M_y kNm	M_{ult} kNm	M_p kNm	M_{ult}/M_p
C1	20.7	6.4	10.5	12.1	13.5	0.90
C2	23.9	25.7	27.2	29.9	38.2	0.78

Table 4.7: Laterally loaded beams - results

Figures 4.28 and 4.29 present the load-displacement hysteresis curves from the two tests. The hysteresis loops of C1 are convex and stable until two bars fractured on one side of the specimen. After this, its resistance fell off dramatically with large displacements occurring and little load resistance offered on one side. The bars fractured at a relatively low displacement level of 32mm, because the specimen failed through the development of a localised crack at the beam-column interface which meant that the longitudinal steel underwent large strains at this point. The hysteresis curves of specimen C2 are pinched from the start of the test, with large displacements occurring with negligible load resistance. A strange aspect of the load-displacement response of C1 is that, even in the first few cycles, the specimen does not appear to have any initial stiffness, since this does not seem feasible, it casts some doubt on the recorded load-displacement results. However, from visual observation, the specimen was seen to fail locally at the joint such that only the longitudinal steel provided resistance over most of the displacement cycles. Outside of the joint area, the specimen did not suffer much damage.

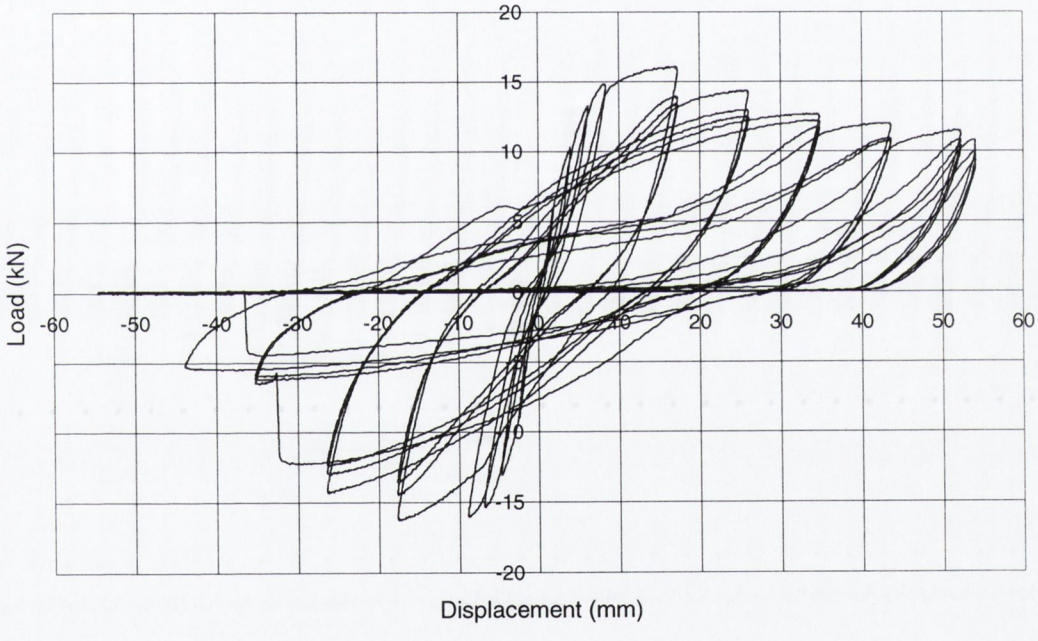

Figure 4.28: C1 Load-displacement hysteresis curve

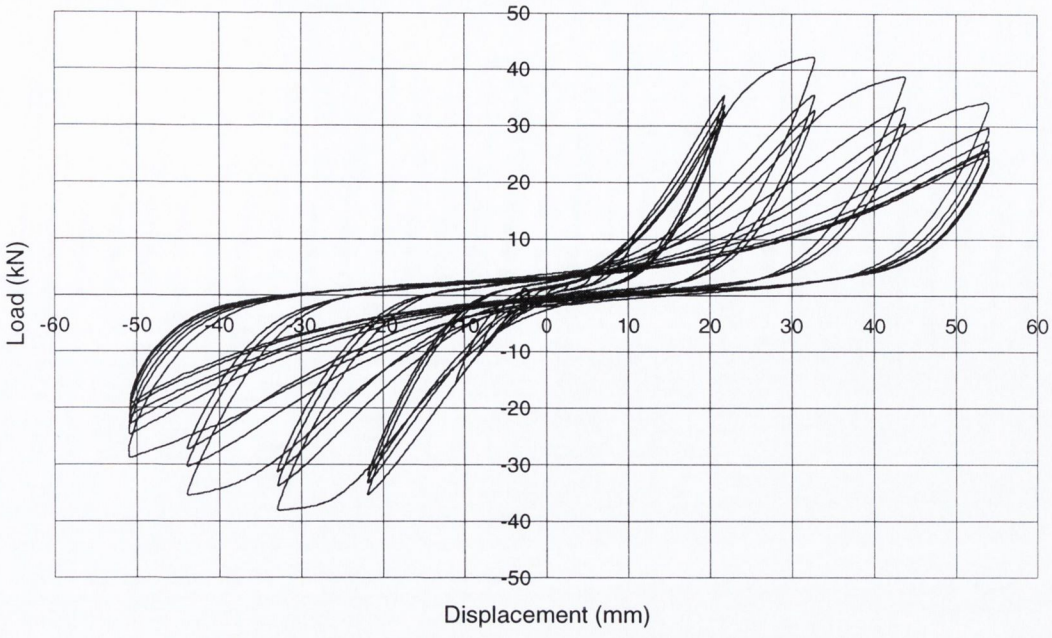

Figure 4.29: C2 Load-displacement hysteresis curve

4.6.2 Conclusions

These two specimens were intended as steps on the path to determining the best conditions, in terms of specimen form and testing type, to investigate the confinement effects of wireballs. Both of these specimens failed due to the formation of a localised plastic hinge region at the joint. This failure mode did not permit the concrete to work adequately in compression and, therefore, the potential of the wireballs was not tested. It was concluded that, to prevent this localised failure and to promote an extensive plastic hinge region, an axial load should be applied to the specimens in combination with the existing lateral loading. It was also considered that a specimen with the same reinforcement content as specimen C2 would behave better than one with the lower steel content of specimen C1 since none of the steel in C2 fractured.

4.7 Summary

Within the initial test series, a range of specimen types subject to different loading arrangements were tested. It was concluded from the first two test series, stub columns under monotonic compression and simply-supported beams in monotonic flexure, that wireballs can enhance confinement and, hence, ductility in compression and flexural members. The data indicated that the use of wireballs, in combination with conventional reinforcement, may allow a reduction in the level of transverse reinforcement required by EC8 without detrimental effect on specimen behaviour. However, the results also suggest that there is a limit on how much the link spacing can

be increased. This ties in with Eurocode 8 provisions for shear resistance and prevention of local buckling. For example, in the EC8 equations for calculating the required link spacing for local ductility, to prevent against longitudinal steel buckling the longitudinal bar diameter is one of the limiting factors. The confinement benefits of wireballs diminish the closer the link spacing is.

The third test series considered simply-supported beams designed to fail in shear. The results suggest that the addition of wireball reinforcement provides an increase in shear strength and a consequent significant increase in ductility. The inclusion of wireballs in these specimens appeared to promote the development of a plastic hinge rather than shear cracking. However, since only four beams were tested in this test series, more work is required to consolidate these findings.

The fourth test series examined the effects of wireballs in poorly reinforced beam-column connections subject to cyclic lateral loading. The failure mode, a localised crack at the beam-column interface, was not conducive to determining the confinement potential of wireballs since the concrete was not permitted to work in compression. However, a tentative link between increased energy dissipation and the presence of wireballs was proposed from the results; otherwise the inclusion of wireballs in these specimens did not appear beneficial. The failure modes of the specimens in the fourth test series did not test the shear enhancement potential of wireballs either.

The first purpose of all the above tests was to examine the effects of wireball in reinforced concrete under difference loading conditions. The second purpose was to determine the optimum specimen type, details and loading arrangement for the final test series which is discussed in the next chapter.

Finally, it should be noted that since the purpose of the above tests was to examine the effects of wireballs in reinforced concrete under different loading arrangements a more extensive range of data would be necessary in order to prove the statistical validity of the results.

CHAPTER 5

BEAM-COLUMN RESULTS

5.1 Introduction

This chapter considers the results from eight beam-column specimens, each subject to a combination of lateral cyclic loading, representative of earthquake loading (ECCS, 1986), and axial loading. The specimens all had the same dimensions and longitudinal steel contents but differed from each other in terms of the following three parameters:

(i) axial load level
(ii) link spacing
(iii) whether or not the specimen contained wireballs.

The aim of these tests was to determine whether, or not, the inclusion of wireballs increases a specimen's resistance to a combination of lateral cyclic and axial loading and, if so, whether their inclusion allows the level of links specified by EC8 to be reduced without detrimental effect on specimen response. The specimen details and test set-up have been discussed in Section 3.7.

The chapter is divided into several sections that discuss different aspects of the results. Section 5.2 considers all specimens together in terms of initial stiffness, yield points, moment capacities, displacement and rotation capacities. Section 5.3 presents the visual observations made during the tests, while Section 5.4 considers the hysteresis and moment-rotation curves of the specimens. In Section 5.5, the specimens are divided into three groups and their hysteresis characteristics are considered in detail in terms of energy dissipation and resistance. Section 5.6 then compares the effect of different link spacing on the specimens' ultimate displacements and total dissipated energy.

5.2 General results

Table 5.1 details the results of the eight specimens for both positive and negative displacements. Table 5.2 presents the average (of the positive and negative displacement responses) ultimate moments, ultimate moment to predicted moment ratios and ductility ratios. The approach of taking an average of the positive and negative values for these properties is considered reasonable since all the specimens were of the same general type and tested within the same laboratory set-up.

Therefore, it is considered that an average value provides a robust result which removes any variability, such as the longitudinal steel being slightly off-line or the specimen being slightly off-centre in the test set-up, which may occur between specimens.

The following properties of the specimens are provided in Table 5.1:

- Concrete cylinder strength (f_{ck})
- Yield load and displacement (P_y and Δ_y)
- Initial Stiffness (K_i)
- Yield and ultimate moment (M_y and M_u)
- Ultimate Displacement (Δ_u)
- Theoretical, or predicted, moment resistance of a full and reduced section (M_p and M_{pR})
- Displacement and rotational ductilities (μ_Δ and μ_ψ)

5.2.1 Cylinder strengths

With the exception of specimens C6.1, C6.4 and C6.6, all the cylinder strengths lie between 29 and 31N/mm^2. Specimens C6.1, C6.4 and C6.6 have lower strengths of 22.6 N/mm^2 and 26.1 N/mm^2 respectively.

5.2.2 Yield loads

Specimen yielding is defined from each specimen's load-displacement response as the last point prior to the beginning of significant non-linear behaviour. The positive yield loads range from 41kN to 52kN while the negative yield loads range between 39.1kN and 49.1kN. Therefore, there is a difference of 10-11kN between the strongest and weakest specimens. This variety in yield strengths could be due to the unavoidable lack of precision inherent with experimental work:

- In the placing of the steel cages, within the formwork, it was inevitable that the cages would become slightly skewed. This introduces eccentricity within the specimens with respect to both axial and lateral loading. The eight specimens were poured in pairs and thus the pair of moulds made for the job, were re-used three times. The re-use of timber formwork can lead to a slight "slackening" of the formwork, and some minor errors when re-constructing the formwork for further use, leading to slight crookedness in the specimens.
- Some errors due to the application of axial load may also occur. A small eccentricity of the axial load (Figure 3.14) may arise if the loading jack is not placed exactly online with the

specimens' central axis. Also, where the target value of axial load for specimens is intended to be the same, some minor differences arose between the axial loads actually applied. For instance, specimen C6.1 was intended to have an axial load of 30% its compressive capacity applied when, actually, a load of 33% its compressive capacity was applied. This is due to the limited accuracy of the equipment used to apply the pressure to the loading jack. Interestingly, this specimen (C6.1) achieved one of the lowest moments of resistance of all the specimens; this may be due to the combination of low cylinder strength and higher applied axial load.

5.2.3 Yield displacements

The yield displacements were taken as those displacements occurring just before the start of significant non-linear behaviour. The yield positive displacement values are all between 9 and 10mm and all the yield negative displacement values, with the exception of C6.3, are slightly higher than this.

5.2.4 Initial stiffness

The initial stiffness values (K_i) were obtained by taking the initial slopes of the first positive and negative load-displacement cycles. The positive initial stiffnesses vary from 6.2kN/mm (C6.1/105/30) to 9.9kN/mm (C5.2/145/30). It is interesting to note that specimen C6.1, which has the lowest cylinder strength, also displays the lowest positive stiffness. The negative stiffness values do not show any similar trend relating stiffness to cylinder strength. However, a consistent trend is that the negative stiffness values are all lower than the positive stiffness values. This is not unexpected since a certain amount of damage is done to the specimens during the first positive displacement causing them to have lost a certain degree of initial stiffness as they enter their first negative displacement.

Specimen	f_{ck} N/mm^2	K_i kN/mm	P_y kN	Δ_y mm	M_y kNm	Δ_u mm	M_u kNm	M_p kNm	M_{pR} kNm	M_u/M_p	M_u/M_{pR}	μ_Δ	μ_ψ	N kN	$N/(f_{ck})(A)$
C5.1	30.94	9	48	9.4	35.76	50	46.81	52.76	45.03	0.89	1.04	5.3	5.3	350	28.3
145,W,30		-6.5	-49.1	-10	-36.58		-53.06			1.01	1.18	-5.0	-5.0		
C5.2	29.06	9.9	48	9.1	35.76	40	48.40	52.01	44.23	0.93	1.09	4.4	4.4	350	30.1
145,30		-7.4	-46	-10.5	-34.27		-47.31			0.91	1.07	-3.8	-3.8		
C6.1	22.62	6.2	45	10	33.53	40	44.53	47.70	40.97	0.93	1.09	4.0	4.0	300	33.2
105,30		-5.3	-39.1	-10.3	-29.13		-42.15			0.88	1.03	-3.9	-3.9		
C6.2	29.21	6.9	46	10	34.27	52+	47.32	51.64	44.21	0.92	1.07	5.2+	5.2+	336	28.8
125,W,30		-4.5	-44.7	-11.3	-33.30		-50.81			0.98	1.15	-4.6+	-4.6+		
C6.3	31.27	8.4	49	9.3	36.51	40	50.95	55.87	44.50	0.91	1.14	4.3	4.3	496	39.7
145,W,40		-6.5	-48.9	-8.2	-36.51		-55.90			1.00	1.26	-4.9	-4.9		
C6.4	26.06	7.9	41	9.2	30.55	40	40.86	55.21	44.06	0.74	0.93	4.3	4.3	486	38.5
125,W,40		-4.4	-44	-9.5	-32.78		-48.55			0.88	1.10	-4.2	-4.2		
C6.5	31.53	9.2	52	9.3	38.74	50	49.70	53.78	45.46	0.92	1.09	5.4	5.4	374	29.7
200,W,30		-5.8	-46.5	-9.5	-34.64		-52.30			0.97	1.15	-5.3	-5.2		
C6.6	26.05	7.5	48	9.6	35.76	30	47.58	49.64	42.69	0.96	1.11	3.1	3.1	313	30.0
175,30		-6.9	-48	-10.8	-35.76		-46.50			0.94	1.09	-2.8	-2.8		

Table 5.1: General results for positive and negative cycles

Specimen	P_y kN	M_y kNm	M_u kNm	M_u/M_p	M_u/M_{pR}	μ_Δ	μ_ψ
C5.1 145,W,30	48.55	36.17	49.93	0.95	1.11	5.2	5.2
C5.2 145,30	47.00	35.02	47.86	0.92	1.08	4.1	4.1
C6.1 105,30	42.05	31.33	43.34	0.91	1.06	4.0	4.0
C6.2 125,W,30	45.35	33.79	49.07	0.95	1.11	5.2+	5.2+
C6.3 145,W,40	48.95	36.51	53.43	0.96	1.20	4.6	4.6
C6.4 125,W,40	42.50	31.67	44.71	0.81	1.02	4.3	4.3
C6.5 200,W,30	49.25	36.69	51.00	0.95	1.12	5.4	5.4
C6.6 175,30	48.00	35.76	47.04	0.95	1.10	3.0	3.0

Table 5.2: Average results for positive and negative cycles

CHAPTER 5

BEAM-COLUMN RESULTS

5.1 Introduction

This chapter considers the results from eight beam-column specimens, each subject to a combination of lateral cyclic loading, representative of earthquake loading (ECCS, 1986), and axial loading. The specimens all had the same dimensions and longitudinal steel contents but differed from each other in terms of the following three parameters:

(i) axial load level
(ii) link spacing
(iii) whether or not the specimen contained wireballs.

The aim of these tests was to determine whether, or not, the inclusion of wireballs increases a specimen's resistance to a combination of lateral cyclic and axial loading and, if so, whether their inclusion allows the level of links specified by EC8 to be reduced without detrimental effect on specimen response. The specimen details and test set-up have been discussed in Section 3.7.

The chapter is divided into several sections that discuss different aspects of the results. Section 5.2 considers all specimens together in terms of initial stiffness, yield points, moment capacities, displacement and rotation capacities. Section 5.3 presents the visual observations made during the tests, while Section 5.4 considers the hysteresis and moment-rotation curves of the specimens. In Section 5.5, the specimens are divided into three groups and their hysteresis characteristics are considered in detail in terms of energy dissipation and resistance. Section 5.6 then compares the effect of different link spacing on the specimens' ultimate displacements and total dissipated energy.

5.2 General results

Table 5.1 details the results of the eight specimens for both positive and negative displacements. Table 5.2 presents the average (of the positive and negative displacement responses) ultimate moments, ultimate moment to predicted moment ratios and ductility ratios. The approach of taking an average of the positive and negative values for these properties is considered reasonable since all the specimens were of the same general type and tested within the same laboratory set-up.

Therefore, it is considered that an average value provides a robust result which removes any variability, such as the longitudinal steel being slightly off-line or the specimen being slightly off-centre in the test set-up, which may occur between specimens.

The following properties of the specimens are provided in Table 5.1:

- Concrete cylinder strength (f_{ck})
- Yield load and displacement (P_y and Δ_y)
- Initial Stiffness (K_i)
- Yield and ultimate moment (M_y and M_u)
- Ultimate Displacement (Δ_u)
- Theoretical, or predicted, moment resistance of a full and reduced section (M_p and M_{pR})
- Displacement and rotational ductilities (μ_Δ and μ_ψ)

5.2.1 Cylinder strengths

With the exception of specimens C6.1, C6.4 and C6.6, all the cylinder strengths lie between 29 and 31N/mm^2. Specimens C6.1, C6.4 and C6.6 have lower strengths of 22.6 N/mm^2 and 26.1 N/mm^2 respectively.

5.2.2 Yield loads

Specimen yielding is defined from each specimen's load-displacement response as the last point prior to the beginning of significant non-linear behaviour. The positive yield loads range from 41kN to 52kN while the negative yield loads range between 39.1kN and 49.1kN. Therefore, there is a difference of 10-11kN between the strongest and weakest specimens. This variety in yield strengths could be due to the unavoidable lack of precision inherent with experimental work:

- In the placing of the steel cages, within the formwork, it was inevitable that the cages would become slightly skewed. This introduces eccentricity within the specimens with respect to both axial and lateral loading. The eight specimens were poured in pairs and thus the pair of moulds made for the job, were re-used three times. The re-use of timber formwork can lead to a slight "slackening" of the formwork, and some minor errors when re-constructing the formwork for further use, leading to slight crookedness in the specimens.
- Some errors due to the application of axial load may also occur. A small eccentricity of the axial load (Figure 3.14) may arise if the loading jack is not placed exactly online with the

specimens' central axis. Also, where the target value of axial load for specimens is intended to be the same, some minor differences arose between the axial loads actually applied. For instance, specimen C6.1 was intended to have an axial load of 30% its compressive capacity applied when, actually, a load of 33% its compressive capacity was applied. This is due to the limited accuracy of the equipment used to apply the pressure to the loading jack. Interestingly, this specimen (C6.1) achieved one of the lowest moments of resistance of all the specimens; this may be due to the combination of low cylinder strength and higher applied axial load.

5.2.3 Yield displacements

The yield displacements were taken as those displacements occurring just before the start of significant non-linear behaviour. The yield positive displacement values are all between 9 and 10mm and all the yield negative displacement values, with the exception of C6.3, are slightly higher than this.

5.2.4 Initial stiffness

The initial stiffness values (K_i) were obtained by taking the initial slopes of the first positive and negative load-displacement cycles. The positive initial stiffnesses vary from 6.2kN/mm (C6.1/105/30) to 9.9kN/mm (C5.2/145/30). It is interesting to note that specimen C6.1, which has the lowest cylinder strength, also displays the lowest positive stiffness. The negative stiffness values do not show any similar trend relating stiffness to cylinder strength. However, a consistent trend is that the negative stiffness values are all lower than the positive stiffness values. This is not unexpected since a certain amount of damage is done to the specimens during the first positive displacement causing them to have lost a certain degree of initial stiffness as they enter their first negative displacement.

Specimen	f_{ck} N/mm^2	K_i kN/mm	P_y kN	Δ_y mm	M_y kNm	Δ_u mm	M_u kNm	M_p kNm	M_{pR} kNm	M_u/M_p	M_u/M_{pR}	μ_Δ	μ_ψ	N kN	$N/(f_{ck})(A)$
C5.1	30.94	9	48	9.4	35.76	50	46.81	52.76	45.03	0.89	1.04	5.3	5.3	350	28.3
145,W,30		-6.5	-49.1	-10	-36.58		-53.06			1.01	1.18	-5.0	-5.0		
C5.2	29.06	9.9	48	9.1	35.76	40	48.40	52.01	44.23	0.93	1.09	4.4	4.4	350	30.1
145,30		-7.4	-46	-10.5	-34.27		-47.31			0.91	1.07	-3.8	-3.8		
C6.1	22.62	6.2	45	10	33.53	40	44.53	47.70	40.97	0.93	1.09	4.0	4.0	300	33.2
105,30		-5.3	-39.1	-10.3	-29.13		-42.15			0.88	1.03	-3.9	-3.9		
C6.2	29.21	6.9	46	10	34.27	52+	47.32	51.64	44.21	0.92	1.07	5.2+	5.2+	336	28.8
125,W,30		-4.5	-44.7	-11.3	-33.30		-50.81			0.98	1.15	-4.6+	-4.6+		
C6.3	31.27	8.4	49	9.3	36.51	40	50.95	55.87	44.50	0.91	1.14	4.3	4.3	496	39.7
145,W,40		-6.5	-48.9	-8.2	-36.51		-55.90			1.00	1.26	-4.9	-4.9		
C6.4	26.06	7.9	41	9.2	30.55	40	40.86	55.21	44.06	0.74	0.93	4.3	4.3	486	38.5
125,W,40		-4.4	-44	-9.5	-32.78		-48.55			0.88	1.10	-4.2	-4.2		
C6.5	31.53	9.2	52	9.3	38.74	50	49.70	53.78	45.46	0.92	1.09	5.4	5.4	374	29.7
200,W,30		-5.8	-46.5	-9.5	-34.64		-52.30			0.97	1.15	-5.3	-5.2		
C6.6	26.05	7.5	48	9.6	35.76	30	47.58	49.64	42.69	0.96	1.11	3.1	3.1	313	30.0
175,30		-6.9	-48	-10.8	-35.76		-46.50			0.94	1.09	-2.8	-2.8		

Table 5.1: General results for positive and negative cycles

Specimen	P_y kN	M_y kNm	M_u kNm	M_u/M_p	M_u/M_{pR}	μ_Δ	μ_ψ
C5.1 145,W,30	48.55	36.17	49.93	0.95	1.11	5.2	5.2
C5.2 145,30	47.00	35.02	47.86	0.92	1.08	4.1	4.1
C6.1 105,30	42.05	31.33	43.34	0.91	1.06	4.0	4.0
C6.2 125,W,30	45.35	33.79	49.07	0.95	1.11	5.2+	5.2+
C6.3 145,W,40	48.95	36.51	53.43	0.96	1.20	4.6	4.6
C6.4 125,W,40	42.50	31.67	44.71	0.81	1.02	4.3	4.3
C6.5 200,W,30	49.25	36.69	51.00	0.95	1.12	5.4	5.4
C6.6 175,30	48.00	35.76	47.04	0.95	1.10	3.0	3.0

Table 5.2: Average results for positive and negative cycles

5.2.5 Yield and ultimate moment capacities

The yield and ultimate moments of resistance were determined by multiplying the yield load and ultimate (i.e. maximum) load by the lever-arm. The lever-arm used to calculate these moments is 745mm as this is the distance between the point of application of the lateral load and the beam-column boundary surface (Figure 5.3). This lever-arm is employed because the maximum moment of resistance of the beam-column must occur at the point of the beam-column furthest from the point of application of the lateral load. It follows that at the point of maximum moment the maximum level of damage should be expected to occur. However, it is worth noting that a visual inspection of all the specimens showed that the maximum level of damage actually occurred consistently slightly above the beam-column boundary surface. This phenomenon is discussed in Section 5.3.

It is appropriate to consider whether the wireball-reinforced specimens display higher resistances than the specimens without wireballs. Figure 5.1 compares a plot of the average ultimate moment in the different specimens. The average ultimate moment refers to the average of the positive and negative ultimate moments. It is clear that the inclusion of wireballs does not significantly enhance the strength of the specimens. This confirms the earlier results as discussed in Section 2.7.3.

The theoretical ultimate moments, for the full beam-column section (M_p) and for the reduced column section (M_{pR}), when the cover concrete has spalled away, were calculated using Equation 3.14. The calculation of M_{pR} is of the same form as for M_p except that the section area used is the reduced area, when the cover concrete has spalled, which is taken as the area within the centreline of a link. When the cover is assumed to have spalled the depth to the top steel (*d'* in Equation 3.14) is reduced by the amount of original concrete cover to the top steel. Likewise, the total depth of the spalled section (*D* in Equation 3.14) is reduced by an amount equal to the depth of original concrete cover to the top and bottom steel.

From Table 5.1, it is clear that the moment capacities differ from specimen to specimen due to different cylinder strengths and axial loads. With the exception of C6.4(125,W,40), the predicted moments for the full section over-predict the observed moment capacities by 5-9%. The predicted moments for the reduced section under-predict the observed moment capacities by between 2% (C6.4) and 20% (C6.3). This suggests that the ultimate moment of the specimens occurs at some point between the specimen having all its cover intact and the specimens having lost all its cover.

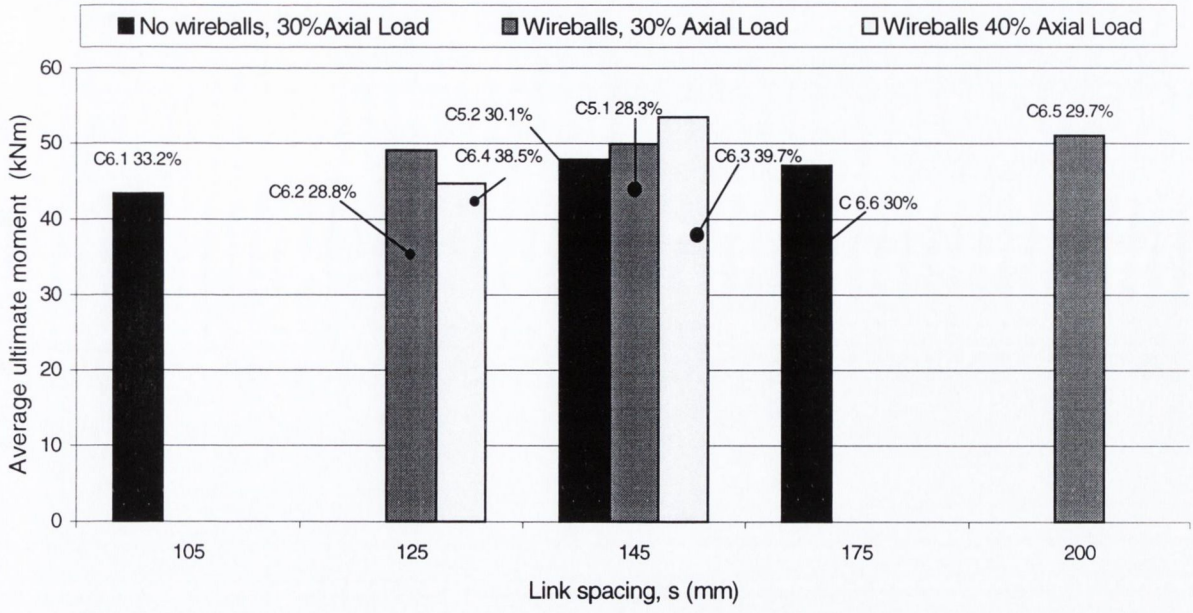

Figure 5.1: Average ultimate moments for beam-columns (Test Series 6)

5.2.6 Ductility ratios

5.2.6.1 Displacement ductilities

The displacement ductility ratio, μ_Δ, is the ratio of the ultimate displacement to the displacement at yield. The yield displacement is defined as the last displacement prior to the start of significant non-linear behaviour. The ultimate displacement is the point in the applied displacement history (i.e. 10, 20, 30, 40, 50 or 52mm) at which the specimen ultimately fails. Unfortunately, due to the displacement history imposed on the specimens, the accuracy of the quoted ultimate displacement values is limited. For example, a specimen that fails close to the end of the 40mm cycles can only be said to have an ultimate displacement of 40mm when, if a higher displacement of 45mm had been applied, the specimen may have behaved just as well. In other words, the quoted value of ultimate displacement cannot quantify how well a specimen maintained its load carrying capacity at this displacement. This issue is considered, with respect to the specimens' losses in resistance, in Section 5.6. A second limitation is the fact that the displacement range of the actuator was limited to ±52mm. However, this was only relevant in the case of specimen C6.2, since all other specimens failed before the full stroke of the actuator was reached. The ultimate displacement of C6.2 is, therefore, written as 52+mm.

5.2.6.2 Rotational ductilities

The rotational ductilities, μ_ψ, are the ratios of the ultimate rotation to the yield rotation. These values are the same as the displacement ductility values since rotation (ψ), in this case, is the angle through which the specimen has deflected when subject to a lateral load, as shown by Figure 5.2 and Equation 5.1.

$$\psi = \Delta/L \tag{5.1}$$

where:

ψ = rotation

Δ = lateral displacement (mm)

L = lever-arm length (mm)

P = applied lateral load

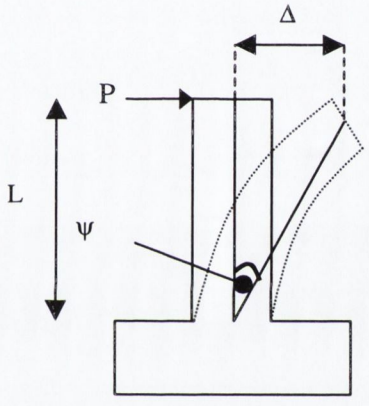

Figure 5.2: Rotation

The ductility values of the specimens, in terms of either displacement or rotation, are one of the key factors to be considered when examining the results of these tests. For simplicity, the average of the positive and negative ductility ratios are considered. These values are presented in Table 5.2. The ratios provide confirmation that the use of wireballs improves ductility. The displacement ductilities of the eight specimens fall into three categories; (i) greater than 5, (ii) between 4 and 5 and (iii) lower than 4. Notably, the three specimens with ductility ratios greater than 5 all contained wireballs.

The three specimens with ductility ratios greater than 5 are specimens C6.2 (125,W,30), C6.5 (200,W,30) and C5.1(145,W,30). All of these specimens contained wireballs and had a nominal axial load of 30%. Of these three specimens, C6.2 was the most ductile. It is no great surprise that this specimen behaved in the most ductile manner since it had a high degree of confinement provided by closely spaced links plus wireballs. However, if the wireballs had been ineffective, specimen C6.1 (105,30) would have been the most ductile. Specimens C6.5 and C5.1, although

having large link spacings of 200mm and 145mm respectively, also achieved ductility ratios of greater than 5. This is an encouraging result in terms of the benefits of wireball reinforcement since specimens without wireballs but containing links at similar, or closer spacings, as these specimens achieved ductility ratios of only 3 and 4.

Specimen C6.1 contained links at 105mm spacing, the DCL required link spacing for a column of its dimensions subject to an axial load of 30% of its compressive capacity. Despite its link spacing complying with Eurocode 8 requirements, the specimen was outperformed by specimens with larger link spacings and the same level of axial load, but which also contained wireballs. Indeed, specimens with both larger link spacings and higher axial loads, but containing wireballs, performed equally well as specimen C6.1.

Comparison of the responses of specimens C5.1 (145,W,30) and C5.2 (145,30), which had exactly the same link spacing and target axial load, highlights further the ductility enhancement effects of wireballs. Both specimens have very similar characteristics in terms of f_{ck}, M_y, K_i and M_u, but display different ductility capacities. Specimen C5.1 (which contained wireballs) achieved a ductility ratio of 5.2, while specimen C5.2 (which did not contain wireballs) achieved a ratio of only 4.1.

A final observation, which consolidates further the ductility benefit of wireballs, is that even under higher axial loads their inclusion appears beneficial. Specimens C6.3 (145,W,40) and C6.4 (125,W,40) had links at 145mm and 125mm respectively, both contained wireballs and both had a target axial load level of 40%. Although they were subject to a higher axial load than the other specimens (almost sufficient to render the specimens over-reinforced) they were not any less ductile. Both reached a ductility ratio of 4, the same as that attained by specimens C5.2 and C6.1 which had lower axial load and similar, or closer, link spacings.

The conclusion to be drawn is that wireballs do appear to enhance member ductility. The results clearly show that specimens containing wireballs display higher ductility capacities than those without wireballs, even when the link spacing of the wireball reinforced specimens is larger than that of a standard specimen. Specimens with wireballs were also seen to display greater ductility at higher axial loads than other specimens without wireballs, which had lower axial loads. The results indicate clearly that there is potential to reduce the amount of transverse reinforcement required for a given ductility demand if wireballs are substituted.

5.3 General observations

This section discusses the visual observations made during all eight tests and relates these observations to the measured load-displacement hysteresis curves. The aim is to provide an accurate description of the response of the specimens in order to provide a clearer understanding of the different behaviour of specimens with and without wireballs. Section 5.3.1 provides an account of the observed behaviours, while Section 5.3.2 discusses these observed behaviours with special attention given to the effects of wireballs and axial loads. The aim is to provide a good insight into the effects of wireballs, before proceeding to Sections 5.4 and 5.5 where the hysteresis characteristics of the specimens are considered in more detail.

5.3.1 Visual observations

While the specimens' responses differed, due to their different link spacings, wireball content and axial loads, in many respects all specimens behaved in a similar fashion. Table 5.3 details the observed behaviour of the specimens, with respect to displacement cycle. This table details when, and what form of, degradation occurred in the specimens, and how this degradation progressed to the ultimate collapse of the specimens.

Throughout this table, certain faces and corners of the specimens are referred to. Figure 5.3 illustrates a specimen with all of its sides identified by the letter "F" followed by a number. Corners are identified by the two faces that meet there, (e.g. corner F2-F6 is the corner on the front column face furthest from the actuator). Table 5.3 also provides details of any damage that occurred to the four longitudinal steel bars. These bars are identified in Figure 5.3 as Bar 1 to Bar 4 inclusive.

The first column of Table 5.3 identifies the displacement cycle, the second column provides details of the observed behaviour of the specimens during that cycle, and the last column indicates whether specimen failure has occurred, and when. The details provide an outline of the overall behaviour of the specimens. Figures 5.4(a) to 5.4(p) present a series of photographs illustrating the specimens at various stages during testing. These photographs are referred to within Table 5.3 when relevant.

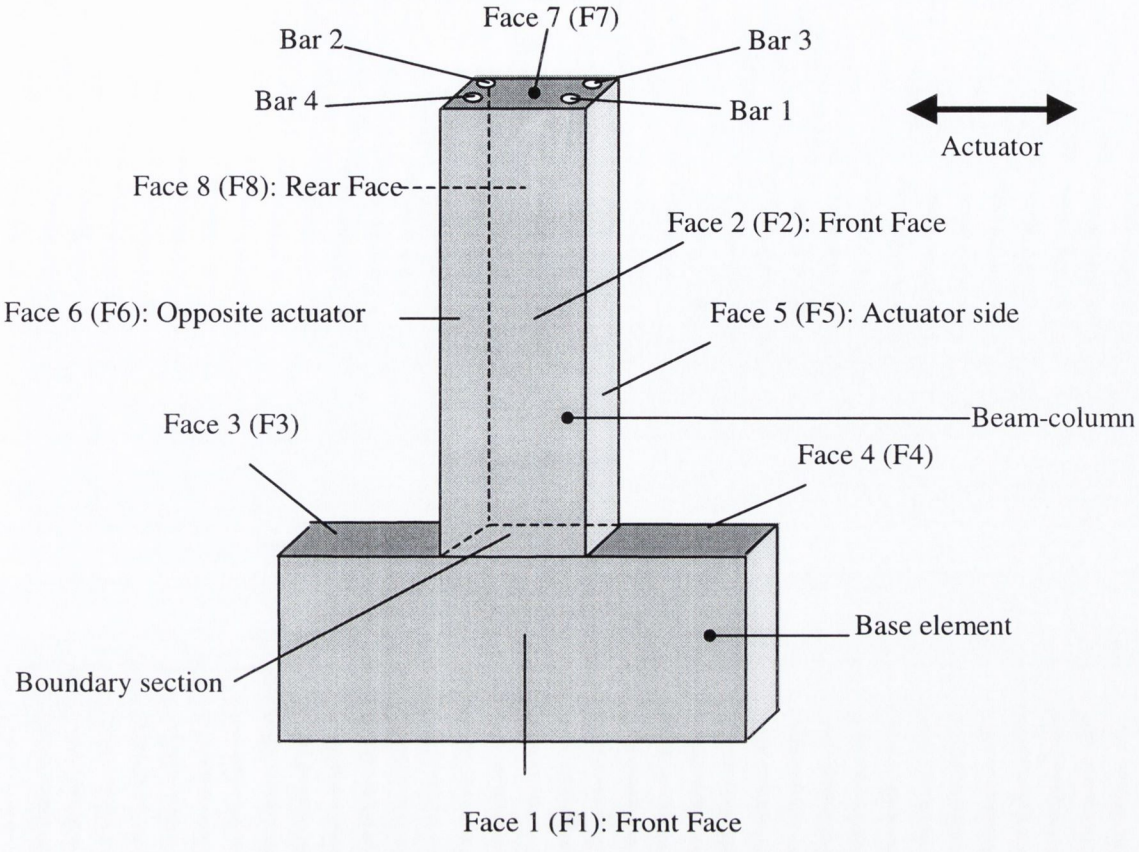

Figure 5.3: Specimen face and bar labelling system

Loading History	General Behaviour	Collapsed Specimens
Application of axial load	• The target level of axial load for each specimen was applied just prior to the application of lateral loading. Its application resulted in the development of some minor shear cracks in the base element of all the specimens. These cracks were superficial and did not develop further during the test	
Cycles 1-4	• The lateral displacement cycles were started immediately after the target axial load was applied. • With increasing lateral displacement, horizontal flexural cracks developed in the beam-columns. During these early cycles these cracks closed up completely when in compression. • The development of horizontal cracks was coupled with the formation of some minor vertical cracks, these cracks propagated more quickly in the specimens subject to higher axial loads.	
Cycle 5a-5c	• For all specimens, increased levels of damage occurred during the first 20mm cycle. • The horizontal cracks observed in cycle 4 became permanently visible (although they were only "pencil-line" cracks at this stage). These cracks formed on F5 and F6 and spread to F2 and F8. • The vertical cracks worsened. These tended to form close to the column corners in all of the specimens and varied in lengths from 100mm to 300mm in all of the specimens (Photo (a) in Figure 5.4). It was observed that these tended to be worse in specimens with the higher axial loads. • Small amounts of spalling occurred, beginning with grain sized particles of concrete falling from the horizontal cracks and corners, and then some more sizeable flakes (10-30mm long) of concrete (Photo (b)). • F6 was observed to suffer more than F5 in all of the tests. • During the course of the 20mm cycles, the level of spalling increased and the cracks (horizontal and vertical) lengthened and deepened. With every 20mm cycle, the region of damage increased. • The level of overall damage observed was slightly higher in the specimens with the higher levels of axial load.	

Table 5.3: Observed specimen behaviour

Loading History	General Behaviour	Collapsed Specimens
Cycle 6a-6c	• The 30mm cycles brought increased spalling to all of the specimens. Sizeable pieces of concrete (from 100mm to 200mm long, and approximately the cover depth) spalled from all the specimens, especially at their corners, such that the cover was becoming badly damaged in the plastic hinge region (Photos (c), (d), (e) and (f)). • In specimen C6.3 a large piece of concrete at 200mm from the boundary surface, and approximately 300mm in length, was observed to be loosening from F2-F5 corner (Photos (g) and (h)). • The vertical cracks lengthened in all the specimens, approaching lengths of 400mm in specimen C6.3. • As in the 20mm cycles, F5 was observed to suffer less than F6. • The specimens subject to the higher levels of axial load continued to suffer a higher degree of damage than the other specimens.	
7a+ (push)	• The level of spall increased with the first 40mm cycle. • Within the plastic hinge region of the specimens, the cover spalled on F5 and F6 such that in the more badly damaged specimens the lower column link was becoming visible. • By this cycle, specimen C6.6 had suffered more cover spall than the other specimens with its four corners damaged to a considerable height (greater than half the lever arm). Corner F6-F8 had spalled so much that the corners of the first two links were visible. • With the exception of C6.6, the cores of all the specimens appeared intact at this stage. Even in the specimens with the higher axial load levels, the cores held together. A 500mm long vertical crack was observed on corner F6-F8 of C6.6.	
7a- (pull)	• During this first 40mm pull cycle, all the specimens except C6.2, which continued to resist load well, were observed to undergo increased degradation as large pieces of concrete spalled from their corners and the vertical cracks deepened into the specimens. In C6.4 the initiation of buckling was observed in Bar 1. • The core of C6.6 had undergone severe degradation by this point. • In all specimens, corner F2-F6 appeared to suffer the most damage.	

Table 5.3 continued: Observed specimen behaviour

Loading History	General Behaviour	Collapsed Specimens
7b+ (push)	• C6.6 collapsed during this cycle after significant amounts of spalling from corner F2-F6 and, buckling of the longitudinal reinforcement bar (Bar 4) at that corner (Photos (i), (j) and (k)). • C5.2 also failed after much spalling - a large piece of concrete, about 600mm long, fell from corner F2-F6 and the specimen sheared. All of the longitudinal steel buckled between the 1st and 2nd links, as these burst open. • All the other specimens continued to carry load, although their corners were visibly deteriorating. • C6.4 suffered a lot during this cycle with its lower link opening up. However, its longitudinal steel did not appear to have buckled any more than had been observed in cycle 7a (Photos (l) and (m)). • Indications of the lower link opening up in C5.1 were also observed.	C6.6(175,30) C5.2(145,30)
7b-(pull)	• The cores of all the remaining specimens were still visibly intact at this stage (Photos (n) and (o)). • A large vertical crack on the rear face of C6.1 was observed to worsen significantly as it extended deeper into the specimen and widened.	
7c+ (push)	• The resistance of C6.1 was observed to decrease significantly during this cycle. • Buckling of the longitudinal steel of C6.3 and C6.4 was observed between the 1st and 2nd links, and in specimen C6.3 this was coupled by the opening up of the lower link. • Two bangs were heard from C6.3 followed by severe buckling of all of the longitudinal steel bars between the 1st and 2nd links. Bars 1 and 4 were observed to have buckled the most.	
7c-(pull)	• Severe damage occurred to all the surviving specimens, although the degree of damage was much less in C6.2 than in C6.1, C6.3 or C6.4. • Bangs were heard from C6.1, coupled with buckling of the longitudinal steel between the 1st and 2nd links, and the lower link opening up. Bars 1 and 4 were the most buckled, Bar 4 was fixed, within the steel cage, to the corner of the link where the link legs/hooks overlap. • In C6.3, a shear crack was observed in the core. The wireballs initially prevented its total disintegration but subsequently, severe buckling of the longitudinal steel occurred, followed by collapse. • The core of C6.4 still appeared to be undamaged.	C6.3(145,W,40)

Table 5.3 continued: Observed specimen behaviour

Loading History	General Behaviour	Collapsed Specimens
8a+(push)	• Both specimens C6.1 and C6.4 collapsed during this cycle. • The collapse of specimen C6.1 was quicker than that of C6.4, the wireballs probably preventing rapid disintegration of the core in the latter case. • C6.2 still resisted load well at this stage. • C5.1 experienced further degradation, especially at corner F2-F6, but its core still seemed intact as the wireballs held it together.	C6.1(105,30) C6.4(125,W,40)
8b-(pull)	• Sizeable pieces of concrete (100mm long) were observed to be just ready to spall from corners F2-F5 and F6-F8 of specimen C5.1.	
8c+	• Two large pieces of concrete spalled from specimen C5.1, one from corner F5-F6 and another from corner F2-F5. • Some degradation of the core of C6.5 was observable, but the wireballs prevented total disintegration. • C6.2 maintained a good load resistance and its core remained intact.	
8c-	• Specimen C5.1 failed after a bang and heavy spall, coupled with heavy buckling of the longitudinal steel between the 1st and 2nd links. Bar 4, fixed on the link corner where the legs overlapped, was badly buckled, Bar 3, the least distorted of the four longitudinal bars, did not buckle too severely. • Specimen C6.5 failed after its lower link was pushed open and buckling of the longitudinal steel occurred.	C5.1(145,W,30) C6.5(200,W,30)
9a-9c	• Only C6.2 remained intact by this stage. It continued to maintain its load capacity and did not collapse. However, some slight buckling of Bar 2, on the link opening, and some degradation of the core was apparent. The links still remained fully closed (Photo (P)).	

Table 5.3 continued: Observed specimen behaviour

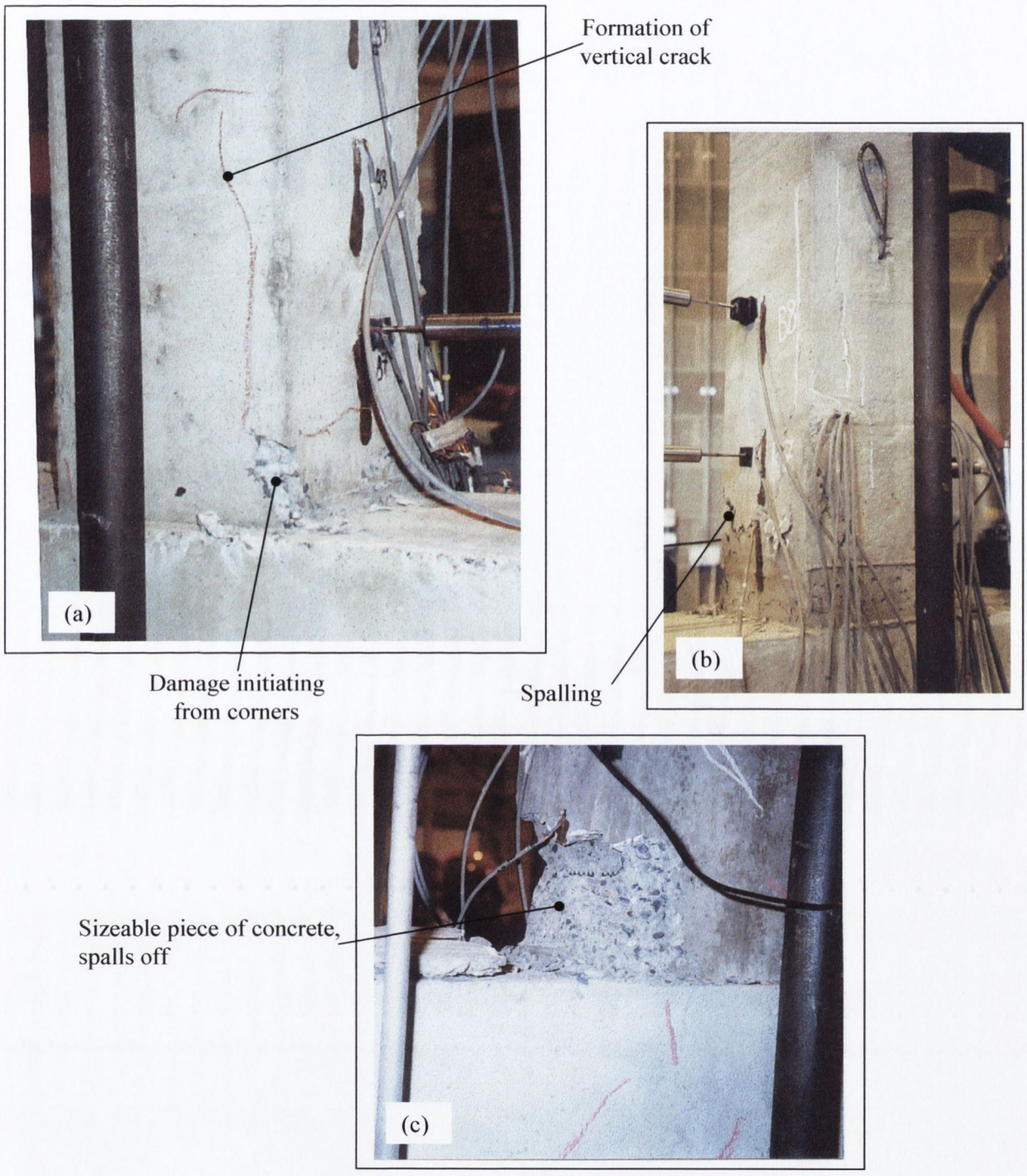

Figure 5.4: (a) C5.1(145,W,30) during Group cycles 5,
(b) C6.3(145,W,40) during Group cycles 5, (c)C6.1(105,30) during Group cycles 6

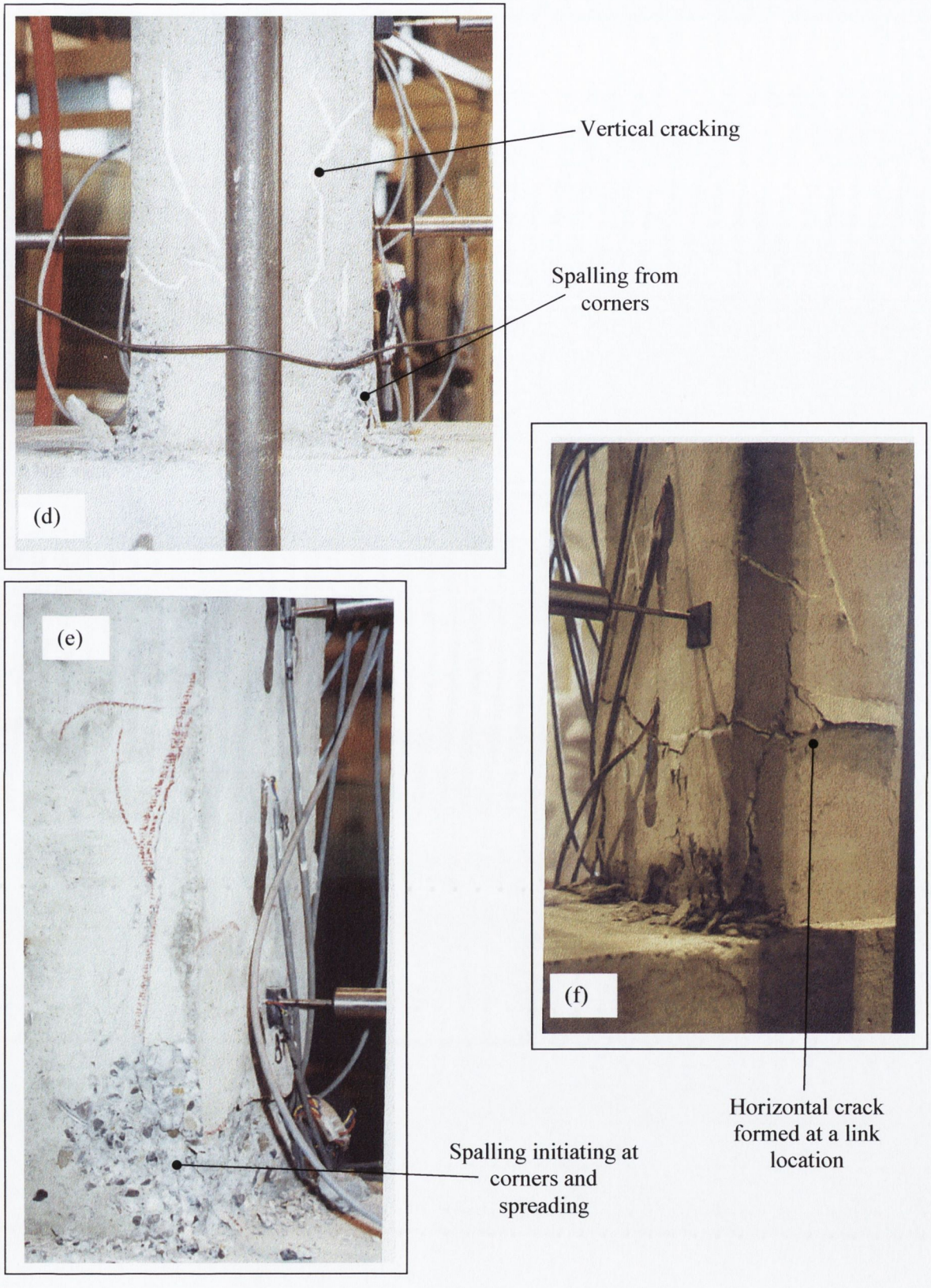

Figure 5.4: (d) C6.2(125,W,30) during Group cycles 6, (e) C5.1(145,W,30), (f) C6.6(175,30) during Group cycles 6

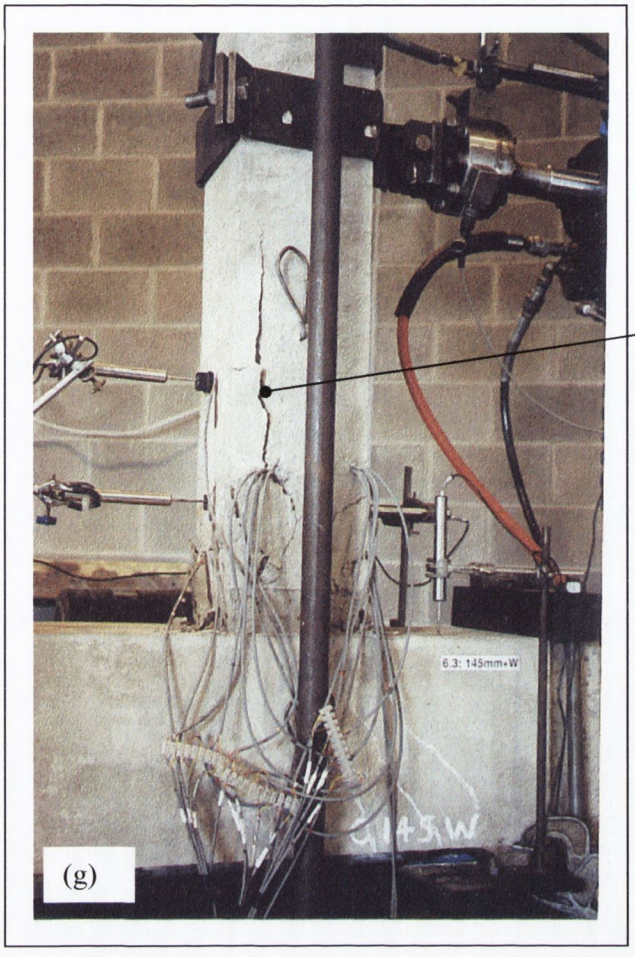

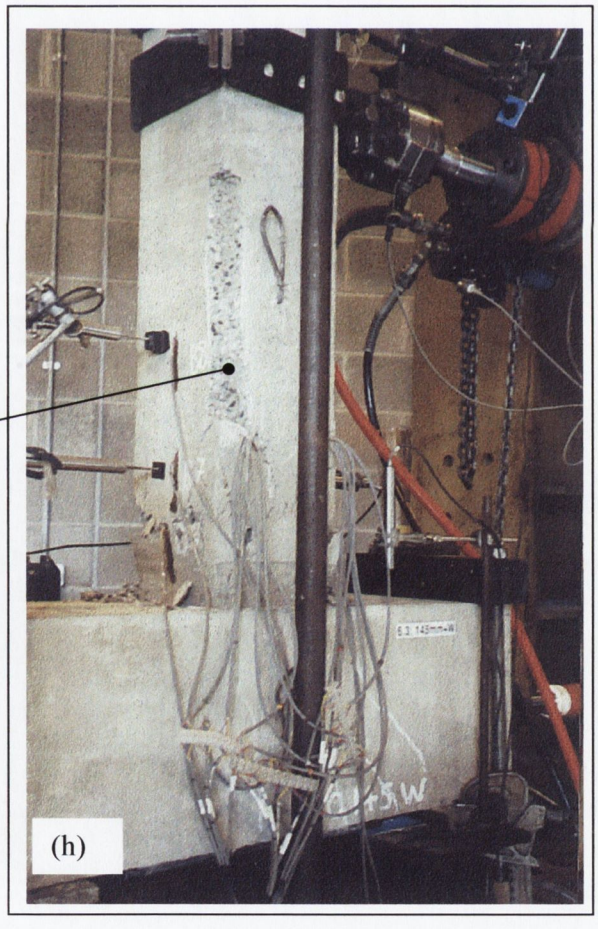

Figure 5.4: (g) and (h) C6.3(145,W,40) during Group cycle 6

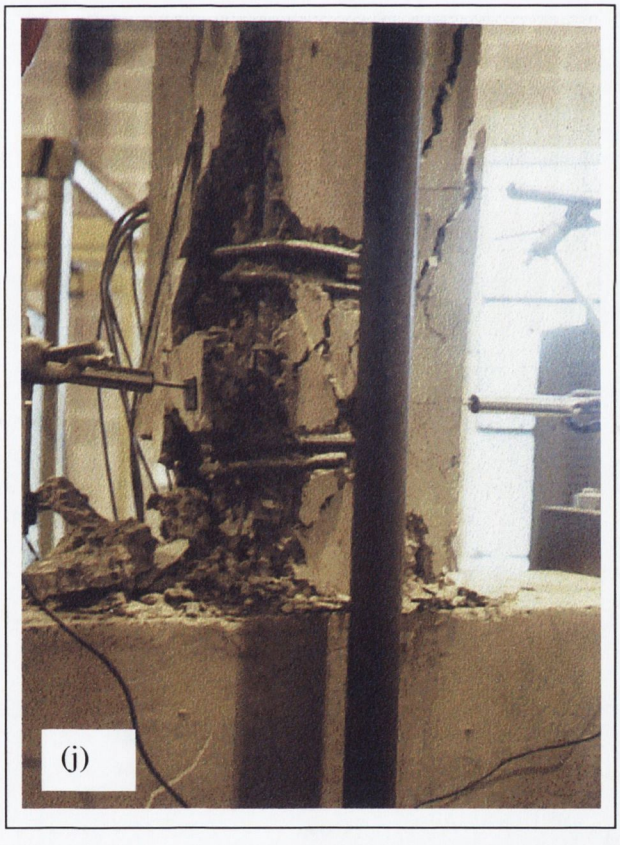

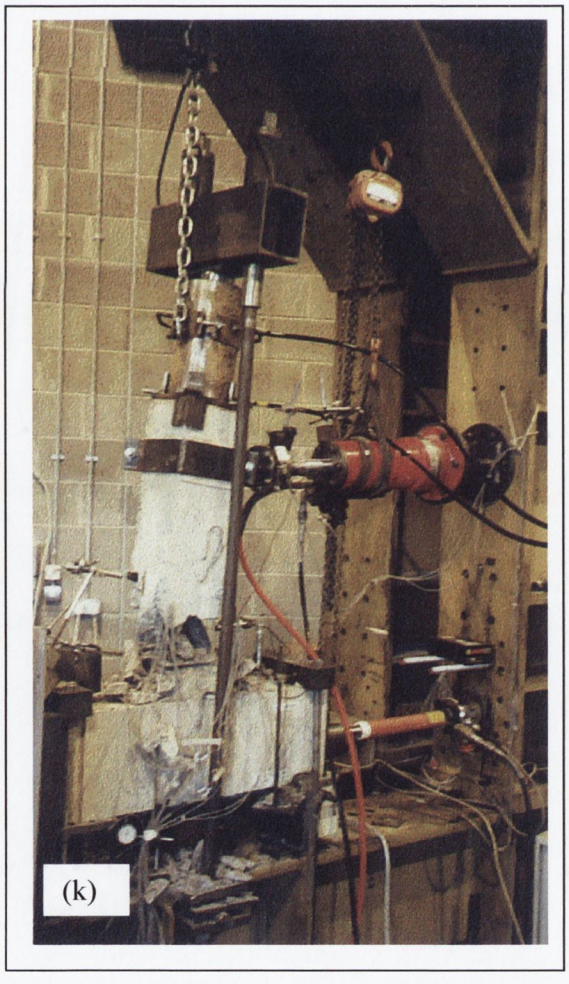

Figure 5.4: (i), (j) and (k): C6.6(175,30) during Group cycle 7

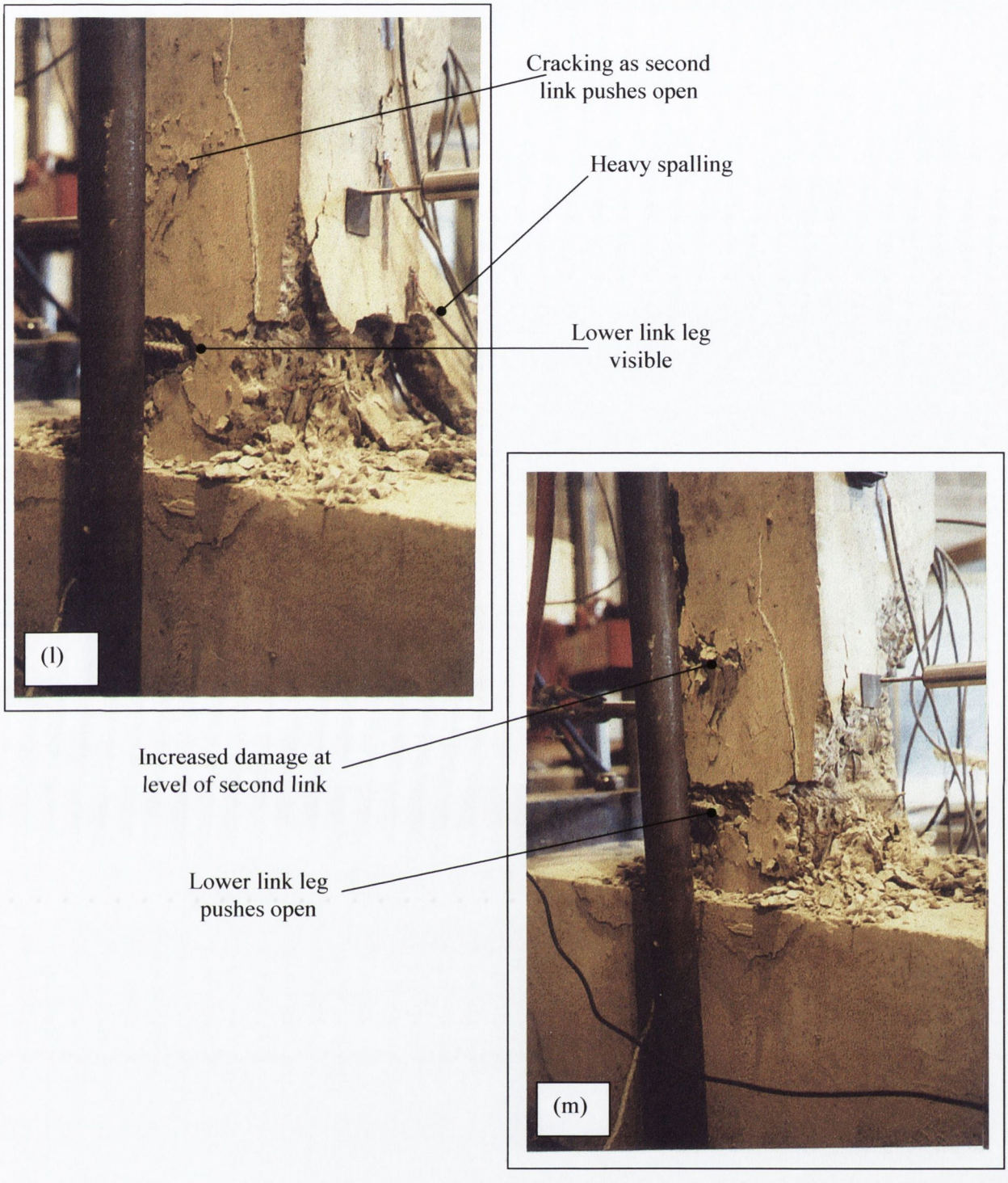

Figure 5.4: (l) and (m): C6.4(125,W,40) during Group cycles 7

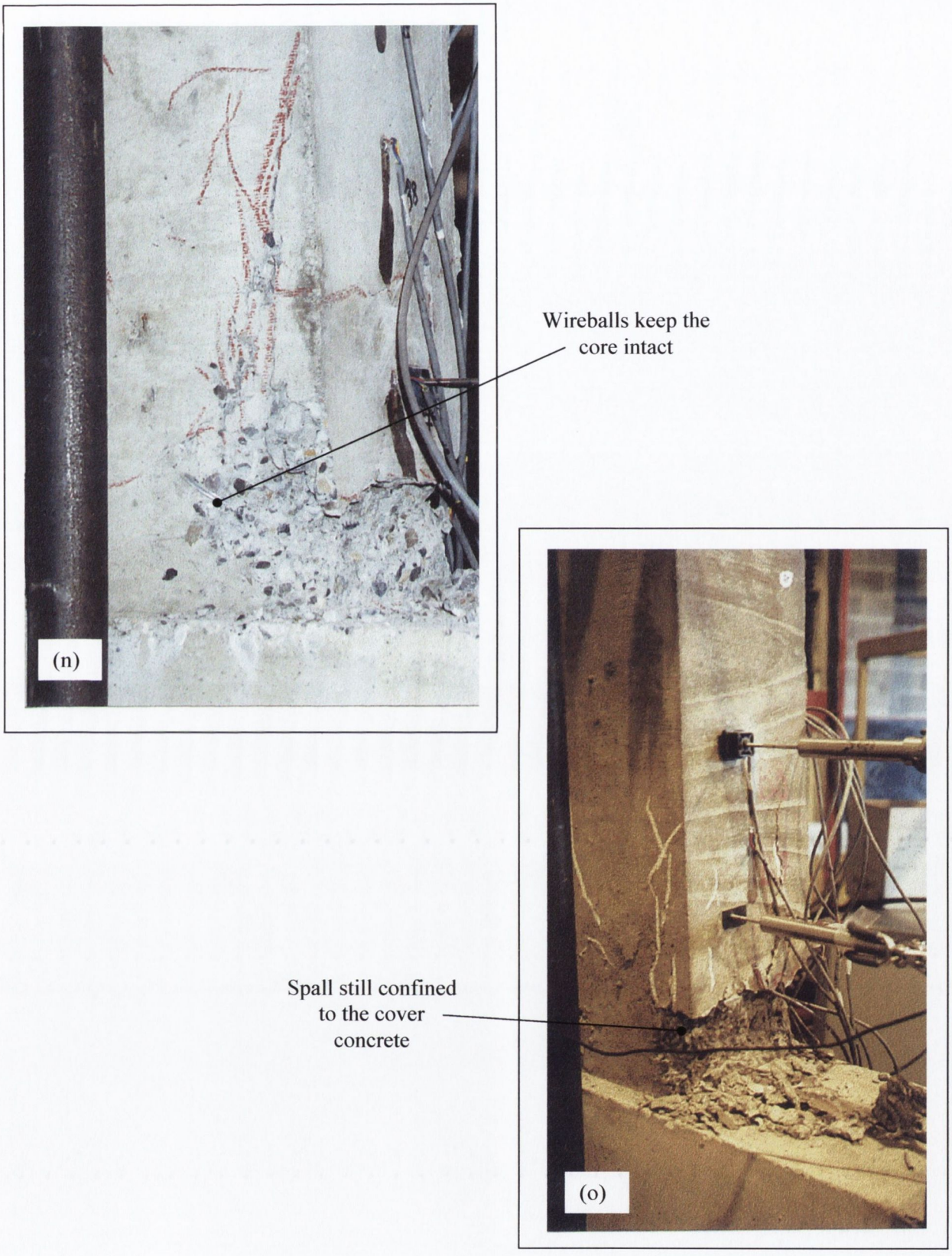

Figure 5.4: (n) C5.1(145,W,30) during Group cycle 7, (o) C6.2(125,W,30) during Group cycle 7

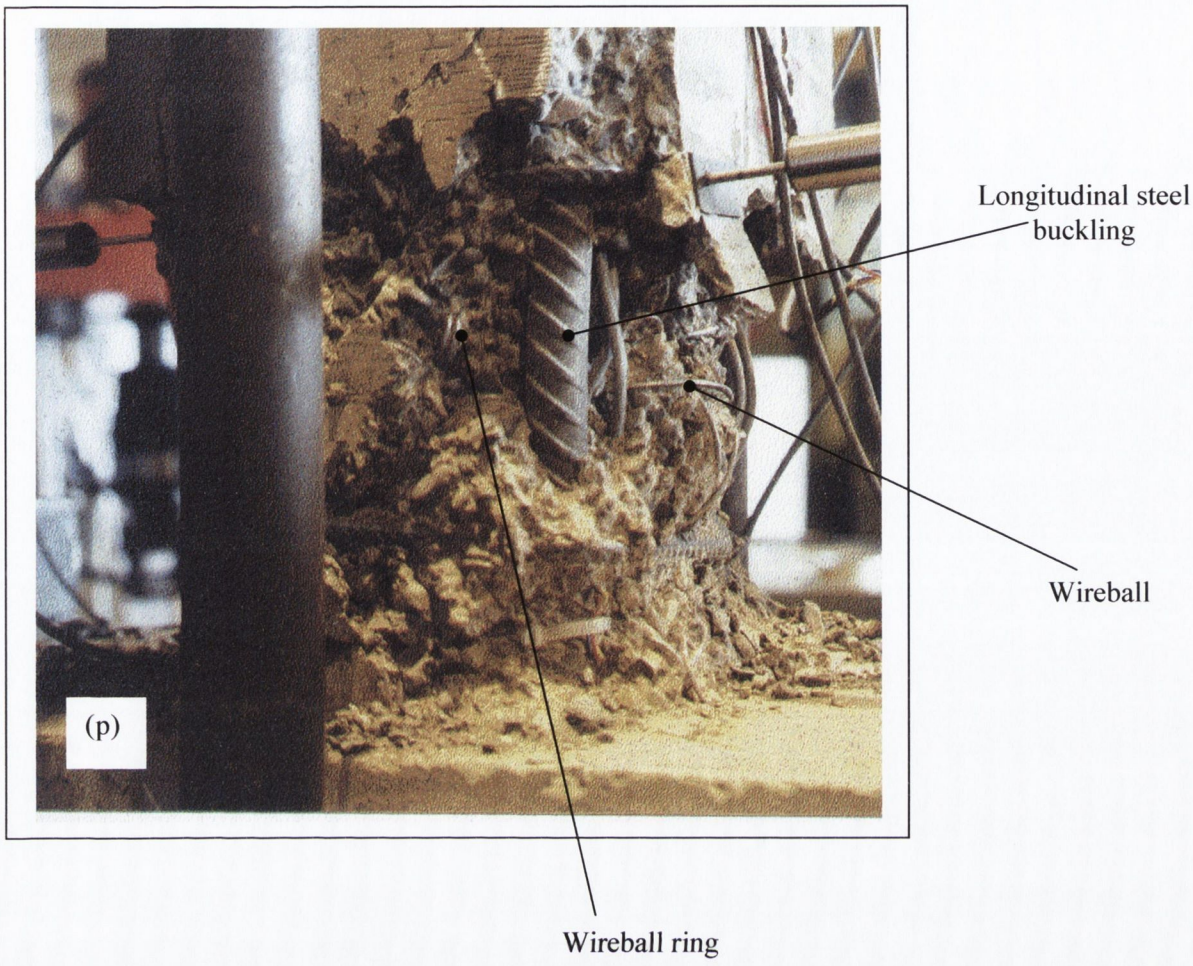

Figure 5.4: (p) C6.2(125,W,30) at end of Group cycles 8

5.3.2 Failure modes

With the exception of specimen C6.2(125,W,30), all of the specimens collapsed. Ultimate failure of all specimens proceeded according to the following sequence:

- Ample amounts of concrete spall.
- Degradation of the confined core.
- The lower column links being forced open as the core expanded.
- Buckling of the longitudinal steel.

However, the presence of wireballs influenced specimen behaviour in the following manner:

- Delayed and reduced degradation of the concrete core.
- Reduced link distortion and opening.
- Reduced longitudinal steel buckling.

Figures 5.5(a) to 5.5(n) present post-failure photographs of all the specimens, with the exception of C5.2(145,30) for which no photographs are available. All of the specimens developed an extensive plastic hinge region along the beam-column length. Table 5.4 provides the approximate plastic hinge lengths of the specimens, measured as the lengths of the damaged area of each specimen from which cover had completely spalled. The hinge lengths range between 200 and 350mm in length. This table also details the number of transverse links that were pushed out and distorted by the end of the test, and provides an indication of the severity of distortion.

Specimen	**Approximate plastic hinge length (mm)**	**Links damaged**	**Level of damage to the links**
C5.1 (145,W,30)	260	1st link only	1st link leg pushed out very slightly
C5.2 (145,30)	350	1st and 2nd link	Both links severely distorted
C6.1 (105,30)	300	1st and 2nd link	Legs of the links pushed out, but they were not very distorted
C6.2 (125,W,30)	200-225	None	None
C6.3 (145,W,40)	300	1st and 2nd link	1st link severely distorted, 2nd link a little distorted
C6.4 (125,W,40)	330	1st and 2nd link	1st link severely damaged, 2nd link a little distorted, similar level of distortion as C6.3
C6.5 (200,W,30)	300	1st and 2nd link	1st link quite severely distorted, 2nd link experienced only minor distortion
C6.6 (175,30)	350	1st and 2nd link	Both links severely distorted but lower link more so, being probably the most distorted link in all tests

Table 5.4: Approximate plastic hinge lengths and distortion of the links

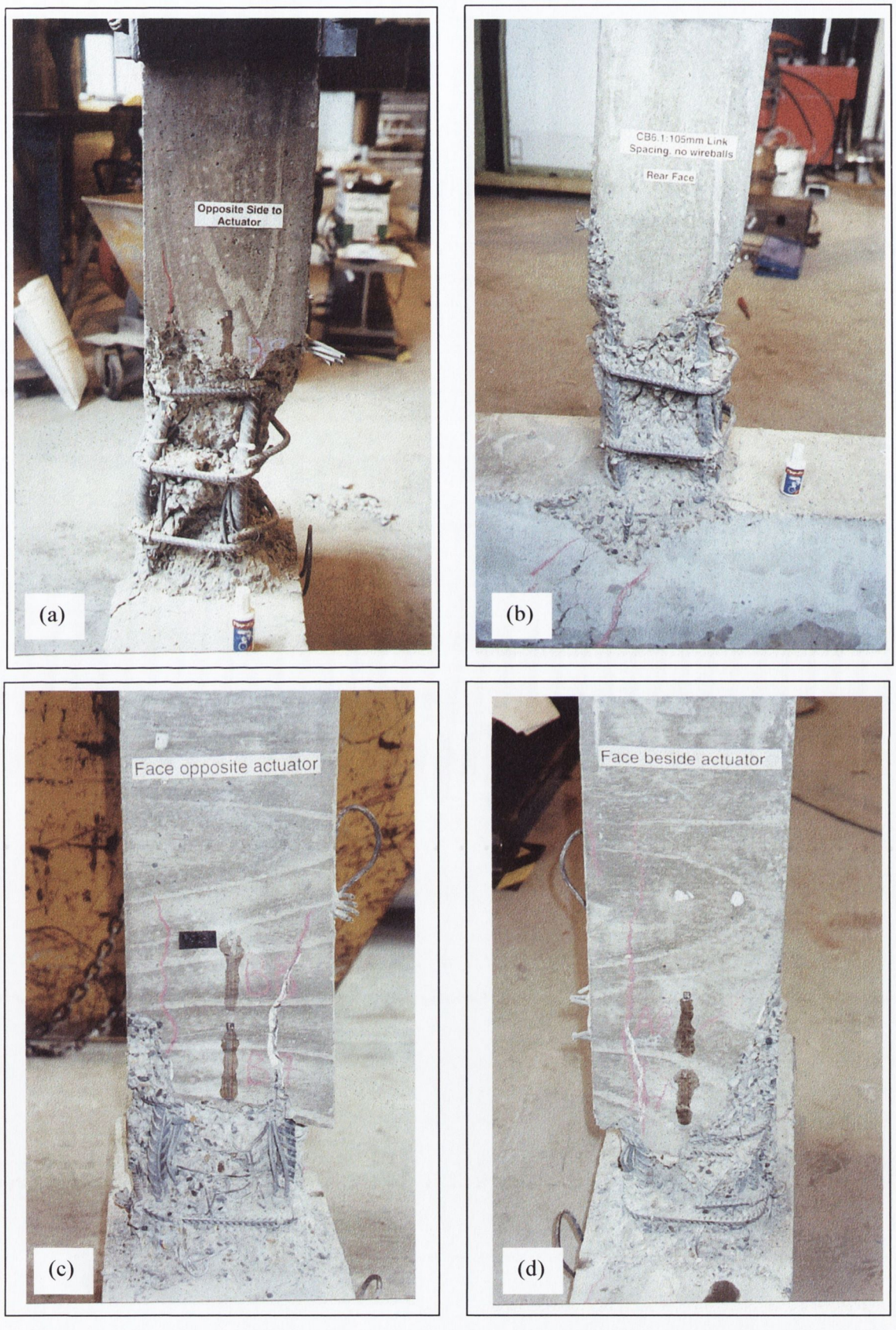

Figure 5.5: Specimens post-failure: (a) and (b): C6.1(105,30), (c) and (d): C6.2(125,W,30)

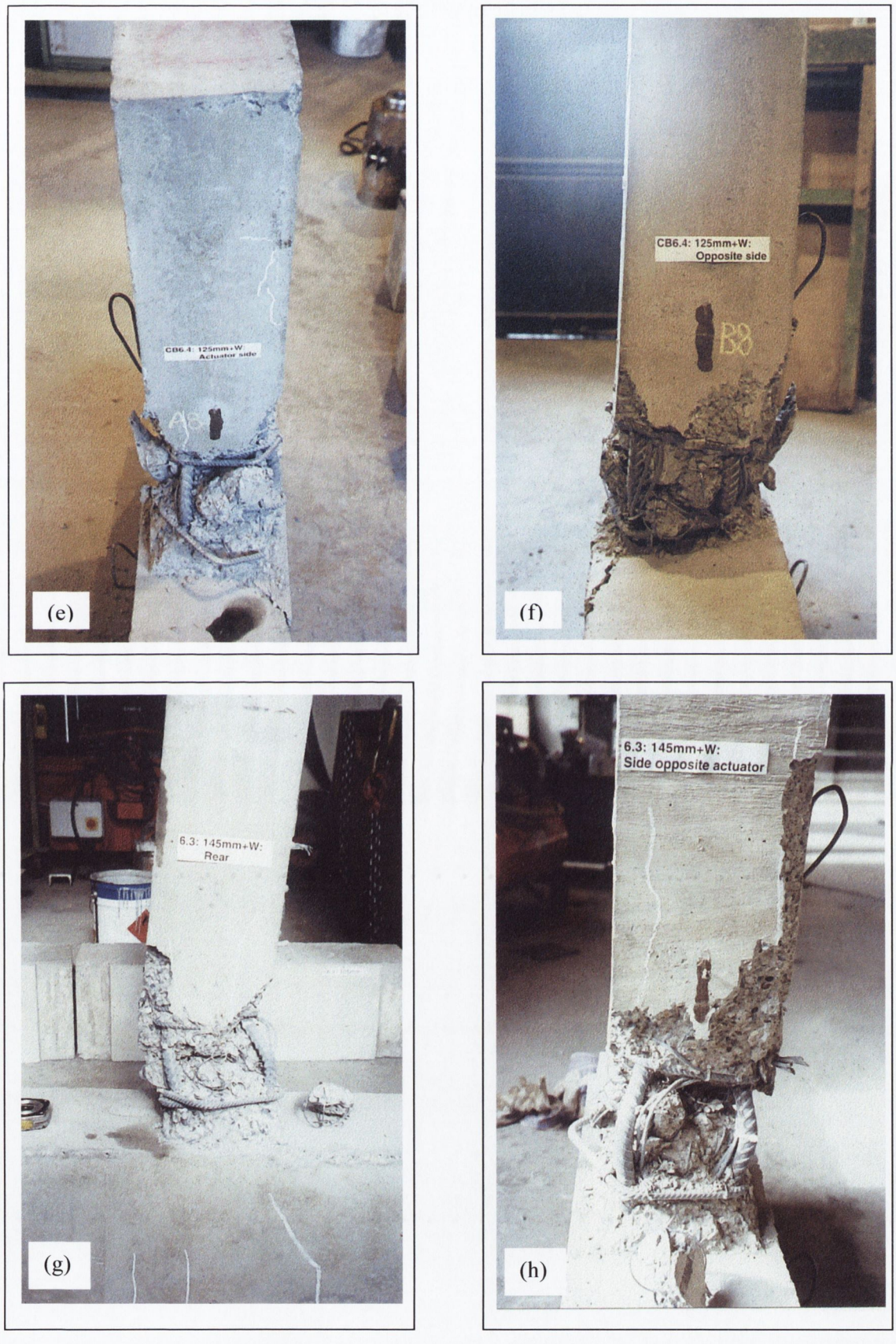

Figure 5.5: Specimens post-failure: (e) and (f): C6.4(125,W,40) and (g) and (h): C6.3(145,W,40)

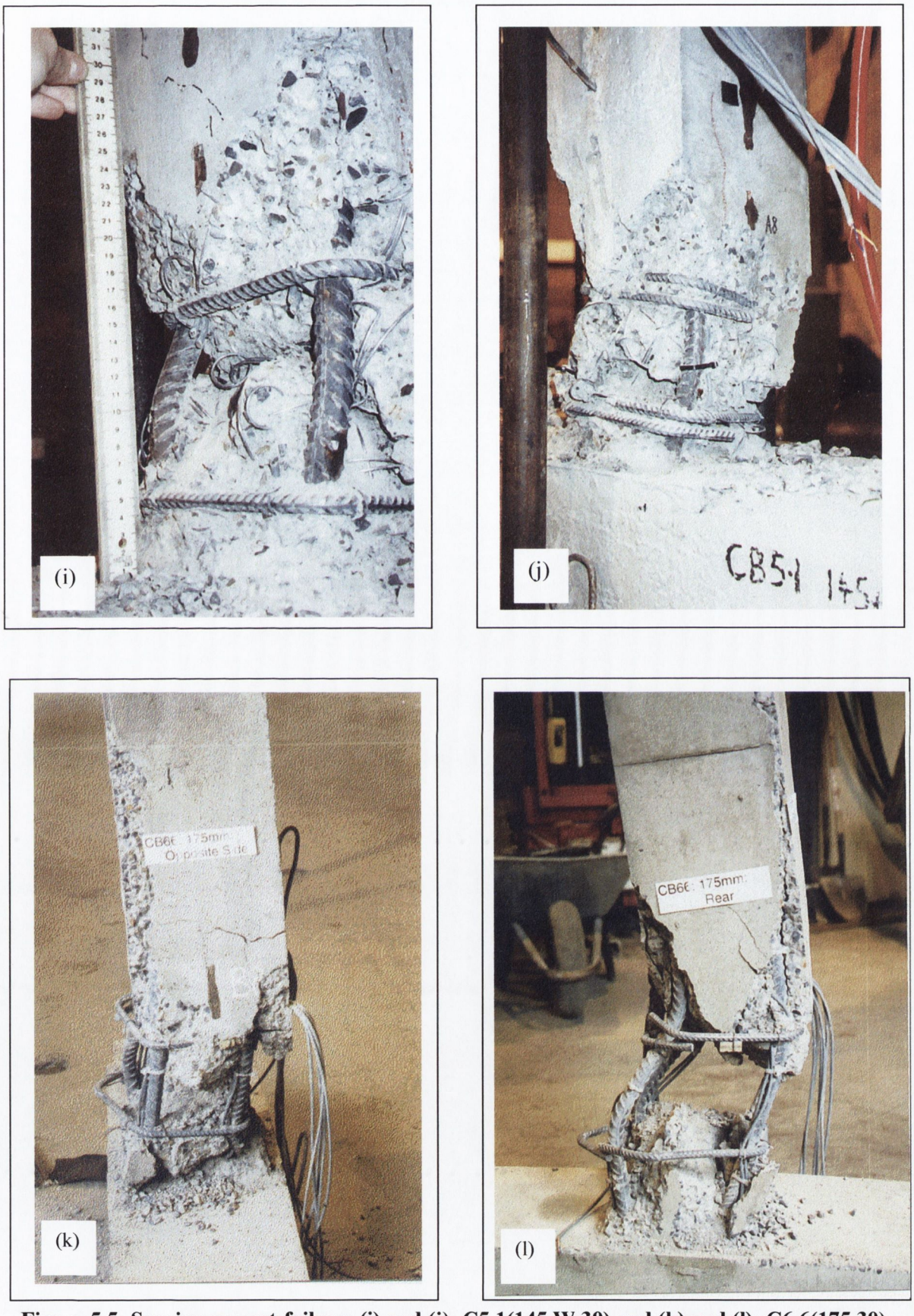

Figure 5.5: Specimens post-failure: (i) and (j): C5.1(145,W,30) and (k) and (l): C6.6(175,30)

Figure 5.5: Specimens post-failure: (m) and (n): C6.5(200,W,30)

Specimen C6.6, with links at 175mm, was the most badly damaged of the specimens. By the end of the test, there was no concrete remaining between the first and second links. This is not surprising since the level of confinement provided in this specimen was too low to offer any restraint against the cracking and degradation of the core. The two lower links of the specimen suffered severe damage - the lower link being probably the most severely damaged of all the specimens. Specimen C6.5, with a link spacing of 200mm, also suffered quite heavy damage but, relative to C6.6, the level of damage was not so severe. Specimen C6.5 had a larger link spacing and yet, was observed to behave better than specimen C6.6. While the core of C6.6 disintegrated totally in the plastic hinge region, this did not occur in specimen C6.5, even at larger displacements. The improved performance may be attributed to the presence of wireballs in specimen C6.5. The specimen that performed best was specimen C6.2 with links at 125mm, and wireballs. Even when this specimen was displaced to the maximum stroke of the actuator it did not collapse. It outperformed specimen C6.1, which had a closer link spacing of 105mm.

Influence of wireballs

The influence of the confinement effects of wireballs is clear when the responses of different specimens are compared. Specimens C5.1 (145,W,30) and C5.2 (145,30) were identical except

that specimen C5.1 contained wireballs. Despite having the same link spacing, axial load, and concrete strengths, there was a marked difference between their observed behaviour. During the cycles just prior to collapse, the core of specimen C5.2 became severely degraded and its two lower links were pushed open and badly distorted. After its collapse, no concrete remained in the region between the first and second link. In contrast, the core within the plastic hinge region of specimen C5.1, remained much more intact, as the wireballs prevented total disintegration. The limited damage to the links of this specimen, in comparison to the links of specimen C5.2, provided strong visual evidence of the confinement effects of wireballs. It is worth noting here, that where specimen C5.2 failed in cycle 7b, specimen C5.1 failed only in cycle 8c.

Comparison of the ultimate states of specimens C6.1 (105,30) and C6.2 (125,W,30) provides further evidence of the benefits of wireballs. Both of these specimens behaved well, but whereas C6.1 failed during cycle 8a specimen C6.2 did not fail, even at the maximum stroke of the actuator. Specimen C6.1 was, therefore, outperformed by specimen C6.2, which had a larger link spacing but which also contained wireballs. Both of these specimens were observed to suffer increased degradation during the 40mm cycles, however, where this damage led to the some opening of the two lower links in specimen C6.1, the links of C6.2 were observed to remain completely closed, even at the end of the test. Therefore, while specimen C6.2 (detailed in accordance with EC8 specifications) performed quite well, the level of confinement offered by its links was not as much as that offered to C6.2 by its combination of links, at a larger spacing (20% larger), and wireballs.

Influence of axial load

It was apparent even during the early stages of the tests, that specimens with target axial loads of 40% suffered more than their counterparts with lower target axial loads of 30%. Degradation of the specimens with the higher levels of axial load began sooner, and was much worse throughout the test, than that of specimens with lower axial loads. Specimens C6.2 (125,W,30) and C6.4 (125,W,40) both had link spacings of 125mm and contained wireballs, but they were subject to axial loads of 30% and 40% their compressive capacities, respectively. Specimens C5.1 (145,W,30) and C6.3 (145,W,40) had link spacings of 145mm and contained wireballs, but were subject to axial loads of 30% and 40% respectively. Within both of these specimen pairs, the influence of the level of axial load was clearly observable. Both specimens with lower axial loads had shorter regions of damage, less distortion and opening of their lower links, and less buckling of their longitudinal steel than their counterparts with higher axial loads. Moreover, the degradations of the cores of the specimens with different levels of axial load were remarkably different. The core of C6.4 was highly degraded, with wireballs being pushed outwards. On the other hand, there was only minor degradation of the core of specimen C6.2. In both specimens C5.1 (145,W,30) and

C6.3 (145,W,40), the wireballs held the specimen cores together and prevented total disintegration. However, in both cases, the wireballs were being forced out of the core, and the expansion of the core was much worse in the specimen with the higher axial load.

Confining influence of the base element

Visual inspection of all the specimens showed that the maximum level of damage occurred, consistently, between the first and second link, which is slightly above the region of maximum moment. In all specimens, the first link was placed at 50mm above the boundary surface, as recommended by EC8 for a beam-column joint. The region just above the boundary surface and beneath the first link, was subject to the maximum moment and yet, in all the specimens, it suffered only minimal damage in its' core. This phenomenon has been observed by many previous researchers (Paultre *et al.*, 2001, Légeron *et al.*, 2000, Bayrak *et al.*, 1998, Sheikh *et al.*, 1994) and is attributed to confinement of the base of beam-column sections by the connected structural element. The confinement offered by this element increases the moment capacity of the sections just above it. Therefore, the resisting moment of the beam-column, without the confinement effects of the base element, is often taken as acting somewhat above the boundary surface. However, in this case, where all the specimens are identical in terms of their end conditions and, therefore, the same level of confinement is provided to each beam-column, the lever-arm is taken as the full lever-arm of 745mm.

5.4 Load-displacement and moment-rotation hysteresis responses

5.4.1 Introduction

This section considers the load-displacement and moment-rotation hysteresis responses of the specimens. The load-displacement responses of all the specimens are discussed in detail in Section 5.5 in terms of energy dissipation and resistance, here they are considered only with respect to the observed behaviour of the specimens during testing. In addition, the influences of wireballs and axial load on the general behaviour of the specimens are considered. Finally, the moment-rotation hysteresis responses are presented.

5.4.2 Load-displacement hysteresis response

Overall, the load-displacement responses of all specimens display many similar general characteristics. They differ in terms of their load capacity degradation, both within a group of cycles and from one group to another, and when their ultimate collapse occurs. All the hysteresis curves are convex displaying little or no pinching; this is a reflection of the flexural, rather than shear, failure of the specimens. However, the hysteresis loops of the specimens differ, somewhat, in terms of their size (energy dissipation), and in the slopes of their descending branches. The load-displacement hysteresis responses are presented in Figure 5.6(a) to 5.6(h).

Over the first four cycles all the specimens remained elastic, displaying no significant non-linearity until cycle 5a. This is clear from the hysteresis plots where the initial stiffness is maintained over the first four cycles. It is only as the concrete started to undergo visible damage that deviation from the initial stiffness occurred.

During each of the tests, the first significant damage was observed during cycle 5a, the first of the 20mm cycles. The previously formed horizontal cracks became permanent and worsened from this cycle on. This is due to the onset of yielding which occurred between cycles 4 and 5a. Referring to Table 5.1, of this chapter, the yield displacements all lie between 8.2 and 11.3mm, which, according to the applied displacement histories, occur in cycle 4 or early in cycle 5a. This yielding indicates significant non-linear behaviour, and this is clearly visible in the hysteresis curves of all the specimens. Small amounts of non-linearity occur in cycle 4 but it becomes much more pronounced during the 20mm cycles. Load-strain plots for the longitudinal steel reinforcement, presented in Appendix A, also illustrate the development of non-linearity during cycles 4 and 5a as the strains reach yield. Appendix B presents load-strain plots for the concrete.

The peak loads of all specimens occur in cycle 5a. In the next two 20mm cycles, the load capacity decreases due to the cyclic degradation of the specimens. Cyclic degradation resulted in spalling of the concrete and plastic elongation of the steel, leading to decreases in load capacity and stiffness.

Similar, but more severe, behaviour to that observed in the 20mm cycles was observed in all later cycles (group cycles 6 to 9), and this behaviour is reflected in the hysteresis curves of the specimens. Further decreases in resistance occur due to more spalling, and flexural cracks open further with plastic elongation of the longitudinal steel. With each displacement group, there was more degradation of the specimens, and this resulted in the decreases in resistance displayed in the hysteresis curves (these falls in load capacity are quantified in terms of resistance ratios in Sections 5.5 and 5.6). The level of degradation of a specimen is reflected by the stability of its hysteresis curves, and this, coupled with the observed behaviour during testing, provides valuable information on the benefits of wireballs.

Comparison of the hysteresis responses of specimens C5.1 (145,W,30), C5.2 (145,30) and C6.3 (145,W,40) provides a very good insight into the benefits of wireballs. The most stable of these three hysteresis curves is that of specimen C5.1 which maintains good load carrying capacity until the 50mm cycles. On the other hand, the hysteresis curve of C5.2 is not so stable, displaying larger drops in load capacity preceding specimen failure during the 40mm cycles. The superior behaviour of C5.1 relative to C5.2 can be attributed to the presence of wireballs. The hysteresis curve of C6.3 was also less stable than that of C5.1, due to the effects of a higher axial load. However, despite having a higher axial load than C5.2, the hysteresis curve of C6.3 is remarkably similar to that of C5.2 providing further positive indication of the confinement benefits of wireballs. Warnings of the imminent collapse of all these specimens is provided by the significant drops in load carrying capacity displayed on the hysteresis curves. These are due to crushing of the core, opening up of the links and finally, buckling of the longitudinal steel.

It was noted in the above comparison that the specimen with the higher axial load has a less stable hysteresis curve than its counterpart with a lower axial load. The effect of axial load on specimens with wireballs is also illustrated by comparison of specimens C6.2 (125,W,30) and C6.4 (125,W,40). C6.2 displayed the most stable behaviour of all the specimens during testing, as it did not fail, suffering only minimal core damage and minor buckling. This stability is reflected in the resulting hysteresis curve in which there are no sudden drops in load carrying capacity, and the shapes of the hysteresis loops within each displacement group remain very similar. In contrast, specimen C6.4 with a higher axial load did fail because its core suffered much degradation. The contrast between the hysteresis curves illustrates, clearly, the effects of axial load on the stability of the specimens. A final point here is that specimen C6.2 outperformed specimen C6.1 despite having a larger link spacing. C6.1 was detailed in accordance with EC8 for DCL conditions. It failed in the last 40mm cycle. The hysteresis curve for specimen C6.1 displays a considerable drop in resistance during cycle 7c. This sudden loss in resistance, together with an observed sudden increase in the width of a large vertical crack on the corner of C6.1, provides warning of the imminent collapse of the specimen.

Specimen C6.6 was observed to perform the least well of all of the specimens. Its poor performance was due to the specimen's large link spacing and absence of wireball reinforcement. The hysteresis curve shows that the specimen failed upon entry into the 40mm cycles. Significant losses of resistance occur before failure due to the rapid disintegration of the specimen core. Relative to specimen C6.5, the performance of C6.6 was very inferior. This is illustrated by the contrast between the hysteresis curves of the two specimens. In specimen C6.5, the hysteresis loops are stable, displaying small decreases in resistance and similar descending curves within each displacement group. In specimen C6.6, there are significant losses of resistance within each displacement group, leading to a decrease in the area of the hysteresis loops.

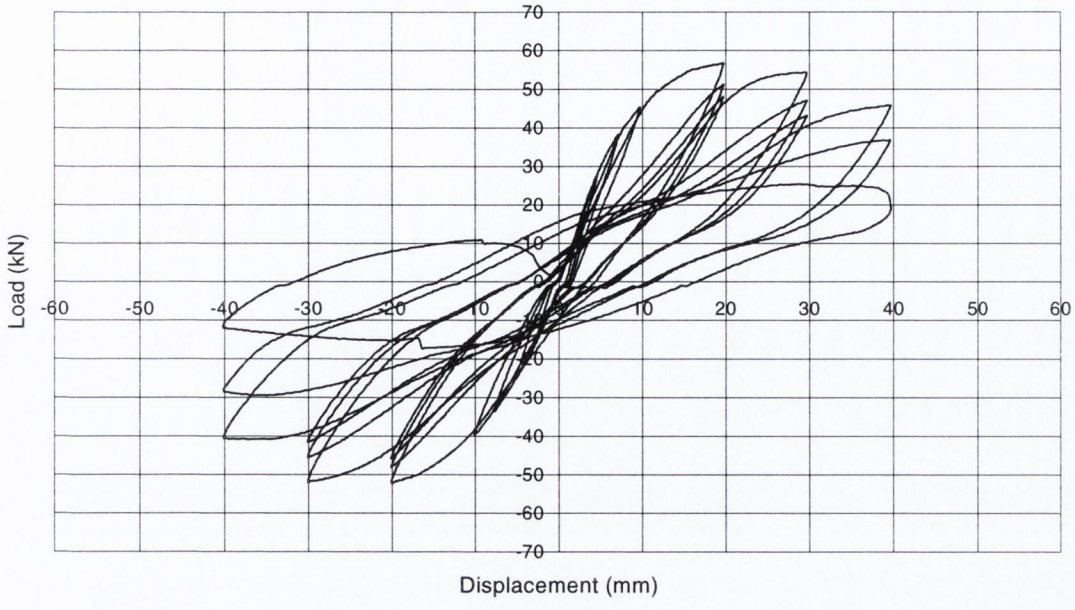

Figure 5.6 (a): C6.1 (105,30) Load-displacement hysteresis response

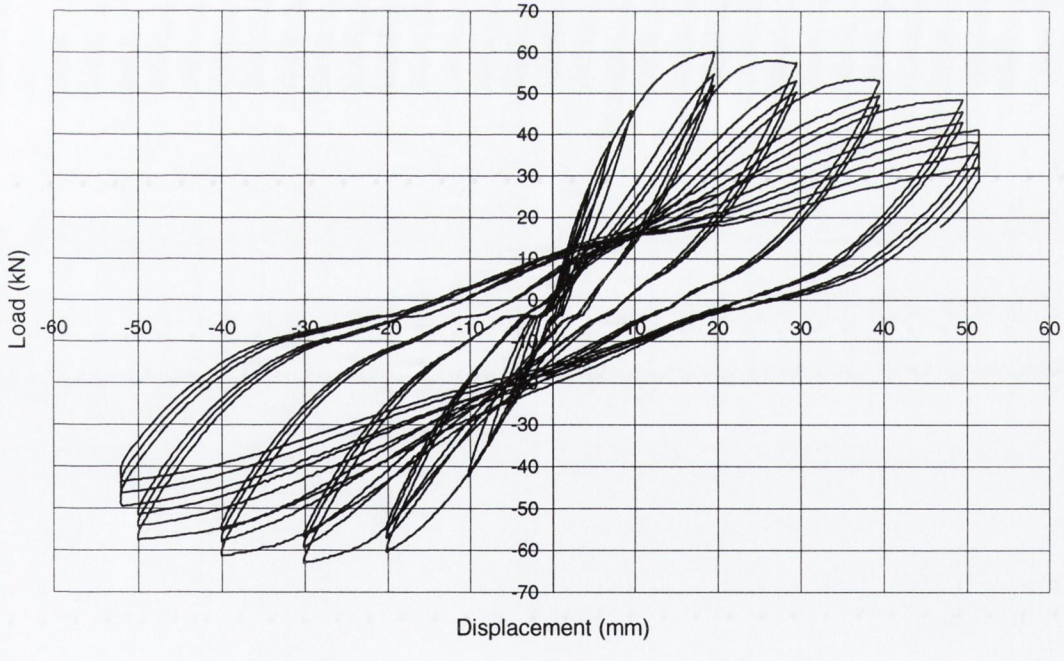

Figure 5.6(b): C6.2 (125,W,30) Load-displacement hysteresis response

Figure 5.6(c): C6.4 (125,W,40) Load-displacement hysteresis response

Figure 5.6(d): C5.1 (145,W,30) Load-displacement hysteresis response

Figure 5.6(e): C5.2 (145,30) Load-displacement hysteresis response

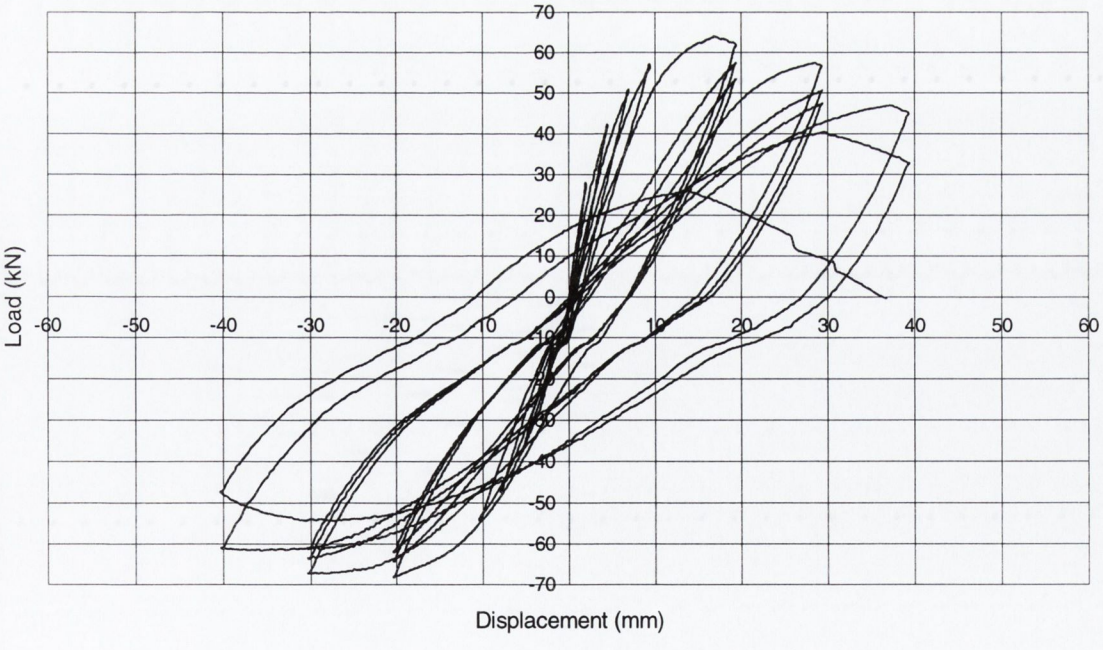

Figure 5.6(f): C6.3 (145,W,40) Load-displacement hysteresis response

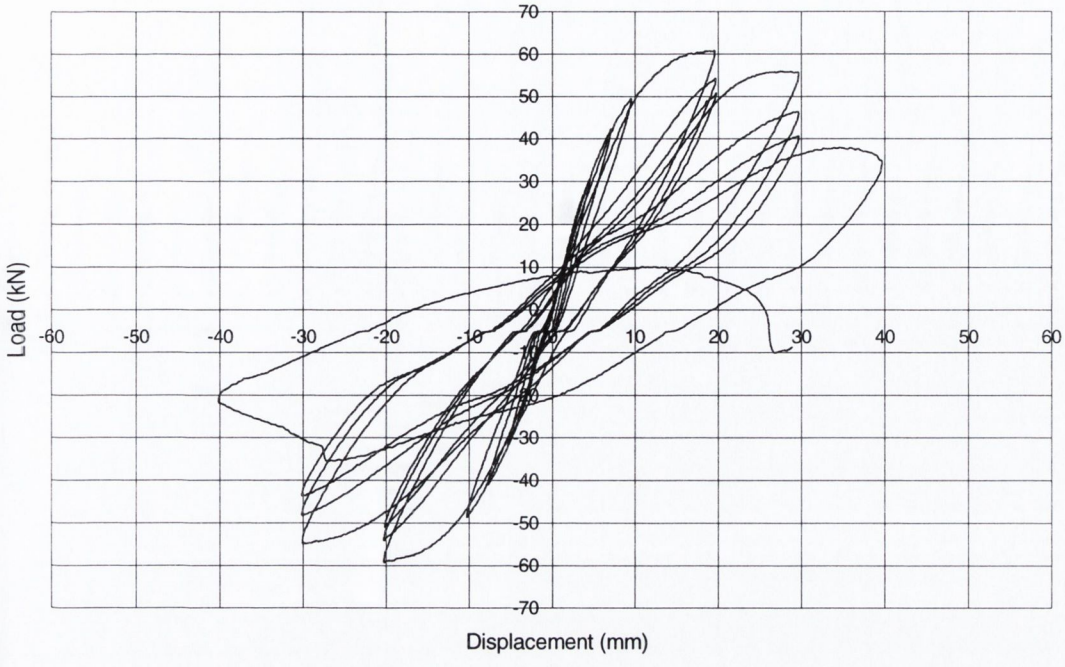

Figure 5.6(g): C6.6 (175,30) Load-displacement hysteresis response

Figure 5.6(h): C6.5 (200,W,30) Load-displacement hysteresis response

5.4.3 Moment-rotation hysteresis response

The moment-rotation curves are plots of the total moment versus rotation. Rotation is defined in Equation 5.1 as the ratio of the applied lateral displacement to the lever-arm length. The moment is the sum of the moment due to the applied lateral force plus the moment arising from the P-Delta effect (Section 3.7.2.1). Figures 5.7(a) to (h) present the moment-rotation hysteresis responses of the specimens. The curves display similar characteristics to the load-displacement curves in terms of reductions in resistance and in the shape of the hysteresis loops. However, the load-displacement curves present the responses to the applied lateral load only, while the moment-rotation curves present the responses to the moment due to the applied lateral loading and that moment due to the P-Delta effect. In the figures, the envelope curves for the maximum moment due to the applied lateral load for each group cycle, are shown by a dashed line. The intention of these plots is solely to illustrate the increase in moment, due to the P-Delta effect, which the specimens are subject to. Outside of this section, the specimen responses are considered in terms of the load-displacement response only.

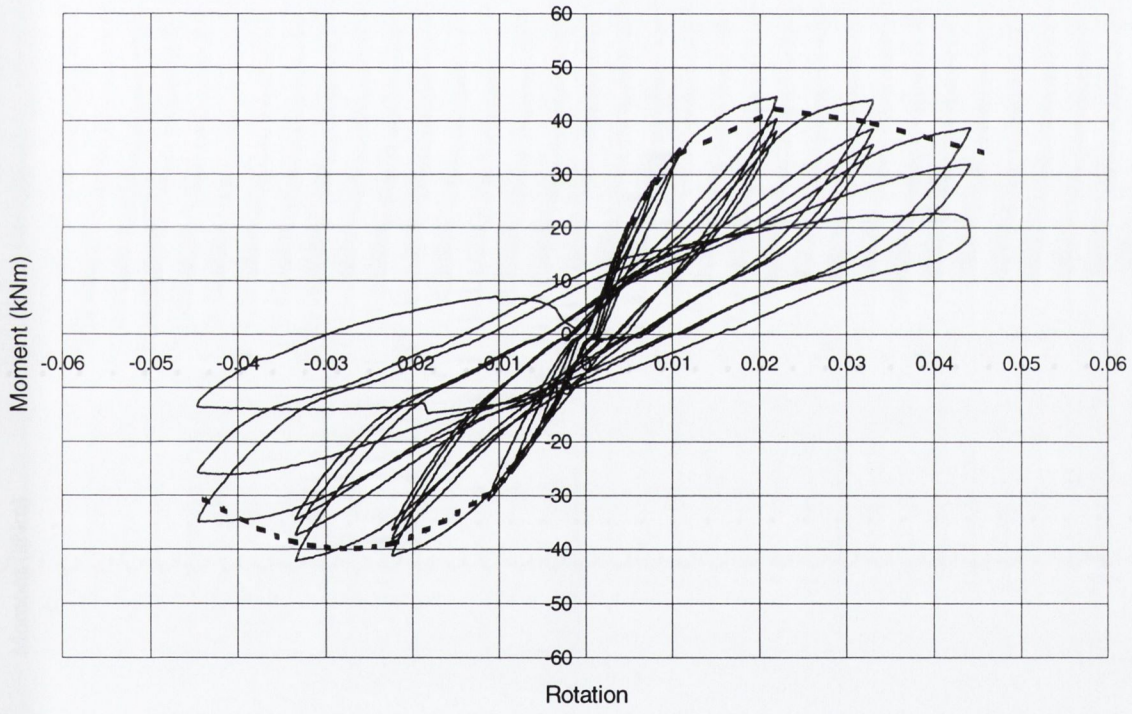

Figure 5.7(a): C6.1 (105,30) Moment-rotation hysteresis response

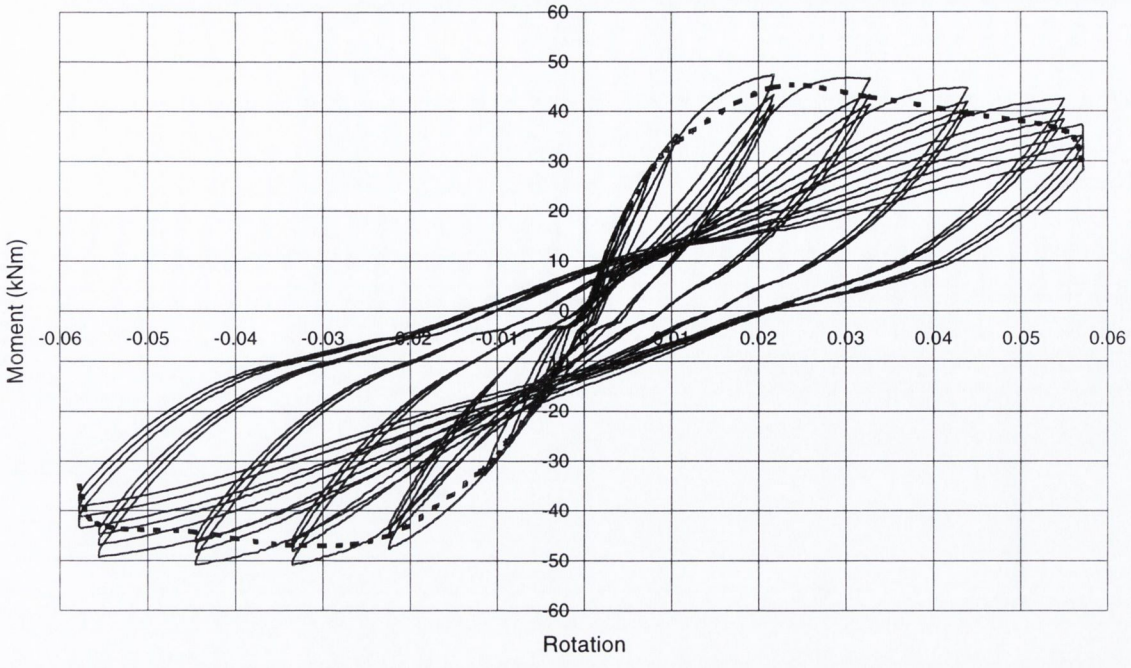

Figure 5.7(b): C6.2 (125,W,30) Moment-rotation hysteresis response

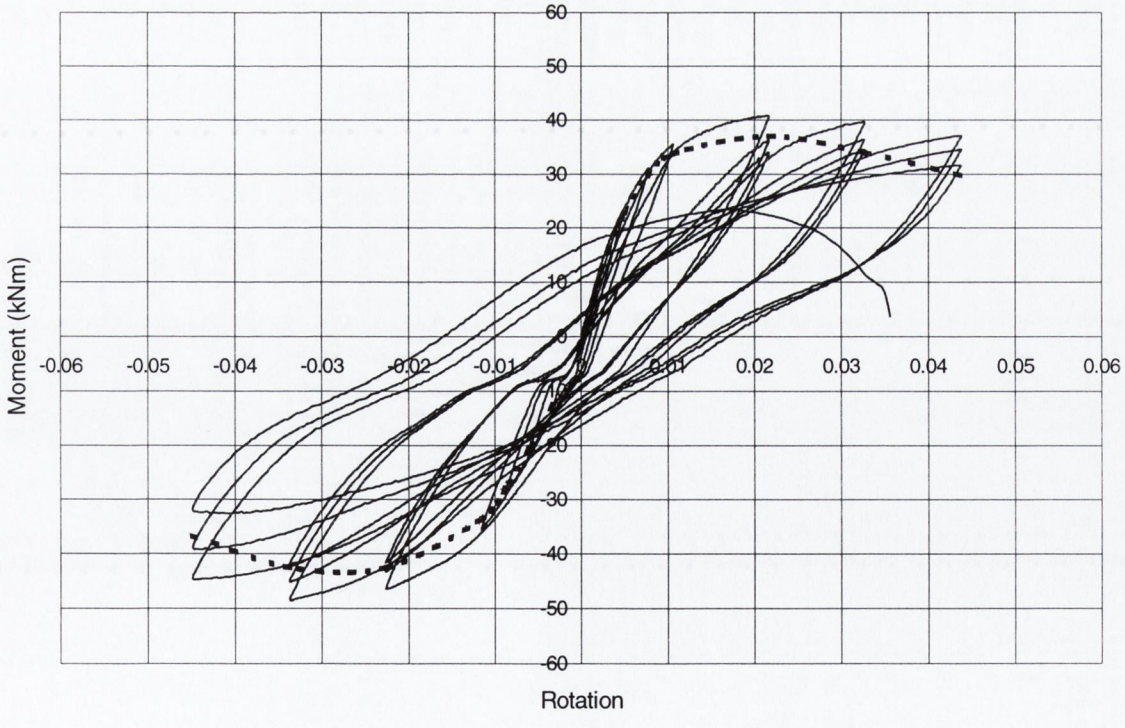

Figure 5.7(c): C6.4 (125,W,40) Moment-rotation hysteresis response

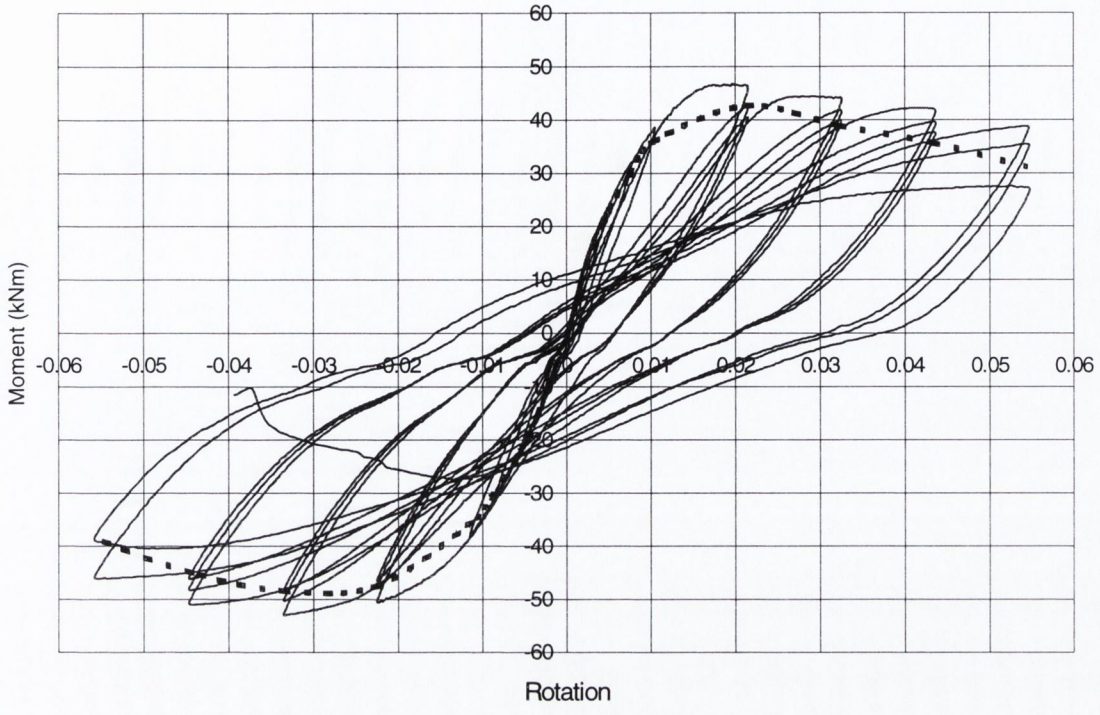

Figure 5.7(d): C5.1 (145,W,30) Moment-rotation response

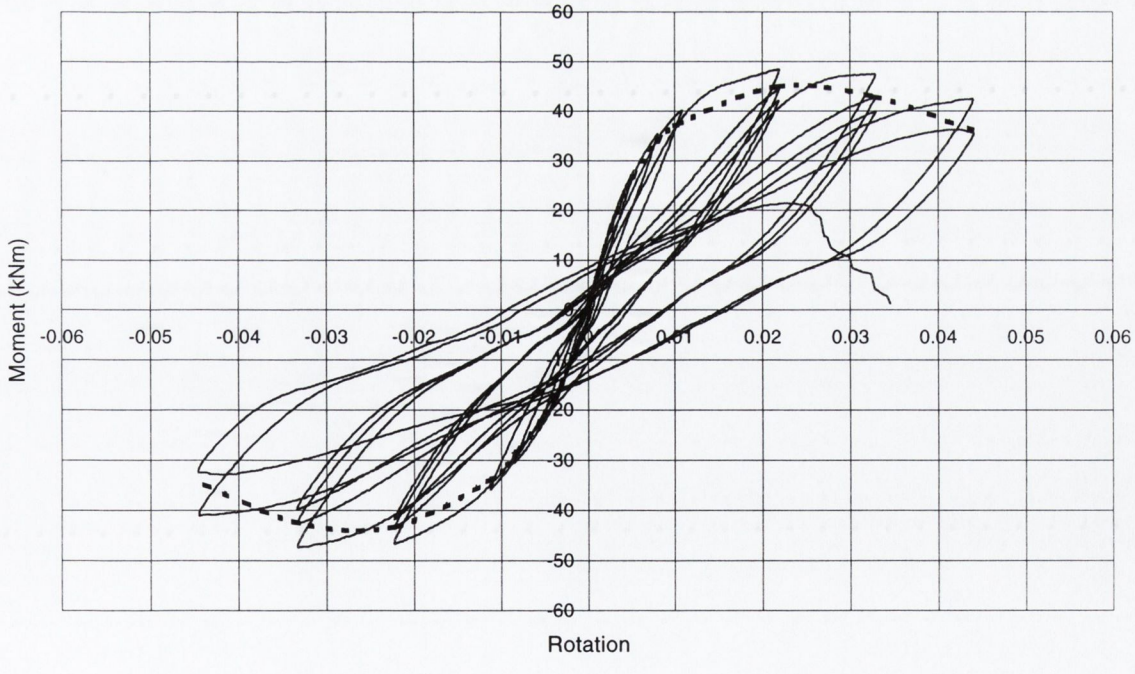

Figure 5.7(e): C5.2 (145,30) Moment-rotation hysteresis response

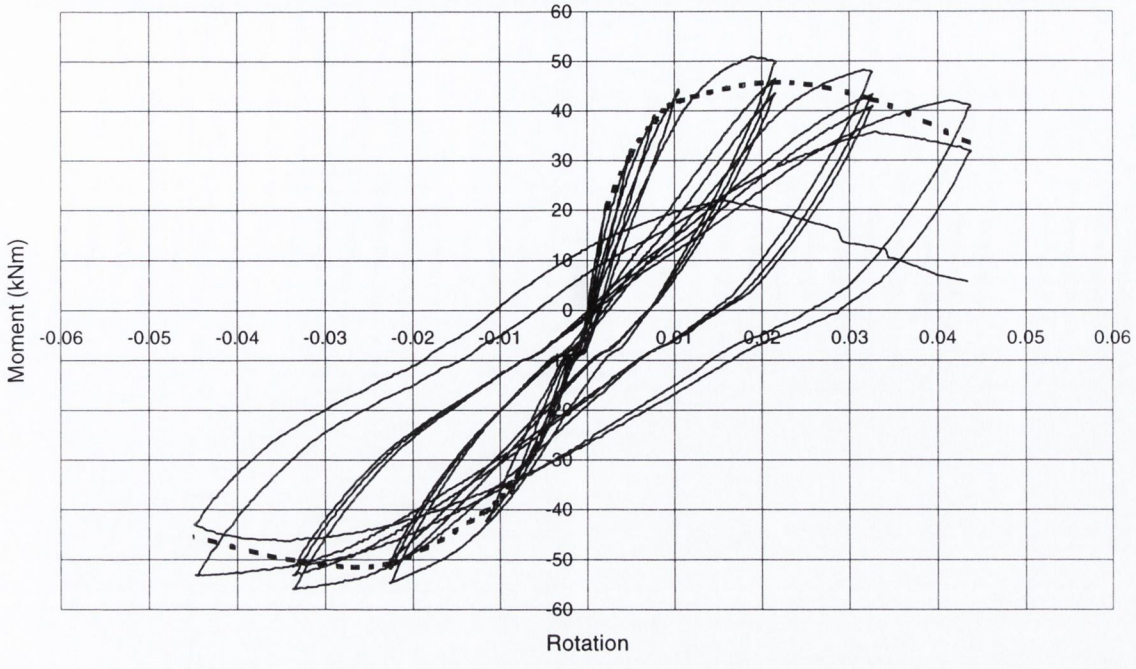

Figure 5.8(f): C6.3 (145,W,40) Moment-rotation response

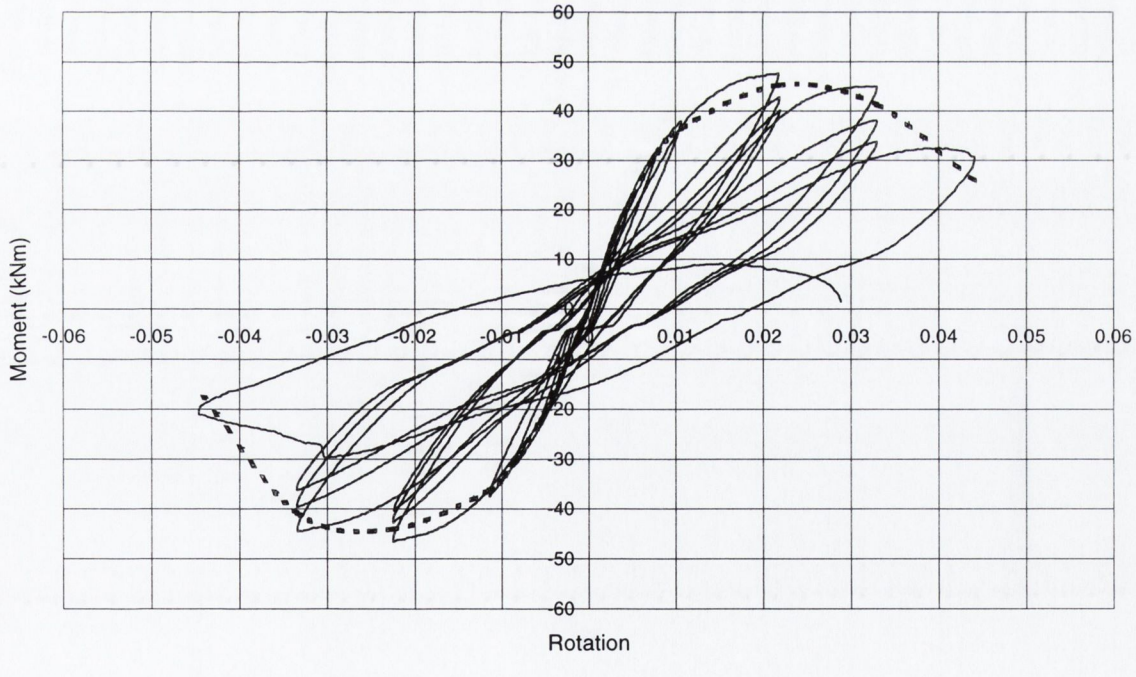

Figure 5.7(g): C6.6 (175,30) Moment-rotation response

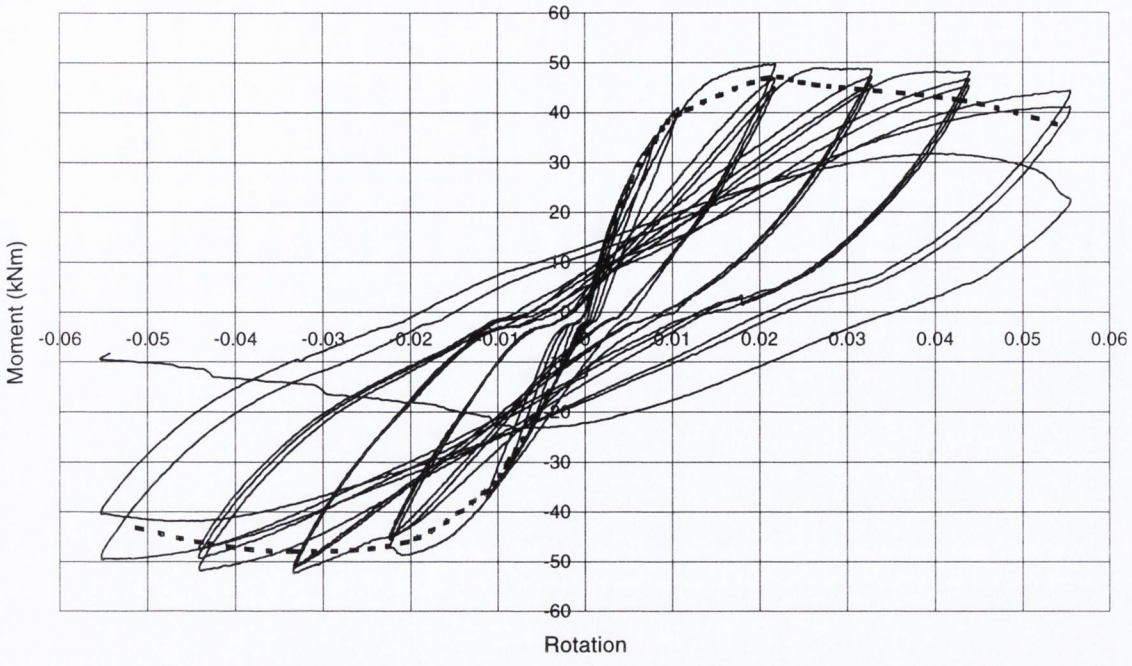

Figure 5.7(h): C6.5 (200,W,30) Moment-rotation response

5.5 Comparison groups

Within this section, the hysteresis characteristics of the specimens are considered in detail to investigate further the extent to which the inclusion of wireballs improves concrete confinement. Previous sections have shown that in terms of ductility capacity and observed behaviour during testing the inclusion of wireballs is certainly beneficial. The aim of this section is to consolidate the information provided in previous sections by considering, in greater depth, the hysteresis characteristics of the specimens in terms of energy dissipation and resistance, since both of these properties are essential for good earthquake resistance. The results of the eight specimens are examined by dividing them into three groups as detailed in Table 5.5. In each group, the specimens possess broadly similar link spacings.

Energy dissipation

The ability of a structure to dissipate energy is of the utmost importance in earthquake resistant design. In reinforced concrete, increased energy dissipation is achieved through confinement. As the area within a hysteresis loop is a measure of the energy dissipation capacity of a system, it is important that large hysteresis loops are maintained, even after a number of load reversals. Within this section, the energy dissipation capacity of the specimens is considered by plotting the area within each hysteresis loop against the corresponding displacement cycle. The aim is to determine

whether the inclusion of wireballs increases energy dissipation capacity, thereby quantifying their effectiveness in confining concrete.

Resistance

The resistance of a specimen is a measure of its ability to maintain load carrying capacity under cyclic loading. It is, therefore, an inverse measure of how much cyclic degradation a specimen suffers. Two evaluations of resistance are considered within this section, as follows:

- Resistance ratio: the ratio of the maximum resistance attained in a cycle to the yield resistance of the specimen. It is calculated as the ratio of the maximum load attained in a cycle to the yield load.
- Minimum resistance: the minimum resistance ratio attained in a group of cycles.

Group Number	Specimen	Link Spacing (mm)	Wireballs (Y/N)	$N/(f_{ck})(A)$ (%)
1	C6.1	105	N	33.2
	C6.2	125	Y	28.8
	C6.4	125	Y	38.5
2	C5.1	145	N	28.3
	C5.2	145	Y	30.1
	C6.3	145	Y	39.7
3	C6.6	175	N	29.7
	C6.5	200	Y	30.0

Table 5.5: Comparison groups of specimens

5.5.1 Group 1 (C6.1, C6.2 and C6.4)

The three specimens considered within this group are, C6.1(105,30), C6.2(125,W,30) and C6.4(125,W,40). The link spacing of 105mm, used in specimen C6.1, is the link spacing recommended for a DCL column subject to an axial load of 30% of its compressive capacity. The 125mm link spacing of the other two specimens was chosen to determine whether these specimens would behave as well as C6.1, due to the inclusion of wireballs, even though their link spacing was 20% larger. Specimen C6.4 had both a larger link spacing and a higher axial load than C6.1. The hysteresis curves of the three specimens are shown in Figure 5.6(a) to 5.6(c), and the contrasts displayed therein were discussed briefly in Section 5.4.2. The most evident contrast was that between the extremely stable behaviour of C6.2 and that of the other two specimens. A second important aspect was that specimen C6.1 did not appear to behave any better than specimen C6.2,

even though it was subject to a lower axial load, and had closer confining links. This section now considers these effects quantitatively.

Energy dissipation

Figure 5.8 compares the energy dissipated in each of the push and pull half cycles of the three tests. The energies dissipated by all specimens are very similar, which is no surprise since all of these specimens are well confined. However, specimen C6.2 continues to dissipate energy long after the other two specimens have failed, implying that, in terms of the *total* energy dissipated, specimen C6.2 outperforms the other two specimens.

Specimen C6.4(125,W,40) displays an energy dissipation capacity as good as that of specimen C6.1 (105,30) even though it was subject to 40% axial load and had a larger link spacing. The EC8 recommended link spacing for a similar column with an axial load of 40% its capacity is 80mm. However, specimen C6.2 has a link spacing 55% greater than this, and still performs as well as C6.1, detailed to EC8 standards for a 30% axial load.

A final point to note is that for all three specimens, the energy dissipated during the "pull" half cycle is consistently larger than that dissipated for the "push" half cycle. This trend is discussed further in Section 5.6.3.

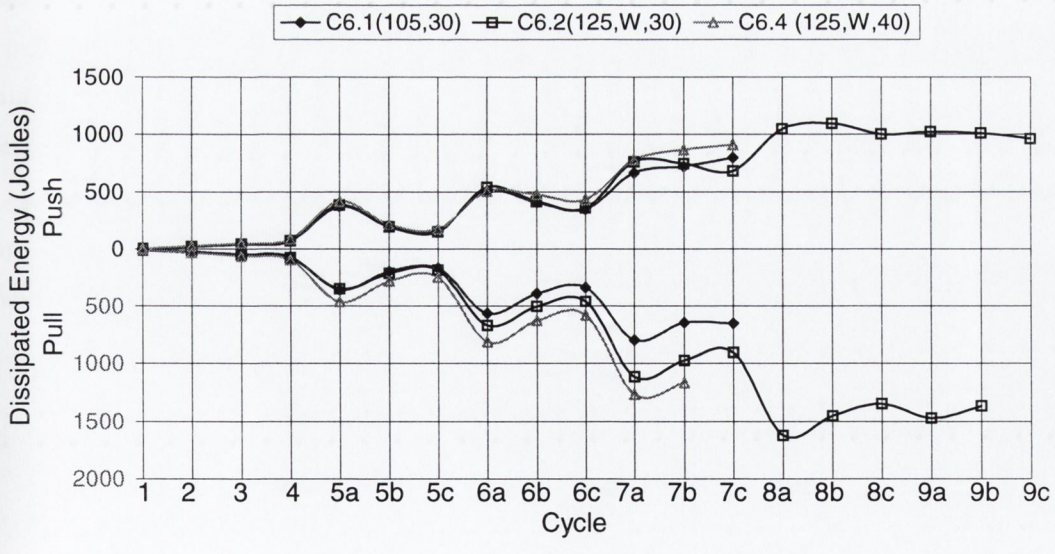

Figure 5.8: Group 1 Dissipated energy versus cycle

Resistance

A plot of the resistance ratios achieved by the specimens in each displacement cycle is presented in Figure 5.9. From the plot, it is easy to identify the point when the specimens attain their maximum resistances and the manner in which their resistances decrease as the specimens undergo increased cyclic degradation. These resistance plots reflect the energy dissipation plots in that the resistance ratios of the specimens are all quite similar. The similarity between the two plots arises because energy dissipation is partly a function of the resistance: the greater a specimen's resistance, the greater its potential for maintaining its load carrying capacity and, hence its increased energy dissipation capacity. However, both this plot and the energy dissipation plot show that the specimen's behaviours diverge a little from cycle 7a (the first 40mm cycle) on.

During the 40mm cycles, specimen C6.1 displays considerable losses in resistance. C6.4 also displays significant losses, but these are smaller than for C6.1. While C6.2 does lose some resistance, the decrease is small. Moreover, specimen C6.2 continues to resist load up to the end of the test. The losses in resistance of these specimens occur first due to the spall of cover concrete and some plastic elongation of the steel. In the later cycles, the more rapid decreases in resistance are due to further plastic elongation of the steel and degradation of the concrete core. Specimen C6.2 continues to resist load to the end of the test because its core does not degrade significantly due to the high level of confinement offered to it by the combination of closely spaced links and wireballs.

Figure 5.10 presents the minimum resistances of the specimens within each group for both push and pull displacements. The change in these resistance values is a good indication of how the stability of a specimen changes from one displacement level to the next. The plot highlights the extremely stable behaviour of specimen C6.2 relative to the other two specimens. It also indicates that specimen C6.4 has a slightly greater stability than specimen C6.1, where in displacement group 7, the minimum resistance of C6.4 is significantly higher than that of C6.1. However, both of these specimens fail before the 50mm cycles (displacement group 8).

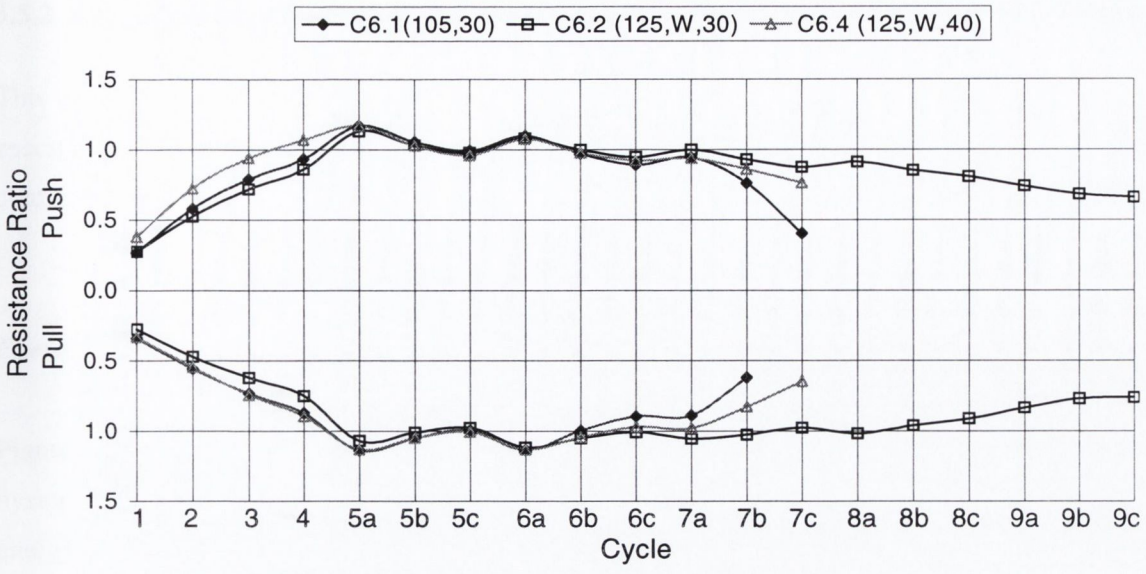

Figure 5.9: Group 1 Resistance ratios versus cycle

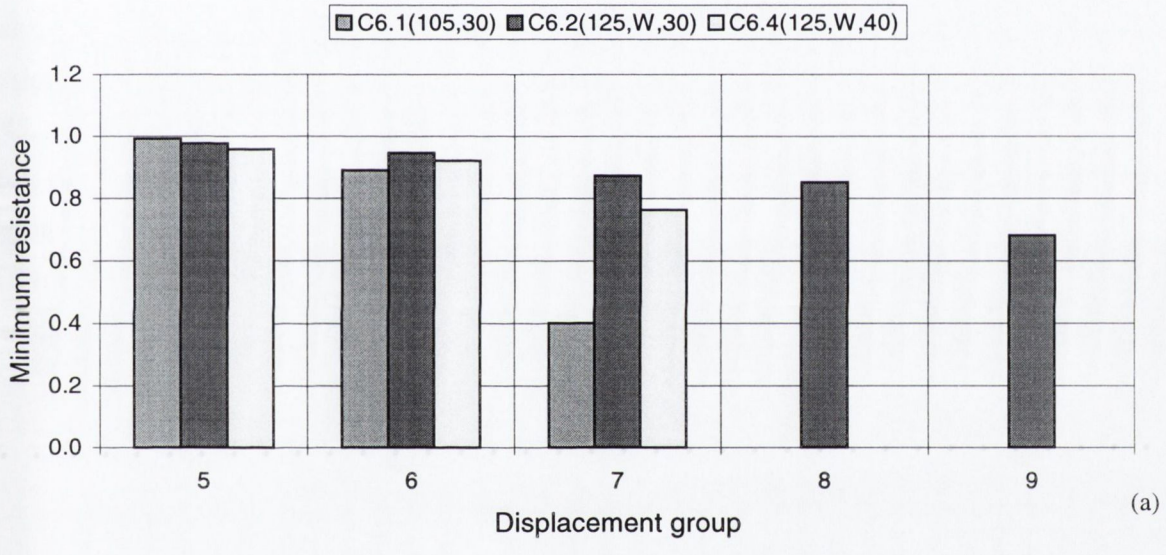

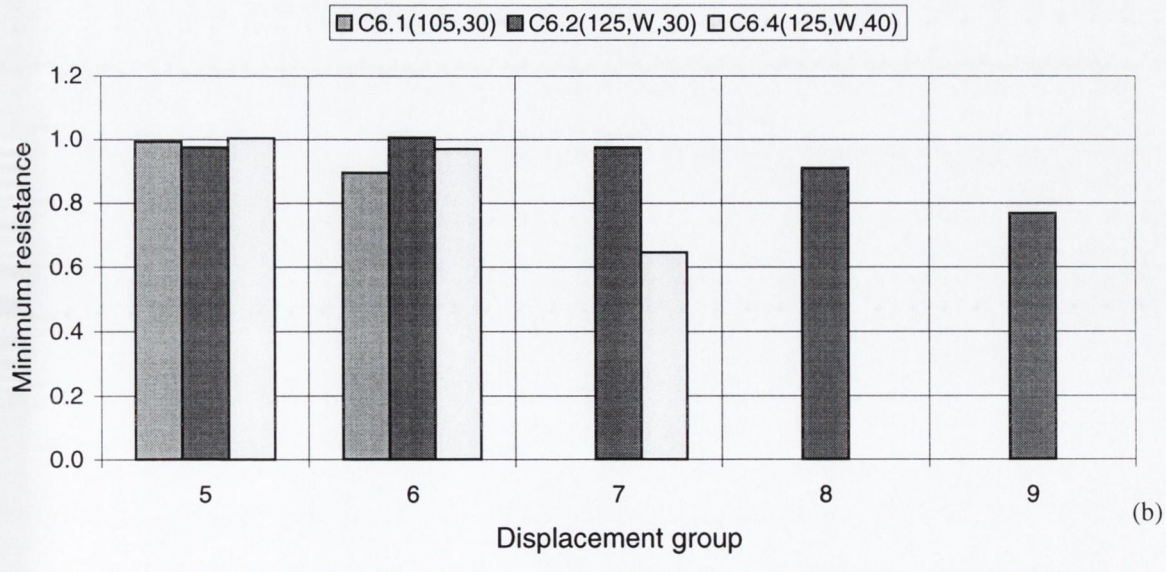

Figure 5.10: Group 1: (a) Minimum push resistances, (b) Minimum pull resistance

5.5.2 Group 2 (C5.1, C5.2 and C6.3)

This group compares specimens C5.1 (145,W,30), C5.2 (145,30) and C6.3 (145,W,40). All the specimens have the same link spacing of 145mm, however, they differ in whether or not they contain wireballs and in the level of axial load applied.

Energy dissipation

Figure 5.11 shows the energies dissipated by the three specimens in the half cycles of each hysteresis loop. Up to and inclusive of cycle 5c, the three specimens dissipate similar quantities of energy. From cycle 6a on, (as in Group 1), the curves diverge somewhat as the specimens undergo different rates of damage. The specimen that performs the best is specimen C5.1. As for specimen C6.2 of Group 1, specimen C5.1 outperforms the other two specimens by its ability to continue resisting load at higher displacements, rather than by possessing significantly superior energy dissipation capacity within each hysteresis loop. The superiority of C5.1(145,W,30) over C5.2 (145,30) shows clearly the confinement benefits of wireballs, as does the fact that specimen C6.3(145,W,40) performs almost as well as specimen C5.1(145,W,30). The hysteresis curves of the latter two specimens are very similar, having almost the same levels of energy dissipation as far as cycle 6c. Again, the dissipated energies of these three specimens are larger for the pull displacement.

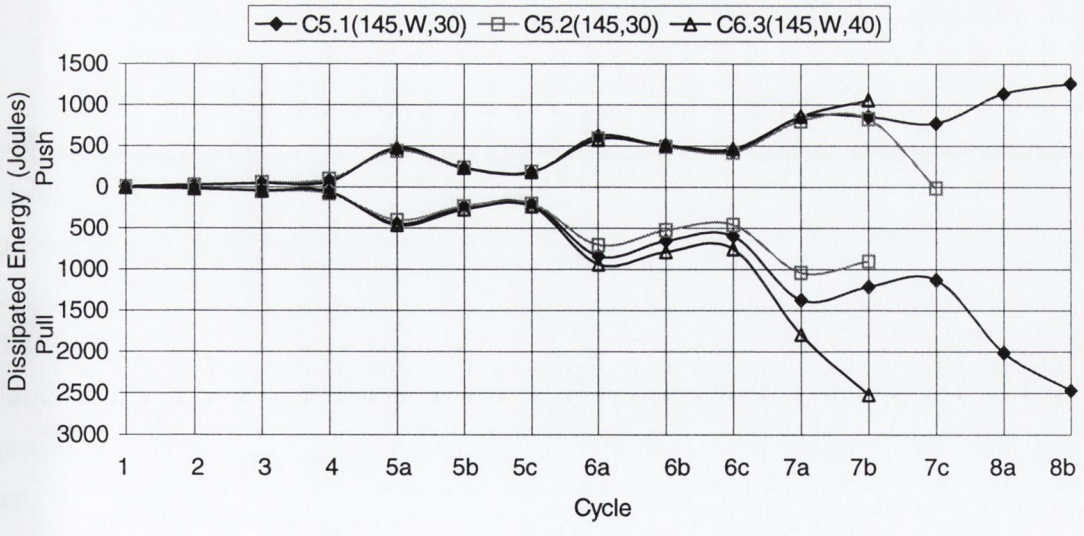

Figure 5.11: Group 2 Dissipated energy versus cycle

Resistance

The resistance ratios achieved in each cycle are plotted in Figure 5.12. As in Group 1, all of the specimens reach their maximum resistance in cycle 5a (just after yield), except for C6.3 which reaches its maximum "pull" resistance in cycle 6a. The resistance levels of all three specimens are alike, except that specimens C5.2 and C6.3 lose all resistance in cycle 7c, whereas specimen C5.1 continues to resist load to cycle 8c. Akin to the energy dissipative capacities of C5.2 and C6.3, the resistance ratios of these two specimens are also comparable, signifying the good confinement capabilities of wireballs even where the axial load level promoted an over-reinforced failure.

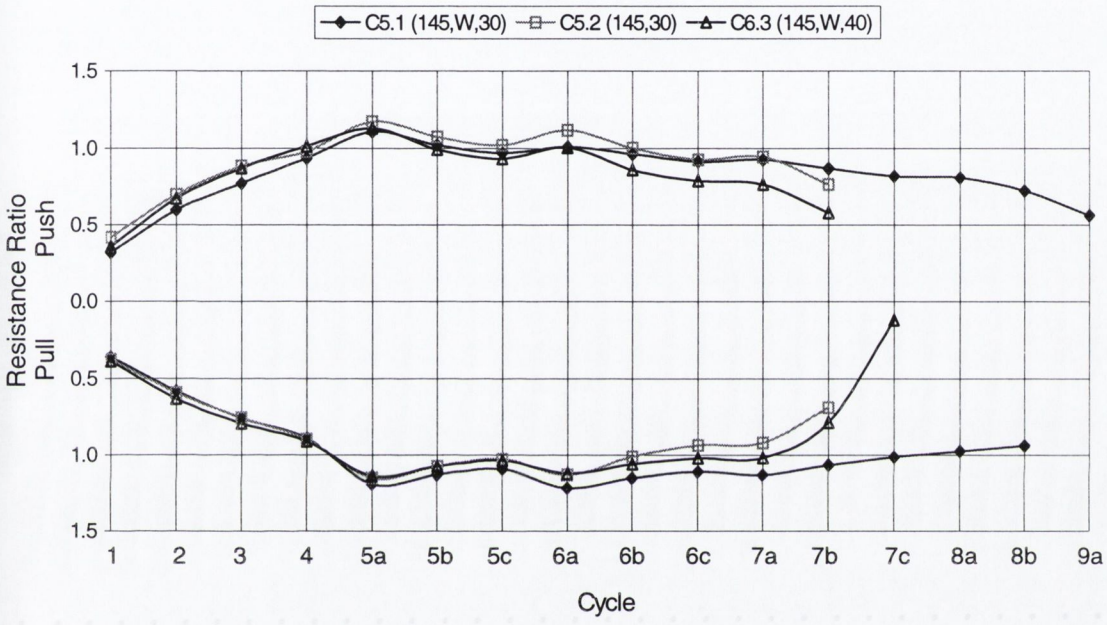

Figure 5.12: Group 2 Resistance ratios versus cycle

Figure 5.13 shows the minimum resistance ratios of the three specimens for each push and pull displacement group. This shows very clearly the superior performance of specimen C5.1 relative to the other two specimens. Where the other two specimens lose their resistance in the 40mm (group 7) cycles, specimen C5.1 still displays a large value of minimum resistance in the 50mm cycles (group 8), for both push and pull half cycles. Also evident from these plots is the similar performances of specimens C5.2 and C6.3. However, while C5.2 loses all of its resistance in displacement group 7, the minimum resistance of C6.3 is still greater than zero for this displacment group. Although specimen C6.3 was observed to have a shear crack running through its core at the end of the 40mm cycles, much more concrete remained within its core than in specimen C5.2 due to the interlocking properties of the wireballs, and hence, the slightly superior resistance of specimen C6.3.

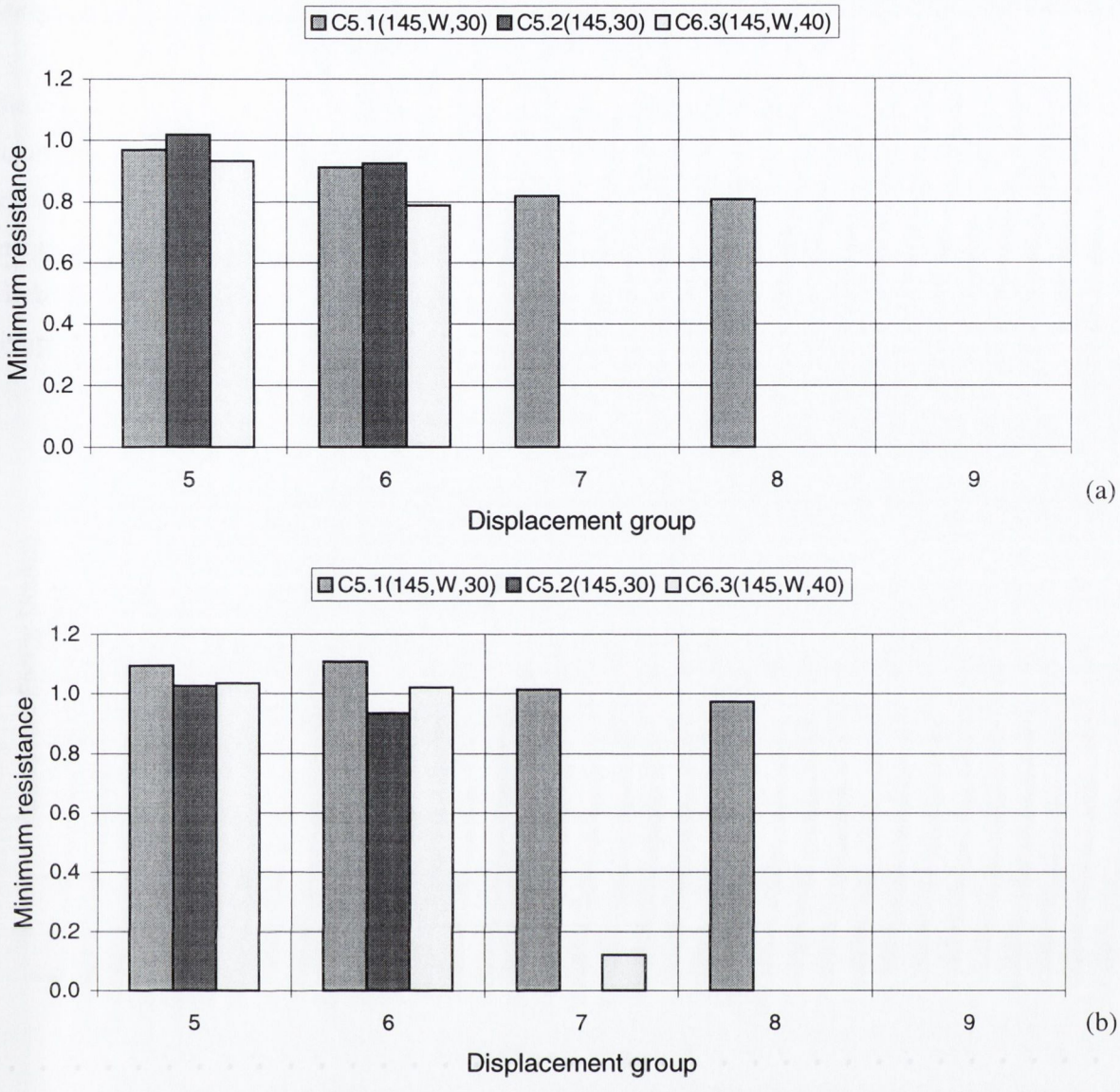

Figure 5.13: (a) Minimum push resistances (b) Minimum pull resistances

5.5.3 Group 3 (C6.5 and C6.6)

Both specimens in this group had an axial load of 30% of their compressive capacities. Specimen C6.5 contained wireballs, and links at 200mm spacing (90% greater than that recommended for DCL conditions). Specimen C6.6 had no wireballs but, its links were at a closer spacing of 175mm (67% greater than that for DCL conditions). The previous two groups provide substantial evidence that the inclusion of wireballs enhances specimen performance by supplying increased confinement. More particularly, the results suggest that through the use of wireballs, the spacing of confining links recommended by EC8 for DCL conditions may be increased without detrimental effect on beam-column ductility. The link spacings previously considered were 125mm and 145mm. Comparison of the results of this last pair of specimens will determine whether wireballs contrive to enhance specimen performance at much larger link spacings.

Energy dissipation

The energy dissipated by specimens C6.5 and C6.6 in each displacement cycle are compared in Figure 5.14. The superior behaviour of C6.5 is very evident in its ability to dissipate energy well beyond the cycle in which C6.6 fails. Also, even during the cycles where C6.6 resists load, its energy dissipation capacity is always slightly less than that of C6.5. This indicates that the use of wireballs can be beneficial even when the link spacing is large. As in all the previous energy dissipation plots, more energy is dissipated when the specimen is being pulled.

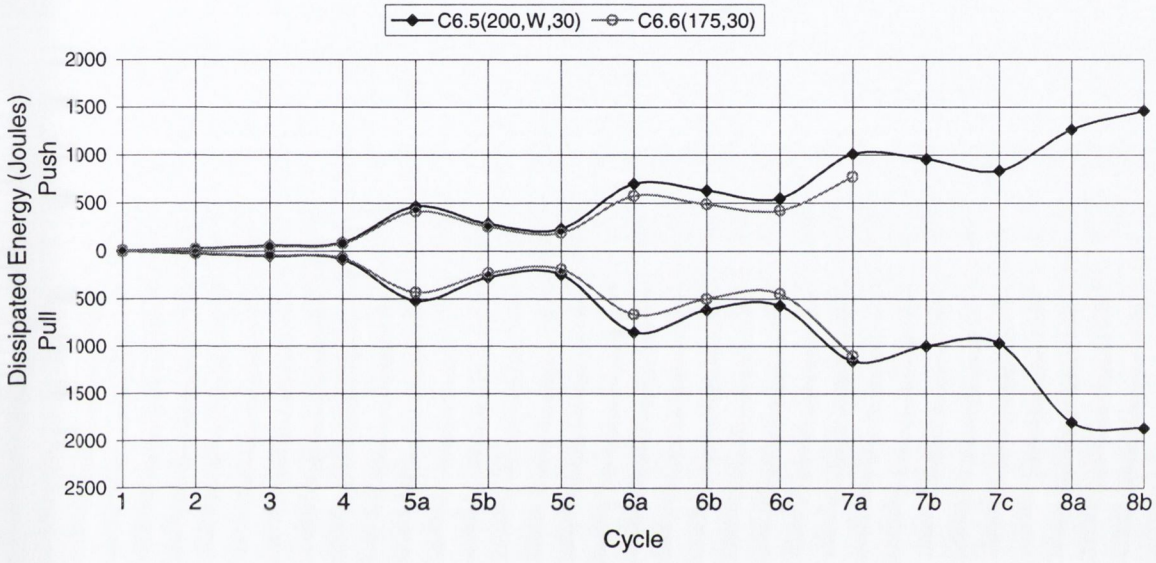

Figure 5.14: Group 3 Dissipated energy versus cycle

Resistance

Figure 5.15 shows the resistance ratios in each cycle for both specimens. From the plot it is clear that both specimens reach their maximum resistances in cycle 5a, just after yield. There is a distinct difference between the peak push and pull resistances of the specimens. When the specimens are being pushed C6.6 is the stronger whereas specimen C6.5 is the stronger when pulled. However, Figure 5.16, which plots the average of these push and pull resistance ratios, shows that the specimen behaviours to peak resistance are almost identical.

The plot of the average push and pull resistance ratios, emphasises the different rates of degradation of the two specimens. Upon reaching its maximum resistance, the capacity of C6.6 decreases rapidly. It does increase a little upon entry to the next displacement group (Group 6) but after this point, no further increases in resistance occur, and the drop in resistance is very rapid. On the other hand, due to the presence of wireballs, the loss in resistance of specimen C6.5 is much more gradual.

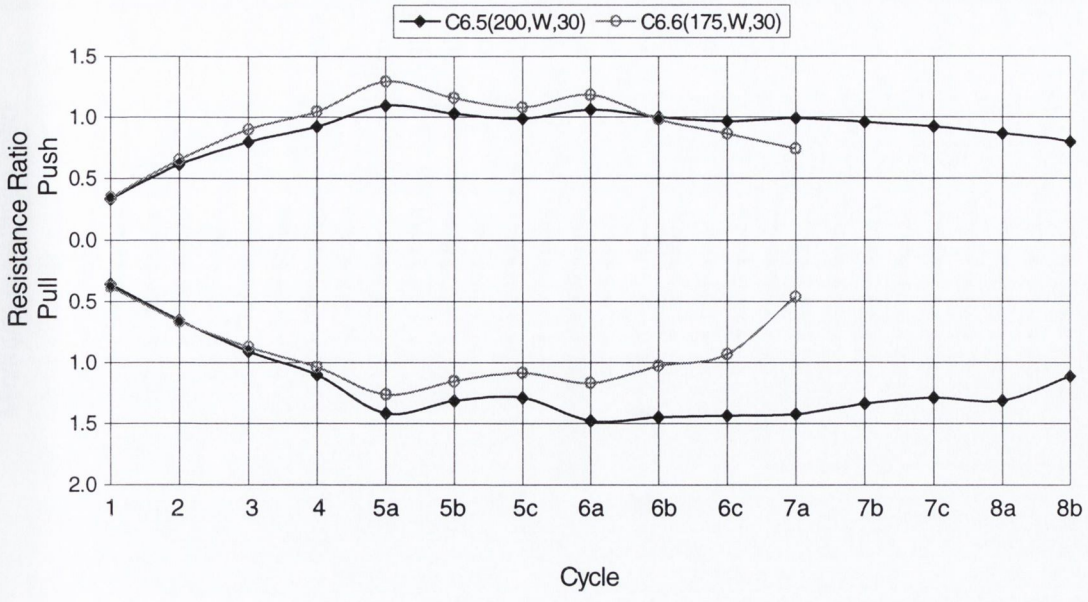

Figure 5.15: Group 3 Resistance ratios

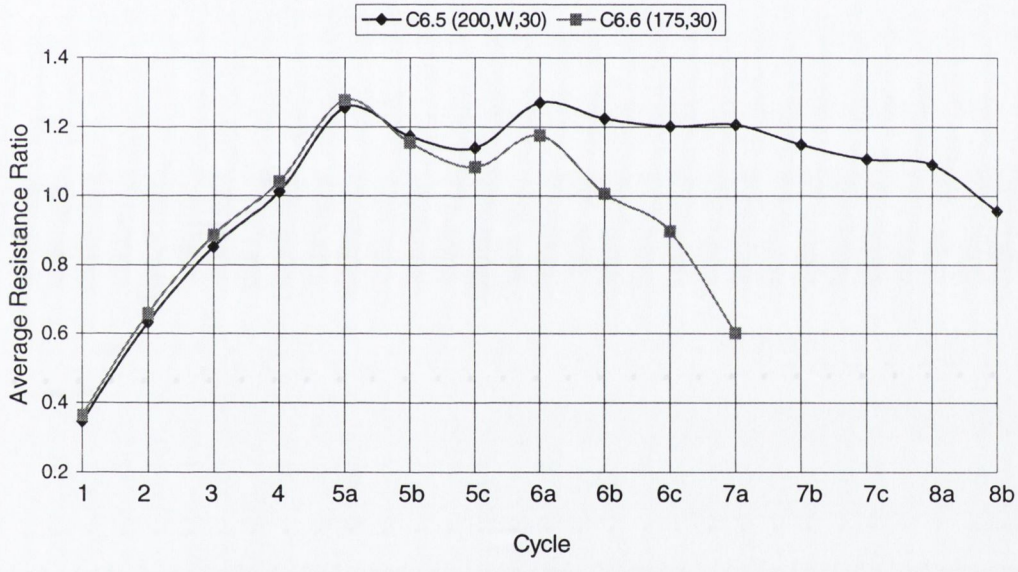

Figure 5.16: Average of push and pull resistances for Group 3

Finally, Figure 5.17 presents the minimum resistance ratios for the push and pull half cycles of each displacement group. These charts highlight the superior performance of specimen C6.5. It is evident that specimen C6.6 loses its resistance in displacement group 7 (40mm) while specimen C6.5 is still able to carry load throughout the 50mm cycles (group 8).

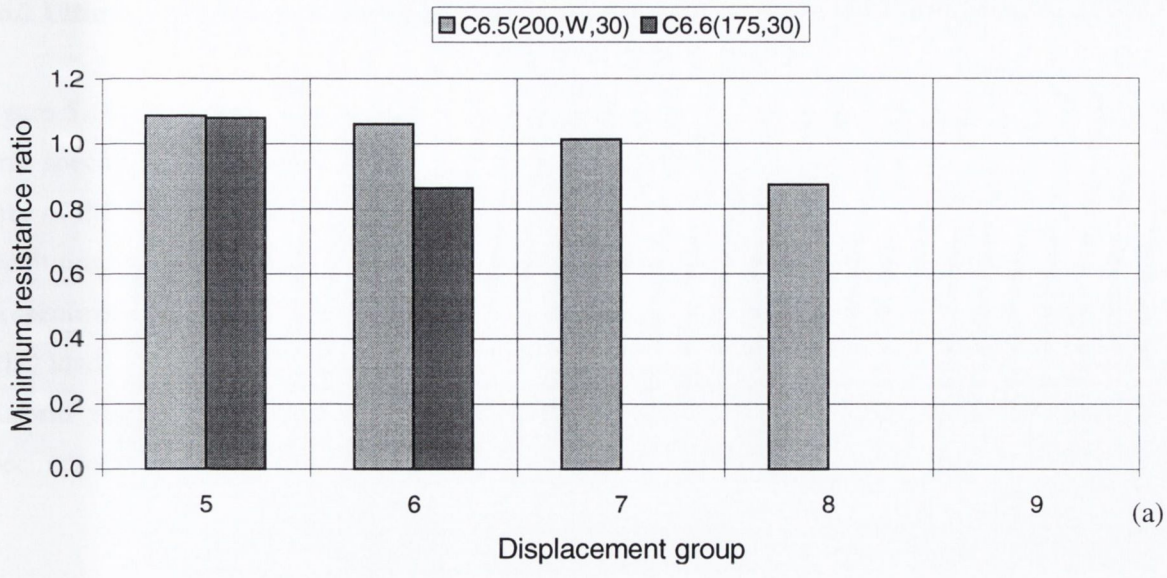

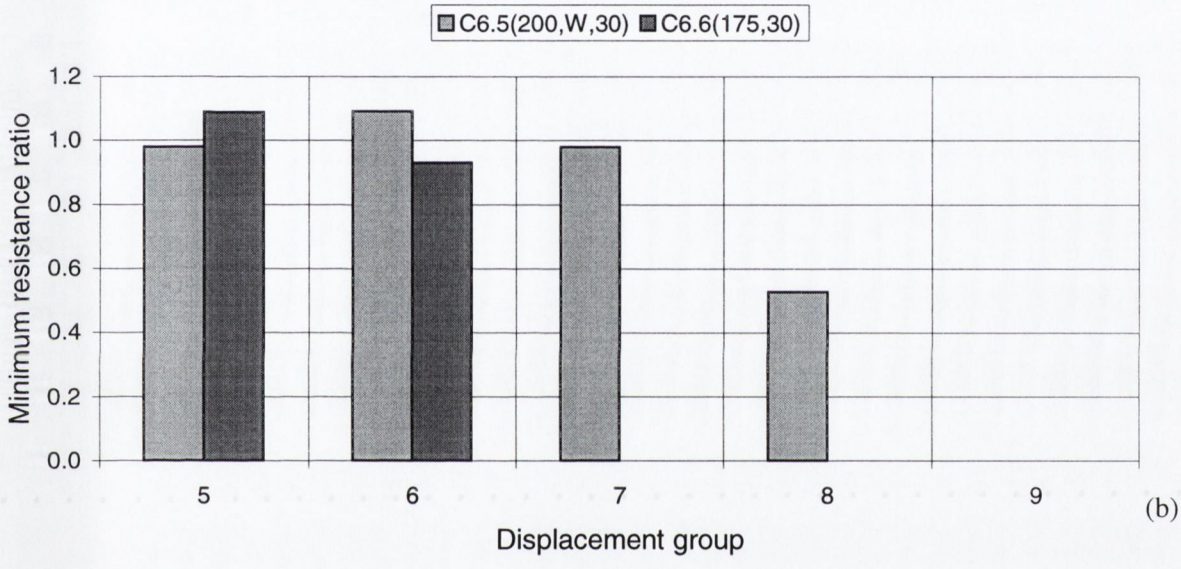

Figure 5.17: Group 3 Minimum resistances (a) push (b) pull

5.6 Effect of link spacing

5.6.1 Introduction

Section 5.5 considered the eight specimens in terms of three comparison groups. The results show that the wireball reinforced specimens behaved better than the specimens with no wireballs. This penultimate section considers the variation in ultimate displacement and total dissipated energy with link spacing.

5.6.2 Ultimate displacement and link spacing

Figure 5.18 compares the ultimate displacements of all specimens in terms of link spacing. The three specimens that continue to carry load into the 50mm cycles all contain wireballs. Notably, all three of these specimens have link spacings larger than the 105mm recommended by EC8 for DCL conditions. All three of these specimens achieve ultimate displacements greater than that achieved by specimen C6.1, which was detailed in accordance with EC8. Furthermore, even under increased axial load levels, close to that for over-reinforced failure, the wireball reinforced specimens perform very well. Specimens C6.3 and C6.4 both achieve the same ultimate ductilities as specimen C6.1, even though, they possess larger link spacings and higher axial loads.

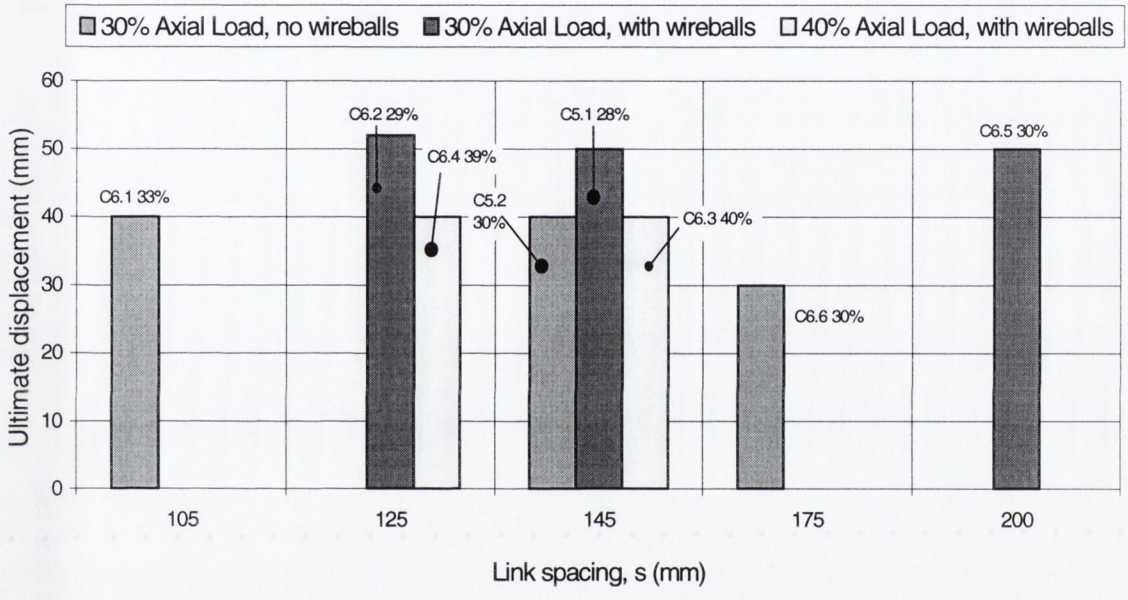

Figure 5.18: Ultimate displacements versus link spacing

In Section 5.2 it was commented that, due to the displacement history imposed on specimens, the ultimate displacement values and, therefore, the quoted displacement ductility values, only have a limited degree of relevance. For example, in the above plot, four specimens have an ultimate displacement of 40mm. While it is true that all four of these collapsed during, or just after, the 40mm displacement cycles, this information cannot distinguish between the varying performances of the specimens at this displacement. In other words, where some specimens may be able to resist the 40mm displacement very well, only failing on entering the 50mm cycles, some of the specimens may not resist the 40mm displacement as well. Therefore, while the above plot of ultimate displacements is accurate, it is somewhat limited. In order to distinguish between the varying capacities of specimens that have the same ultimate displacements, plots of the Resistance drop ratios are provided in Figures 5.19 and 5.20. The resistance drop ratio is the ratio of the load carrying capacity of a specimen at the end of a group of displacement cycles (say cycle 8c) relative

to its load carrying capacity at the beginning of the group cycle (say cycle 8a). The ratio shows how much the resistance of a specimen changes within a displacement group, and therefore, is a measure of the level of damage that occurs to the specimen at a particular displacement.

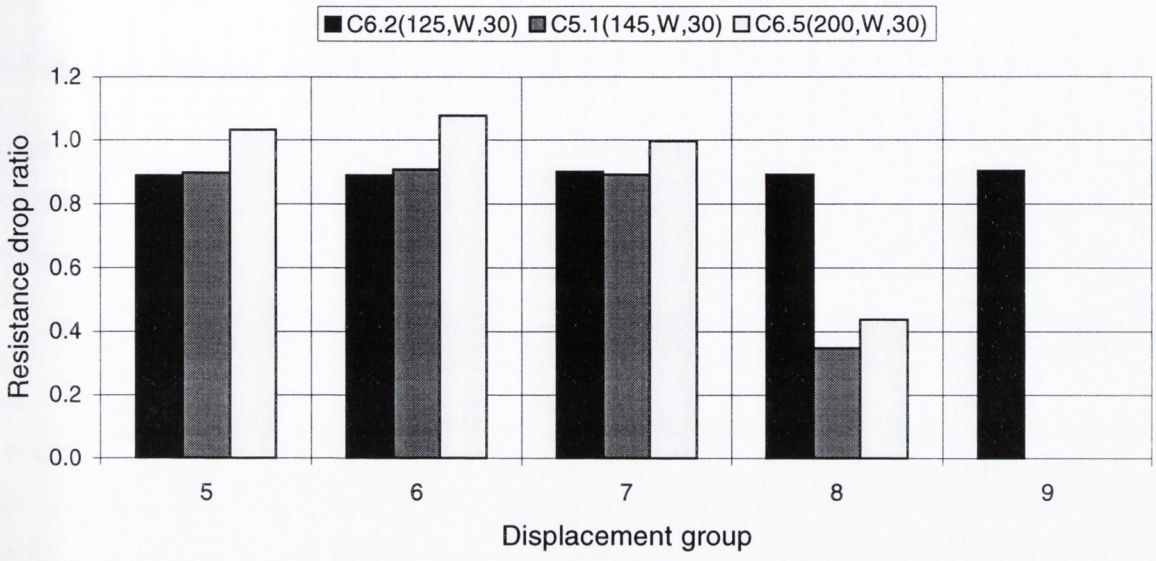

Figure 5.19: Resistance drop ratios for specimens C6.2, C5.1 and C6.5

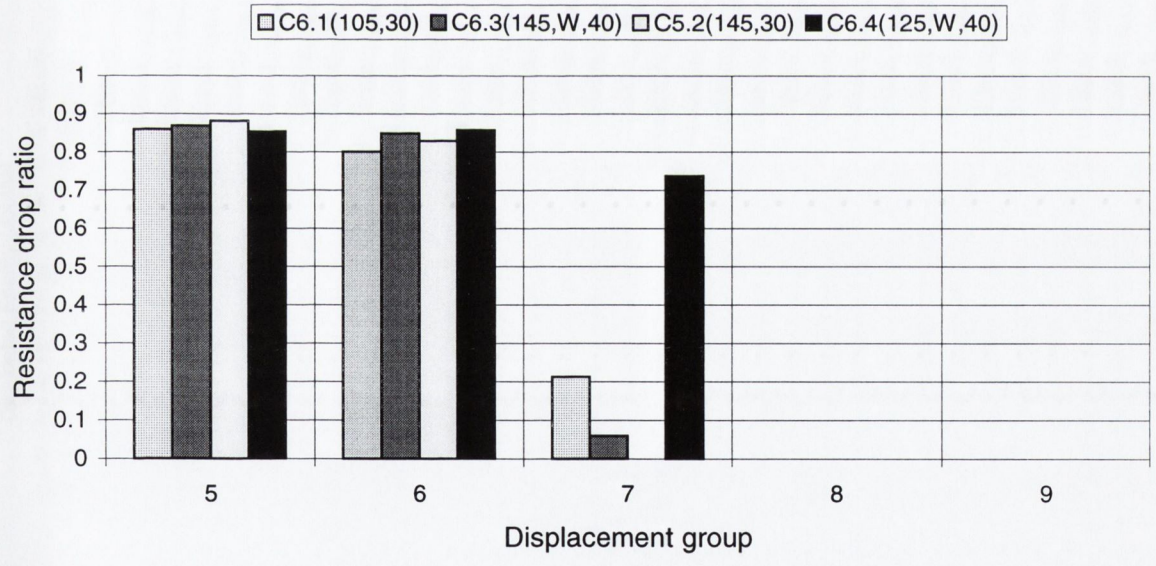

Figure 5.20: Resistance drop ratios for specimens C6.1, C6.3, C5.2 and C6.4

Figure 5.19 shows that of the three specimens quoted as having an ultimate displacement of 50mm, specimen C6.2 performed best in terms of resistance drop ratios. Figure 5.20 presents the resistance drop ratios of the four specimens with ultimate displacements of 40mm. Here it is clear that of the four specimens, C6.4 (125,W,40) performs the best. This is affirmation of the benefits of wireballs since this specimen had a larger link spacing, and higher axial load, than specimen C6.1 (105,W,30). The similar results of specimens C6.3 (145,W,40) and C5.2 (145,30) also

confirm the benefits to ductility of wireballs. It is not necessary to plot the resistance ratios of specimen C6.6 because this specimen was the only specimen that had a ductility ratio of less than 4 and, hence, stands out on its own.

5.6.3 Dissipated energy and link spacing

Figure 5.21 compares the average of the total energy dissipated in the push and pull half cycles of each test. The specimens with the highest energy dissipation capacities are specimens C6.2, C6.5 and C5.1 respectively. These specimens also had the largest ultimate displacements. The superior performance of these specimens relative to those with closer link spacings emphasises the capacity of wireballs to be used to partially replace confinement links. The specimen that dissipates the least amount of energy is specimen C6.6 with the large link spacing of 175mm, and no wireballs. A noteworthy feature of the plot is that all of the specimens with wireballs dissipate more energy than the specimens without wireballs, even when the axial load levels are high, and the link spacings are large.

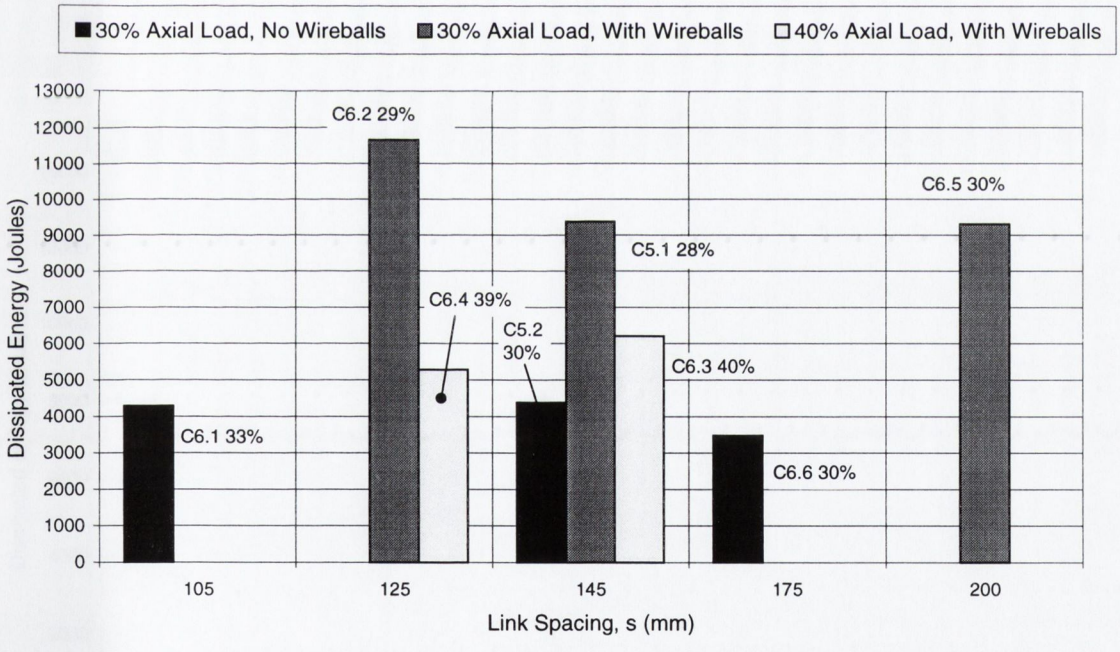

Figure 5.21: Average total dissipated energy with link spacing

Figure 5.22 presents separately the energies dissipated when specimens are being pushed and pulled. This purpose of this plot is to illustrate a point that arose in Section 5.4 when each of the three comparison groups were being discussed. In each group, it was observed that the energy dissipated in the pull half cycles is always greater than that dissipated in the push half cycles. This phenomenon is clear in Figure 5.22, where in the majority of specimens the energy dissipated in the pull half cycles is greater than the energy dissipated in the push half cycles. However, an

interesting point is that for the specimens without wireballs, the push and pull energies are more similar. Interestingly, in the visual observations of Section 5.3, it was noted that the column side furthest from the actuator (F6) always appeared to suffer higher levels of degradation than the side nearest the actuator (F5). Also, it is clear from the hysteresis curves that more of the displacement range occurs within the negative force range than within positive force range.

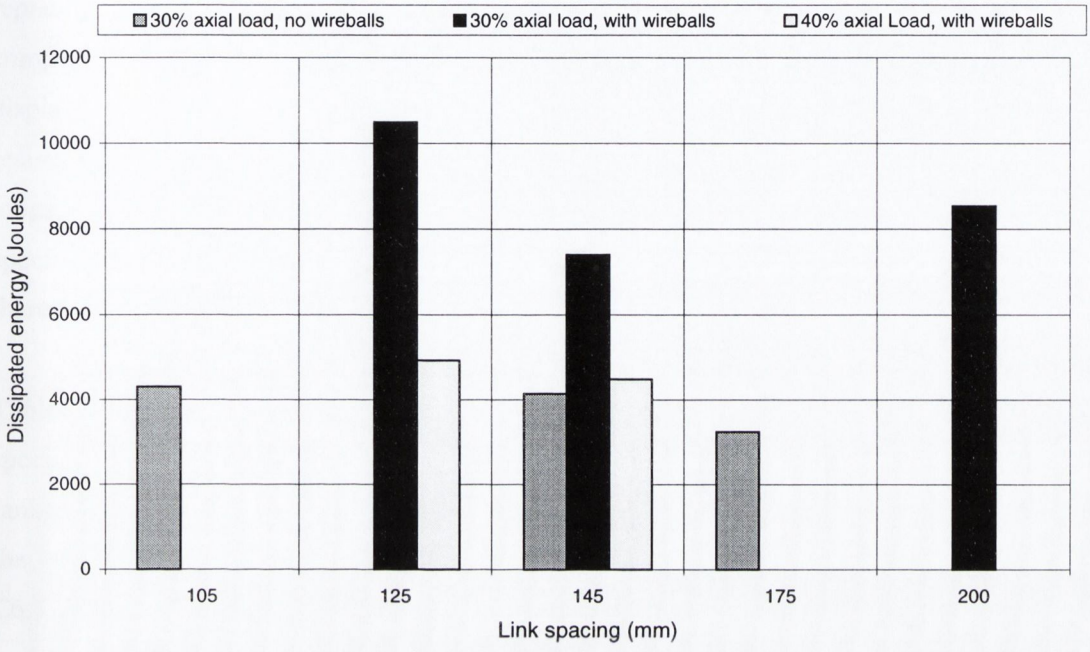

(a)

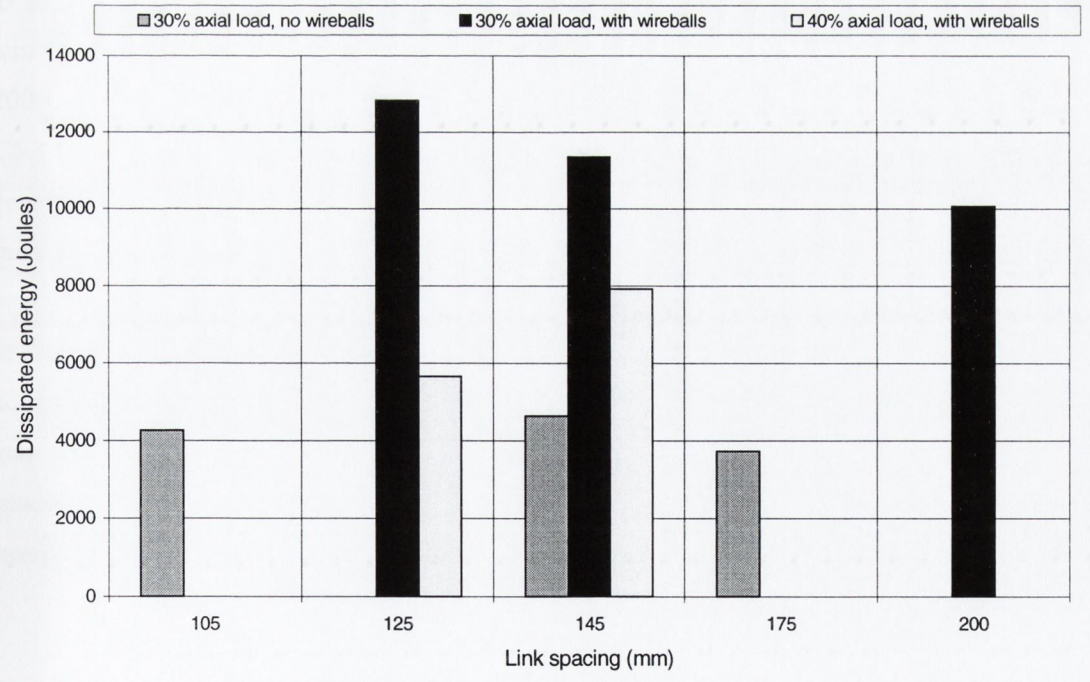

(b)

Figure 5.22: (a) Positive (push) dissipated energy, (b) Negative (pull) dissipated energy

5.7 Conclusions

Wireball reinforcement provides increased confinement in reinforced concrete. This was observed visually in the slower degradation of specimens with wireballs in comparison to those without, and it was also evident in the increased energy dissipation and displacement ductility capacities of the wireball reinforced specimens. Hence, it is clear that wireballs improve the earthquake resistance of reinforced concrete beam-columns, and that there is scope for wireballs to be used in partial replacement of the large amount of confinement links otherwise necessary. Table 5.6 provides a comparison summary of the specimens by ranking them in terms of energy dissipation capacity and displacement ductility. Where specimens displayed the same displacement ductilities, the resistance-drop ratios in their ultimate displacement group, plus the stability of their final hysteresis loops were considered in order to determine which specimens were the most ductile. The specimens are ranked from 1 to 5 where a ranking of 1 indicates the best performance. Where there is a negligible difference in performance, the specimens are given the same ranking.

Table 5.6 illustrates clearly the superior performance of the wireball reinforced specimens over the specimens without wireballs, even when the axial loads are high. Specimen C6.1 (125,W,30), ranked first, outperformed all other specimens, whereas C6.6 (175,30) stood on its own as having the least ability to dissipate energy and the lowest displacement ductility. Specimens C5.1 and C6.5 are ranked second in the table. Their superior behaviour to specimen C6.1 (105,30), detailed to EC8 specifications, highlights the scope to increase link spacing, through the inclusion of wireballs, without detrimental effect on specimen behaviour. Their link spacings of 145mm and 200mm are 38% and 90% greater than the recommended 105mm for a DCL column. Specimens C6.4 (125,W,40) and C6.3 (145,W,40) are ranked third and fourth, respectively, demonstrating the benefits of wireballs even in specimens with axial loads approaching those for over-reinforced failure. These specimens perform as well (even better, in the case of C6.4) than specimen C6.1.

In conclusion, wireball reinforcement has been seen to be very beneficial in terms of concrete confinement, as it improves the energy dissipation capabilities and ductility capacities of conventionally reinforced specimens. The positive effects of wireball inclusion means that the link spacing specified by EC8 for DCL conditions may be increased considerably, even under high levels of axial load, without adverse effect on member performance.

Specimen	Link Spacing (mm)	% increase in link spacing over that for DCL column	Wireball Content (Y/N)	$N/(f_{ck})(A)$ %	Ranking
C6.1	125	19	Y	33.2	1
C5.1	145	38	Y	28.3	2
C6.5	200	90	Y	29.7	2
C6.4	125	19	Y	38.5	3
C6.3	145	38	Y	39.7	4
C6.1	105	0	N	33.2	4
C5.2	145	38	N	30.1	4
C6.6	175	67	N	30.0	5

Table 5.6: Performance ranking of specimens

CHAPTER 6

MODEL THEORY

6.1 Introduction

This chapter describes the numerical modelling of the beam-column specimens considered in this research. The experimental results described in the previous chapter were very positive, indicating that the inclusion of wireballs in reinforced concrete is beneficial to its ductility and energy dissipation capacity. The development of a model of the test specimens allows this experimental data to be extended to the behaviour of a wider range of reinforced concrete members containing wireball reinforcement.

Section 6.2 describes the material models used, while Sections 6.3 and 6.4 describe the moment-curvature and moment-displacement relationships employed. The implementation of the model is presented in Section 6.5.

6.2 Material models

Mander *et al.* (1988) developed a stress-strain model for concrete subjected to uniaxial compressive loading and confined by transverse reinforcement. The concrete sections considered contained any general type of confining steel – either spiral or circular links, or rectangular links, with and without supplementary cross-ties. A single equation (Equation 6.1) is used to describe the stress-strain response. The influence of various types of confinement is taken into account by defining an effective lateral confining stress, which is dependent on the configuration of the transverse and longitudinal reinforcement. With respect to available ultimate displacement capacity, or ductility, the model also describes a method through which the ultimate concrete compression strain may be predicted. The following sections detail Mander's model and its application to rectangular concrete sections. They also discuss the modifications required to make the model more applicable to the beam-columns tested in this research. The material laws used to describe the unconfined concrete and the reinforcing steel are also presented.

6.2.1 Confined concrete in compression

Mander's stress-strain model is illustrated in Figure 6.1. For a slow (quasi-static) strain rate and monotonic loading, the longitudinal compressive concrete stress f_c is given by:

$$f_c = \frac{f'_{cc}\, x\, r}{r - 1 + x^r} \tag{6.1}$$

where f'_{cc} is compressive strength of confined concrete, (defined in Section 6.2.2.2), and,

$$x = \frac{\varepsilon_c}{\varepsilon_{cc}} \tag{6.2}$$

$$r = \frac{E_c}{E_c - E_{\text{sec}}} \tag{6.3}$$

$$E_c = 5000\sqrt{f'_{co}} \tag{6.4}$$

$$E_{\text{sec}} = \frac{f'_{cc}}{\varepsilon_{cc}} \tag{6.5}$$

$$\varepsilon_{cc} = \varepsilon_{co}\left[1 + 5\left(\frac{f'_{cc}}{f'_{co}} - 1\right)\right] \tag{6.6}$$

where f'_{co} and ε_{co} are unconfined concrete strength and corresponding strain, respectively, (ε_{co} is assumed to be 0.002), and E_c is the tangent modulus of elasticity of concrete. For the cover concrete, the part of the falling branch for which $\varepsilon_c > 2\varepsilon_{co}$ is assumed to be a straight line which reaches zero stress at the spalling strain, ε_{sp}.

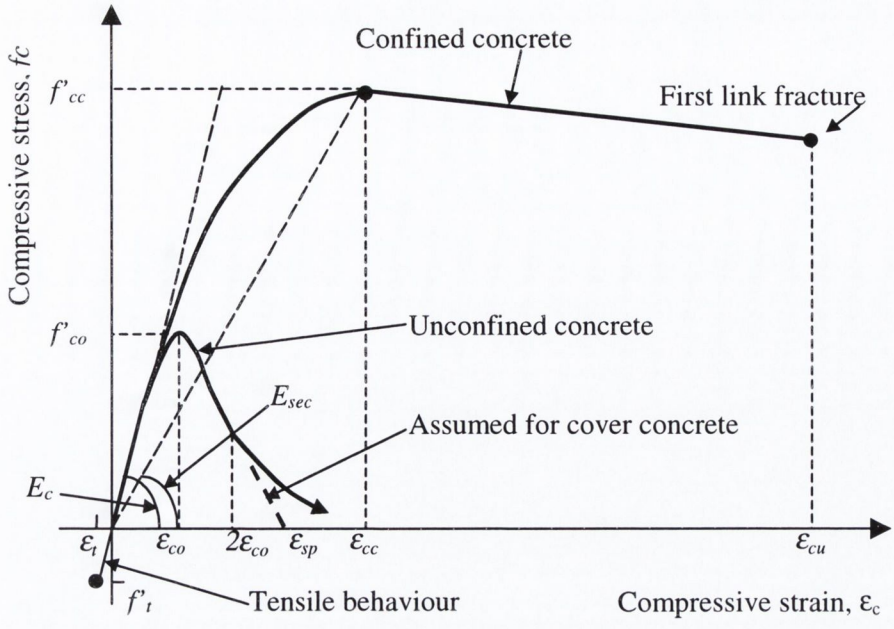

Figure 6.1: Stress-strain model for monotonic loading of confined and unconfined concrete, (after Mander *et al.*, 1988)

6.2.1.1 Lateral confinement in rectangular sections

According to Mander, the maximum transverse pressure from the confining steel can only be exerted effectively on that part of the concrete core where the confining stress has fully developed due to arching action (Section 2.6.1). Figure 6.2 shows the arching action assumed to occur between adjacent levels of transverse reinforcement in a rectangular section. Midway between these levels of transverse reinforcement, the area of ineffectively confined concrete will be the largest and the area of effectively confined concrete core, A_e, will be the smallest.

It is assumed for convenience that the area of the confined core, A_{cc}, is the area within the centrelines of the perimeter link excluding the area of longitudinal steel. To allow for the fact that A_e is less than A_{cc}, the effective lateral confining pressure, f'_l, is given as:

$$f'_l = f_l k_e \tag{6.7}$$

where f_l = lateral pressure from the transverse reinforcement, assumed to be uniformly distributed over the surface of the concrete core and,

$$k_e = \frac{A_e}{A_{cc}} \tag{6.8}$$

where k_e = confinement effectiveness factor and,

$$A_{cc} = A_c(1-\rho_{cc}) \tag{6.9}$$

where ρ_{cc} = ratio of longitudinal steel reinforcement area to the area of the core section, and A_c = area enclosed by the centrelines of the perimeter link (= $b_c \times d_c$, where b_c and d_c are the core dimensions illustrated in Figure 6.2).

In rectangular sections, arching is assumed to act in the form of second-degree parabolas with an initial tangent slope of 45°. Vertical arching occurs between the layers of transverse reinforcement and horizontal arching occurs between the longitudinal bars, as illustrated in Figure 6.2.

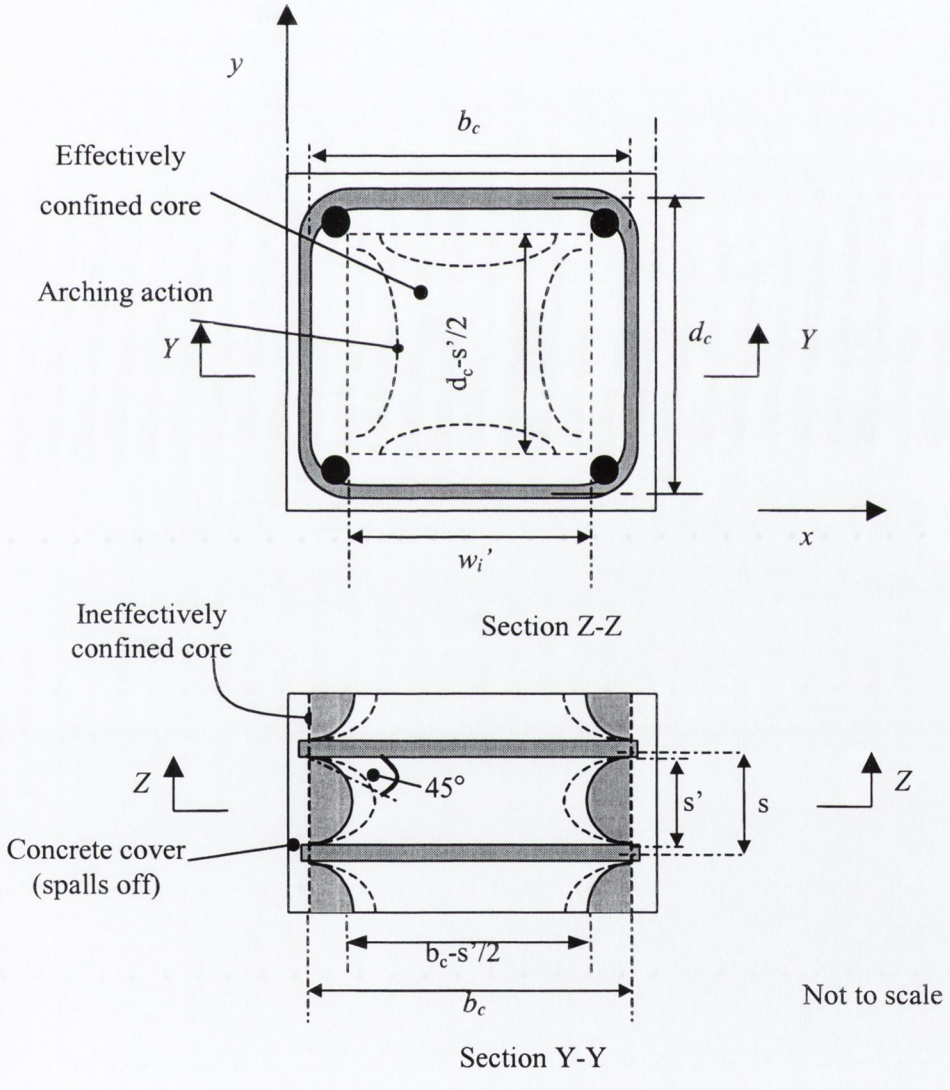

Figure 6.2: Effectively confined core for rectangular link reinforcement, (after Mander *et al.*, 1988)

The effectively confined area of concrete at link level is found by subtracting the area of the parabolas containing the ineffectively confined concrete from the area A_c enclosed by the centrelines of the perimeter link. For one parabola, the ineffectual area (A) is:

$$A = \frac{(w'_i)^2}{6} \tag{6.10}$$

where $w_i = i^{th}$ clear distance between adjacent longitudinal bars (Figure 6.2).

Hence, the total plan area of ineffectually confined core concrete at link level, for number n longitudinal bars is:

$$A_i = \sum_{i=1}^{n} \frac{(w'_i)^2}{6} \tag{6.11}$$

Incorporating the influence of the ineffective area in elevation (Figure 6.2, Section Y-Y), the area of effectively confined concrete core, A_e, midway between the levels of transverse reinforcement is:

$$A_e = \left(b_c d_c - \sum_{i=1}^{n} \frac{(w'_i)^2}{6} \right) \left(1 - \frac{s'}{2b_c} \right) \left(1 - \frac{s'}{2d_c} \right) \quad \text{from Figure 6.2} \tag{6.12}$$

where:

b_c and d_c = core dimensions to the centrelines of the perimeter link in the x and y directions

s' = clear vertical spacing between links (Figure 6.2)

The area of concrete core enclosed by the perimeter links is given by Equation 6.9. Hence, substituting Equations 6.9 and 6.12 into Equation 6.8 the confinement effectiveness coefficient, k_e, for rectangular links is:

$$k_e = \frac{\left(1 - \sum_{i=1}^{n} \frac{(w'_i)^2}{6 b_c d_c} \right) \left(1 - \frac{s'}{2b_c} \right) \left(1 - \frac{s'}{2d_c} \right)}{(1 - \rho_{cc})} \tag{6.13}$$

In rectangular sections, where there may be different quantities of transverse steel in the x and y directions, these quantities may be expressed as:

$$\rho_x = \frac{A_{sx}}{s d_c} \tag{6.14}$$

$$\rho_y = \frac{A_{sy}}{sb_c} \tag{6.15}$$

where A_{sx} and A_{sy} = the total areas of transverse bars running in the x and y directions, respectively and, s = centre to centre link spacing (Figure 6.2)

The lateral confining stress, which is the total transverse bar force divided by the vertical area of confined concrete, is given for the x and y directions as follows:

$$f_{lx} = \left(\frac{A_{sx}}{sd_c}\right)(f_{yh}) = (\rho_x)(f_{yh}) \tag{6.16}$$

$$f_{lyx} = \left(\frac{A_{sy}}{sb_c}\right)(f_{yh}) = (\rho_y)(f_{yh}) \tag{6.17}$$

where f_{yh} = yield strength of the transverse reinforcement.

From Equation 6.7 the effective lateral confining stress in the x and y directions are:

$$f'_{lx} = k_e(\rho_x)(f_{yh}) \tag{6.18}$$

$$f'_{ly} = k_e(\rho_y)(f_{yh}) \tag{6.19}$$

6.2.1.2 Compressive strength of confined concrete

Mander provides a general solution of the multi-axial failure criterion in terms of the two lateral confining stresses (f'_{lx} and f'_{ly}, or f'_{l1} and f'_{l2}, respectively). Figure 6.3 presents this general solution. Knowing the two lateral confining stresses, the confined strength ratio (f'_{cc}/f'_{co}, where f_{co}' is the unconfined strength which corresponds to the concrete cylinder strength) may be determined, and hence, the confined concrete strength, f'_{cc}.

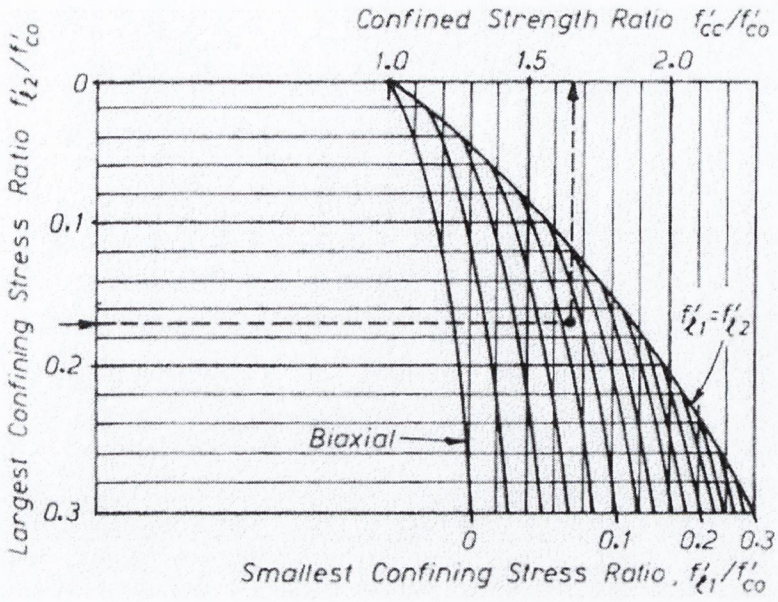

Figure 6.3: Confined strength determination from lateral stresses for rectangular sections, (Mander *et al.*, 1988)

6.2.1.3 Ultimate concrete compression strain

While it is essential to be able to predict the confined strength of reinforced concrete, it is also important, especially in earthquake resistant design, to be able to calculate the ultimate rotation capacity of a flexural plastic hinge in a reinforced concrete member. To achieve this, it is necessary to be able to predict the ultimate compressive strain, ε_{cu} (Figure 6.1).

Mander *et al.* (1988) define the ultimate compressive strain as the longitudinal strain at which the first link fracture occurs, since this strain is regarded as the end of the useful region of the stress-strain curve for the confined concrete core. Subsequently, Mander *et al.* (1988) propose a method for predicting the longitudinal concrete compressive strain at the first link fracture using an energy balance approach. In this approach, the additional ductility available to concrete due to its confinement is determined from the strain energy stored in the transverse reinforcement.

Consider the stress-strain curves for unconfined and confined concrete presented in Figure 6.1. The area under each curve represents the total strain energy per unit volume that will cause the concrete to fail. According to Mander, the increase in concrete strain energy at failure due to its confinement is equivalent to the strain energy capacity of the confining reinforcement as it yields in tension. Mander calculates the longitudinal concrete compressive strain corresponding to link fracture by equating the ultimate strain energy capacity of the confining reinforcement per unit volume of concrete core (U_{sh}), to the difference in areas between the confined (U_{cc}) and the

unconfined (U_{co}) concrete stress-strain curves, plus additional energy required to maintain yield in the longitudinal steel in compression (U_{sc}). Thus,

$$U_{sh} = U_{cc} + U_{sc} - U_{co} \tag{6.20}$$

where:

U_{sh} = ultimate strain energy capacity of the confining reinforcement

U_{cc} = area under confined concrete stress-strain curve

U_{co} = area under unconfined concrete stress-strain curve

U_{sc} = energy required to maintain the longitudinal steel in compression

Upon expansion of Equation 6.20, Mander obtains the following relationship:

$$\rho_s A_{cc} \int_0^{\varepsilon_{sf}} f_s d\varepsilon_s = A_{cc} \int_0^{\varepsilon_{cu}} f_c d\varepsilon_c + \rho_{cc} A_{cc} \int_0^{\varepsilon_{cu}} f_{sl} d\varepsilon_c - A_{cc} \int_0^{\varepsilon_{sp}} f_c d\varepsilon_c \tag{6.21}$$

where:

ρ_s = ratio of volume of transverse reinforcement to volume of concrete core

A_{cc} = area of concrete core (mm^2)

f_s and ε_s = stress (N/mm^2) and strain in the transverse reinforcement

ε_{sf} = fracture strain of transverse reinforcement

f_c and ε_c = longitudinal compressive stress (N/mm^2) and strain in concrete

ε_{cu} = ultimate longitudinal compressive strain

ρ_{cc} = ratio of longitudinal reinforcement to volume of concrete core

f_{sl} = stress in longitudinal reinforcement (N/mm^2)

ε_{sp} = spalling strain of unconfined concrete

In other words, the strain energy capacity of the confining reinforcement per unit volume of concrete core is equal to the strain energy capacity of the confined concrete plus the strain energy capacity of the longitudinal steel less the strain energy capacity of the concrete in its unconfined state (i.e. the strain energy capacity that the concrete has when the concrete strains are so low that the transverse steel does not provide a confinement pressure).

On the left hand side of Equation 6.21 the expression:

$$\int_0^{\varepsilon_{sf}} f_s d\varepsilon_s = U_{sf} \tag{6.22}$$

where U_{sf} = strain energy (MJ/m^3) of the transverse reinforcement up to the fracture strain ε_{sf}.

Results from tests carried out by Mander *et al.*, (1984) on grade 275 and grade 380 reinforcement of various bar diameters indicates that U_{sf} is effectively independent of bar size and yield strength and may be taken as:

$$U_{sf} = 110 MJ / m^3 \tag{6.23}$$

For the steel considered, ε_{sf} ranged between 0.24 and 0.29.

6.2.1.4 Ultimate strain in beam-column specimens

The above theory is based on the assumption that ultimate failure occurs due to fracture of a transverse link. However, in the beam-columns considered in this research, ultimate failure occurred when the links began to open up. The links did not actually fracture. This was because the links used did not have 135° hooks extending into the core, but 90° hooks as discussed in Section 3.7.1. Therefore, as the concrete core expanded and the cover spalled, these hooks were not restrained within the core, and simply opened up. This implies that the equations described above for the ultimate concrete compression strain are not readily applicable to this case, since the left hand side of Equation 6.21 should be integrated between zero strain and the strain at link opening, rather than the strain at link fracture. Likewise, in Equation 6.23, the value of U_{sf} equal to 110MJ/m^3 is not applicable. Hence, for this research, Equation 6.21 is redefined by replacing the strain at link fracture by a strain corresponding to link opening:

$$\rho_s A_{cc} \int_0^{\varepsilon_{sop}} f_s d\varepsilon_s = A_{cc} \int_0^{\varepsilon_{cu}} f_c d\varepsilon_c + \rho_{cc} A_{cc} \int_0^{\varepsilon_{cu}} f_{sl} d\varepsilon_c - A_{cc} \int_0^{\varepsilon_{sp}} f_c d\varepsilon_c \tag{6.24}$$

where ε_{sop} = strain at link opening.

Therefore,

$$\int_0^{\varepsilon_{sop}} f_s d\varepsilon_s = U_{so} \tag{6.25}$$

where U_{sop} = strain energy (MJ/m^3) of the transverse reinforcement up to the opening strain, ε_{sop}.

Equation 6.21 was developed for concrete subject to uniaxial compressive loading in which all of the core concrete is in compression (i.e. no bending). However, because of the combination loading applied to the beam-columns considered in this research, some of the core concrete is in tension and the core area in compression varies with neutral axis depth. This implies that the A_{cc} variable in the first and third terms on the right-hand side of Equation 6.24, for confined and unconfined concrete, is not valid. The area A_{cc} should, therefore, be replaced with the actual area of concrete core in compression. Therefore, A_{cc} becomes dependent on the stress state and the position of the neutral axis. The area of steel in compression is also dependent on the stress state and position of the neutral axis. Thus, Equation 6.24 becomes:

$$\rho_s A_{cc} \int_0^{\varepsilon_{sop}} f_s d\varepsilon_s = \sum_{i=1}^{n} A_i \int_0^{\varepsilon_{cu}} f_{ci} d\varepsilon_{ci} + \rho_{cc} A_{cc} \int_0^{\varepsilon_{cu}} f_{sl} d\varepsilon_c - \sum_{i=1}^{n} A_i \int_0^{\varepsilon_{sp}} f_{ci} d\varepsilon_{ci} \tag{6.26}$$

where:

n = number of concrete core elements in compression

A_i =area of core element i (mm)

f_{ci} and ε_{ci} = longitudinal compressive stress (N/mm^2) and strain in core element i

f_{sl} = stress in the longitudinal reinforcement in compression only (N/mm^2)

Equation 6.26 is also further refined to include the effects of the confinement provided by wireballs, such that it becomes:

$$\rho_{sw} A_{cc} \int_0^{\varepsilon_{sw}} f_{sw} d\varepsilon_s + \rho_s A_{cc} \int_0^{\varepsilon_{sop}} f_s d\varepsilon_s = \sum_{i}^{n} A_i \int_0^{\varepsilon_{cu}} f_{ci} d\varepsilon_{ci} + \rho_{cc} A_{cc} \int_0^{\varepsilon_{cu}} f_{sl} d\varepsilon_c - \sum_{i}^{n} A_i \int_0^{\varepsilon_{sp}} f_{ci} d\varepsilon_{ci} \tag{6.27}$$

where:

ρ_{sw} = ratio of volume wireball steel in the x and y directions (these directions being defined in Figure 6.2) to volume of concrete core

f_{sw} = stress in the wireball reinforcement (N/mm^2)

ε_{sw} = strain in the wireball reinforcement

6.2.2 Unconfined concrete in compression

According to Mander's model, unconfined compressed concrete behaves the same as confined concrete up to the unconfined concrete strength, f'_{co}, which occurs when the strain, ε_{co}, reaches 0.002, and is equivalent to the concrete's cylinder strength. Therefore, up to this peak stress, the compression cover concrete has a stress-strain relationship as defined by Mander's stress-strain curve (Figure 6.1). With respect to Figure 6.1, the cover resistance is assumed to decrease linearly to zero stress, from 0.002 strain to ε_{sp}.

6.2.3 Concrete in tension

The following relationship for concrete in tension (Neville, 1995) is assumed:

$$f_t = 0.12(f_{cu})^{0.7} \tag{6.28}$$

where:

f_t = concrete tensile strength (N/mm^2)

f_{cu} = concrete cube compressive strength (N/mm^2)

The tension cover reaches its maximum tensile strength, f_t, at a strain, ε_t. Hence, the elastic modulus in tension, E_{ct}, is:

$$E_{ct} = \frac{f_t}{\varepsilon_t} \tag{6.29}$$

Upon reaching stresses of f_t, the tension cover is assumed to lose strength instantaneously.

6.2.4 Reinforcing steel

The reinforcing steel is assumed to have bilinear stress-strain characteristics as depicted in Figure 6.4. The first branch represents the elastic behaviour of the steel. The second branch represents strain hardening as the steel strength increases from yield to ultimate.

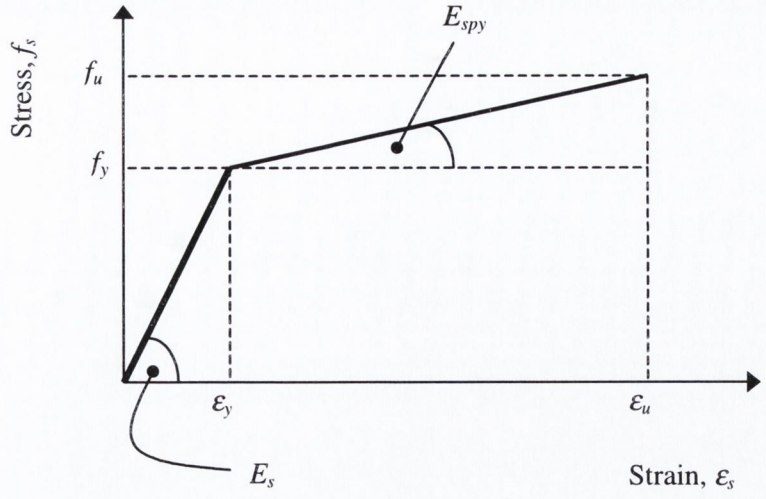

Figure 6.4: Bilinear stress-strain curve for reinforcing steel

where:

f_y, ε_y = yield stress (N/mm^2) and strain

f_u, ε_u = ultimate stress (N/mm^2) and strain

E_s = Young's modulus (N/mm^2)

E_{spy} = post-yield stiffness (N/mm^2)

6.3 Moment-curvature response

This section describes the general process employed to determine the moment-curvature response of a member. Consider a beam-column subject to lateral and axial loading as presented in Figure 6.5. The beam-column section consists of four different 'material regions':

- Core concrete
- Longitudinal steel
- Cover concrete in compression
- Cover concrete in tension

Figure 6.6 presents a cross-section of a reinforced concrete column (such as section A-A in Figure 6.5). The cross-section is divided into N strip elements. The width of the cross-section is B (mm) and its depth is D (mm). The elements may vary in height, D_n. The depth of an element below the extreme compression fibre is x_n. For example, element *"N-3"* is D_{N-3} deep and its centreline is a depth x_{N-3} below the extreme compression fibre. The strain, stress, force and moment equations for such a generalised cross-section are now discussed.

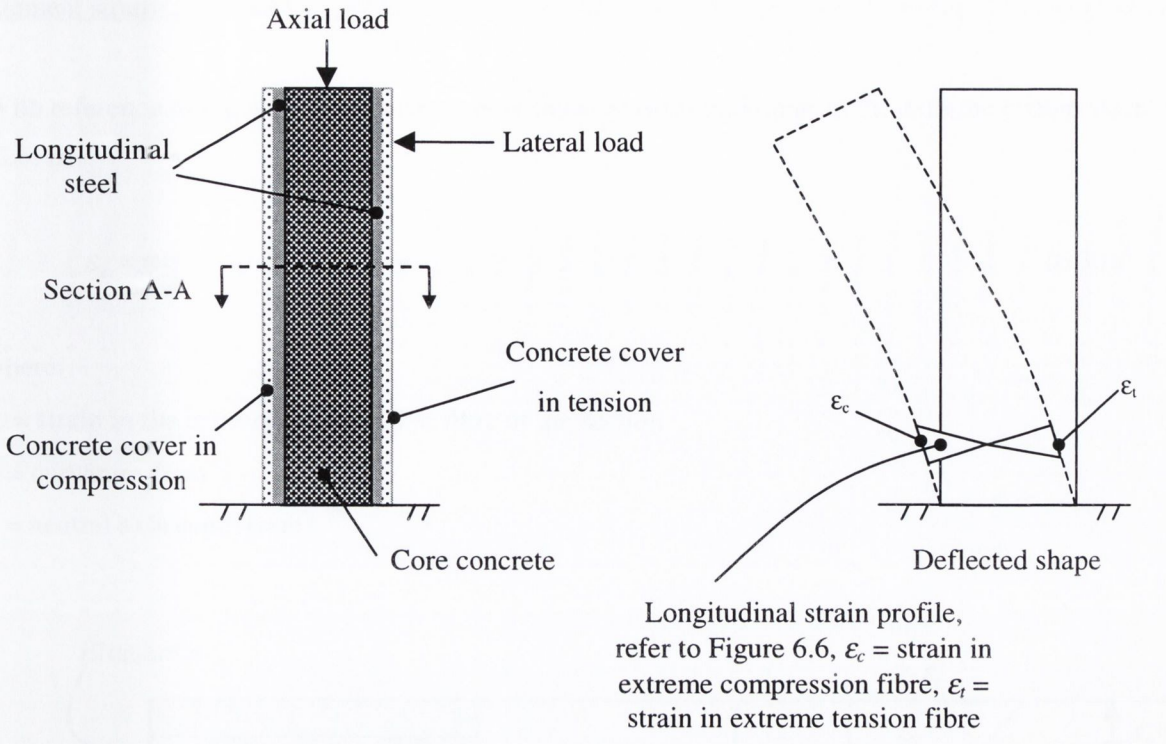

Figure 6.5: Beam-column loading, deflected shape and different 'material regions'

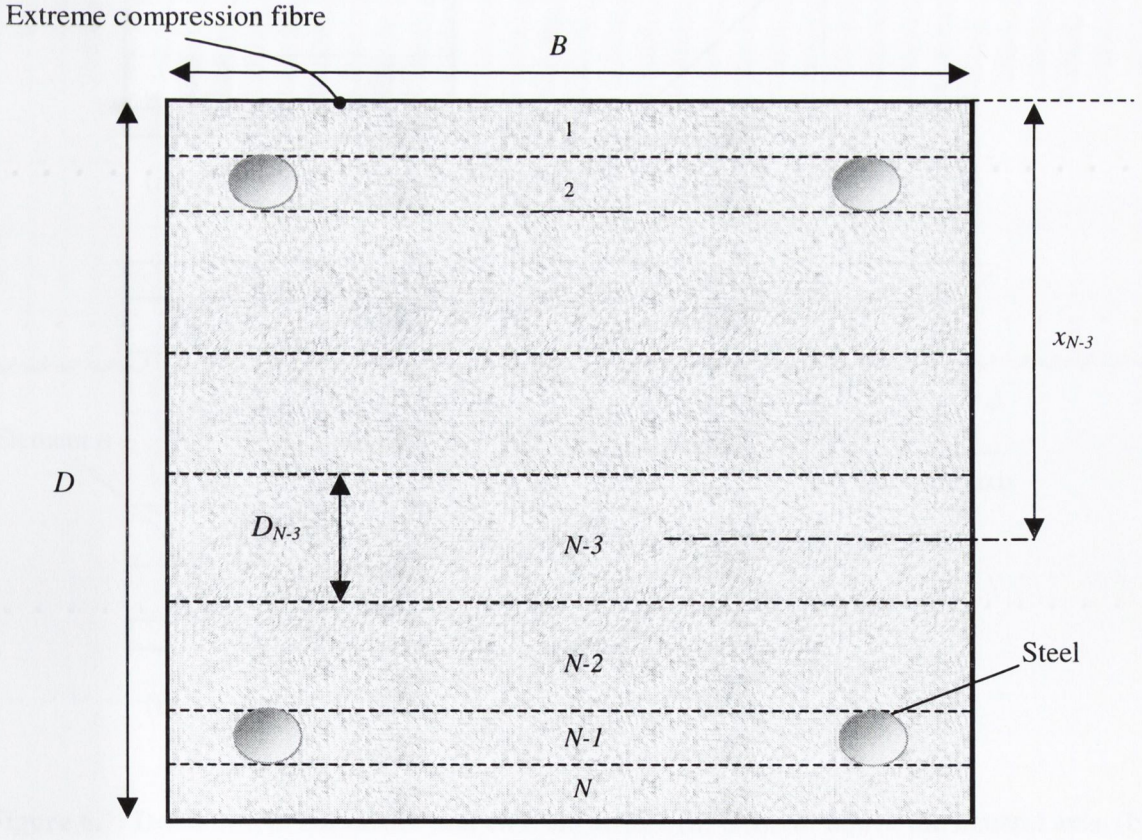

Figure 6.6: Cross-section divided into N strip elements on Section A-A in Figure 6.5

Element strains:

With reference to Figure 6.7, the strain, under linear elastic conditions, at the extreme compression fibre is:

$$\varepsilon_c = \phi x \tag{6.30}$$

where:

ε_c = strain in the extreme compressive fibre of the section

ϕ = curvature (mm^{-1})

x = neutral axis depth (mm)

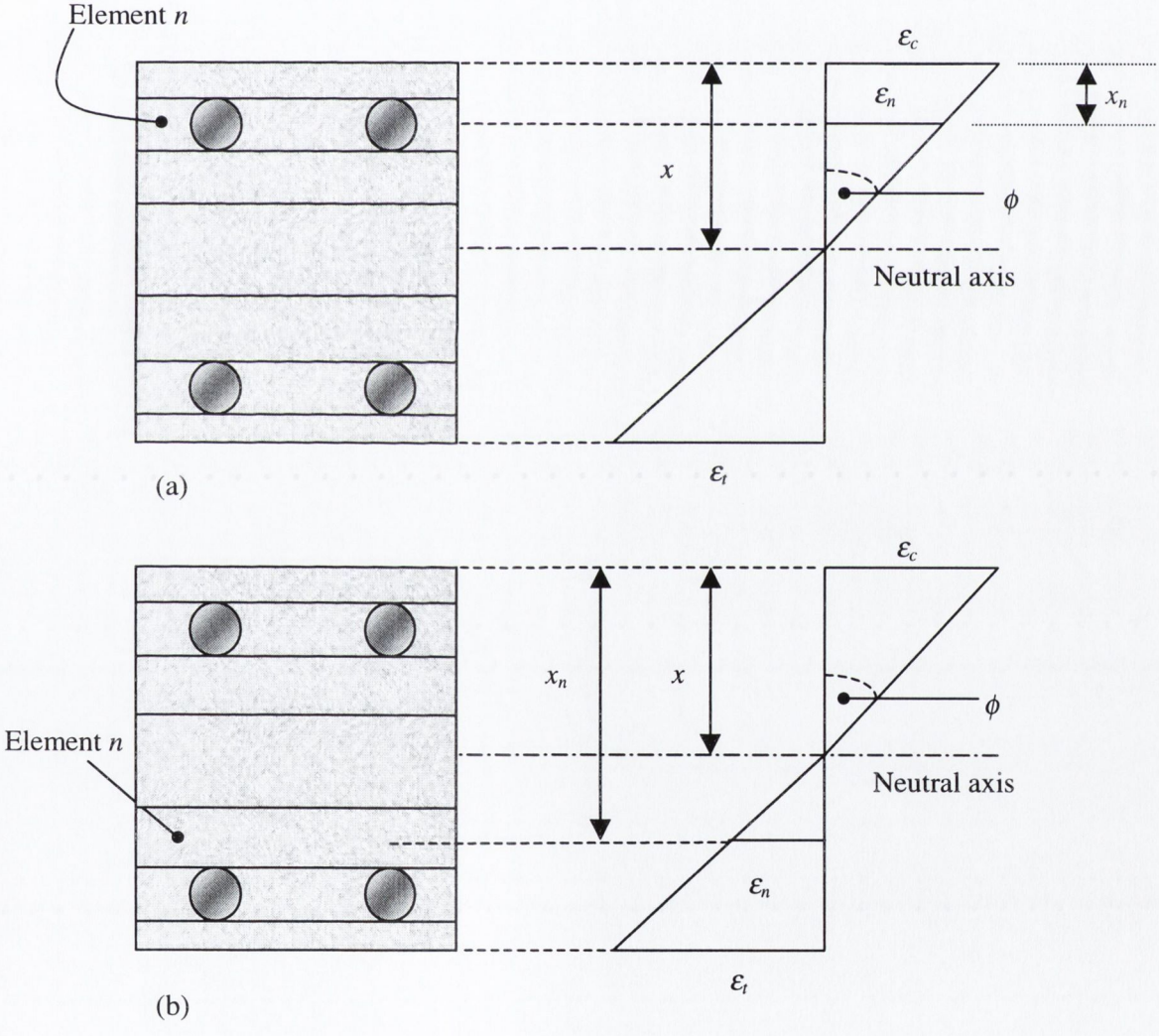

Figure 6.7: Definition of curvature and element strain, (a) element above the neutral axis, (b) element below the neutral axis

Hence, the strain in element n is given by:

$$x_n < x : \varepsilon_n = \left(\frac{\varepsilon_c}{x}\right)(x - x_n) \tag{6.31}$$

$$x_n > x : \varepsilon_n = \left(\frac{\varepsilon_c}{x}\right)(x_n - x) \tag{6.32}$$

where:

x_n = distance from the centre of element n to the extreme compression fibre (mm)

ε_n = strain in element n

Note: Equations 6.31 and 6.32 are such that the strain, ε_n, is always a positive value.

Element stresses:

The stresses in the steel elements are:

$$\varepsilon_n < \varepsilon_y : \sigma_n = (E_s)(\varepsilon_n) \tag{6.33}$$

$$\varepsilon_y < \varepsilon_n < \varepsilon_u : \sigma_n = (E_s)(\varepsilon_y) + (E_{spy})(\varepsilon_n - \varepsilon_y) \text{ from Figure 6.4} \tag{6.34}$$

$$\varepsilon_n > \varepsilon_u : \sigma_n = 0 \tag{6.35}$$

where σ_n = stress in element n (N/mm^2)

The stress in the element representing the concrete cover in tension is:

$$\varepsilon_n < \varepsilon_t : \sigma_n = (\varepsilon_n)(E_{ct}) \tag{6.36}$$

$$\varepsilon_n = \varepsilon_t : \sigma_n = f_t \tag{6.37}$$

$$\varepsilon_n > \varepsilon_t : \sigma_n = 0 \tag{6.38}$$

where:

ε_t = strain at which tensile strength is reached

E_{ct} = concrete modulus in tension (N/mm^2)

f_t = tension strength of concrete, from Equation 6.28 (N/mm^2)

The stress in the element representing the concrete cover in compression (unconfined) is determined from the following equations:

$$\varepsilon_n < 0.002: \sigma_n = f_c \text{ found from Equation 6.1} \tag{6.39}$$

$$\varepsilon_n = 0.002 : \sigma_n = f'_{co} \tag{6.40}$$

$$0.002 < \varepsilon_n < \varepsilon_{sp} : \sigma_n = \left(\frac{f'_{co}}{\varepsilon_{sp} - 0.002} \right) \left(\varepsilon_{sp} - \varepsilon_n \right) \text{ from Figure 6.1 and Section 6.22} \tag{6.41}$$

$$\varepsilon_{sp} \leq \varepsilon_n : \sigma_n = 0 \tag{6.42}$$

where f_c = longitudinal compressive concrete stress according to Mander's stress-strain model for confined concrete up to $\varepsilon_n = 0.002$

The stresses in the strip elements representing the concrete core are as follows:

$$x_n < x : \sigma_n = f_c \text{ of Equation 6.1} \tag{6.43}$$

$$x_n \geq x : \sigma_n = 0 \tag{6.44}$$

Equation 6.43 takes into account that some of the concrete core will be in tension depending on the position of the neutral axis. Therefore, once the element lies outside of the compressive region it contributes zero resistance.

Element forces

The force in each strip element is obtained by multiplying the element stress by its area, as in Equations 6.45 and 6.46. These equations take into account the position of each element's force relative to the neutral axis, such that the forces are either positive (compressive) or negative (tensile). In the case of the strips containing steel these are assumed to contain steel only and their area is taken as the area of reinforcement within the strip and neglects the concrete area.

$$x_n < x : F_n = (A_n)(\sigma_n) \tag{6.45}$$

$$x_n > x : F_n = -(A_n)(\sigma_n) \tag{6.46}$$

where:

F_n = force in element n (N)

A_n = element area (mm^2)

Neutral axis depth:

The neutral axis depth, x, (measured from the compressive face) for a given value of curvature, is solved by iteration. The actual value of x occurs when the following equilibrium condition is satisfied:

$$\sum_{i=1}^{n} F_i + N = 0 \tag{6.47}$$

where:

F_n = force in element n (N)

i = element number

N = applied axial load (N)

Moments of resistance:

The moment of resistance due to each element force is:

$$M_n = (F_n)(D/2 - x_n) \tag{6.48}$$

where:

M_n = moment due to force in element n (Nmm)

$D/2$ = distance from the extreme compression fibre to the section centre (mm)

Note: In Equation 6.48, an element's moment of resistance, M_n, is negative when x_n is greater than $D/2$.

The total moment acting on the section is the sum of all these element moments:

$$M = \sum_{n=1}^{N} M_n \tag{6.49}$$

where:

M = total moment (Nmm)

Following the above procedure, for any series of input curvature values, a corresponding set of resistance moments may be calculated and the moment-curvature responses plotted.

6.4 Moment-displacement response

This section presents the relationships that exist between member curvature, rotation and displacement and, hence, how a moment-displacement response may be extrapolated from existing moment-curvature data.

6.4.1 Basic equations

Consider an elastic cantilever beam, as presented in Figure 6.8(a.1), subject to a load P, which induces a tip displacement Δ and rotation θ. In this case, the beam is also subject to an axial load, N. The moment decreases linearly to zero in the x-direction. For an elastic beam, curvature (the rate of change in rotation) is given by the familiar expression:

$$\phi = \frac{M}{EI} \tag{6.50}$$

where EI = slope of the linear ascending section of the moment-curvature curve (Nmm^2).

Equation 6.50 for an elastic beam implies that, for a linear change in moment along a beam, there is a linear change in curvature, hence, the linear curvature profile of Figure 6.8(a.3).

It is well known that the following relationships between displacement, rotation and curvature exist (Englekirk, 1994):

$$\Delta = y = \text{displacement} \tag{6.51}$$

$$\theta = \frac{dy}{dx} = \text{rotation} \tag{6.52}$$

(6.53)

or:

(6.54)

That is, with respect to Figures 6.8(a.3) to 6.8(a.5), the rotation of the beam is equal to the area under the curvature profile, and the displacement of the beam is equal to the area under the rotation profile. These relationships hold equally well for an inelastic beam (Figure 6.8(b)), although, in this case, the curvature profile will not be linear.

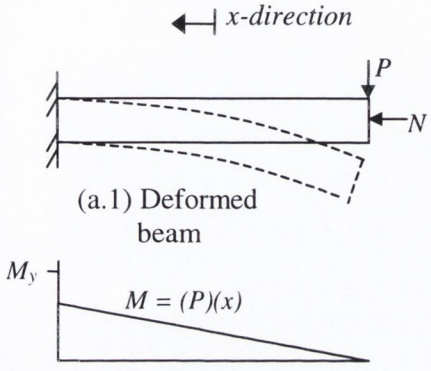

(a.1) Deformed beam

(a.2) Moment profile

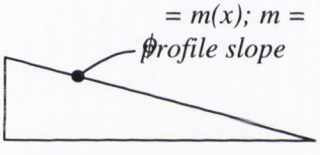

(a.3) Curvature profile

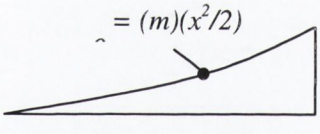

(a.4) Rotation profile

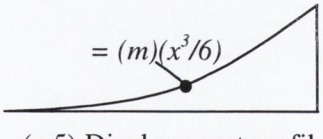

(a.5) Displacement profile

(a) Elastic

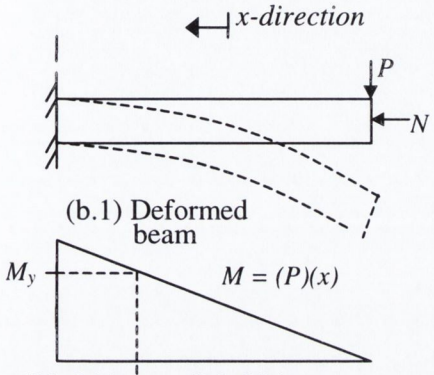

(b.1) Deformed beam

(b.2) Moment profile

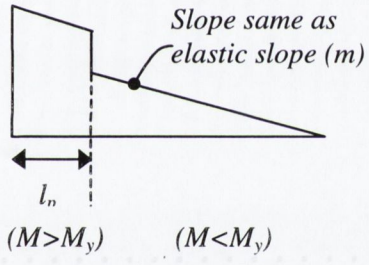

(b.3) Curvature profile, where l_p = plastic hinge length

(b) Inelastic

Figure 6.8: Cantilever beam, (a) elastic, (b) inelastic

6.4.2 Displacement equations

Consider the cantilever beam in Figure 6.9, which is subject to a lateral load P resulting in a deflection Δ. The beam is divided into a number of elements, where the element at the fixed end is referred to as the 'plastic hinge element', since this is the region where potential plastic deformation will occur. If the beam remains elastic, the curvature profile will be linear (Figure 6.9(c)).

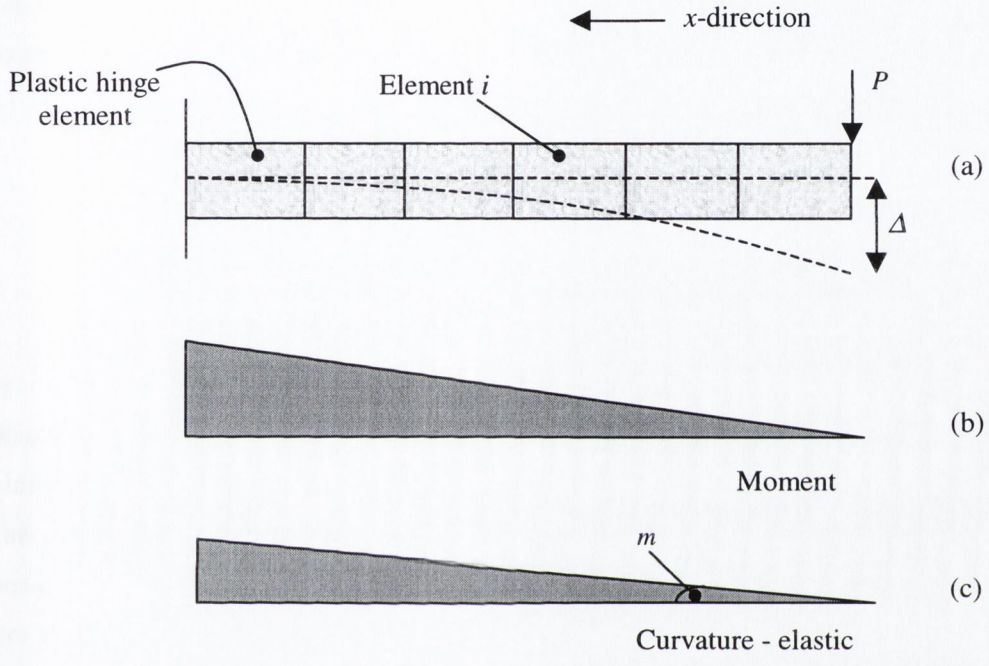

Figure 6.9: Elastic curvature profile for cantilever beam

Therefore, for an elastic beam, curvature along the member is defined as:

(6.56)

where:

m = slope of curvature profile (mm^{-2}) which can be determined the curvature profile is known

x = distance along the beam (mm)

Substituting into Equation 6.55 the total displacement occurring between the beam tip and element i, is:

(6.57)

where:

Δ_{Ti} = total displacement occurring between beam tip and element i (mm)

x_i = distance from beam tip to element i (mm)

C_2 = constant of integration = 0

Consider an inelastic beam, as illustrated in Figure 6.10, with a corresponding curvature profile of the form depicted in Figure 6.10(c) or (d). For the curvature profile in Figure 6.10(d), a 'curvature step' equal to a curvature of 'h' occurs at the change in profile slope. Equation 6.55 is still applicable to both these curvature profiles once the changes in profile slope are taken account of. For both of the curvature profiles depicted in Figures 6.10(c) and (d) the following conditions apply:

(6.58)

(6.59)

where:

x_p= distance from beam tip to the point at which the slope of the curvature profile changes (mm)

m_1 = initial slope of curvature profile (mm^{-2})

m_2 = second slope of curvature profile (mm^{-2})

L = beam length (mm)

z as per Figure 6.10 (mm)

Hence, the total displacement occurring between the beam tip and any point within the plastic hinge element is:

(6.60)

Δ_{Tiph}= total displacement between beam tip to some point i in the plastic hinge element (mm)

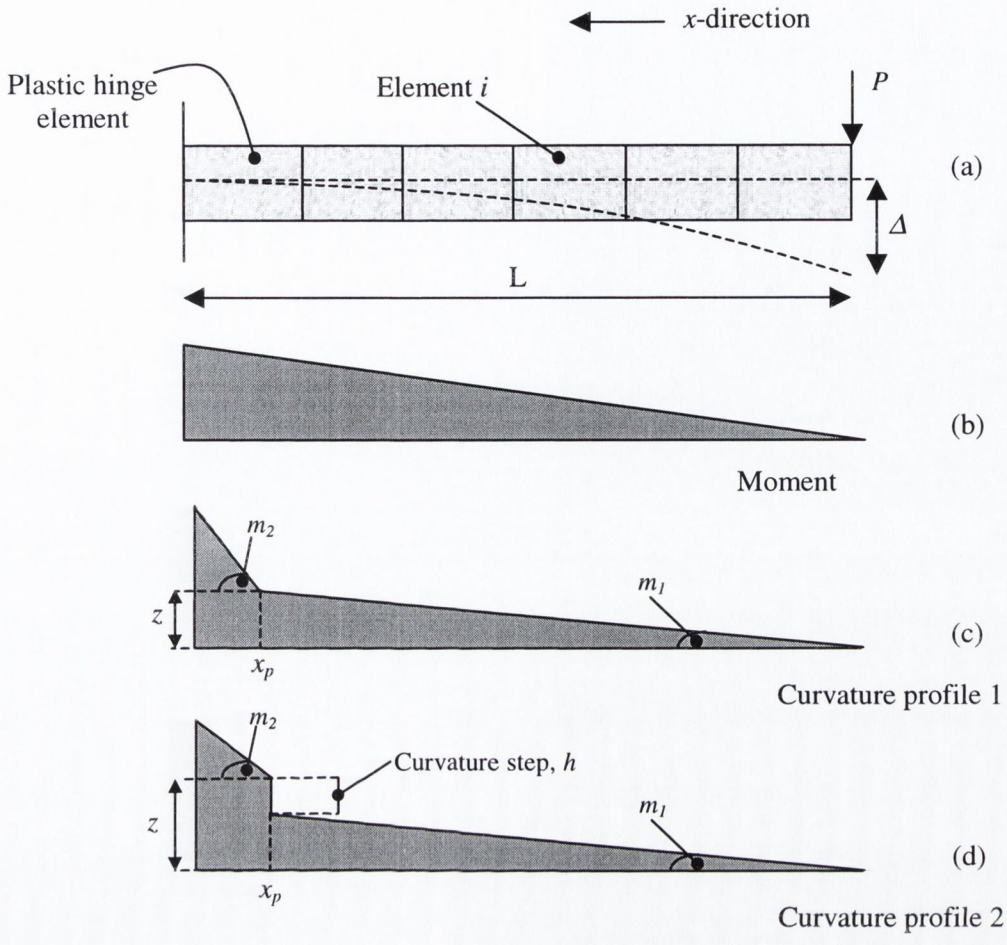

Figure 6.10: Inelastic curvature profiles

6.5 Implementation of numerical model

Both the moment-curvature and moment-displacement responses for each beam-column specimen are determined using an EXCEL-based implementation of the numerical equations represented by the above equations. The cross-section and material details required to compute the moment-curvature response are presented in Section 6.5.1. Section 6.5.2 describes the transformation of moment-curvature data to moment-displacement data, while Section 6.5.3 describes how the strain and strain energy corresponding to failure of the specimens are determined.

6.5.1 Moment-curvature response

The beam-column cross-section was described in Section 4.7.1, it is 200mm × 200mm, with longitudinal steel areas, top and bottom, of 628mm^2, and concrete cover of 15mm. Table 6.1

presents the concrete characteristics, in terms of unconfined and confined compressive strength (f'_{co} and f'_{cc}), compressive elastic modulus (E_c), tensile strength (f_t) and the tensile elastic modulus (E_{ct}). In the implementation of this model the strain, ε_{sp}, is assumed as 0.0035 (O'Brien *et al.*, 1995), and the strain ε_t (the strain at which the concrete reaches its tensile strength) is assumed as 0.001. Table 6.2 presents the characteristics of the steel reinforcement. As described in Section 6.3 the beam-column cross-section is divided into a number of strip elements. The details of the strip elements are provided in Table 6.3, in terms of element material, height, area, depth from the extreme compressive fibre, and lever-arm distance about the midsection ($D/2-x_n$).

The element strains, and, hence, the element stresses and forces are determined for increasing values of curvature (Section 6.3). For each input value of curvature an iterative process is carried out, whereby values of neutral axis depth are iterated until equilibrium of forces is achieved (Equation 6.47). Hence, the element moments are calculated using Equation 6.48 and the total moment acting on the section for a certain input curvature value is determined using Equation 6.49.

Specimen	f'_{co} (N/mm^2)	f'_{cc} (N/mm^2)	E_c (N/mm^2)	f_{ct} (N/mm^2)	E_t (N/mm^2)
C5.1(145,W,30)	30.9	34.4	27800	1.6	1550
C5.2(145,30)	29.1	33.4	26950	1.5	1483
C6.1(105,30)	22.6	29.9	23780	1.2	1245
C6.2(125,W,30)	29.2	35.1	27025	1.5	1489
C6.3(145,W,40)	31.3	35.7	27960	1.6	1562
C6.4(125,W,40)	26.1	31.3	25525	1.4	1375
C6.5(200,W,30)	31.5	33.1	28075	1.6	1571
C6.6(175,30)	26.1	28.9	25520	1.4	1374

Table 6.1: Concrete characteristics

Property	Value
Steel yield strength, f_y (N/mm^2)	360
Strain at yield, ε_y	0.0018
Young's Modulus, E_s (N/mm^2)	200000
Steel ultimate strength, f_u (N/mm^2)	620
Strain at ultimate, ε_u	0.0765
Post-yield stiffness, E_{spy} (N/mm^2)	3480

Table 6.2: Steel characteristics

Element number	Material	D_n mm	A_n mm^2	x_n mm	$(D/2)-x_n$ mm
1	Concrete cover compression	15	3000	7.5	92.5
2	Compression steel	20	628	25	75
3	Concrete core	10	2000	40	60
4	Concrete core	10	2000	50	50
5	Concrete core	10	2000	60	40
6	Concrete core	10	2000	70	30
7	Concrete core	10	2000	80	20
8	Concrete core	10	2000	90	10
9	Concrete core	10	2000	100	0
10	Concrete core	10	2000	110	-10
11	Concrete core	10	2000	120	-20
12	Concrete core	10	2000	130	-30
13	Concrete core	10	2000	140	-40
14	Concrete core	10	2000	150	-50
15	Concrete core	10	2000	160	-60
16	Tension steel	20	628	175	-75
17	Concrete cover tension	15	3000	192.5	-92.5

Table 6.3: Element details

6.5.2 Moment-displacement response

This final section presents, in step-by-step format, how the moment-displacement response is obtained from the moment-curvature response. The beam-columns are 845mm long, but the lever-arm of the applied lateral load is 745mm. Therefore, neglecting the last 100mm, beyond the point of application of lateral load, the beam-column is divided into 10 elements as illustrated in Figure 6.11. Element 10, at the fixed end, is the 'plastic hinge element'. It is assumed that any plastic deformation occurs in the plastic hinge element only, the rest of the beam is assumed to remain linear elastic.

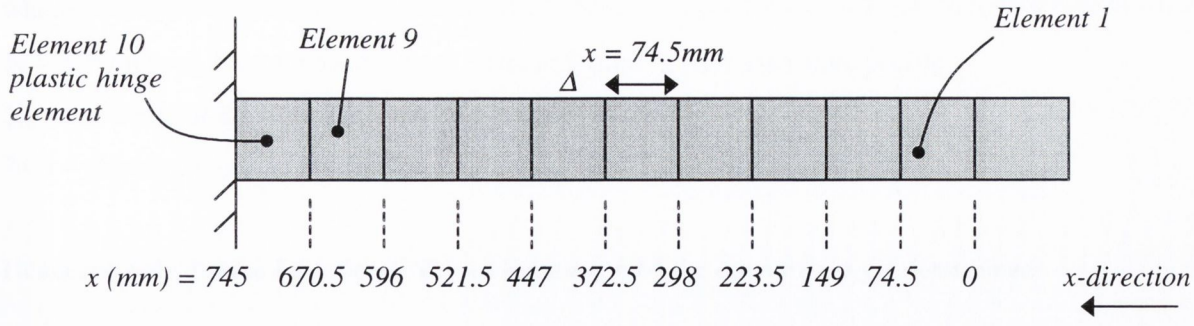

Figure 6.11: Beam-column divided into elements along its length

The procedure for determining the moment-displacement response is:

1. The experimental moment (including the P-Delta component) at the end of each displacement cycle is identified and converted to an equivalent load value.
2. For this load, the moment in each beam-column element, with the exception of the plastic hinge element, is calculated, providing a moment profile.
3. For these moments, the corresponding curvature profile is determined using the known moment-curvature response (Section 6.51).
4. By assuming the z-value as zero and also that any plastic deformation occurs only in the plastic hinge element Equation 6.60 becomes:

(6.61)

where:

Δ_T = total beam displacement (mm)

m_1 = slope of curvature profile from beam tip to element 9, i.e. the assumed linear elastic section

m_2 = slope of curvature profile over the plastic hinge region

The only unknown in Equation 6.61 is the value m_2, since Δ_T is equal to the peak experimental displacement of each cycle and m_1 is calculated from the slope of the curvature profile obtained in step 3 above.

The value m_2 is equal to the curvature gradient occurring over the plastic hinge element:

(6.62)

where:

ϕ_9 = curvature at the right hand side of element 9 (mm^{-1}), from curvature profile

ϕ_{10} = curvature at the right hand side of element 10 (mm^{-1})

74.5 = element length in millimetres

Hence, by substituting Equation 6.62 into Equation 6.61 the curvature ϕ_{10} is determined.

5. The moment corresponding to the curvature value ϕ_{10} is determined from the moment-curvature response. Since this implies a different load on the beam to that obtained in step 1, an iterative procedure is followed until the two loads converge.
6. The moment-displacement response is plotted.

6.5.3 Strain energy and strain in transverse steel

In order to compare the displacement capacity of the specimens and, hence, predict the ductility enhancing influence of wireballs, the strain energy and strains at failure are predicted using the equations outlined in Section 6.2.1.3. It is observed from the experimental results that the specimens yielded on entry into the first of the Group 5 cycles. Therefore, for modelling purposes the specimens are assumed not to have yielded in the first four cycles and to have yielded by Group Cycle 5. The strain energy and strains are determined as follows:

The strain energy of the transverse steel (U_{sl}) for the peak moment of any displacement cycle is calculated using Equation 6.26. The cover strain value ε_{sp} is assumed to be 0.002 since this is the strain corresponding to peak stress in the unconfined concrete (Figure 6.1). To minimise computational effort, it is assumed that beyond this strain, the concrete loses strength instantaneously. This is an approximation, as the concrete actually loses strength in the manner described for the compression cover in Equation 6.41. The strain energies are converted to strain values as follows:

Elastic: Cycles 1-4:

For these cycles, the term on the left-hand side of Equation 6.26 becomes:

(6.63)

where U_{sl} = strain energy in the link at the respective cycle (MJ/m^3).

With the exception of ε_s, everything else in Equation 6.81 is known, hence ε_s may be calculated.

Inelastic: Group Cycles 5-9:

For these cycles, the term on the left-hand side of Equation 6.26 becomes:

(6.64)

Again, with the exception of ε_s, everything else in Equation 6.82 is known and hence, ε_s may be calculated.

6.6 Summary

This chapter describes both the theory and implementation for the prediction of the moment-curvature and moment-displacement response of the beam-columns considered in this research. It also presents a method through which the strain energy and strain in the transverse steel may be predicted such that the benefits of wireballs, with respect to the rotational capacity of reinforced concrete members, may be quantified. Chapter 7 presents the predicted responses of the beam-columns and compares them with the experimental results. It also compares the different predicted strains in the transverse steel at failure for the different specimens in order to quantify the ductility enhancement properties of wireballs.

CHAPTER 7

MODEL PREDICTIONS

7.1 Introduction

Chapter 6 presented the theory and methodology used to create a numerical model to predict the moment-displacement response of the beam-column specimens considered in earlier chapters. Included within this model is a prediction of the strain at which failure of the beam-column occurs. This chapter compares the predicted moment-displacement responses to the experimental responses, while also comparing the predicted failure strains of the beam-columns with and without wireballs.

Section 7.2 presents the predicted moment-curvature responses and Section 7.3 presents the moment-displacement responses. Section 7.4 discusses the predicted failure strains and strain energies of the beam-columns, while Section 7.5 provides some conclusions.

7.2 Moment-curvature response

The predicted moment-curvature response of each beam-column specimen was obtained using Mander's theoretical stress-strain model for confined concrete described in Chapter 6. Figures 7.1 to 7.3 present the predicted moment-curvature responses, where the specimens are grouped according to the three comparison groups defined in Table 5.5 of Chapter 5.

The moment-curvature responses display similar trends, but also some differences, depending on the levels of confinement (in terms of link spacing) and axial load. Of the eight specimens considered, the predicted moment-curvature relationships all followed one of three general shapes, illustrated in Figures 7.4 to 7.6. Critical points on these curves are marked with a number. The three moment-curvature shapes are now discussed.

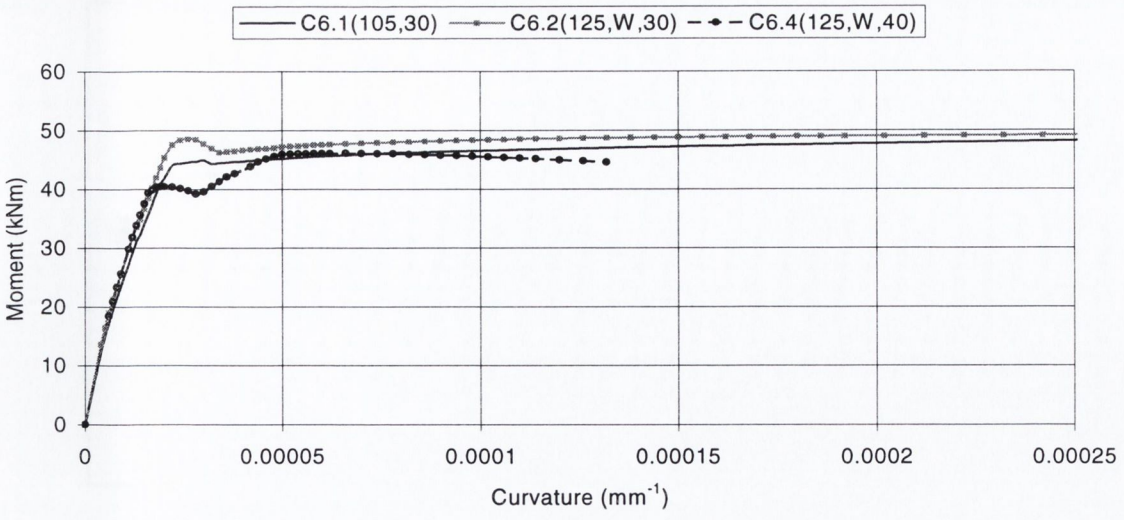

Figure 7.1: Predicted moment-curvature response, Group 1 (C6.1, C6.2 and C6.4)

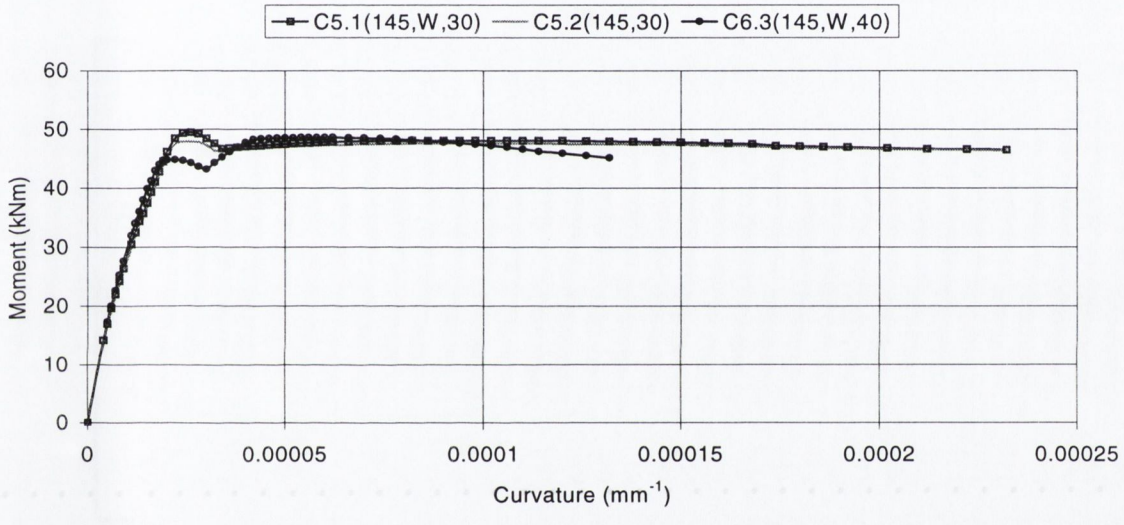

Figure 7.2: Predicted moment-curvature response, Group 2 (C5.1, C5.2 and C6.3)

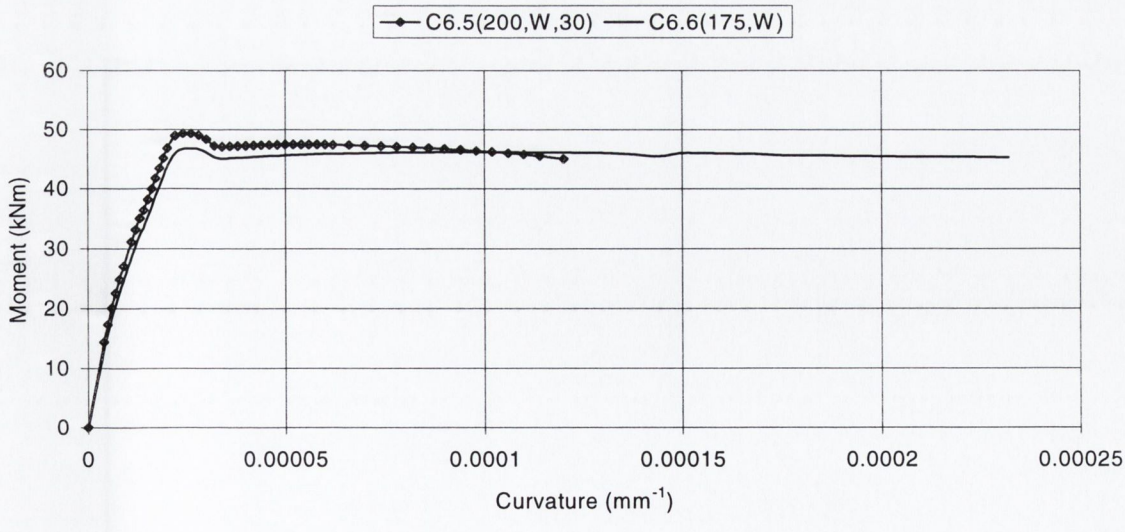

Figure 7.3: Predicted moment-curvature response, Group 1 (C6.5 and C6.6)

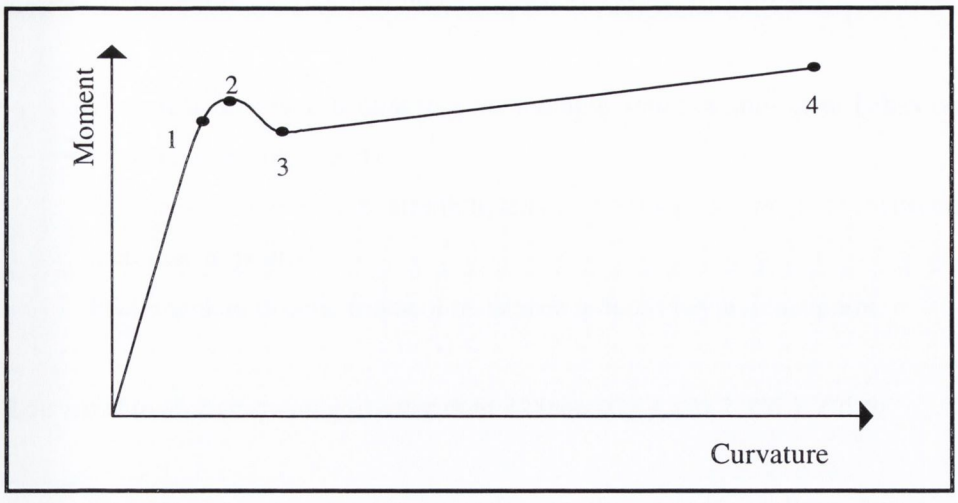

Figure 7.4: Moment-curvature response: Shape 1

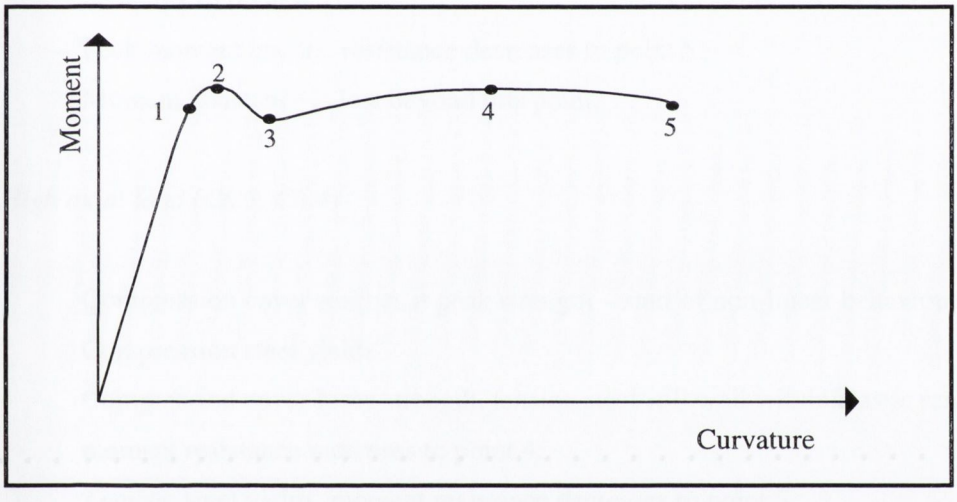

Figure 7.5: Moment-curvature response: Shape 2

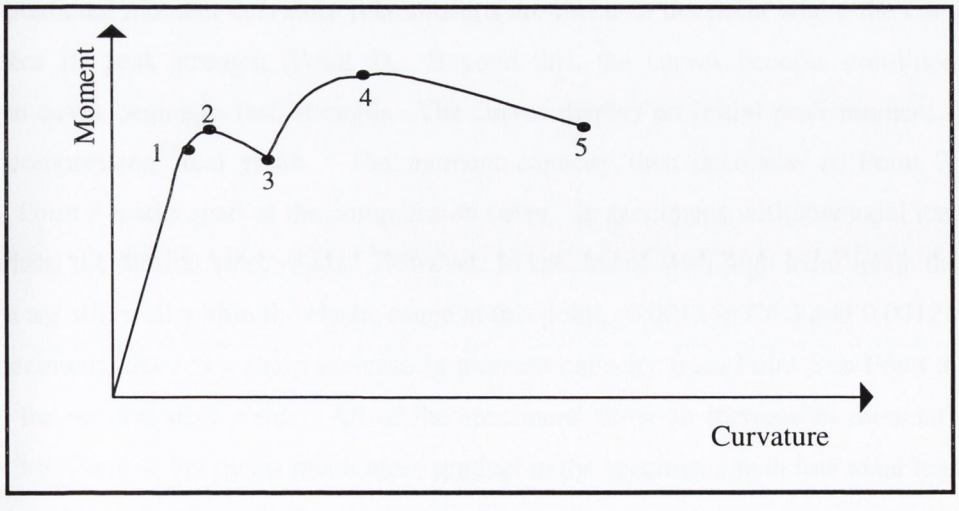

Figure 7.6: Moment-curvature response: Shape 3

Shape 1: Low axial load, link spacing less than or equal to 125mm (C6.1, C6.2)

Point1: Compression cover reaches its peak strength - start of non-linear behaviour.

Point 2: Compression steel yields.

Point 3: Compression cover loses strength, tension steel yields – moment resistance increases to point 4.

Point 4: Peak moment occurs, moment resistance reduces beyond this point.

Shape 2: Low axial load, link spacing greater than 125mm (C5.1, C5.2, C6.5, C6.6)

Point 1: Compression cover reaches its peak strength – start of non-linear behaviour.

Point 2: Compression steel yields.

Point 3: Compression cover loses strength, tension steel yields - moment resistance increases to point 4.

Point 4: Peak moment occurs, resistance decreases to point 5.

Point 5: Moment resistance is lost beyond this point.

Shape 3: High axial load (C6.3, C6.4)

Point 1: Compression cover reaches it peak strength – start of non-linear behaviour.

Point 2: Compression steel yields.

Point 3: Compression cover loses strength, tension steel still well within elastic range, moment resistance increases to point 4.

Point 4: Tension steel yields, moment resistance decreases to point 5.

Point 5: Moment resistance is lost beyond this point.

All of the predicted moment-curvature relationships are linear to the point where the compression cover reaches its peak strength (Point 1). Beyond this, the curves become non-linear as the compression cover begins to lose strength. The curves display an initial peak moment (Point 2) when the compression steel yields. The moment capacity then decreases to Point 3. In all specimens, Point 3 marks spall of the compression cover. In specimens with low axial loads, Point 3 is also where the tension steel yields. However, in specimens with high axial loads the tension steel strains are still well within the elastic range at this point, (0.0013 in C6.3 and 0.0012 in C6.4). In these specimens, there is a sharp increase in moment capacity from Point 3 to Point 4, (Figure 7.6), when the tension steel yields. All of the specimens show an increase in moment capacity from Point 3 to Point 4, but this is much more gradual in the specimens with low axial loads where the tension steel has already yielded.

Upon tension steel yielding, the specimens with low axial loads display an increase in their moment resistance. However, in specimens with the larger link spacings (145mm), this increase in followed by a decrease in resistance prior to ultimate curvature. No such losses in resistance occur in specimens with closely spaced links (105mm and 125mm) where the maximum moment occurs at the final curvature value predicted by the model. In specimens with high axial loads, moment resistance decreases steadily once the tension steel has yielded. Reduction in resistance between Points 4 and 5, in Figures 7.5 and 7.6, occur as the neutral axis depth (measured from the extreme compression fibre) decreases, the region of concrete core in tension increases, and the remaining compressive core elements begin to lose strength. In specimens with close link spacings, exactly the same phenomena occur, yet the specimens do not lose moment capacity. This is related to the different rates at which resistance is lost in the concrete core elements of the specimens. Figure 7.7 presents the normalised stress versus curvature relationships displayed by the concrete core element closest to the extreme compression fibre in six of the specimens. Here the element stress is normalised by the maximum stress occurring in that element at any point in the response. This illustrates that the rate at which resistance is lost is dependent both on link spacing and axial load level. The specimens with closer link spacings, that is more confinement, do not lose strength as rapidly as specimens with larger link spacings or higher axial loads.

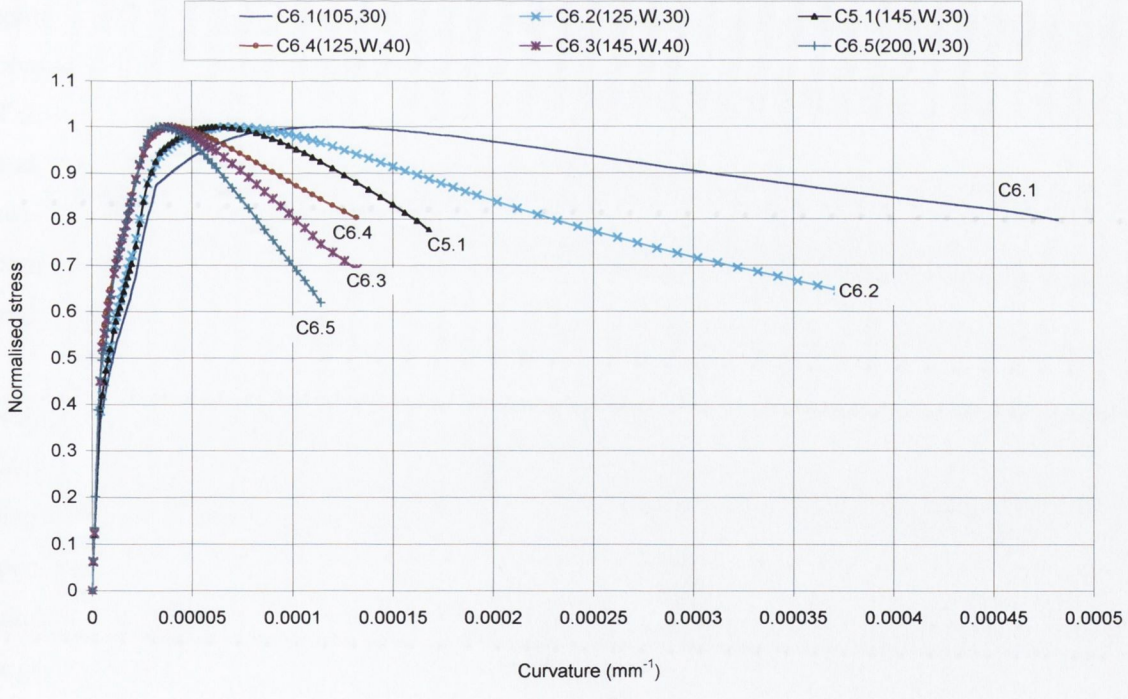

Figure 7.7: Different rates of resistance loss

With respect to the moment-curvature responses presented in Figures 7.1 to 7.3, all the specimens fail at curvature values significantly less that the final curvature value predicted by the model. Beyond this final curvature value further iterations in the model fail to converge. The curvature values of the predicted moment-curvature response which correspond to the experimental moment

values recorded for the last displacement cycle before failure are presented in Table 7.1, along with the corresponding neutral axis depth values and ultimate stresses in the tension and compression steel.

Specimen	Neutral axis depth mm	Curvature mm^{-1}	Compression steel stress N/mm^2	Tension steel stress N/mm^2
C5.1(145,W,30)	99.0	0.000066	365	366
C5.2(145,30)	103.6	0.000054	364	364
C6.1(105,30)	104.6	0.000054	364	363
C6.2(125,W,30)	96.6	0.000070	366	366
C6.3(145,W,40)	126.8	0.000054	366	361
C6.4(125,W,40)	137.9	0.000052	367	360
C6.5(200,W,30)	104.5	0.000062	365	364
C6.6(175,30)	107.0	0.000044	363	362

Table 7.1: Ultimate neutral axis depth, curvature and steel stresses in the predicted moment-curvature responses

With the exception of the specimens with high axial loads, (C6.3 and C6.4), the neutral axes generally fall close to 100mm, i.e. close to mid-depth of the section. At this point, strains in the compression and tension steel are the same, so their stresses balance each other. It is clear from Table 7.1 that, with the exception of the specimens with high axial loads, the stresses in the tension and compression steel are more or less identical. In both specimens with higher axial loads, the stress is higher in the compression steel. In all specimens the stresses in both the tension and compression steel are greater than or equal to the steel yield strength. Notably, in specimens with high axial loads, failure is predicted to occur once the tension steel has yielded.

Notably, of the following specimen pairs: C5.1(145,W,30)/C5.2(145,30), C6.1(145,30)/C6.2(125,W,30) and C6.5(200,W,30)/C6.6(175,30), the specimens with wireballs display larger ultimate curvatures and smaller neutral axis depths than those without wireballs. In specimens with higher axial loads, C6.3(145,W,40) and C6.4(124,W,40) the neutral axis depth values are significantly higher than those for specimens with lower axial loads. This is because a larger area of compressed concrete is required for equilibrium of forces when the applied axial load is higher.

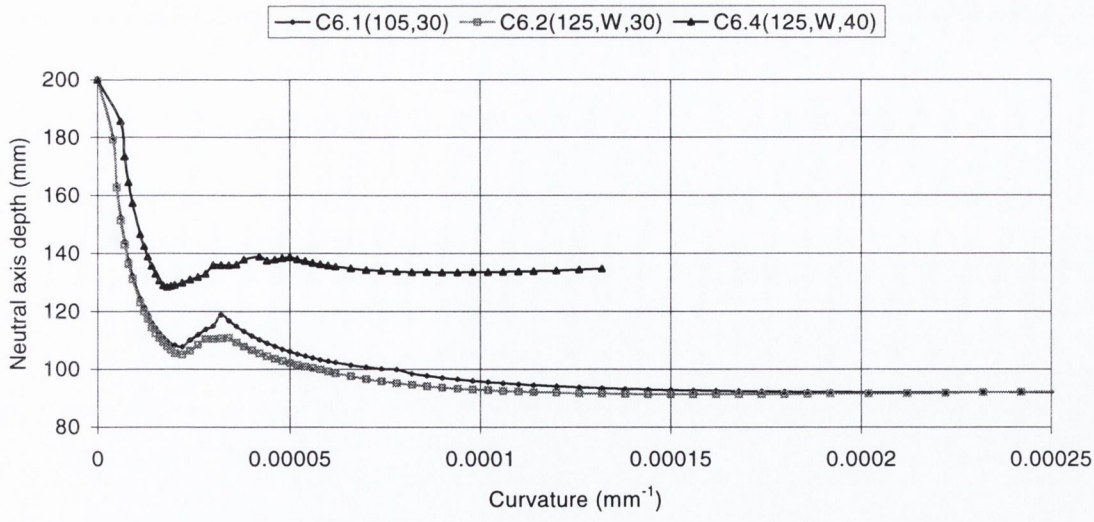

Figure 7.8: Group 1 Neutral axis depth variation with curvature

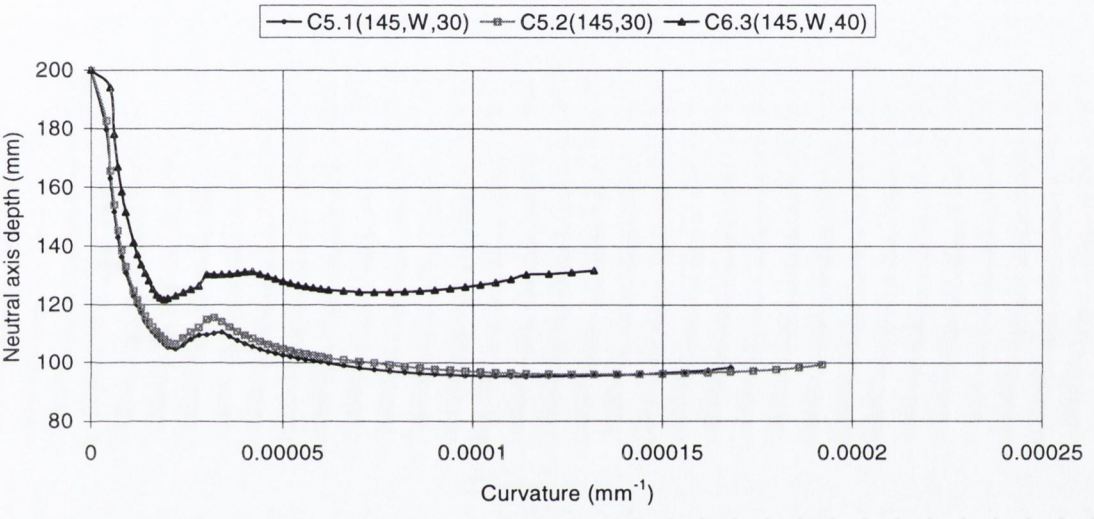

Figure 7.9: Group 2 Neutral axis depth variation with curvature

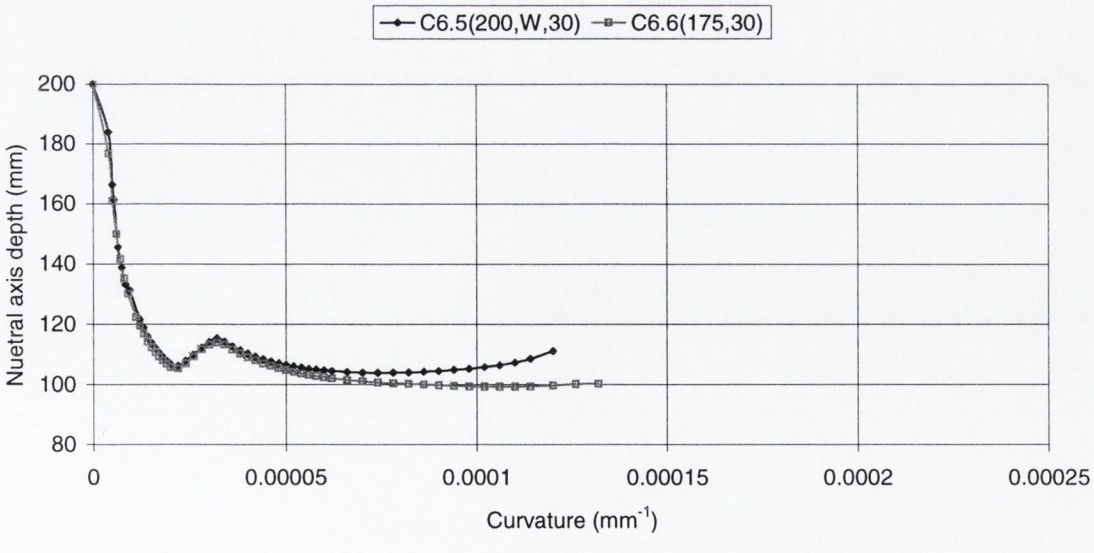

Figure 7.10: Group 3 Neutral axis depth variation with curvature

Figures 7.8 to 7.10 present the predicted variation in neutral axis depth with curvature for the three comparison groups. These curves illustrate that, while the neutral axis depth generally decreases, it increases in value over a certain region of all the moment-curvature responses. A core element lying just outside of the compression region will experience small tensile strains, therefore, as the neutral axis depth gradually increases, these strains will reduce to zero. In other words, to attain force-equilibrium for certain curvature values, the model increases the neutral axis depth such that the core element lying just outside the compression region contributes zero force.

Finally, it is worth noting here that Section 7.4 presents the predicted ultimate strains for link opening. These strains may not correspond to the ultimate curvature values presented in Table 7.1.

7.3 Moment-displacement response

The predicted moment-displacement responses for the eight beam-columns are presented in Figures 7.11 to 7.18, while Table 7.2 provides the ratios of predicted to experimental moment for each displacement level. The first ratio, corresponding to a displacement of 2.5mm, is also the ratio of the predicted initial stiffness to the experimental initial stiffness. The experimental curves presented in Figure 7.11 to 7.18 are envelope curves of the cyclic test results.

It is clear from the moment-displacement responses and Table 7.2 that the model over-predicts initial stiffness. The over-prediction is not consistent, varying from 22% (C6.3) to 65% (C6.1). Indeed, in the case of C6.3, the predicted moments are the most accurate of all the specimens, while the moment predictions for C6.1 for the first four cycles are the most inaccurate of all the specimens. However, there is consistency, in that in all cases the predicted curve lies outside of the experimental curve, up to and including the 10mm displacement cycle.

It is reasonable that the predicted curves lie outside the experimental curves. Mander's model was developed to predict the response of concrete subject to monotonic compressive loading, not the combination of lateral cyclic loading and axial load imposed on the specimens here. Cyclic loading implies quicker stiffness degradation than monotonic loading, and this explains, at least in part, why the experimental curves lie within the predicted curves for the ascending branch.

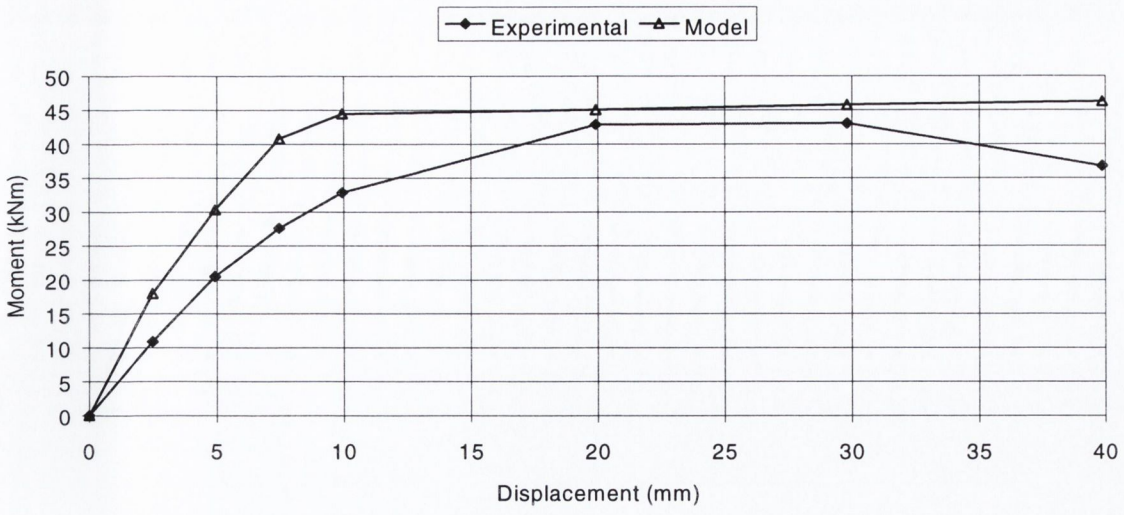

Figure 7.11: C6.1(105,W) Predicted moment-displacement response

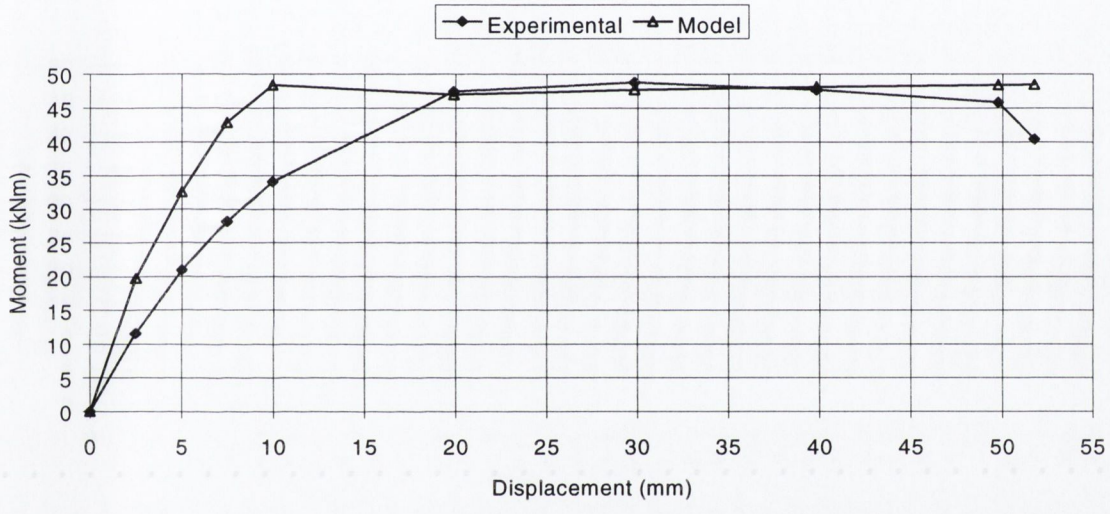

Figure 7.12: C6.2(125,W,30) Predicted moment-displacement response

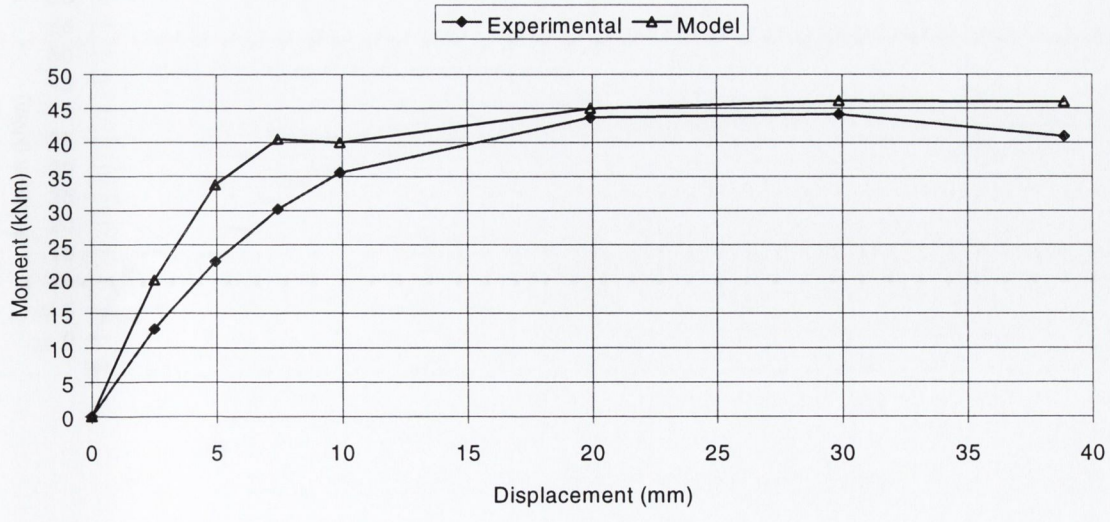

Figure 7.13: C6.4(125,W,40) Predicted moment-displacement response

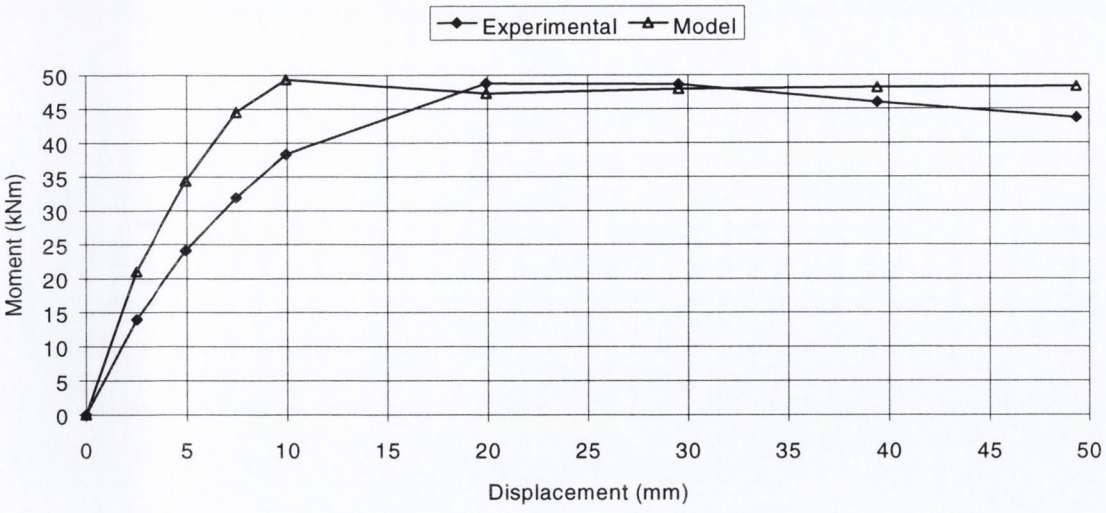

Figure 7.14: C5.1(145,W,30) Predicted moment-displacement response

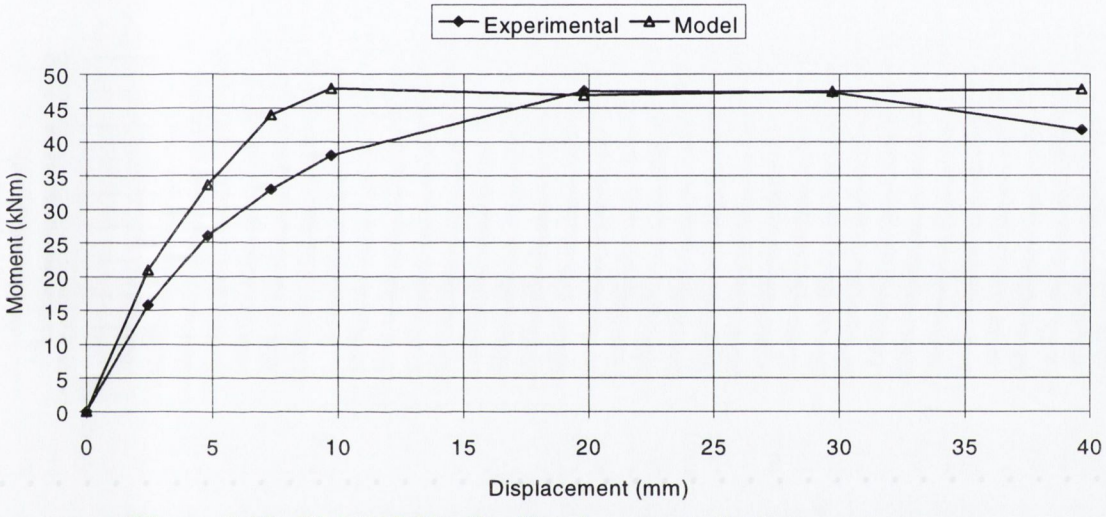

Figure 7.15: C5.2(145,30): Predicted moment-displacement response

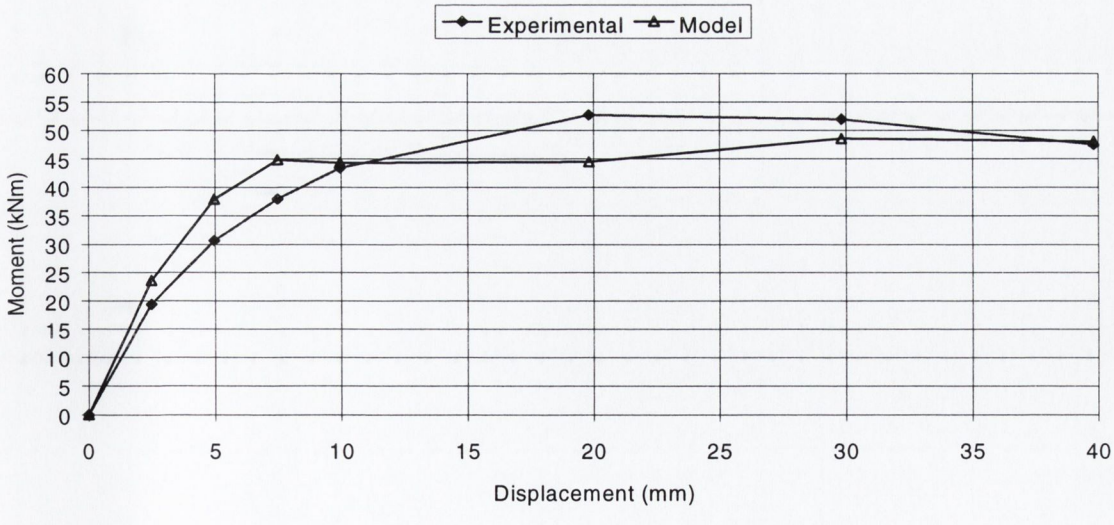

Figure 7.16: C6.3(145,30,W) Predicted moment-displacement response

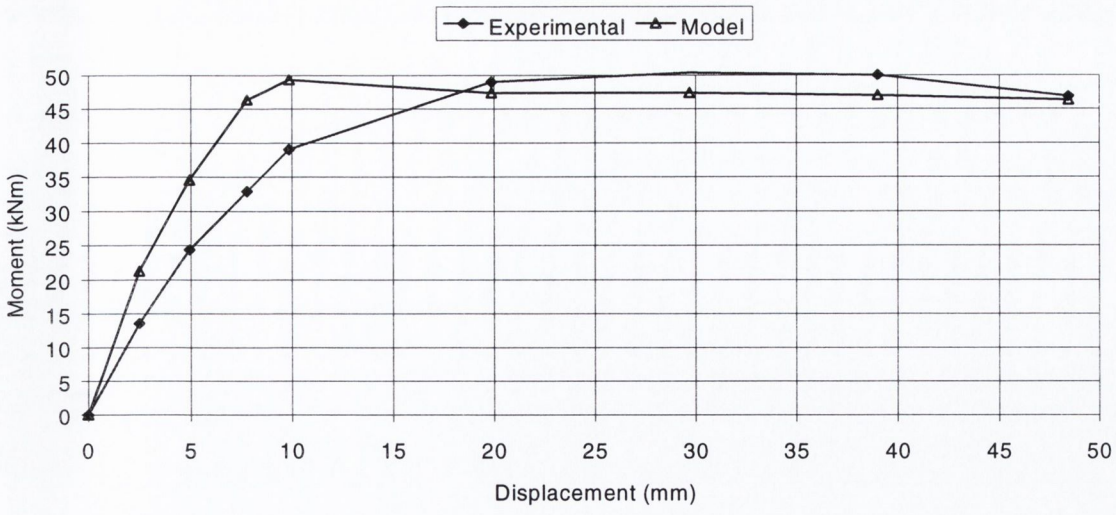

Figure 7.17: C6.5(200,W,30) Predicted moment-displacement response

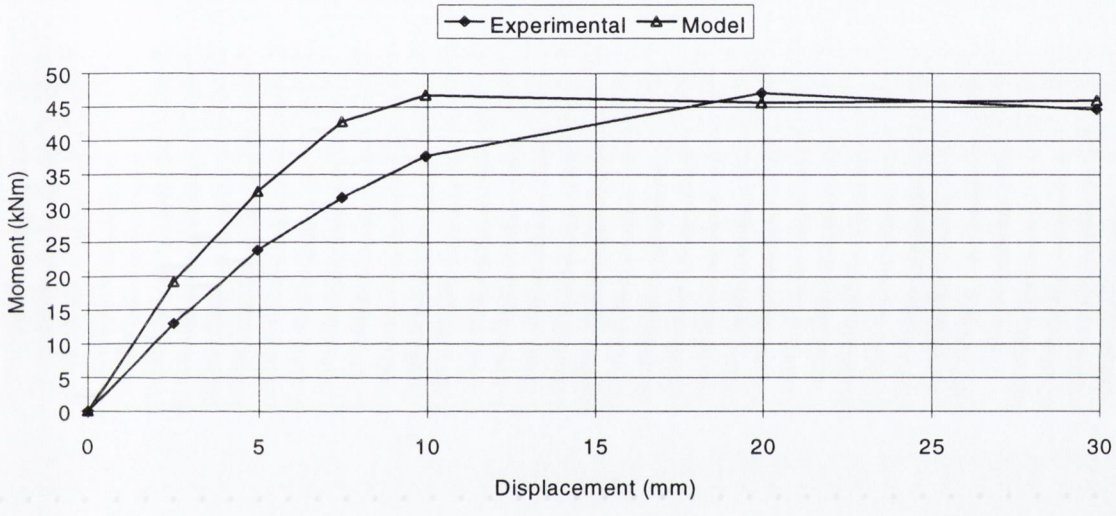

Figure 7.18: C6.6(200,W,30) Predicted moment-displacement response

Cycle/Group Cycle	Displacement mm	C5.1 145/W/30	C5.2 145/30	C6.1 105/30	C6.2 125/W/30	C6.3 145/W/40	C6.4 125/W/40	C6.5 200/W/30	C6.6 175/30
1	2.5	1.50	1.33	1.65	1.71	1.22	1.56	1.56	1.48
2	5.0	1.43	1.29	1.48	1.56	1.24	1.42	1.42	1.36
3	7.5	1.39	1.33	1.48	1.52	1.18	1.41	1.41	1.35
4	10.0	1.29	1.26	1.35	1.42	1.02	1.26	1.26	1.23
5	20.0	0.97	0.99	1.05	0.99	0.84	0.98	0.98	0.97
6	30.0	0.99	-	1.06	0.98	0.93	0.94	0.94	1.03
7	40.0	1.05	1.00	1.26	1.01	1.01	0.99	0.99	-
8	50.0	1.10	1.14	-	1.06	-	-	-	-
9	52.0	-	-	-	1.20	-	-	-	-

Table 7.2: Model Accuracy: Ratios of predicted to experimental moment for each displacement cycle

Note: Ratios for Cycle 1 represent the ratio of predicted to experimental initial stiffness

However, some of the model's over-predictions are so large other possible contributions need to be addressed. The immediate question is whether the model takes account of all external influences acting on the beam-column specimens. Outside of the imposed lateral loading and axial force, other forces acting on the specimen arise from the P-Delta effect, and possible movement of the base element of the beam-columns as they were subject to lateral loading.

The P-Delta effect was discussed in Section 3.7.2.1 and is included in the experimental results. Within the model, the P-Delta effect is taken account of since the experimental moment values used in the model calculations consist of two components – the moment due to the applied lateral load and the moment due to the P-Delta effect. As regards possible vertical movement of the base element, an LVDT was mounted from the laboratory frame to the base element to monitor any movement there. Unfortunately, in two beam columns (C5.1 and C5.2) there were not enough LVDTs available in the laboratory at the time to monitor movement of the base element. However, a dial gauge was used instead and monitored by eye throughout the test – negligible movement was observed. In two other specimens, the LVDT failed to read. However, of the four remaining specimens, displacement versus scan plots are presented in Appendix C. It is clear from these plots that there was negligible movement of the base element.

With respect to the predicted moment capacity of the beam-columns, the model proved very accurate. All of the specimens reach their peak moments at Group Cycles 5 or 6, when they have reached yield. It is clear from Table 7.2 that during these cycles, the predicted moments are very accurate. With the exception of C6.6, all of the predicted moments for Group Cycles 5 and 6 are between 1% and 7% of the experimental moment.

In most cases, from displacements of 10mm to the ultimate displacement, the model curves are approximately straight lines with small positive slopes. Whereas the experimental curves all display a decrease in moment resistance before the ultimate displacement, the predicted curves actually display small increases in resistance. This increase in moment is related to the predicted moment-curvature responses, which also all display some increase in moment capacity after the tension steel yields (Points 3 to Points 4 in Figures 7.4 to 7.6).

A last point to note on the predicted moment-displacement responses, is the almost right-angled transition from linearity to non-linearity between the 10 and 20mm cycles. This is where the steel yields. Where the experimental curves display quite a uniform transition, the predicted curves do not show evidence of yield. This must be related to some change in material properties that the model fails to incorporate properly. Again, cyclic loading effects, such as the Bauschinger effect (Comité Euro-International du Béton, 1996) displayed by steel, which lead to a less well-defined experimental yield point, may play a role. Notably, if the moment-displacement responses are re-

plotted, this time excluding the 7.5mm and 10mm displacement points, the predicted curves represent a much better match to the experimental curves. The slopes of the predicted curves from 5 to 20mm are almost equal the slopes from 10 to 20mm on the experimental curves. These curves are presented in Appendix D.

7.3.1 Sensitivity of the predicted moment-curvature response to material characteristics

Naturally, the predicted moment-curvature response is sensitive to the input material factors, such as the steel reinforcement's characteristics and the unconfined concrete strength, and changes in the moment-curvature response may affect the predicted moment-displacement response. For example, changing the slope of the strain-hardening plateau for the reinforcing steel will change the form of the moment-curvature response in the inelastic range. Figure 7.19 presents the moment-curvature response of specimen C6.1 for lower and upper bound strain-hardening characteristics. The two sets of characteristics are provided in Table 7.3. The lower bound characteristics are those previously presented in Chapter 6 as the reinforcing steel properties used throughout the model while the upper bound properties presented here are the same as for the lower bound conditions except that the ultimate strain is assumed to be twice that for lower bound conditions.

Property	Lower bound	Upper bound
Stress at yield, f_y	360	360
Strain at yield, ε_y	0.0018	0.0018
Young's Modulus, E_s (N/mm^2)	200000	200000
Steel ultimate strength, f_u (N/mm^2)	620	620
Strain at ultimate, ε_u	0.1530	0.0765
Post-yield stiffness, E_{spy} (N/mm^2)	1724	3490

Table 7.3: Upper and lower bound properties for steel reinforcement

It is clear in Figure 7.19 that the strain-hardening slope plays a significant role in determining the slope of the moment-curvature response from its yield point to the final curvature value. For upper bound conditions, the strain-hardening slope is greater than for lower bound conditions. Hence, the slope of the moment-curvature response for upper bound conditions is greater than for lower bound conditions. However, it is clear from the predicted moment-displacement response for lower and upper bound conditions presented in Figure 7.21 that the influence of strain-hardening characteristics is negligible in this case.

Changing the input unconfined concrete strength will also affect the moment-curvature response, since it governs the spalling strength of unconfined concrete as well as being an important factor in determining the confined concrete strength. A lower concrete strength will decrease the predicted initial stiffness and ultimate moment. Figure 7.22 presents the moment-curvature response of specimen C6.6 for the actual unconfined concrete strength of 26.1N/mm^2 and an unconfined strength of 15N/mm^2.

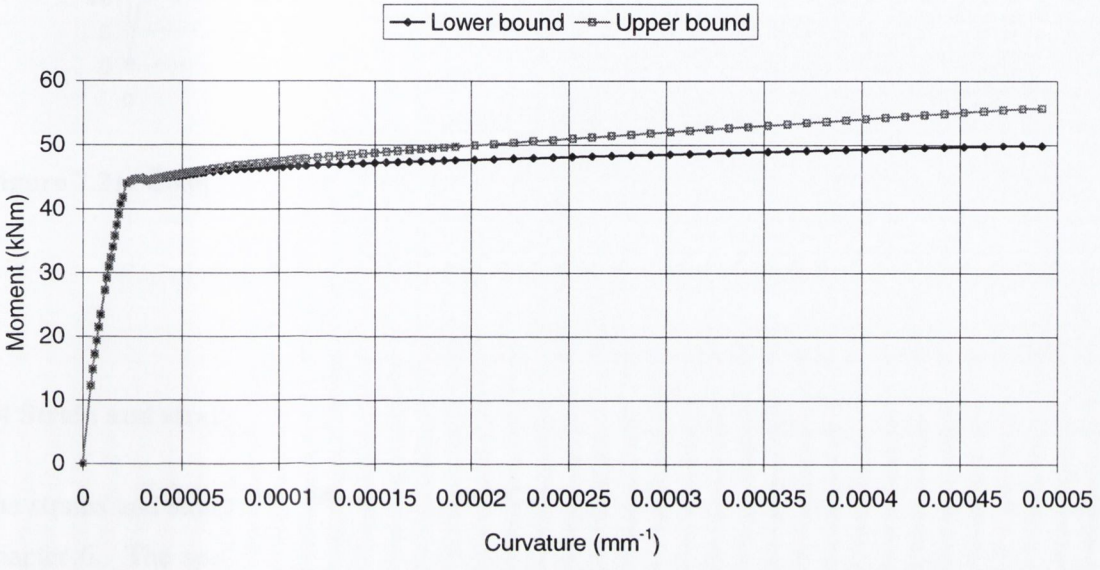

Figure 7.19: C6.1(105,30) Moment-curvature response for lower and upper bound strain-hardening of reinforcing steel

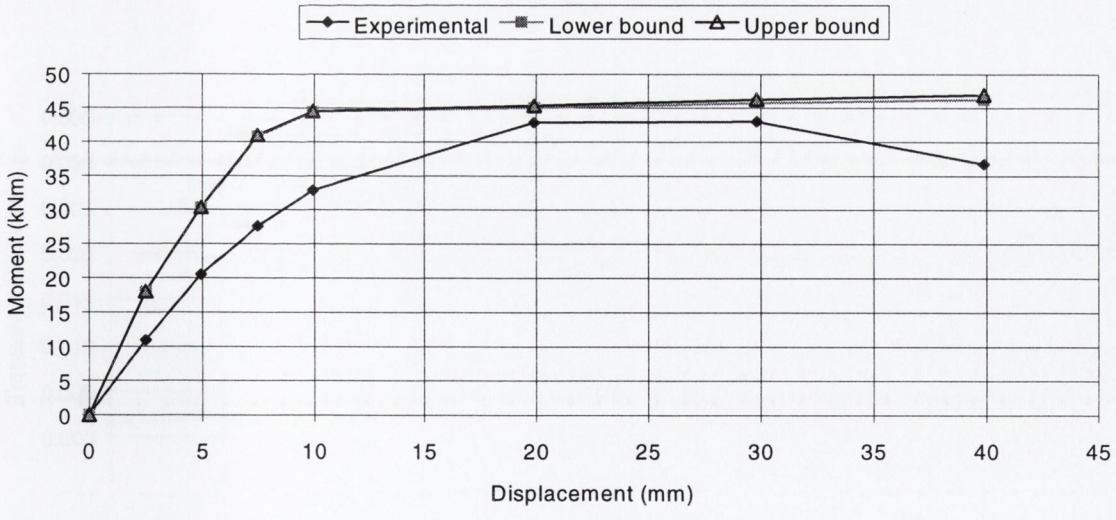

Figure 7.21: C6.1(105,30) Moment-displacement response for lower and upper bound strain-hardening of reinforcing steel

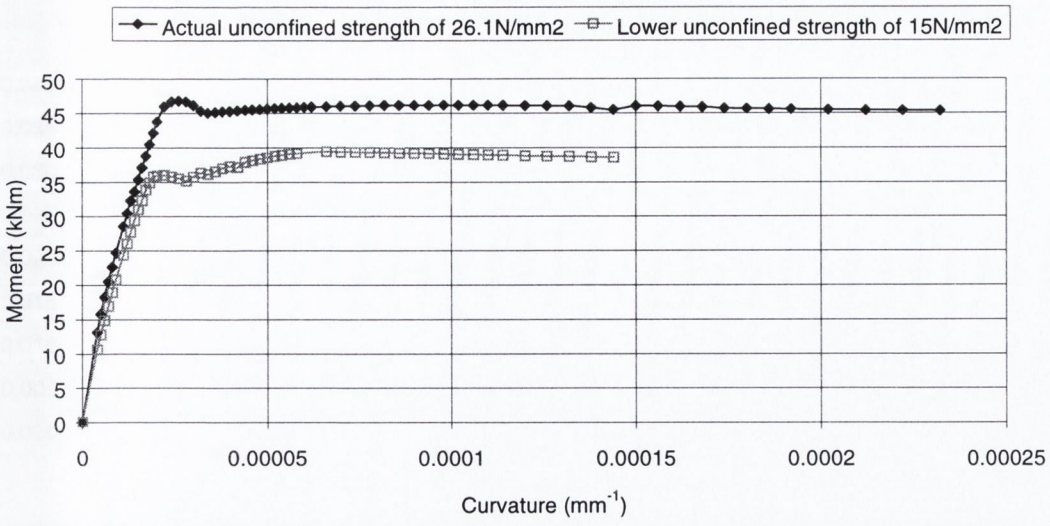

Figure 7.21: C6.6(175,30) Moment-curvature response for two different unconfined concrete strengths

7.4 Strain and strain energies in transverse steel

The strains and strain energies in the transverse steel were predicted using the theory described in Chapter 6. The specimens are considered in the three comparison groups previously defined in Table 5.5. Figures 7.22 to 7.24 present plots of the predicted strain in the transverse steel with respect to displacement cycle. The failure strain, taken as the strain corresponding to the displacement cycle at which the beam-column links were observed to begin to open, is indicated on the plots by a large circle.

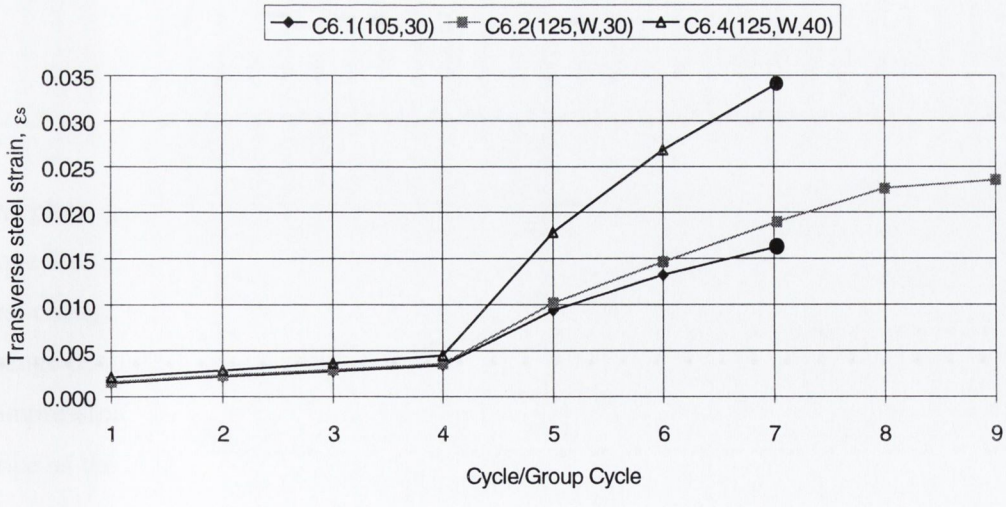

Figure 7.22: Group 1 Transverse steel strain versus Cycle/Group Cycle

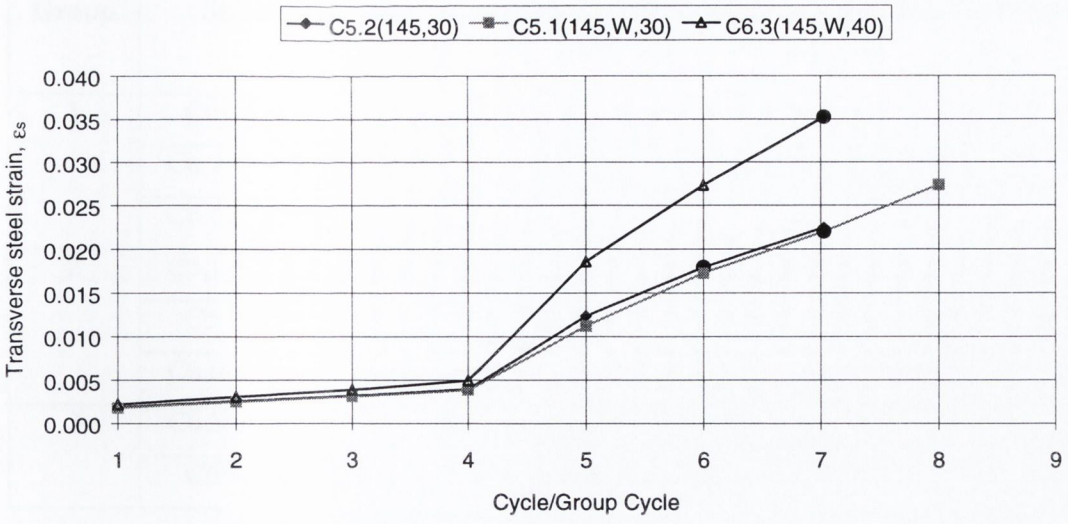

Figure 7.23: Group 2 Transverse steel strain versus Cycle/Group Cycle

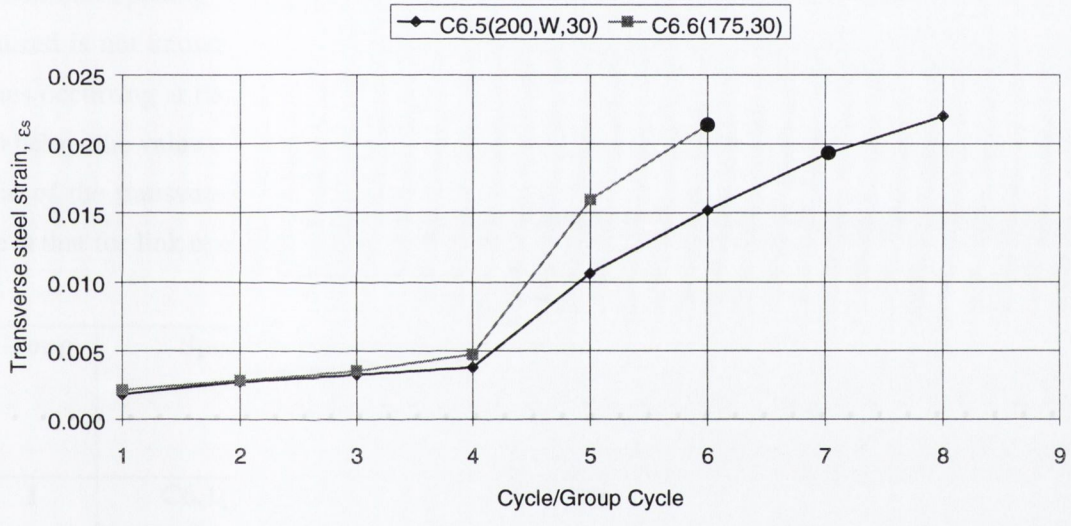

Figure 7.24: Group 3 Transverse steel strain versus Cycle/Group Cycle

The plots are similar in that all the lines display at least three changes in slope. These changes in slope are related to significant changes in the stress-strain characteristics of the two materials. The first change corresponds to yielding of the longitudinal steel, which occurs in cycle 5. The second change occurs when the first concrete core element, that is the core element closest to the extreme compression fibre, reaches its peak stress. Beyond this point, the strain plots display a reduced slope as the core begins to lose resistance. Table 7.4 presents the different slopes of the plots and the corresponding cycles over which these slopes exist.

Group	Specimen	1st slope (cycles)	2nd slope (cycles)	3rd slope (cycles)	4th slope (cycles)
1	C6.1(105,30)	0.001 (1-4)	0.006 (4-5)	0.002 (5-7)	-
	C6.2(125,W,30)	0.001 (1-4)	0.007 (4-6)	0.004 (6-8)	0.0018
	C6.4(125,W,40)	0.001 (1-4)	0.013 (4-5)	0.008 (5-7)	-
2	C5.1(145,W,30)	0.001 (1-4)	0.007 (4-5)	0.005 (5-8)	-
	C5.2(145,30)	0.001 (1-4)	0.008 (4-5)	0.005 (5-7)	-
	C6.3(145,W,40)	0.001 (1-4)	0.014 (4-5)	0.008 (5-7)	-
3	C6.5(200,W,30)	0.001 (1-4)	0.008 (4-5)	0.006 (5-8)	-
	C6.6(175,30)	0.001 (1-4)	0.011 (4-5)	0.052 (5-6)	-

Table 7.4: Transverse steel strains different regions of slope

Table 7.5 presents the transverse steel strain and strain energies in the different specimens at the point of link opening. Specimen C6.2(125,W,30) did not fail and, hence, the strain at which failure occurred is not known. Therefore, the quoted values of strain and strain energy for C6.2 are the values occurring at the last displacement cycle. It is noteworthy, that all of the strain energies are well below the value of 110MJ/m^3, of Equation 6.23, quoted by Mander *et al.* (1998) as the fracture strain of the transverse reinforcement. This is not unexpected since the strain energy calculated here is that for link opening rather than fracture, which naturally will be much less.

Group	Specimen	Strain at link opening	Strain energy at link opening MJ/m^3	Cycle/Cycle Group of link opening
1	C6.1(105,30)	0.016	5.72	7
	C6.2(125,W,30)	0.024	8.56+	9+
	C6.4(125,W,40)	0.034	13.31	7
2	C5.2(145,30)	0.018	6.35	7
	C5.1(145,W,30)	0.022	7.94	6
	C6.3(145,W,40)	0.035	12.78	7
3	C6.5(175,30)	0.021	7.70	6
	C6.6(200,W,30)	0.033	12.36	6

Table 7.5: Strain and strain energy at link opening

Group	Specimen	% increase in strain energy	% increase in strain capacity
1	C6.1(105,30)	-	-
	C6.2(125,W,30)	50+	50+
	C6.4(125,W,40)	113	133
2	C5.2(145,30)	-	-
	C5.1(145,W,30)	22	25
	C6.3(145,W,40)	94	101
3	C6.6(175,30)	-	-
	C6.5(200,W,30)	54	61

Table 7.6: Percentage increase in strain and strain energy capacities

The strain results reflect the ductility enhancing properties of wireball reinforcement. Table 7.6 details the percentage increase in strain and strain energy capacities of the specimens within each comparison group. The results show that the percentage increase in strain and strain energy capacities are similar but not identical. Combination plots, included in Appendix E, of normalised strain (with respect to the maximum achieved strain) and normalised strain energy (with respect to the maximum achieved strain energy), for Group Cycles 5 to 9, illustrate that the two lines are very similar but not exactly the same. However, that said, the percentage increases are very close in value, and the trends within each group are consistent.

In all of the comparison groups, the specimens with wireballs display increased strain and strain energy capacities over those of the specimens without wireballs. In Group 1, specimens C6.2(125,W,30) and C6.4(125,W,40) have strain energy capacities which are 50% and 113% respectively, greater than that of specimen C6.1(105,30). They show similar, although slightly greater, increases in strain capacity. The same trend is evident in Group 2 where the specimens with wireballs, C5.1(145,W,30) and C6.3(145,W,40), have strain energy capacities 22% and 94% greater than the specimen without wireballs, C5.2(145,30). Again, the percentage increases in strain capacity are slightly higher, than the percentage increases in strain capacity. Finally, in Group 3, specimen C6.5(200,W,30) with a larger link spacing but also containing wireballs, displays a 54% increase in strain energy capacity over specimen C6.6(175,30) with a closer link spacing but no wireballs.

In other words, the model is capable of predicting the ductility enhancing effect of wireballs. Taking into account the differences between the percentage increases in strain and strain energy capacity, and disregarding the specimens with the higher axial loads, the model predicts percentage increases in strain or strain energy capacities of between approximately 20 and 55%.

The strain energies presented in Table 7.5 were calculated using Equation 6.26, which is repeated below for convenience:

$$\rho_s A_{cc} \int_0^{\varepsilon_{sop}} f_s d\varepsilon_s = \sum_{i=1}^{n} A_i \int_0^{\varepsilon_{cu}} f_{ci} d\varepsilon_{ci} + \rho_{cc} A_{cc} \int_0^{\varepsilon_{cu}} f_{sl} d\varepsilon_c - \sum_{i=1}^{n} A_i \int_0^{\varepsilon_{sp}} f_{ci} d\varepsilon_{ci} \qquad (6.26)$$

In this equation, the wireball reinforced specimens' strain energies consist of two components: the strain energy in the links plus the strain energy in the wireballs. Therefore, Equation 6.26 was modified to include the component of strain energy associated with the wireballs such that it becomes:

$$\rho_{sw} A_{cc} \int_0^{\varepsilon_{sw}} f_{sw} d\varepsilon_s + \rho_s A_{cc} \int_0^{\varepsilon_{sop}} f_s d\varepsilon_s = \sum_{i}^{n} A_i \int_0^{\varepsilon_{cu}} f_{ci} d\varepsilon_{ci} + \rho_{cc} A_{cc} \int_0^{\varepsilon_{cu}} f_{sl} d\varepsilon_c - \sum_{i}^{n} A_i \int_0^{\varepsilon_{sp}} f_{ci} d\varepsilon_{ci} \qquad (6.27)$$

It is this additional component, the first term on the left-hand side of Equation 6.27, that leads to the higher strain values presented in Table 7.5. The ratio of the first term (for wireball reinforcement) to the second term (for link reinforcement) of the left-hand side of Equation 6.27 equals the percentage increase in strain energy capacity. Therefore, it should be expected that this ratio should be similar to the percentage increases in strain and strain energy capacities presented in Table 7.6, and is written as follows:

$$\frac{\rho_{sw} A_{cc} \int_0^{\varepsilon_{sw}} f_{sw} d\varepsilon_s}{\rho_s A_{cc} \int_0^{\varepsilon_{sop}} f_s d\varepsilon_s} = \text{increase in strain capacity with wireballs} \qquad (7.1)$$

Assuming a uniform volumetric change within the concrete core implies that the strain in the wireballs will equal the strain in the links. Then for:

$$E_s = E_{sw} \Rightarrow f_{sw} = f_s \qquad (7.2)$$

where:

E_s, E_{sw} = Young's Modulus of link steel and wireball steel respectively (N/mm^2)

Therefore, Equation 7.1 reduces to:

$$\frac{\rho_{sw}}{\rho_s} \equiv \frac{Volume\ of\ wireball\ \ steel}{Volume\ of\ link\ steel} = \frac{V_w}{V_L} \qquad (7.3)$$

where:

V_w = volume of wireball steel (mm^3)

V_L = volume of link steel (mm^3)

Table 7.7 presents the ratios of the volume of wireball steel to the volume of link steel for link spacings of 125, 145, and 200mm. The length of the wireball-reinforced region and the number of wireballs within that length are included. The effective volume of wireball steel acting in the horizontal plane is assumed to be half of the total volume of wireball steel.

Link spacing mm	**Wireball reinforced length mm**	**Number of wireballs**	**Number of links**	V_w **mm^3**	V_L **mm^3**	V_w/V_L **%**
125	425	49	3	72735.7	160221.2	45
145	485	56	3	83126.6	160221.2	52
200	450	52	2	77188.9	106814.2	72

Table 7.7: Volumes of wireball and link steel

The V_w/V_L ratios agree quite well with the percentage increases in strain energy presented in Table 7.6, for wireball reinforced specimens with low axial loads. In Table 7.6 specimens C6.2(125,W,30) and C6.5(200,W,30) display percentage increases in strain energy capacity of 50% and 54% relative to their respective group specimens, C6.1(105,30) and C6.6(175,30), which contained no wireballs. These percentages are reasonably close to the respective 45% and 72% values quoted in Table 7.6. However, for the specimens with 145mm link spacing and low axial loads, there a considerable difference between the 22% increase in strain energy capacity of Table 7.6 and the predicted value of 52% quoted in Table 7.7. Indeed, the 22% increase in strain energy capacity observed seems very low in comparison with the general level of ductility enhancement displayed by wireball-reinforced specimens.

With respect to specimens with higher axial loads, the percentage increases in strain and strain energy capacity, are considerably larger than those of similar specimens with lower axial loads. While representing a positive indication of the ductility enhancing capacity of wireballs, these large percentage increases may be somewhat deceptive. With higher axial loads, the strain demand on the specimens increases. The results presented in Table 7.7 suggest that wireballs can sufficiently enhance the strain capacity to meet this increased strain demand. The higher the axial load the larger the strain energy in the longitudinal steel in compression, and hence, with regard to Equation 6.26, the greater the predicted strain energies.

Figures 7.22 to 7.24 presented the transverse steel strains in each displacement cycle. It is clear that in specimens with higher axial loads, these predicted transverse steel strains are also higher. This is consolidated by the slopes of the different regions of the transverse steel strain plots (Table 7.4), where the second slope is consistently steeper in specimens with higher axial loads. However, in specimens with large link spacings but low axial loads, (C6.5(200,W,30) and C6.6(175,30)), the second slope value is also high. The larger transverse steel strains in specimens with high axial loads or large link spacings are related to the predicted neutral axis depth value. Figures 7.8 to 7.10, show the variation in neutral axis depth with curvature for all specimens. These confirm that the neutral axis depth is always greater for higher axial loads. This is because a larger compressive area of concrete is required to maintain stability in specimens subject to higher axial loads. However, the larger the compressed area of concrete, the greater the area of concrete imparting strain energy to the transverse steel and hence, the apparent greater strain energy capacity.

Finally, it is important to remember that specimen C6.2(125,W,30) did not fail. Indeed, by the end of the last displacement cycle the specimen remained substantially intact with no core damage and no signs of the links opening. In other words, the strain energy at which the links would have opened is probably significantly greater than the value of 8.56MJ/m^3 quoted in Table 7.5. Therefore, the percentage increase in strain capacity of this specimen, through the inclusion of wireballs, relative to specimen C6.1, could be as high as the 113% increase observed in specimen C6.4(125,W,40) with the higher axial load.

7.5 Conclusions

The numerical model results presented in this chapter illustrate that the model is capable of predicting the moment-curvature and moment-displacement responses of the test specimens. Further, the model is able to distinguish between the transverse strain demands in specimens with different link spacings and with or without wireball reinforcement. This is the key factor in determining the ductility capacity of reinforced concrete beam-columns.

The moment-curvature response has been illustrated as being sensitive to the levels of confinement (in terms of link spacing) and axial load, and to the input material factors. The moment-displacement responses are accurate in terms of the predicted moment capacities but less accurate with respect to the initial stiffnesses.

Beyond the prediction of a moment-displacement response for each beam-column specimen, the ultimate aim of the numerical model was to check whether Mander's approach to calculating the strain at failure of the beam-columns could be modified to predict failure in wireball-reinforced

specimens. A good correlation with the increase in strain capacity of the specimens with the volume of wireball steel was observed, however, some discrepancies did exist, especially with respect to the predicted strain capacity of specimens with higher axial loads.

CHAPTER 8

CONCLUSIONS

8.1 Introduction

The objective of this research was to assess the confinement effectiveness of wireball reinforcement with a view to improving the ductility, and hence the earthquake resistance, of reinforced concrete members.

Experimental studies were performed to investigate whether the use of wireballs, in combination with conventional longitudinal and transverse reinforcement, increases the rotational capacity of dissipative flexural members. Initial tests considered the response of wireball-reinforced members to different loading types: monotonic compression, flexure and shear. The main test series considered the response of beam-column specimens subject to simultaneous lateral cyclic loading, representative of earthquake loading, and axial compression. A numerical model was also developed to predict the moment-displacement response of reinforced concrete members containing wireballs.

8.2 Experimental studies

8.2.1 Initial tests

The initial test series examined the effect of the inclusion of wireballs in different member types. Tests on stub columns tested under monotonic compression and on simply-supported beams tested in flexure indicated that wireballs, used in combination with conventional reinforcement, enhance confinement in compression and flexural members, leading to improved ductility. It is observed that the inclusion of wireballs in these member types allows a reduction in the amount of transverse reinforcement specified by Eurocode 8 for a certain ductility level. However, the results indicate that there may be a limit to how great this reduction can be before detrimental effects on the shear and buckling resistance of the members occur. It was also observed that the confinement effects of wireballs decreases for smaller transverse link spacings. Monotonic shear on wireball-reinforced beams indicate that the inclusion of wireballs may increase shear resistance and promote the development of a plastic hinge rather than shear cracking. However, the available data is very limited.

8.2.2 Main tests

A series of eight beam-column specimens were considered within this test series. It was quite difficult to find the specimen details and test arrangements that allowed the benefits of wireballs to be demonstrated with the restrictions of the laboratory equipment, and, therefore, preliminary test specimens were considered before the specimen size and detailing could be finalised.

The beam-column specimens were tested under a combination of axial loading and lateral cyclic loading, representative of seismic response conditions. In each test, the applied axial load was kept constant, while the displacement controlled lateral cyclic loading was applied with increasing amplitude. All the specimens had the same dimensions and longitudinal steel contents but differed with respect to (i) transverse steel spacing (ii) inclusion of wireballs and, (iii) level of axial load. The transverse steel consisted of standard rectangular links and the link spacings were related to DCL of Eurocode 8. The applied axial loads were typical values for 'real' columns, being 30-40% of the specimen's cross-sectional capacity.

It was concluded from tests that:

- Wireball reinforcement can increase the earthquake resistance of reinforced concrete beam-columns.

- Wireball reinforcement provides increased confinement in reinforced concrete. Visually this was observed in the slower degradation of beam-column specimens containing wireballs relative to those without. The presence of wireballs delayed and reduced degradation and expansion of the concrete core, while also reducing link distortion and opening and longitudinal steel buckling.

- Quantitatively, the inclusion of wireballs improved energy dissipation capacity and displacement ductility. Even in specimens where the axial load level approached that for over-reinforced conditions, the inclusion of wireballs provided increased rotational ductility capacity and promoted a more stable mode of failure.

- All of the wireball-reinforced beam-column specimens dissipated more energy that specimens without wireballs, even when the axial load levels were high and the link spacings were large.

- There exists much scope for wireballs to be used as partial replacement for the large amount of confinement links otherwise required for good earthquake resistance. Alternatively, the normal

link spacing could be used and extra ductility ensured, through the inclusion of wireballs. This could be of benefit in strategic structures such as hospitals or large bridges.

8.3 Numerical model

A numerical model, based on Mander's theoretical stress-strain model for confined concrete, was developed. It is capable of predicting the moment-curvature and moment-displacement responses of the beam-column specimens considered in this research. It is also able to distinguish between the transverse steel strain demands in specimens with different link spacings and wireball reinforcement.

The moment-curvature response was shown to be sensitive to link spacing, axial load and the input material characteristics. The moment-displacement responses were very accurate in terms of ultimate moment resistance, but less accurate with respect to initial stiffness. Within the elastic range, the predicted moment-displacement response curves always lie outside of the experimental curves since the model considers monotonic loading rather than the lateral cyclic loading conditions considered here and, therefore, the model does not take into account the quicker stiffness degradation implicit with cyclic loading.

It was shown that Mander's approach to the prediction of failure strain may be extended to predict the failure strain of wireball-reinforced beam-columns. A good correlation exists with the increase in strain capacity and the volume of wireball steel. Therefore, the proposed model should allow the ultimate displacements to be determined numerically, and hence, the displacement ductility of members to be predicted.

8.4 Further work

This study explored the confinement effectiveness of wireball reinforcement with a view to enhancing the ductility, and hence the earthquake resistance, of reinforced concrete members. It also proposes a model whereby the displacement ductility of wireball-reinforced members may be predicted. However, while many issues have been addressed, the use of wireball reinforcement in earthquake resistant members still deserves further research. Some of the areas which should be investigated are:

- Within the beam-column specimens tested, various link spacings were considered as well as two different axial load levels. However, an extended range of test specimens with different

link spacings and axial loads would provide greater insight into the confinement enhancing effects of wireball reinforcement. Also, the consideration of a broader spectrum of specimen sizes: larger square sections, rectangular sections and walls, would provide further data on the confinement effects of wireballs.

- The links used in the beam-column specimens were standard rectangular links with 90° hooks. Eurocode 8 recommends the use of 135° hooks that extend into the concrete core. If the code recommended hooks were used, the beam-columns' responses would have been different and, therefore, the confinement benefits of wireballs would not be as obvious. Further experimental studies with members employing the code required link shape would assess the impact of different link shapes on the confinement benefits of wireballs reinforcement. The experience of this study suggests that if this were to be done, larger test specimens would need to be considered. In a similar vein, the use of wireball reinforcement instead of the cross-tie details required in higher ductility members should also be examined.

- The issue of high strength concrete and its application to earthquake resistant structures is an area undergoing increasing research. Since this material displays much less ductility than normal strength concrete, it requires larger amounts of confinement steel to ensure a ductile response. The confinement benefits of wireballs could mitigate the need for the otherwise large amounts, and complex configurations, of transverse steel required.

- The proposed numerical model has shown that Mander's approach to the prediction of failure strain may be extended to predict the failure strain of wireball-reinforced beam-columns. However, a more accurate prediction of the length of the plastic hinge region and on the form of the curvature profile within the plastic hinge is required to make the model more applicable to the analysis of different types of sections and to the analysis of whole frames. Further work could also be performed on relating the predicted failure strains to the predicted ultimate curvatures. A necessary first step in any further work in this regard would be to implement the model in a more efficient form using any standard programming language.

- It is likely that more sophisticated modelling approaches, such as the finite element approach, could be employed to further investigate the applicability of wireball reinforcement. However, this work would require consideration of the inelastic response of concrete subjected to multi-axial strains. This is not a simple issue, and it is not certain that any such studies would provide useful results.

REFERENCES

1. ACI, 'Building code requirement for reinforced concrete', 1983, *American Concrete Institute*
2. ACI, 'Building code requirements for reinforced concrete', 1992, *American Concrete Institute*
3. Ahn, J.M., Lee, J.Y., B.Y., Bahn, 'An experimental study of the behaviour of high strength reinforced concrete columns subjected to reverse cyclic shear under axial compression', 2000, *Magazine of Concrete Research*, 52(3), 209
4. AIJ, 'Design Guidelines for Earthquake Resistant Reinforced Concrete Buildings based on Ultimate Strength Concept', 1990, *Architectural Institute of Japan*
5. Al-Haddad, M., 'Curvature Ductility of Reinforced Concrete Beams under Low and High Strain Rates', 1995, *ACI Structural Journal*, 92(5), 526
6. Andriono, T., Park, R., 'Seismic design considerations of the properties of New Zealand manufactured steel reinforcement bar', 1986, *Bulletin of the New Zealand National Society for Earthquake Engineering*, 19(3), 213
7. Aziznamini, A., Corley, W.G., Johal, L.S.P., 'Effects of transverse reinforcement on seismic performance of columns', 1992, *ACI Structural Journal*, 89(4), 442
8. Bayrak, O., Sheikh, S.A., 'Confinement reinforcement for ductile HSC columns', 1998, *ASCE Journal Structural Div.*, 124(9), 999
9. Beeby, A.W., 'Ductility of Reinforced Concrete: Why is it needed and how is it achieved?", 1997, *The Structural Engineer*, 75(18), 311
10. Bischoff, P.H., Perry, S.H., 'Compressive behaviour of concrete at high strain rates', 1991, *Materials and Structures*, 24, 425
11. Booth, E.D., 'Concrete structures in earthquake regions. Design and analysis', 1994, *Longman Scientific and Technical*
12. BS 1881: Part 108: 1983, 'Testing concrete, Method for making test cubes from fresh concrete', 1983, *British Standards Institution, London*
13. BS 1881: Part 116: 1983, 'Testing concrete, Method for determining the compressive strength of concrete cubes', 1983, *British Standards Institution, London*
14. BS 4466: 1989, 'Scheduling, dimensioning, bending and cutting of steel reinforcement for concrete', 1989, *British Standards Institution, London*
15. BS EN 10 002-1: 1990, 'Tensile testing of metallic materials, Part 1. Method of test at ambient temperature', 1990, *British Standards Institution, London*

16. Booth, E.D.'Earthquake Engineering in the 1990s: achievements, concerns and future directions', 1998, *Proc. Institute of Civil Engineers Structures and Buildings* 128, May, 154
17. Booth, E.D., Kappos, A.J., Park, R., 'A critical review of international practice on seismic design of reinforced concrete buildings', 1998, *The Structural Engineer*, 76(11), 213
18. Burdette, E.G., Hilsdorf, H.K., 'Behaviour of laterally reinforced concrete columns', 1971, *ASCE Journal Structural Div.*, 97(ST2), 587
19. Cheong, H.K., Perry, S.H., 'Concrete columns with lateral prestressing', 1991, *ASCE J. Engineering Mech.*, 117(1), 70
20. Cheung, P.C., Paulay, T., Park, R., 'Behaviour of beam-column joints in seismically-loaded RC frames', 1993, *The Structural Engineer*, 71(8), 129
21. Comité Euro-International du Béton, 'RC elements under cyclic loading', 1996, *CEB*, Bulletin 230
22. Comité Euro-International du Béton, 'Seismic Design of RC Structures for controlled inelastic response. Recent advances in design concepts and codes', 1997, *CEB*, Bulletin 236
23. Comité Euro-International du Béton, "Seismic design of reinforced concrete structures for controlled inelastic response", 1998, *CEB*, Bulletin 240
24. Cusson, D., Paultre, P., 'High-strength concrete columns confined by rectangular ties', 1994, *ASCE Journal Structural Div.*, 120(3), 783
25. Di Cioccio, S., 'Impact of spherically reinforced concrete', *BAI Disstn.*, 1997, Trinity College Dublin.
26. ECCS, 'Recommended testing procedure for assessing the behaviour of structural steel elements under cyclic loading', 1986, *ECCS-Technical Committee 1 – Structural safety and loading Technical Working Group 1.3 – Seismic Design*
27. Englekirk, R., 'Steel structures. Controlling behaviour through design.', 1994, *John Wiley & Sons*
28. Eurocode 2, 'Design of concrete structures – Part 1: General rules and Rules for Buildings, European Prestandard ENV 1992-1-1', 1991, *European Committee for Standardisation TC 250,* Brussels.
29. Eurocode 8, 'Design provisions for earthquake resistance of structures-Part 1-3: General rules - Specific rules for various materials and elements, European Prestandard ENV 1998-1-3', 1998, *European Committee for Standardisation TC 250*, Brussels.
30. Fardis, M.N., 'Current trends in earthquake resistant analysis and design of reinforced concrete structures', 1995, *European Seismic Design Practice, 5th SEDEC Conference (ed. Elnashai, A.S.)*, 375

31. Foster, S.J., 'On behaviour of high strength concrete columns: cover spalling, steel fibers, and ductility', 2001, *ACI Structural Journal*, 98(4), 583
32. Foster, S.J., Attard, M.M., 'Strength and ductility of fiber-reinforced high-strength concrete columns', 2001, *ASCE Journal Structural Div.*, 127(1), 28
33. Fu, H.C., Erki, M.A., Seckin, M., 'Review of effects of loading rate on concrete in compression', 1991, *ASCE Journal Structural Div.,* 17(12), 3645
34. Furukawa, J., Kouji, O, 'Effect of yield strength of longitudinal reinforcing bar on ductility of R/C beam yield hinge', 1996, *11th World Conference on Earthquake Engineering (eds. Sociedad Mexican Ingenierí),* Acapulco, Mexico, Paper No. 1197.
35. Hakuto, S., Park, R., Tanaka, H., 'Seismic load tests on interior and exterior beam-column joints with substandard reinforcing details', 2000, *ACI Structural Journal*, 97(1), 11
36. Jansson, M., 'Betonbalker armenade med tradballer ar 5 millimetres staltrad, 1994, *BELAB*, Gottenburg.
37. Kent, D.C., Park, R., 'Flexural members with confined concrete', 1971, *ASCE Journal Structural Div.*, 97(ST7), 1969
38. Légeron, F., Paultre, P., 'Behaviour of high-strength concrete columns under cyclic flexure and constant axial load', 2000, *ACI Structural Journal*, 97(4), 591
39. Levins, C.T., 'Spherical reinforced in short concrete columns, *MSc Disstn.*, 1994, Trinity College Dublin.
40. Lin, C.H, Lee, F.S., 'Ductility of high-performance concrete beams with high-strength lateral reinforcement', 2001, *ACI Structural Journal*, 98(4), 600
41. Mander, J.B., Priestley, M.J.N., Park, K., 'Seismic design of bridge piers', 1984, *Research Report No. 84-2*, University of Canterbury, New Zealand
42. Mander, J.B., Priestley, M.J.N., Park, R., 'Theoretical stress-strain model for confined concrete', 1988, *ASCE Journal Structural Div.*, 114(8), 1804
43. Mander, J.B., Priestley, M.J.N., Park, R., 'Observed stress-strain behaviour of confined concrete', 1988, *ASCE Journal Structural Div.*, 114(8), 1827
44. Mendis, P.A., Kovacic, D., Setunge, S., 'Basis for the design of lateral reinforcement for high-strength concrete columns', 2000, *Structural and Engineering Mechanics*, 9(6), 589
45. Mo, Y.L., Wang, S.J., 'Behaviour of reinforced concrete columns', 2000, *Magazine of Concrete Research*, 52(6), 419
46. Mau, S.T., Holland, J., Hong, L., 'Small-column compression tests on concrete confined by WWF', 1998, *ASCE Journal Structural Div.*, 124(3), 252
47. Moehle, J.P., Cavanagh, T., 'Confinement effectiveness of cross ties in RC', 1985, *ASCE Journal Structural Div.*, 111(10), 2105
48. Neville, A.M., 'Properties of Concrete', 1995, *Longman Group Limited*

49. NZ S 3101: Part 1, 'Code of practice for the design of concrete structures', 1995, *Standards Association of New Zealand*, Wellington, New Zealand
50. O'Connor, T., 'Spherical reinforcement in short concrete columns, 1996, *BAI Disstn.*, Trinity College Dublin.
51. O'Brien, E.J., Dixon A.S., 'Reinforced and prestressed concrete design. The complete process', 1995, *Longman Scientific and Technical*
52. O'Rourke, J., 'Spherical reinforcement in short concrete columns, 1995, *BAI Disstn.*, Trinity College Dublin.
53. Park, R., Paulay, T., "Reinforced Concrete Structures", 1975, *John Wiley & Sons*
54. Park, R., Priestley, M.J., Gill, W.D., 'Ductility of square-confined concrete columns', 1982, *ASCE Journal Structural Div.*, 108(ST4), 929
55. Park, R., 'Capacity Design of Ductile RC Building Structures for earthquake resistance', 1992, *The Structural Engineer*, 70(16), 279
56. Paultre, P., Légeron, F., Mongeau, D., 'Influence of concrete strength and transverse reinforcement yield strength on behaviour of high-strength concrete columns', 2001, *ACI Structural Journal*, 98(4), 490
57. Razvi, R., Saatcioglu, M., 'Confinement of reinforced concrete columns with welded wire fabric', 1989, *ACI Structural Journal*, 86(5), 615
58. Razvi, R., Saatcioglu, M., 'Confinement of high-strength concrete columns for seismic applications', 1996, *11th World Conference on Earthquake Engineering (eds. Sociedad Mexican Ingenierí),* Acapulco, Mexico, Paper No. 1855.
59. Richart, F.B., A. Brandtzaeg, Brown, R.L., 'A study of the failure of concrete under combined compressive stress', 1928, *Engineering Research Station*, University of Illinois, Bulletin No. 185
60. Richart, F.B., A. Brandtzaeg, Brown, R.L., 'The failure of plain and spirally reinforced concrete in compression', 1929, *Engineering Research Station*, Univ. of Illinois, Bulletin No. 190
61. Ryan, C.A., West, R.P., Broderick, B.M., 'Wireballs-their genesis and future', 2001, *Colloquium on Concrete Research in Ireland*, National University of Ireland, Galway, 25
62. Ryan, C.A., Broderick, B.M., West, R.P., 'Performance of wireball reinforced concrete under seismic loading conditions', *CONSEC'01 3rd International Conference on Concrete under Severe Conditions: Environment & Loading*, Vanvcouver, 707
63. Ryan, C.A., Broderick, B.M., West, R.P., 'Confinement effects in RC members employing wireball reinforcement', 2001, *Proceedings of the 12th European Conference in Earthquake Engineering*, Paper No. 067 (under review)
64. Saaticioglu, M. Razvi, S.R., 'Strength and Ductility of Confined Concrete', 1992, *ASCE Journal Structural Div.*, 118(6), 1591

65. Samra, R.M., 'Ductility analysis of confined columns', 1991, *ASCE Journal Structural Div.*, 116(11), 3148
66. Scott, R.H., 'The effects of detailing on RC beam/column connection behaviour', 1992, *The Structural Engineer*, 70(18), 318
67. Sheikh, S.A.,Uzumeri, J.M. 'Strength and ductility of tied concrete columns', 1980 , *ASCE Journal Structural Div.*, 106(ST5), 1079
68. Sheikh, S.A., Toklucu, M., 'Reinforced concrete columns confined by circular hoops', 1993, *ACI Structural Journal*, 90(5), 542
69. Sheikh, S.A., Shah, D.V., Khoury, S.S., 'Confinement of high strength concrete columns', 1994, *ACI Structural Journal*, 91(1), 100
70. Teychenne, D.C, 'Design of Normal Concrete Mixes', 1988, *Building Research Establishment*, Department of the Environment, U.K.
71. Thomson, A. W., 'Seismic Resistance of Flush End-Plate Joints', 2001, *PhD Thesis*, Trinity College Dublin
72. Uniform Building Code, 1982, *International Conference of Building Officials*, Whittier, California, 1982, 780
73. Watson, S., Park, R., 'Simulated seismic load tests on reinforced concrete columns', 1994, *ASCE Journal Structural Engineering,* 120(6), 1825
74. Whelan, L., 'Quasi-static loading of spherically reinforced concrete columns', 1988, *BAI Disstn.*, Trinity College Dublin.
75. West, R.P., Levins, C.T., 'Spherical "Wireball" reinforcement in columns', 1997, *Proceedings 4th International Congress Structural Engineering Analysis and Modelling,* Ghana, 102-114.
76. Yong, Y., Nour, M.G., Nawy, E.G., 'Behaviour of laterally confined high-strength concrete under axial loads', 1988, *ASCE Journal Structural Div.*, 114(2), 332
77. Zahn, F., Park, R., Priestley, M.J.N., 'Design of reinforced concrete bridge columns for strength and ductility', 1986, *University of Canterbury,* Christchurch, New Zealand, Research Report 86-7

APPENDIX A

TEST SERIES 6: STEEL STRAINS TO YIELD

Figures A.2 to A.10 present steel load-strain curves for the specimens to either the positive or negative peak displacement of cycle 5a, where the specimens yielded. The strain gauges are identified by a number (1, 2,3 or 4), which is the longitudinal steel bar number the gauge was on, and a letter (A, B, C, or D) which corresponds to the level of the gauge with respect to the boundary section of the specimen. Both longitudinal steel bar numbers and levels are illustrated in Figure A.1.

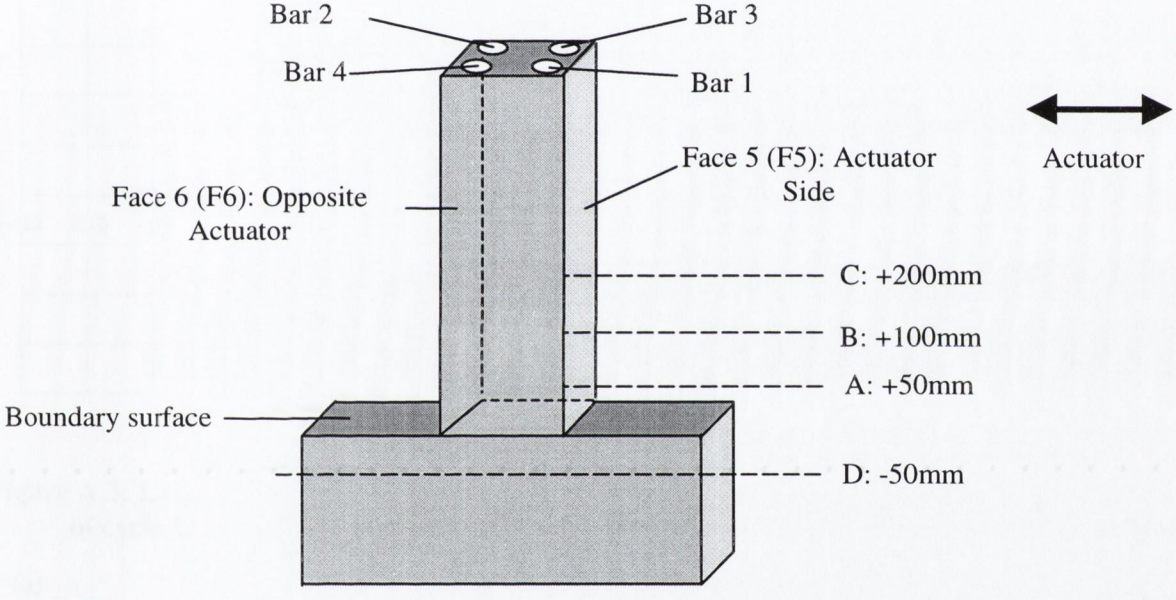

Figure A.1: Strain gauge positioning

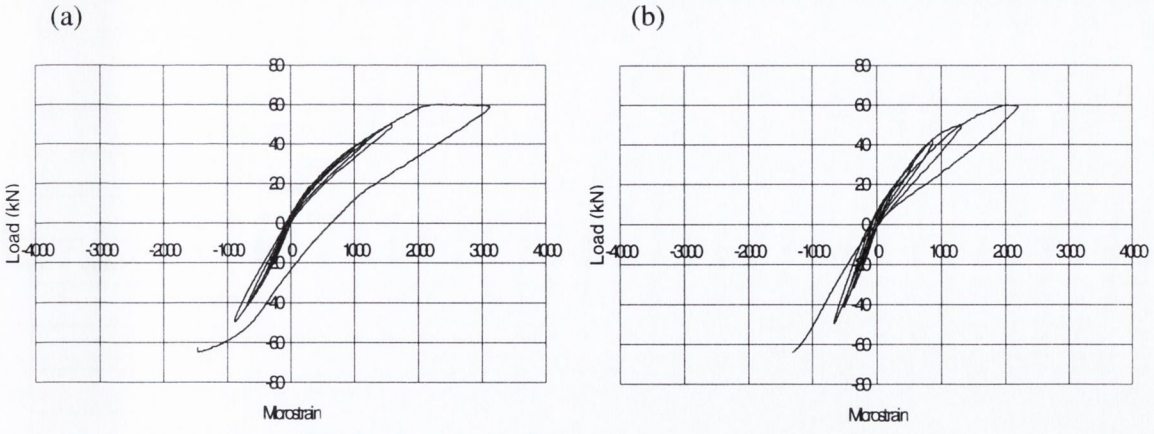

Figure A.2: Load-strain response to negative peak displacement of cycle 5a (a) C5.1(145,W,30) gauge A1, (b) C5.1(145,W,30) gauge B1

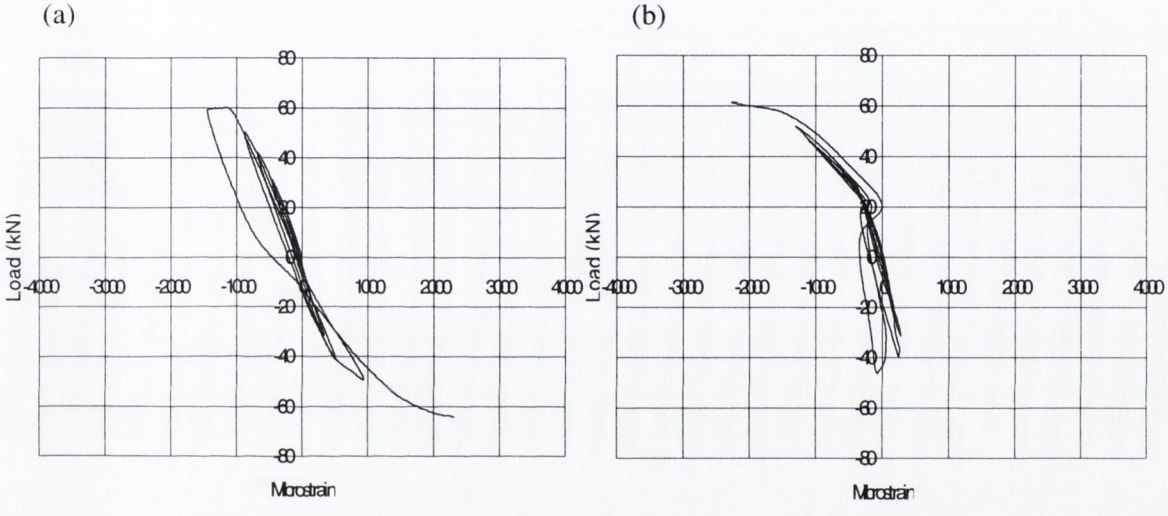

Figure A.3: Load-strain response (a) C5.1(145,W,30) gauge B2 to positive peak displacement of cycle 5a, (b) C5.2(145,30) gauge D2 to negative peak displacement of cycle 5a

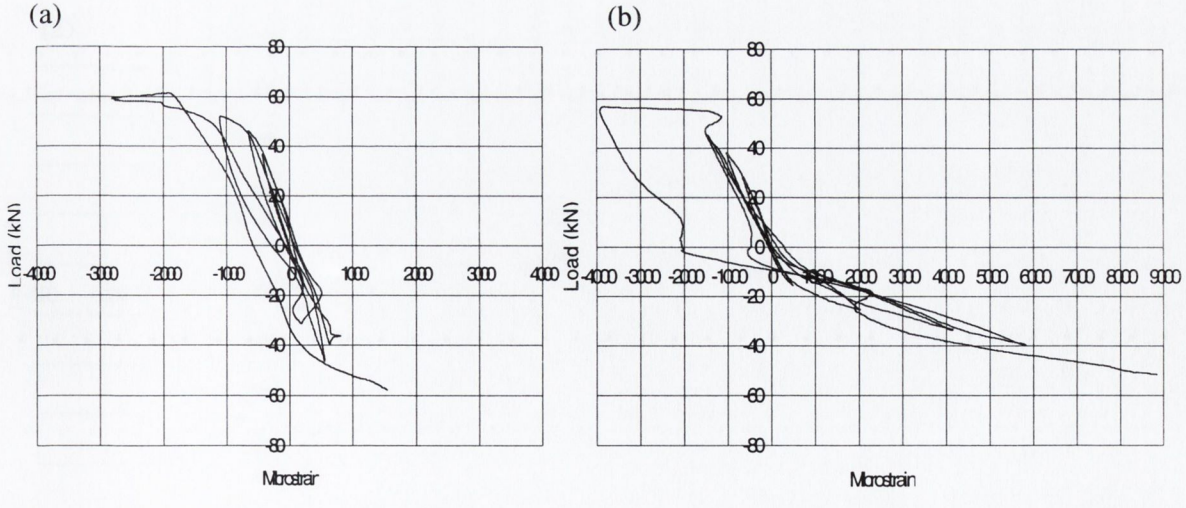

Figure A.4: Load-strain response to positive peak displacement of cycle 5a (a) C5.2(145,30) gauge A4, (b) C6.1(105,30) gauge D2

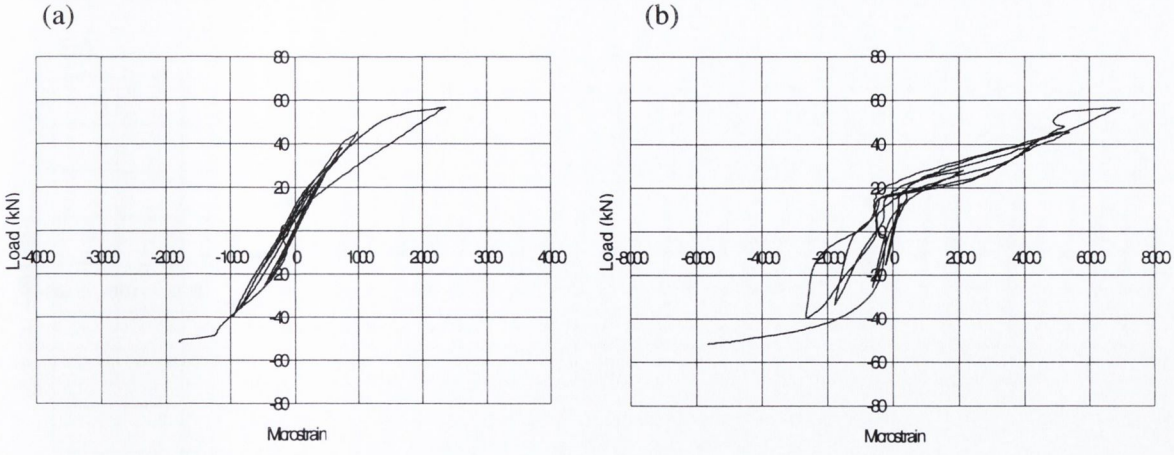

Figure A.5: Load-strain response to positive peak displacement of cycle 5a (a) C6.1(105,30) gauge A1, (b) C6.1(105,30) gauge D1

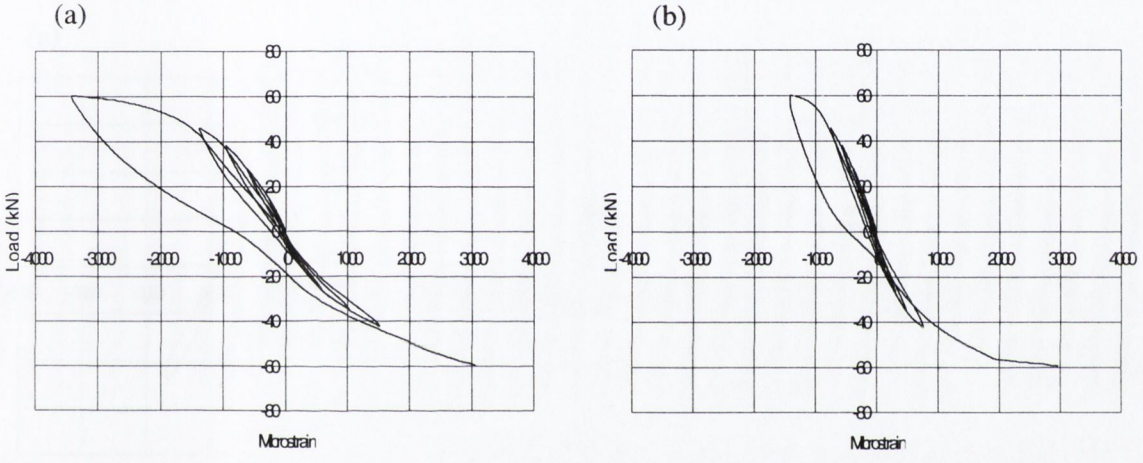

Figure A.6: Load-strain response to positive peak displacement of cycle 5a (a) C6.2(125,W,30) gauge A2, (b) C6.2(125,W,30) B2

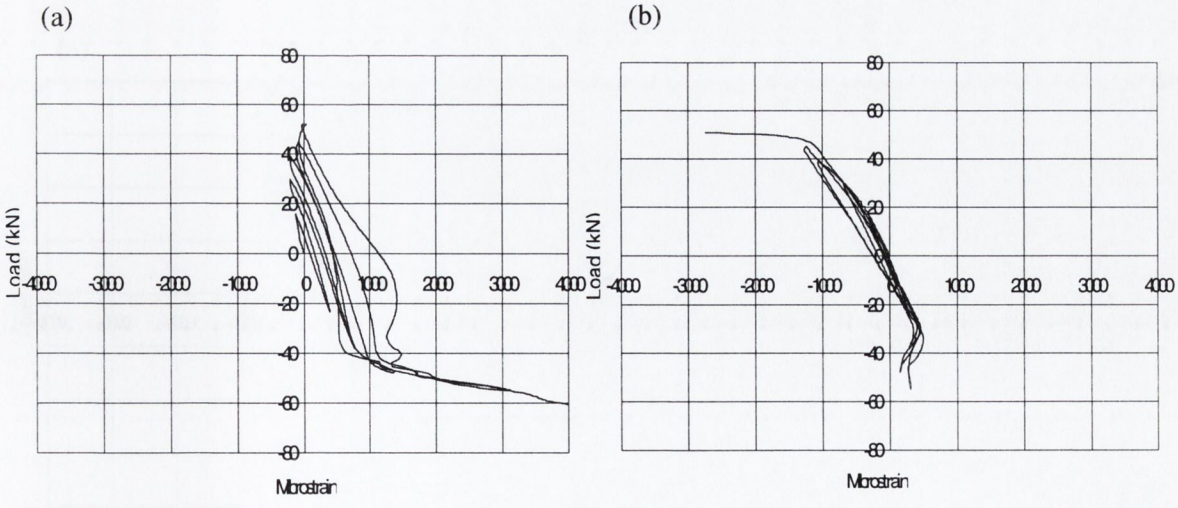

Figure A.7: Load-strain response to positive peak displacement of cycle 5a (a) C6.3(145,W,40) gauge D2, (b) C6.3(145,W,40) gauge A2

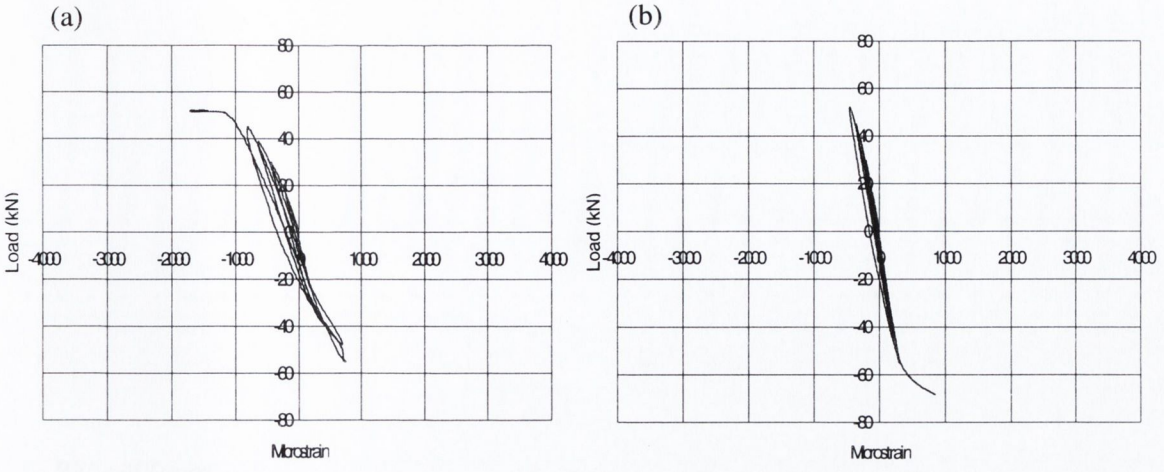

Figure A.8: Load-strain response to positive peak displacement of cycle 5a (a) C6.3(145,W,40) gauge B2, (b) C6.3(145,W,40) gauge C2

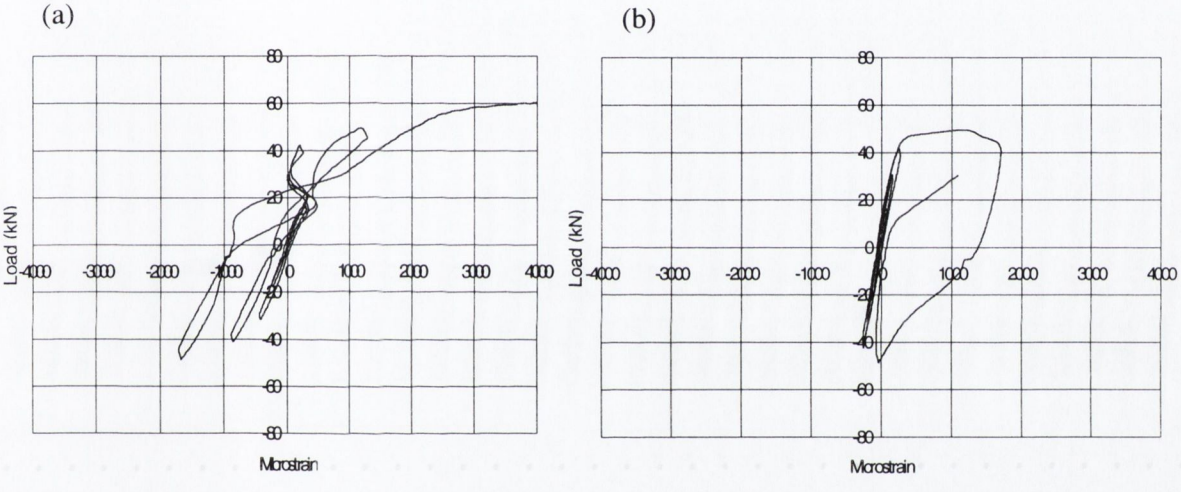

Figure A.9: Load-strain response to positive peak displacement of cycle 5a (a) C6.6(175,30) gauge D1, (b) C6.6(175,30) gauge A1

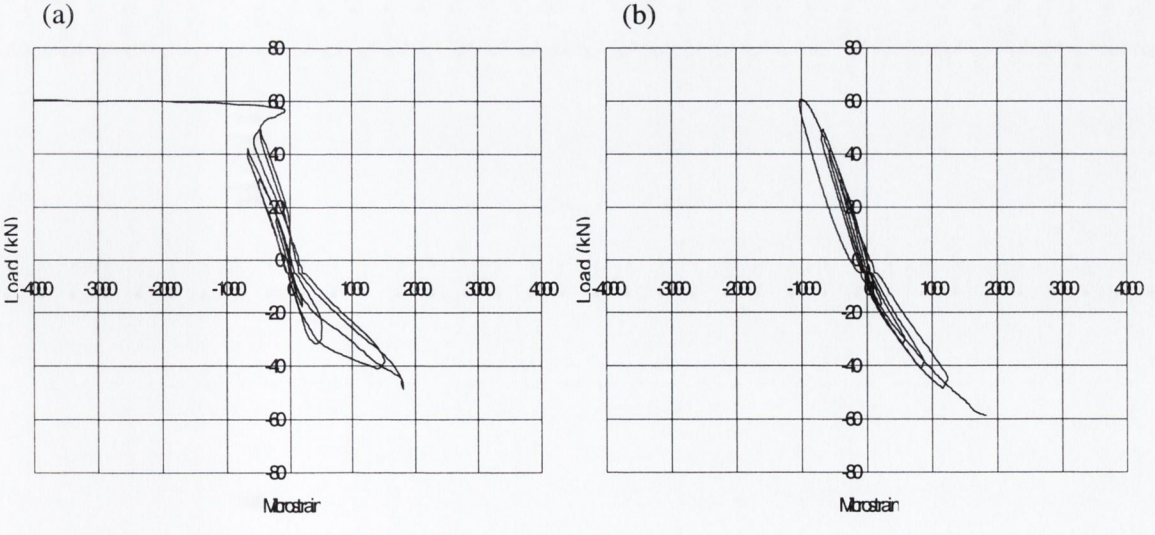

Figure A.10: Load-strain response (a) to peak negative displacement of cycle 5a C6.6(175,30) gauge D2, (b) to peak positive displacement of cycle 5a C6.6(175,30) gauge A2

APPENDIX B

TEST SERIES 6: CONCRETE STRAINS

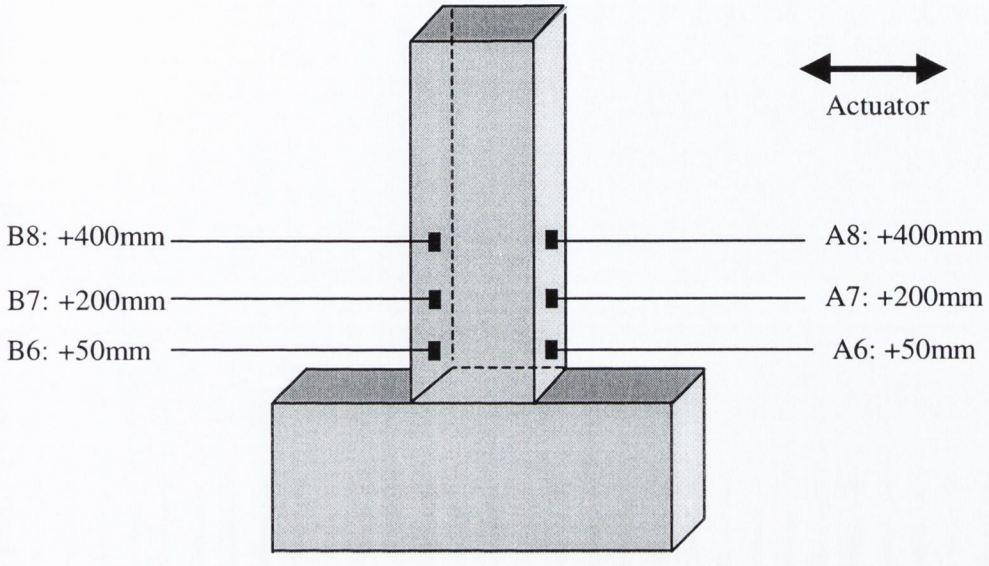

Figure B.1: Strain gauge positions on the beam-column

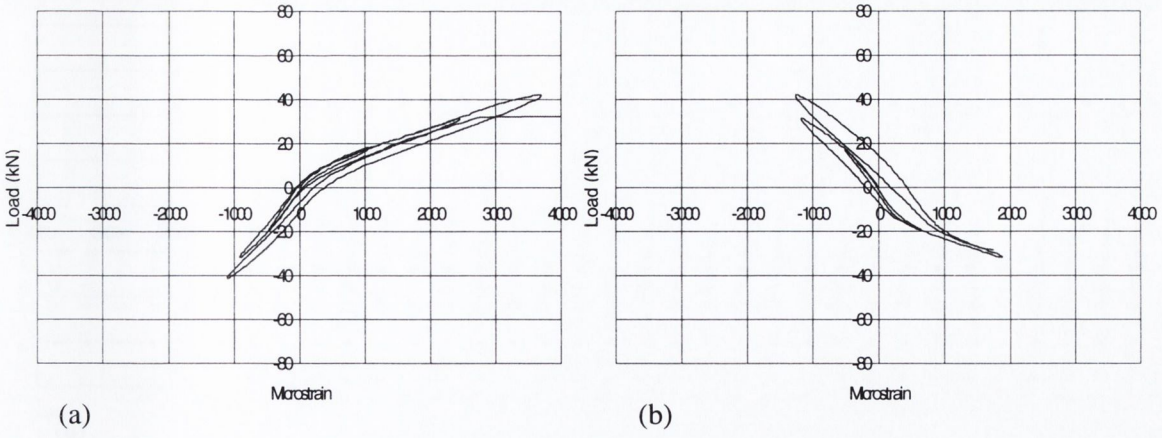

Figure B.2: Load-strain response (a) C5.1(145,W,30) gauge A6 (b) C5.1(145,W,30) gauge B6

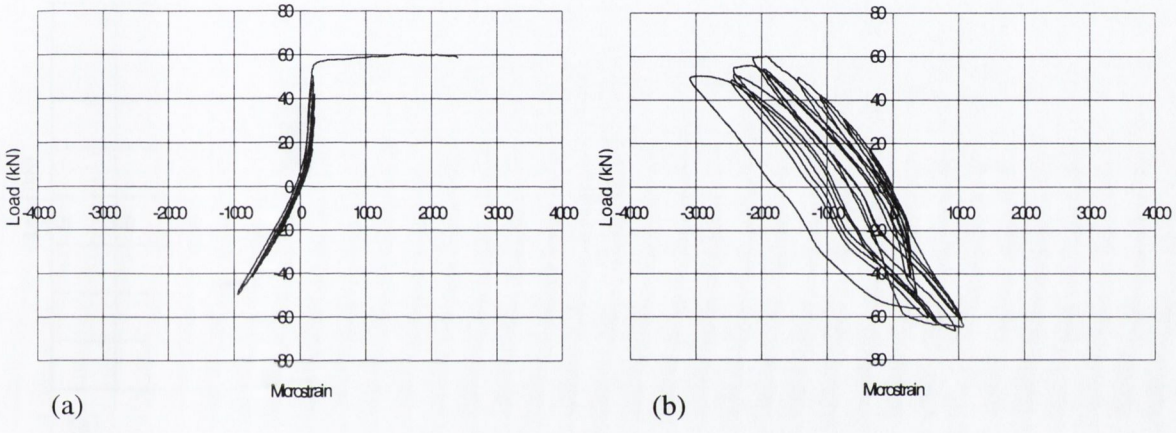

Figure B.3: Load-strain response (a) C5.1(145,W,30) gauge A7 (b) C5.1(145,W,30) gauge B7

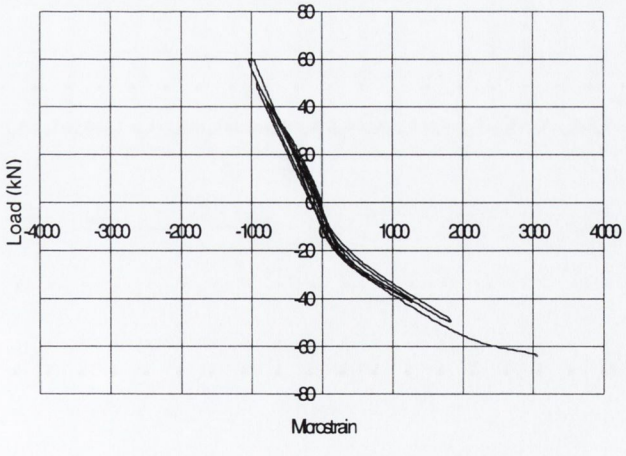

Figure B.4: Load-strain response C5.1(145,W,30) gauge B8

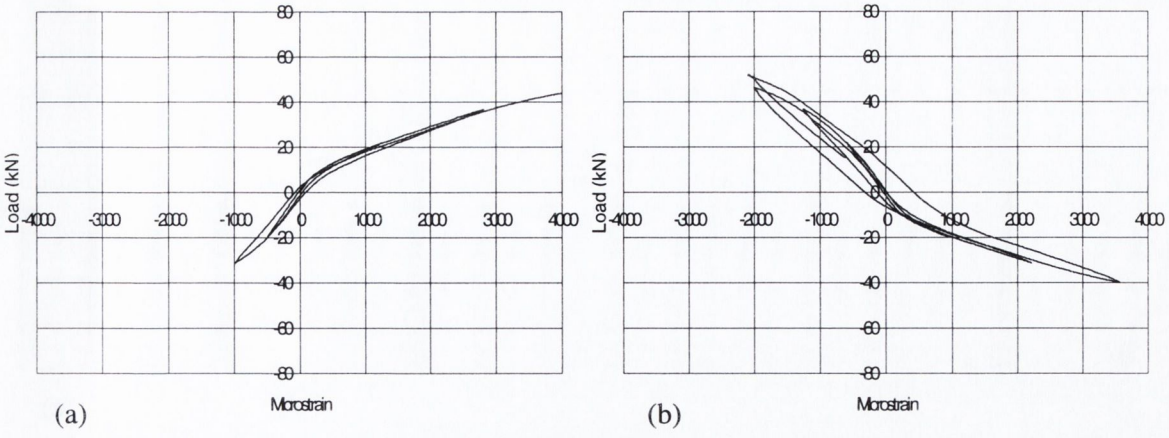

Figure B.5: Load-strain response (a) C5.2(145,30) gauge A6, (b) C5.2(145,30) gauge B6

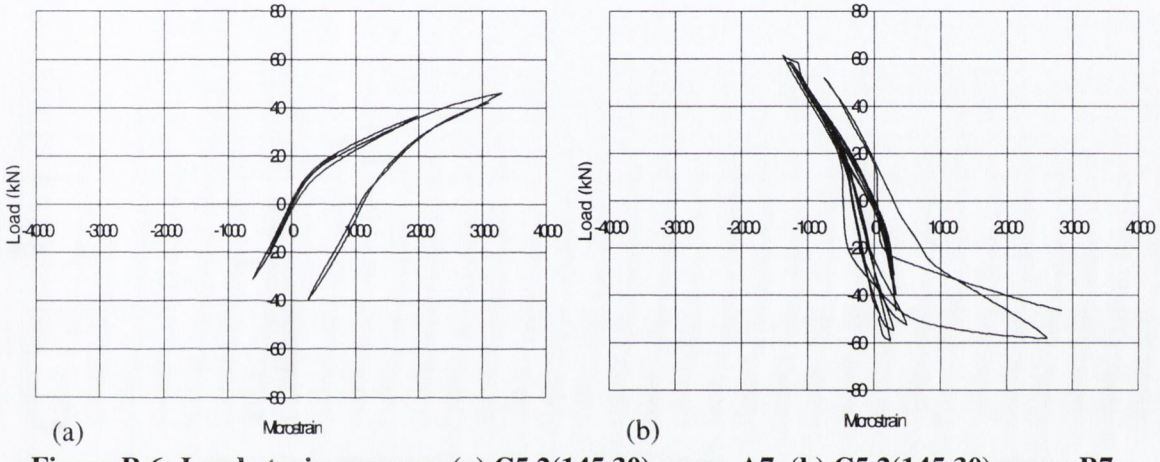

Figure B.6: Load-strain response (a) C5.2(145,30) gauge A7, (b) C5.2(145,30) gauge B7

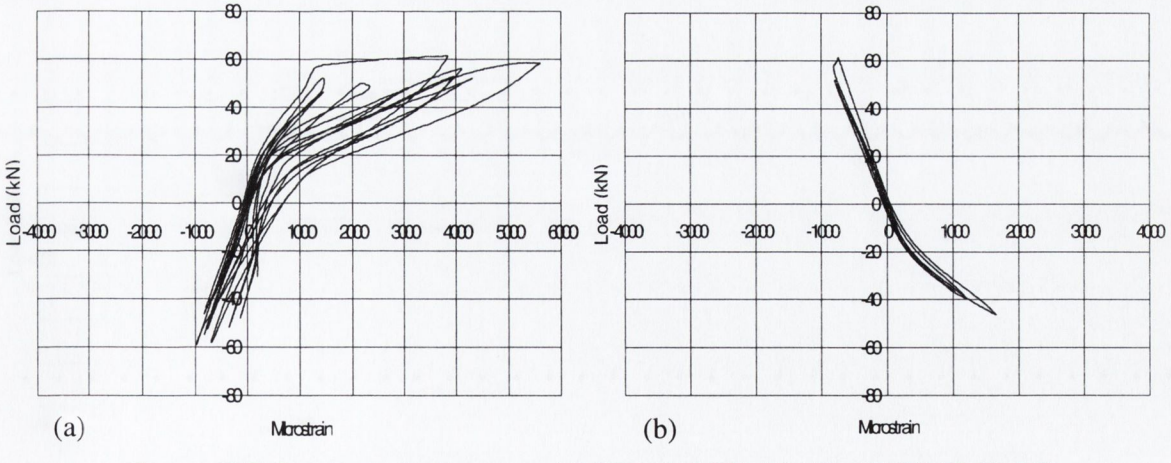

Figure B.7: Load-strain response (a) C5.2(145,30) A8, (b) C5.2(145,30) B8

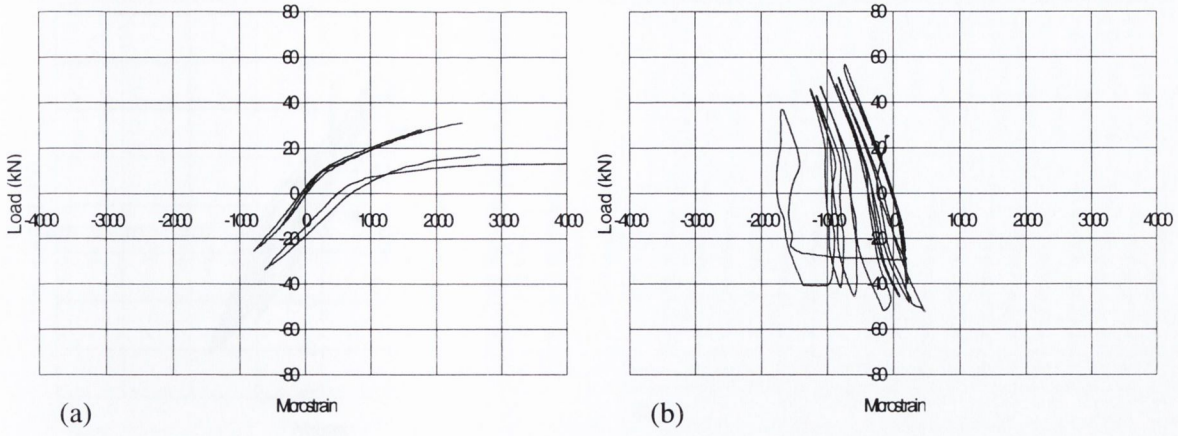

Figure B.8: Load-strain response (a) C6.1(105,30) gauge A6, (b) C6.1(105,30) gauge B6

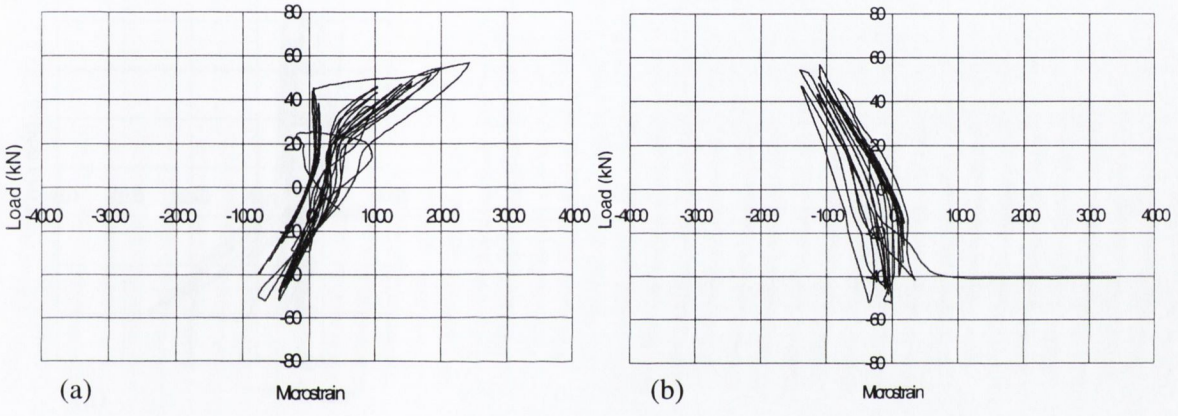

Figure B.9: Load-strain response (a) C6.1(105,30) gauge A7, (b) C6.1(105,30 gauge B7

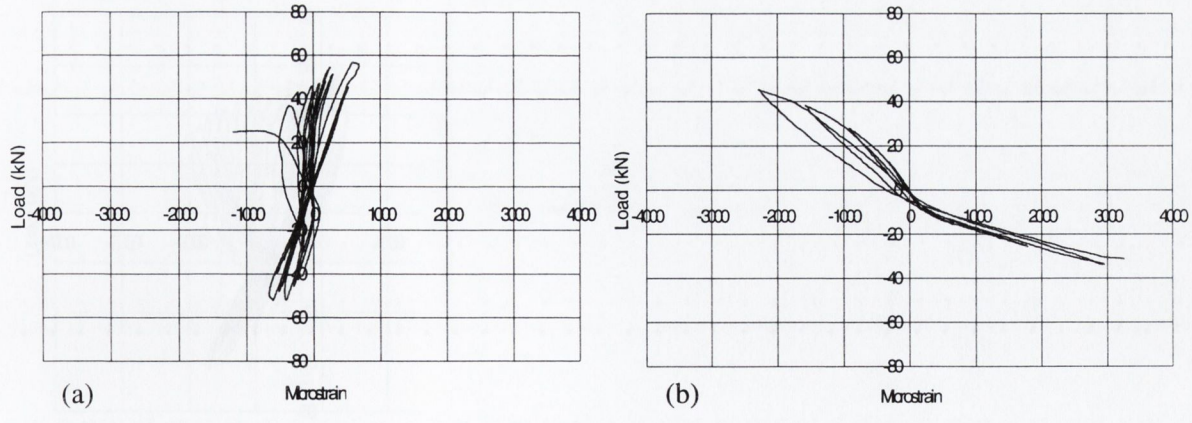

Figure B.10: Load-strain response (a) C6.1(105,30) gauge A8, (b) C6.1(105,30) gauge B8

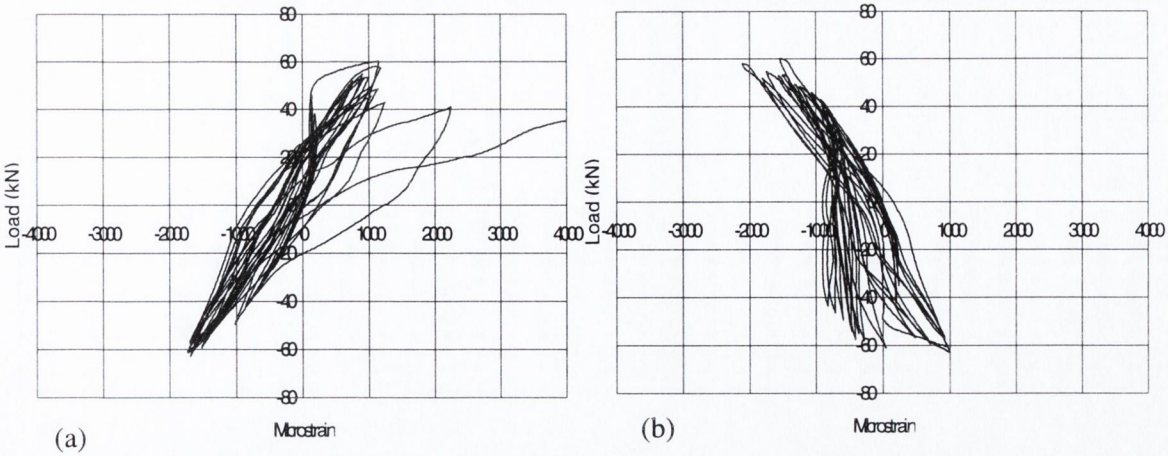

Figure B.11: Load-strain response (a)C6.2(125,W,30) gauge A6, (b) C6.2(125,W,30) gauge B6

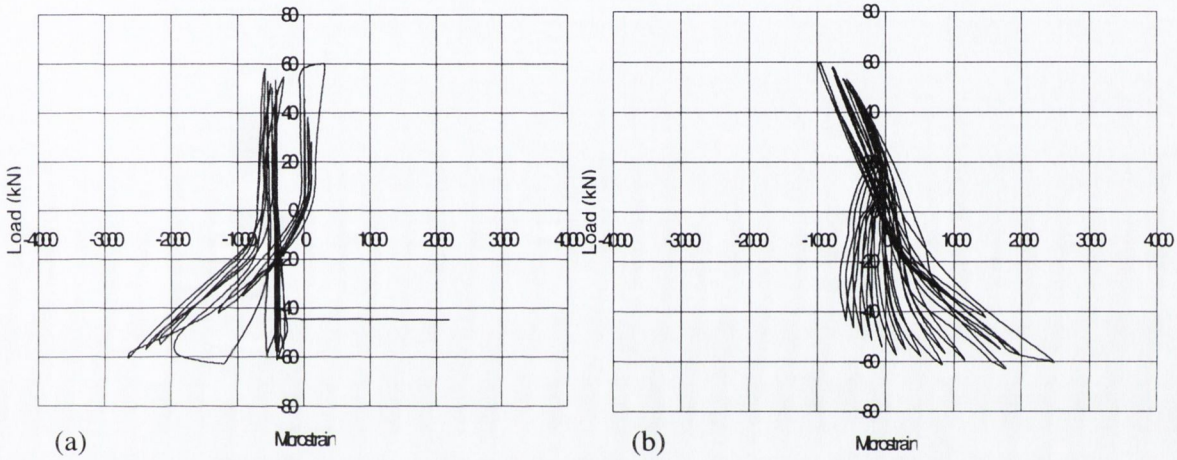

Figure B.12: Load-strain response (a) C6.2(125,W,30) gauge A7, (b) C6.2(125,W,30) gauge B7

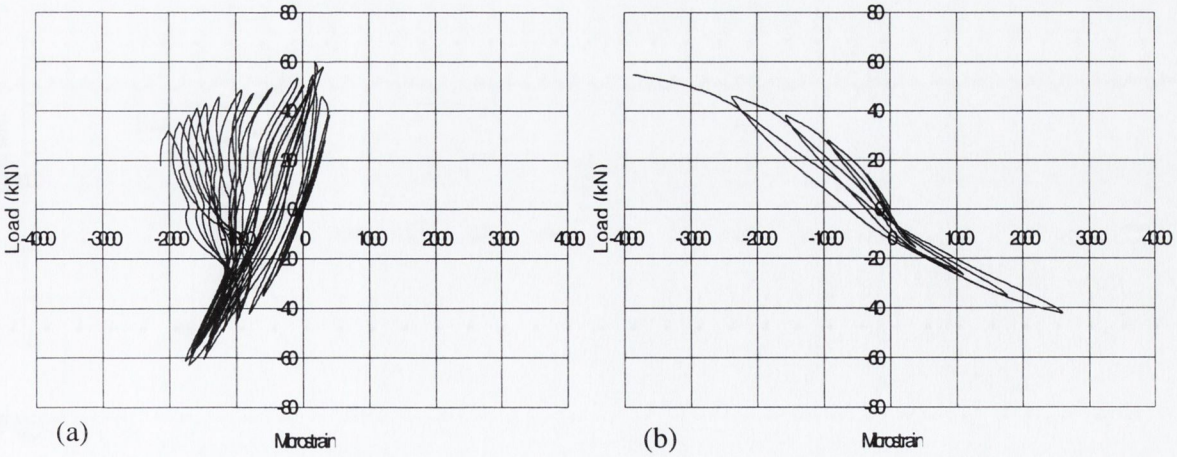

Figure B.13: Load-strain response (a) C6.2(125,W,30) gauge A8, (b)C6.2(125,W,30) gauge B8

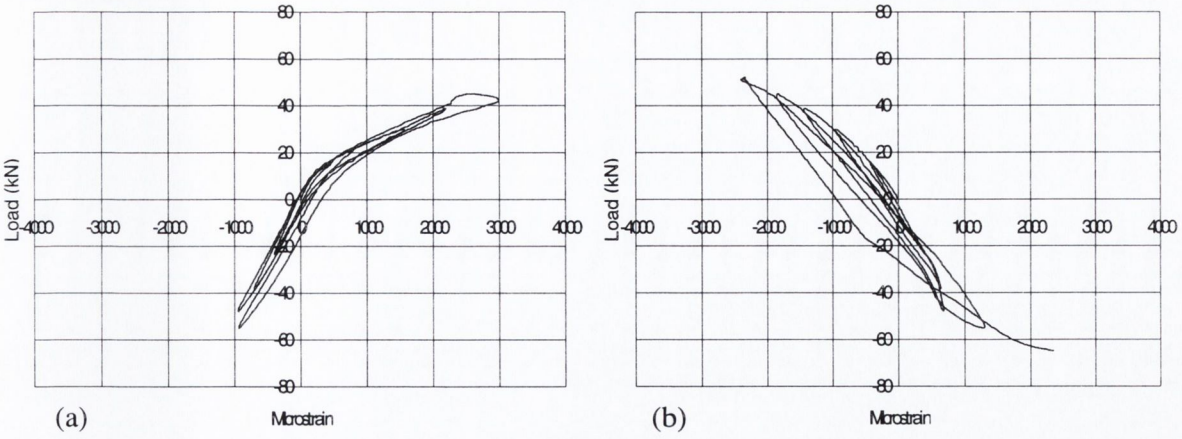

Figure B.14: Load-strain response (a)C6.3(145,W,40) gauge A6, (b) C6.3(145,W,40) gauge B6

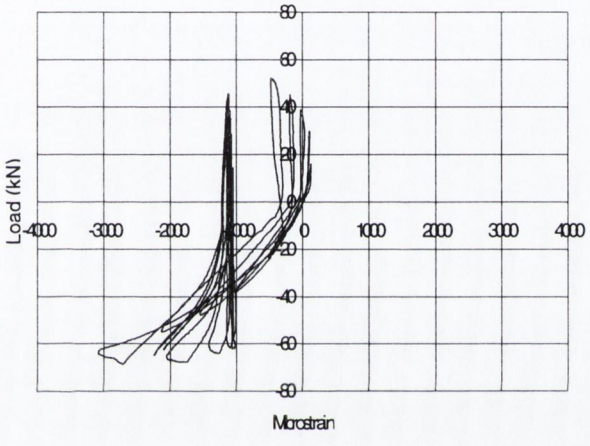

Figure B.15: Load-strain response (a) C6.3(145,W,40) gauge A7, (b) C6.3(145,W,40) gauge B8

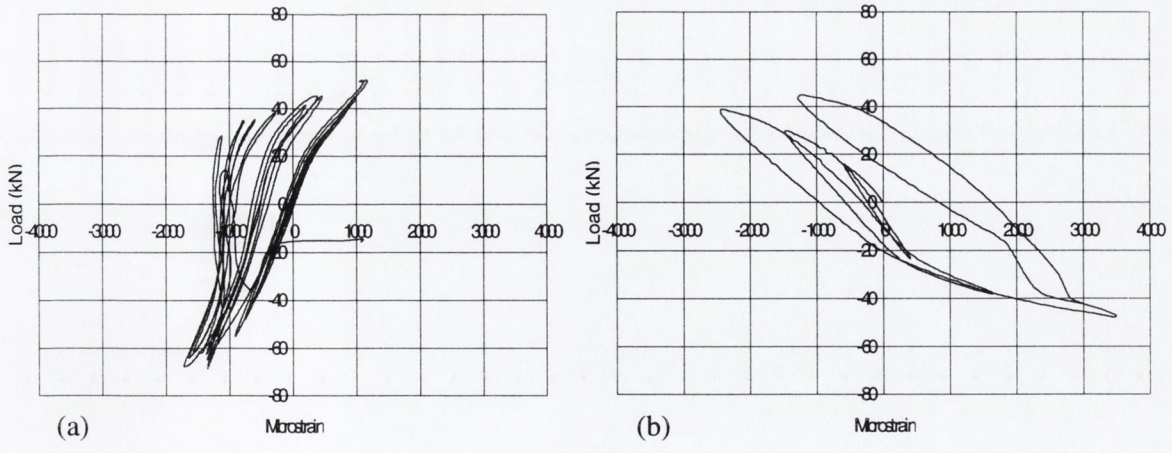

Figure B.16: Load-strain response (a)C6.3(145,W,40) gauge A8, (b) C6.3(145,W,40) gauge B8

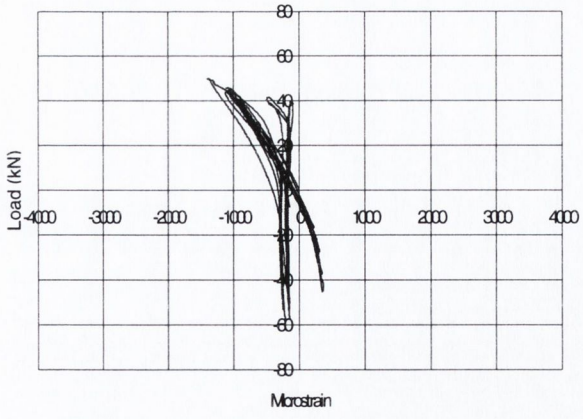

Figure B.17: Load-strain response C6.4(125,W,40) gauge B6

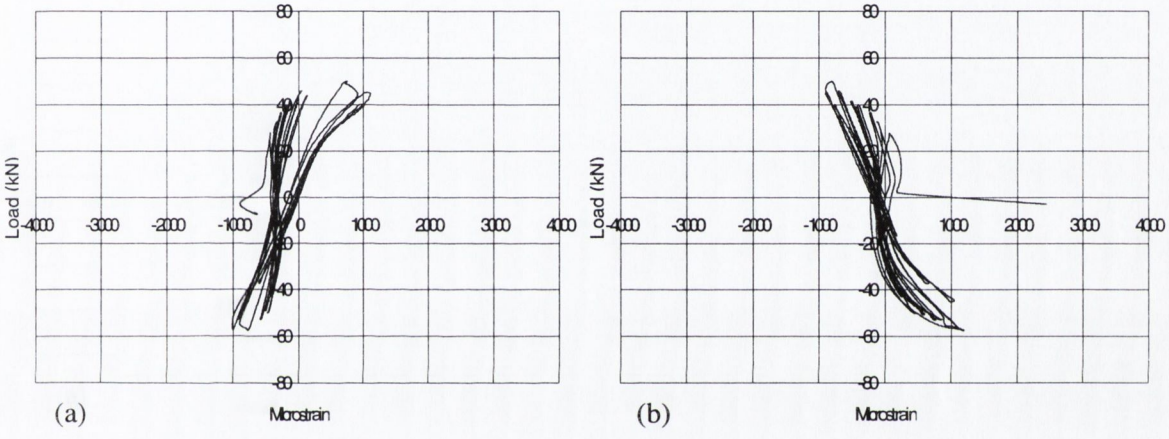

Figure B.18: Load-strain response (a)C6.4(125,W,40) gauge A7, (b) C6.4(125,W,40) gauge B7

Figure B.19: Load-strain response C6.4(125,W,40) gauge A8

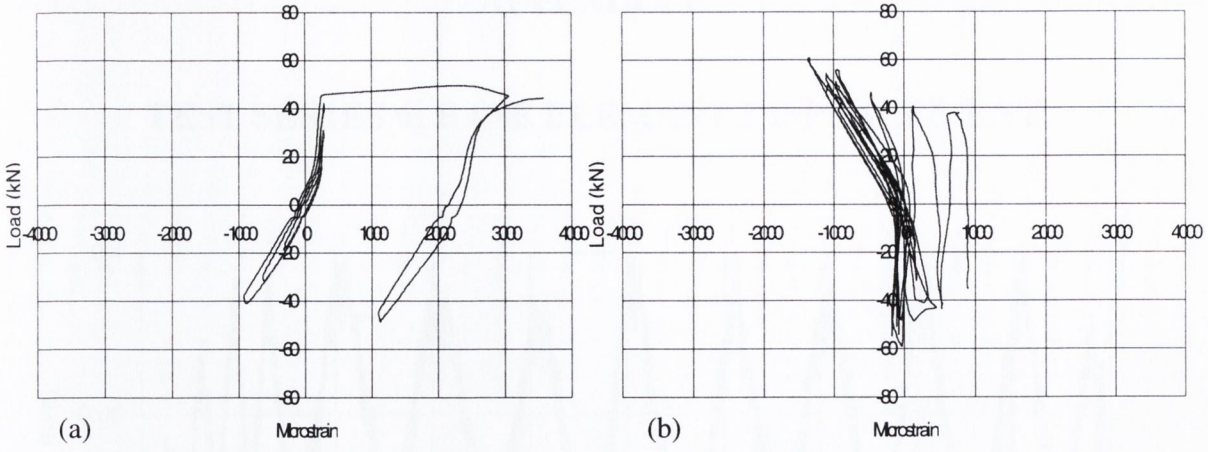

Figure B.20: Load-strain response (a) C6.6(175,30) gauge A6, (b) C6.6(175,30) gauge B6

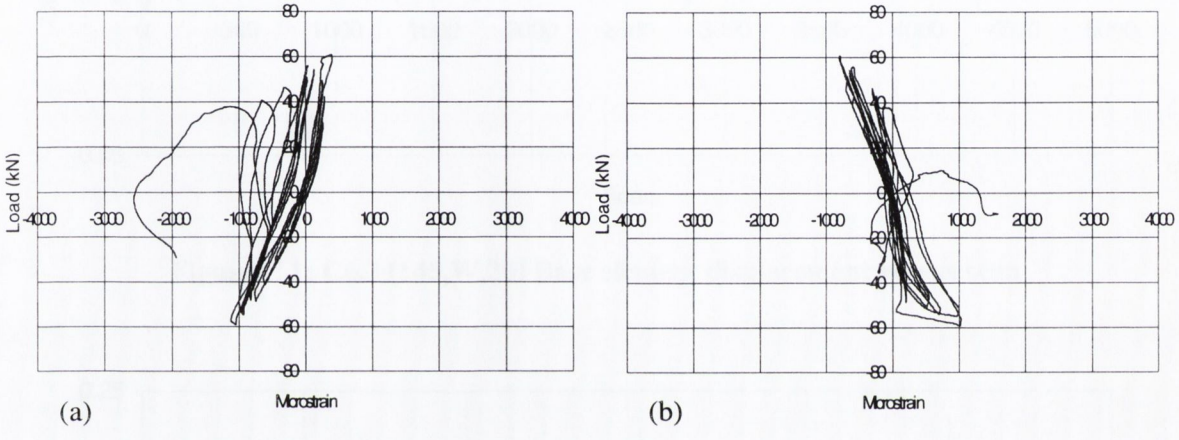

Figure B.21: Load-strain response (a)C6.6(175,30) gauge A7, (b) C6.6(175,30) gauge B7

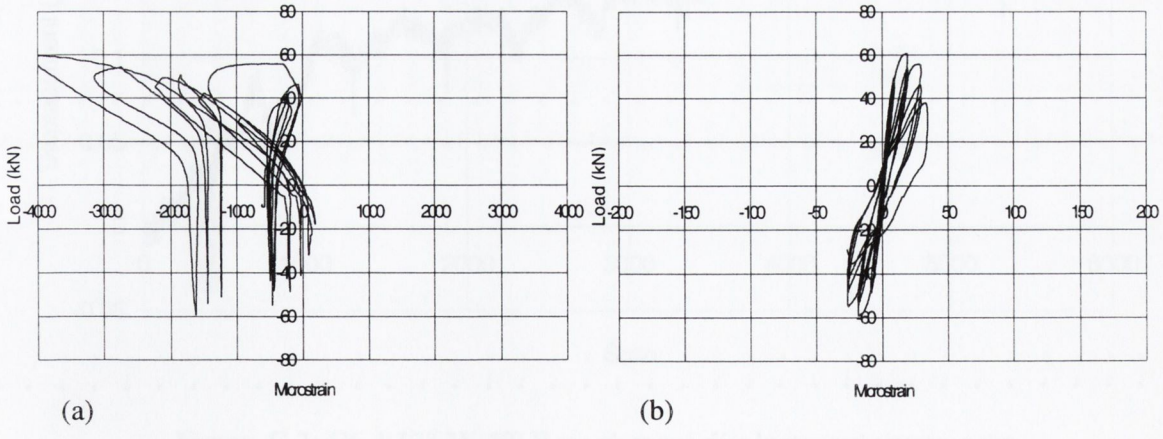

Figure B.22: Load-strain response (a) C6.6(175,30) gauge A8, (b) C6.6(175,30) gauge B8

APPENDIX C

TEST SERIES 6: BASE ELEMENT DISPLACEMENT

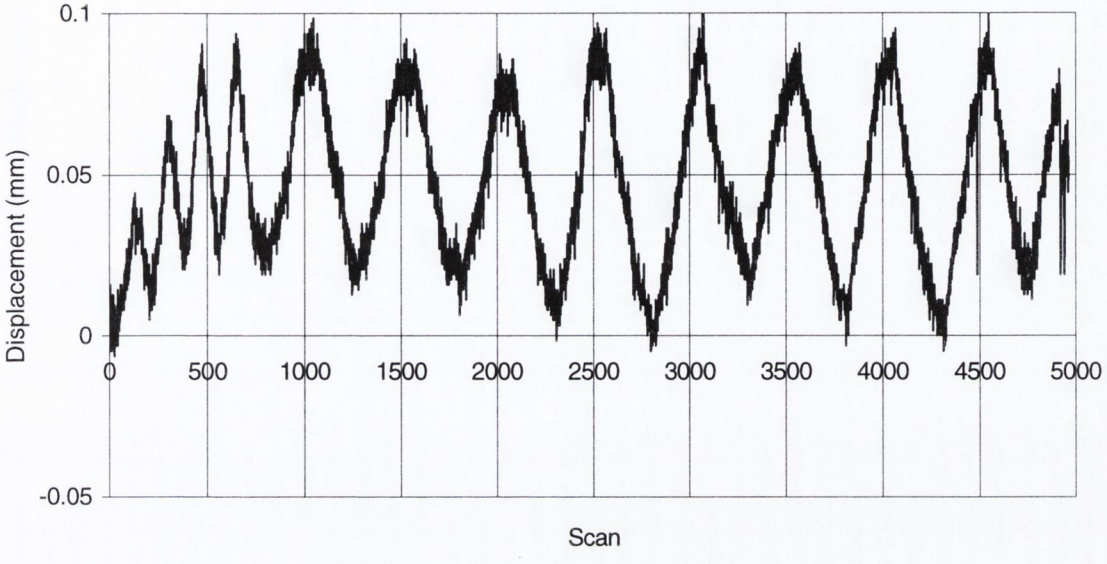

Figure C.1: C6.3 (145,W,30) Base element displacement versus scan

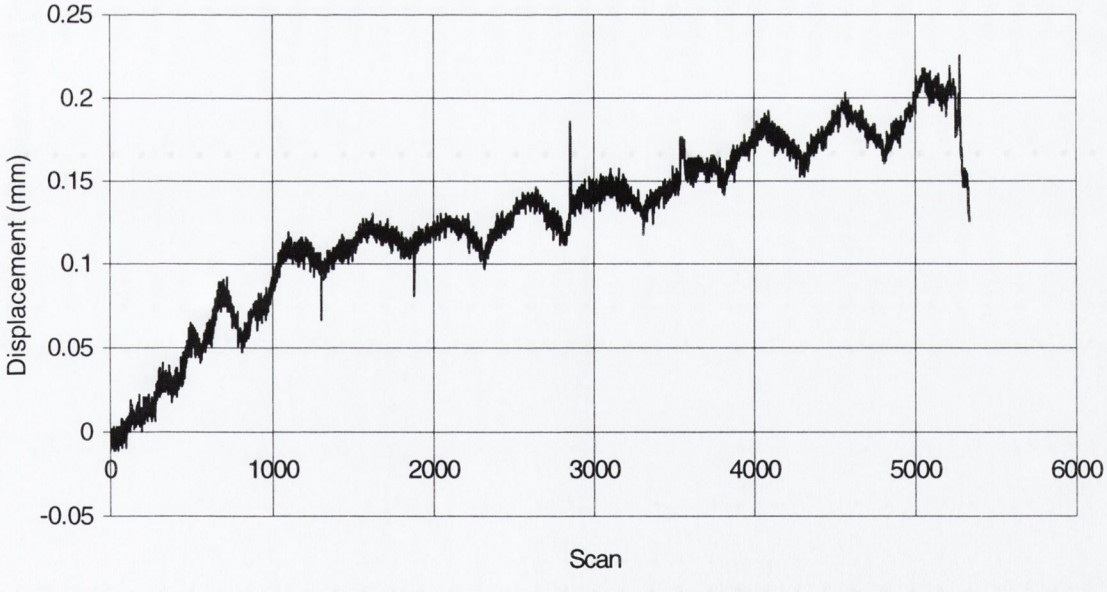

Figure C.2: C6.4(125,W,40) Base element displacement versus scan

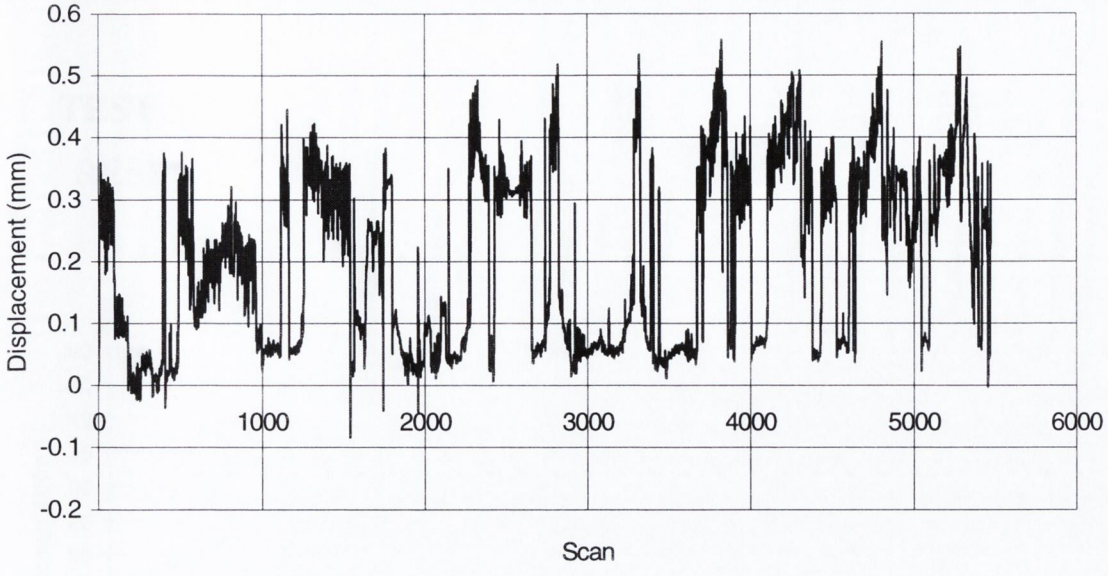

Figure C.3: C6.5(200,W,30) Base element displacement versus scan

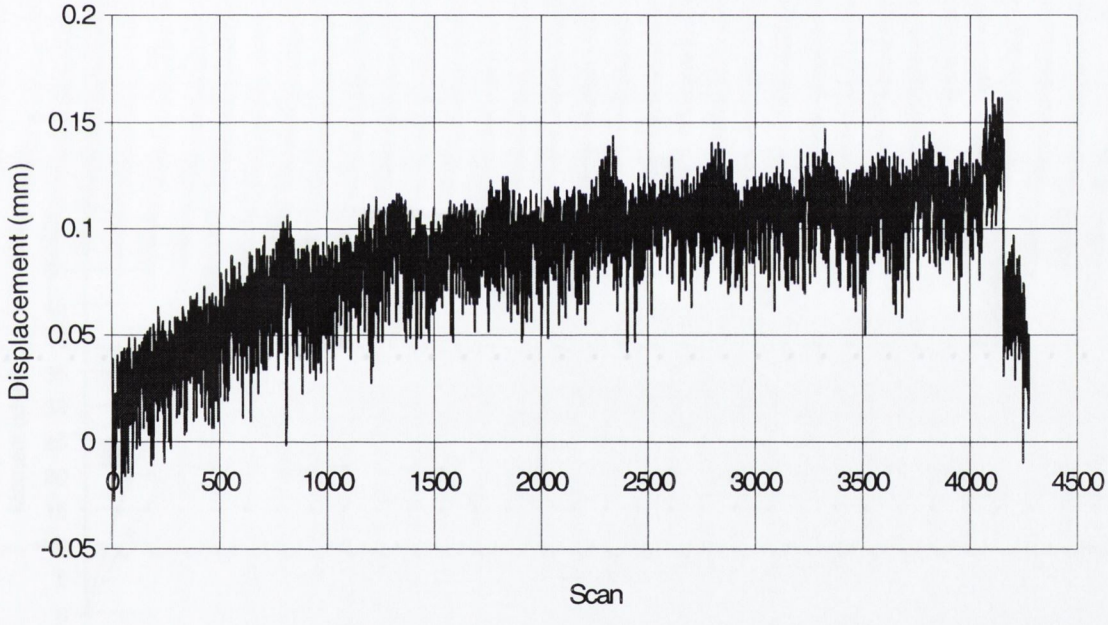

Figure C.4: C6.6(175,30) Base element displacement versus scan

APPENDIX D

TEST SERIES 6: PREDICTED MOMENT-DISPLACEMENT RESPONSE WITHOUT 7.5 AND 10mm DISPLACEMENTS

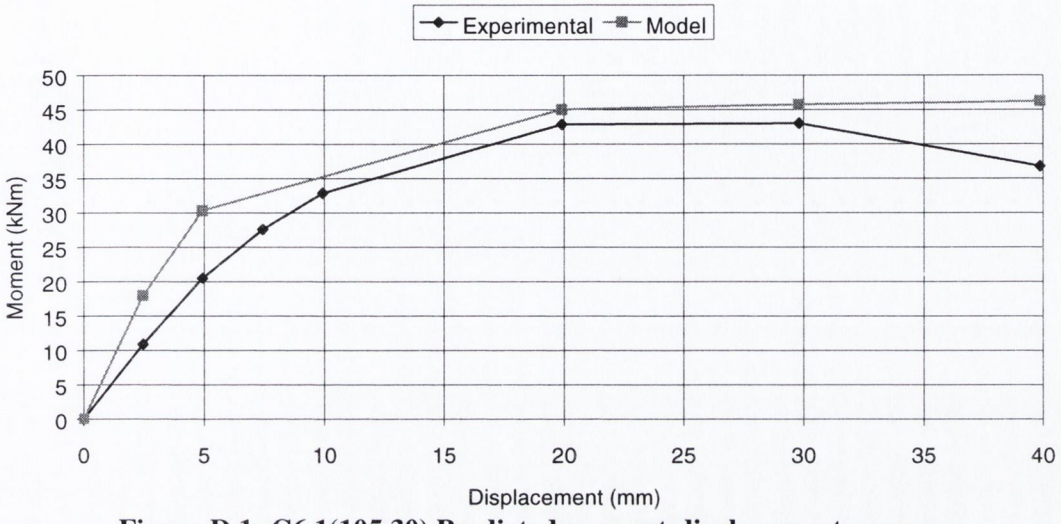

Figure D.1: C6.1(105,30) Predicted moment-displacement response

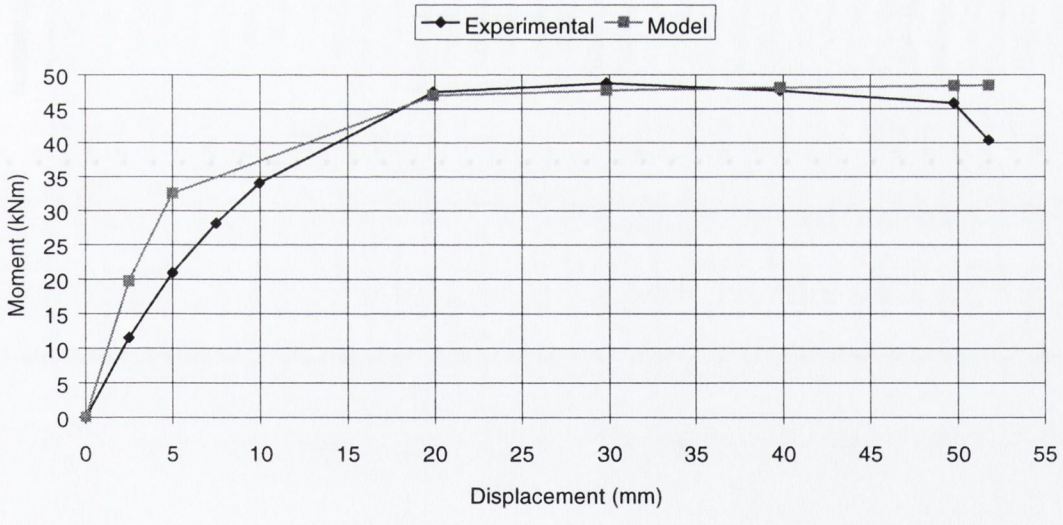

Figure D.2: C6.2(125,W,30) Predicted moment-displacement response

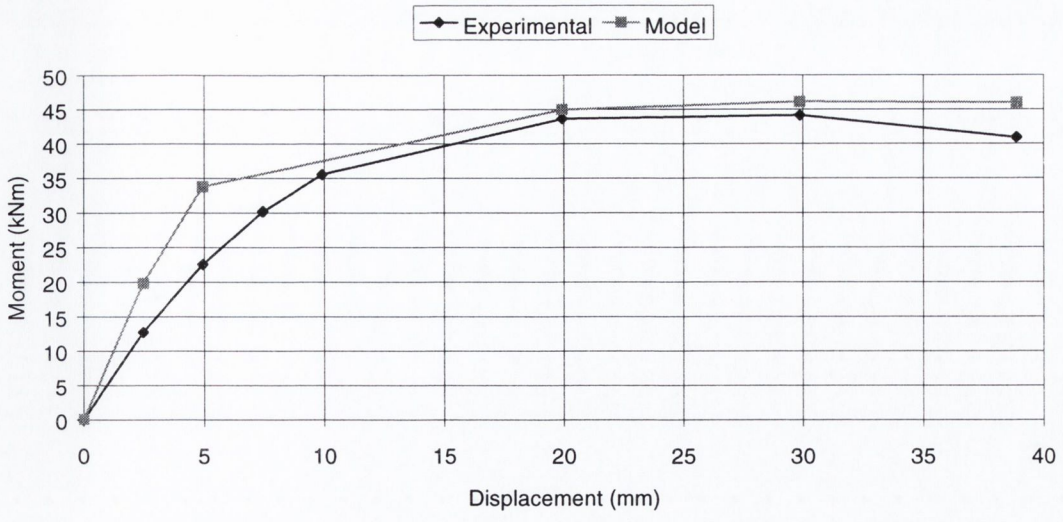

Figure D.3: C6.4(125,W,40) Predicted moment-displacement response

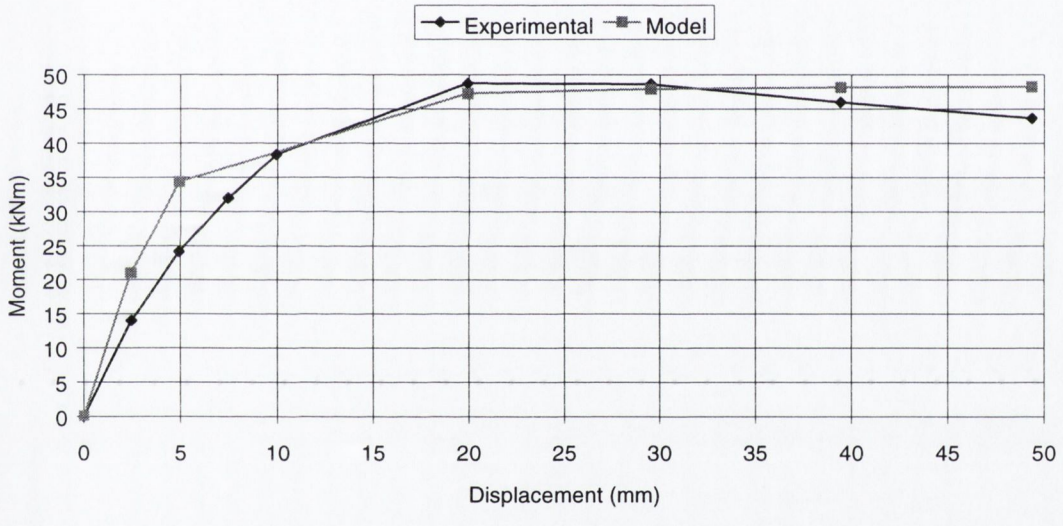

Figure D.4: C5.1(145,W,30) Predicted moment-displacement response

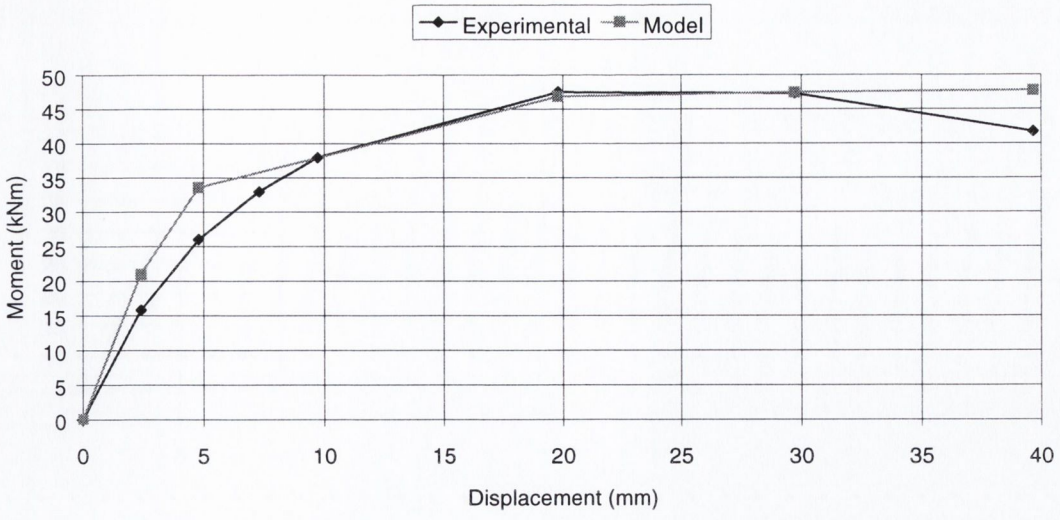

Figure D.5: C5.2(145,30) Predicted moment-displacement response

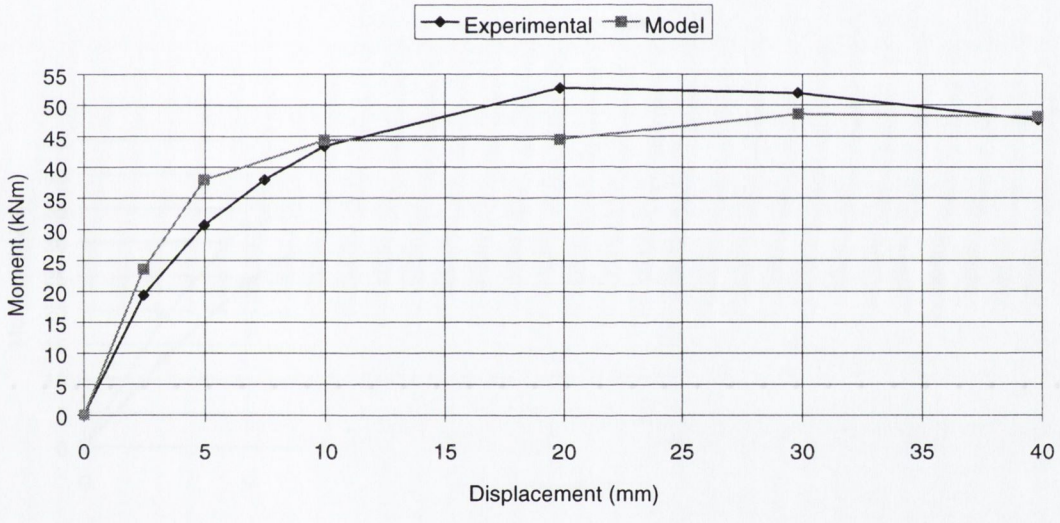

Figure D.6: C6.3(145,W,40) Predicted moment-displacement response, in this case only the 7.5mm point is excluded from the predicted response

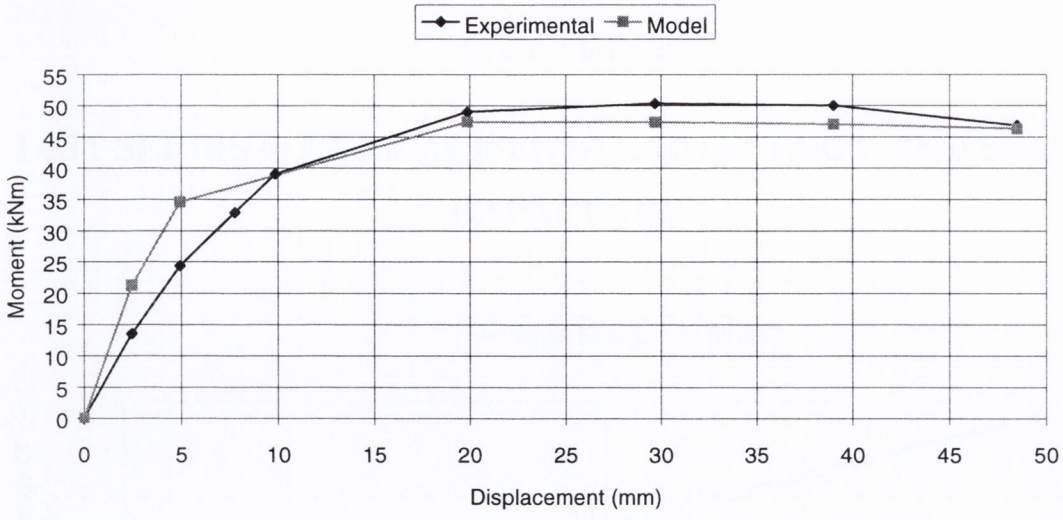

Figure D.7: C6.5(200,W,30) Predicted moment-displacement response

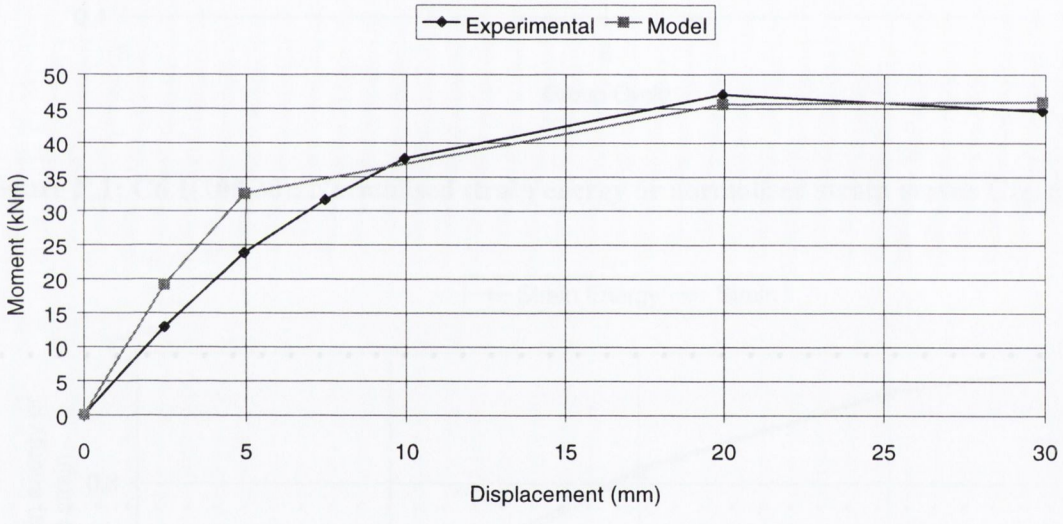

Figure D.8. C6.6(175,30) Predicted moment-displacement response

APPENDIX E

TEST SERIES 6: NORMALISED STRAIN ENERGY AND STRAIN CAPACITIES

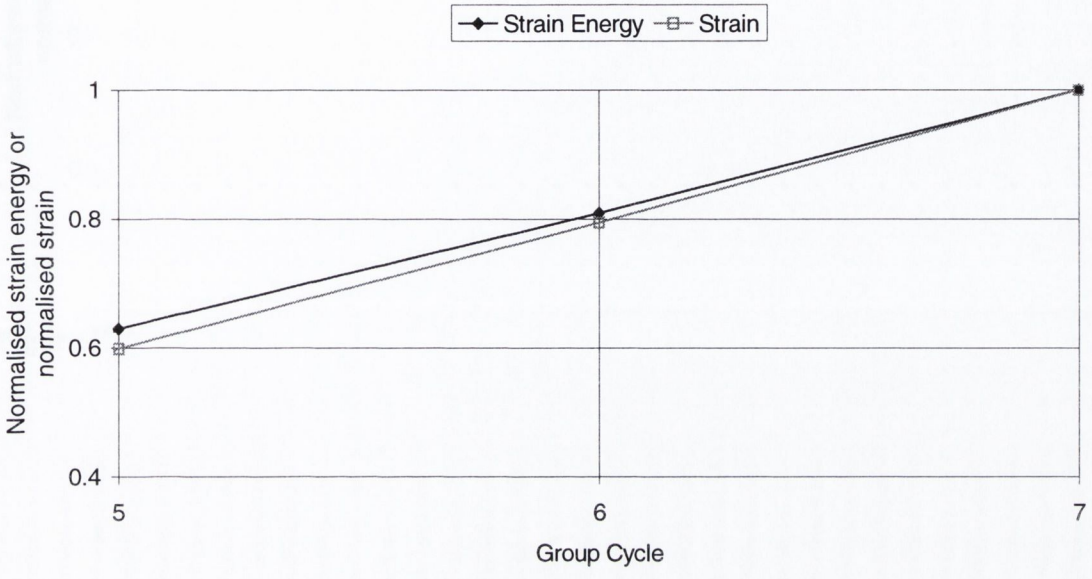

Figure E.1: C6.1(105,30): Normalised strain energy or normalised strain versus Group Cycle

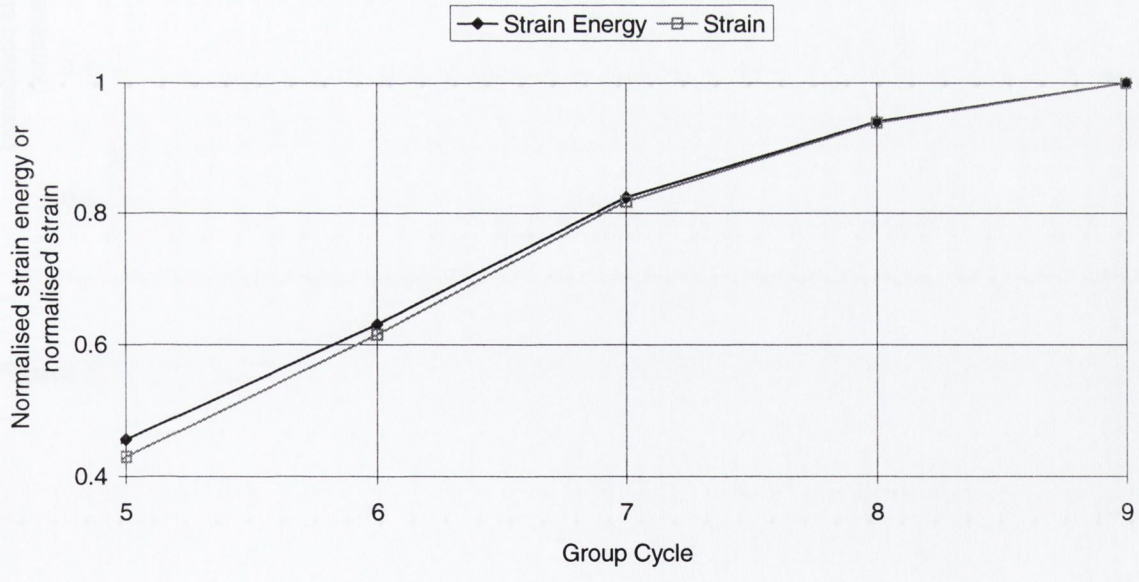

Figure E.2: C6.2(125,W,30): Normalised strain energy or normalised strain versus Group Cycle

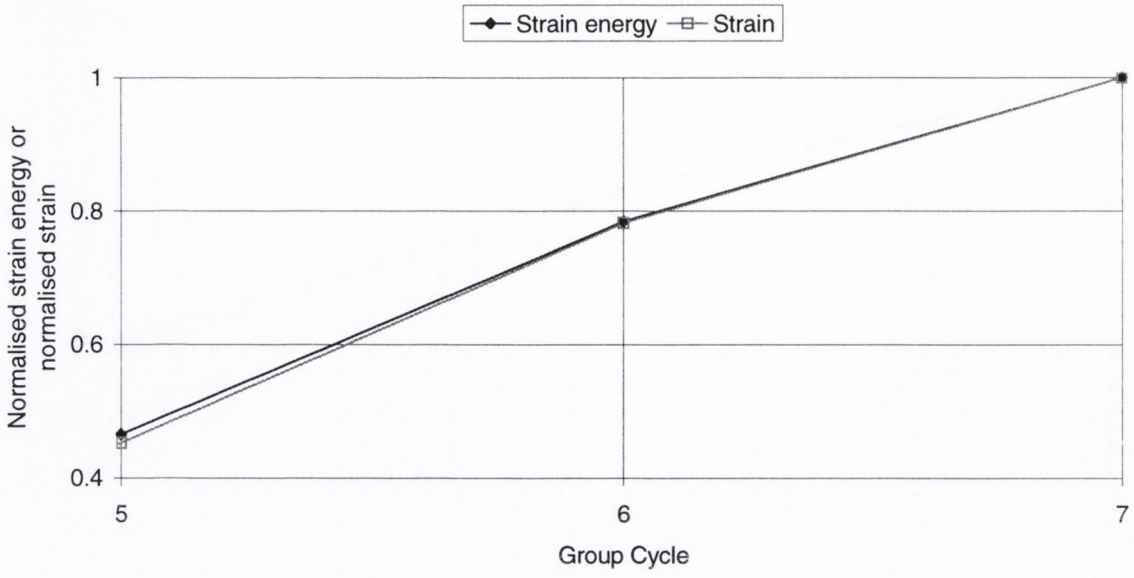

Figure E.3: C6.4(125,W,40): Normalised strain energy or normalised strain versus Group Cycle

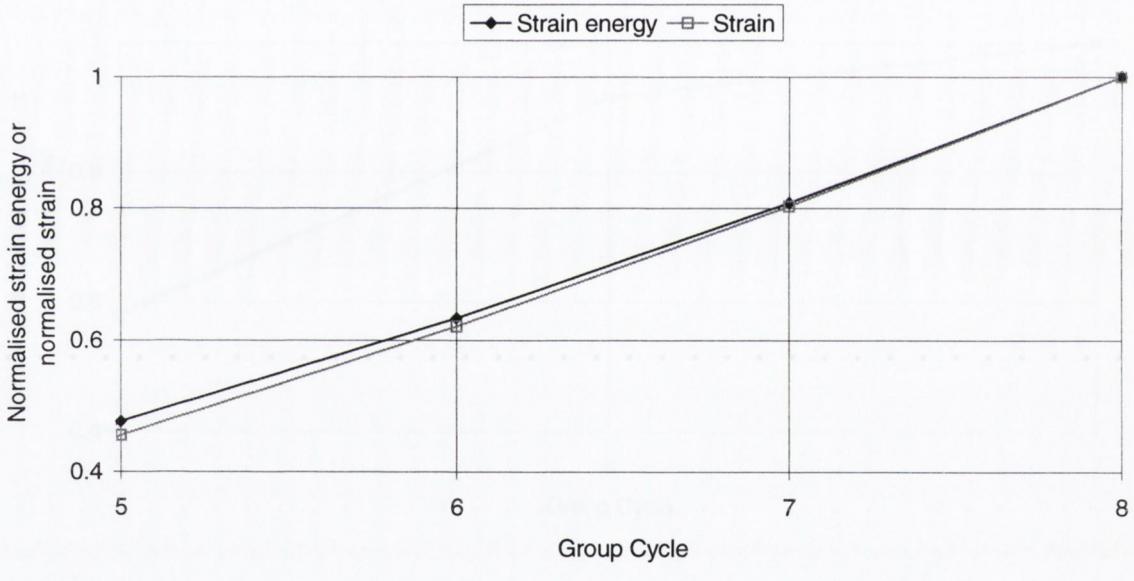

Figure E.4: C5.1(145,W,30): Normalised strain energy or normalised strain versus Group Cycle

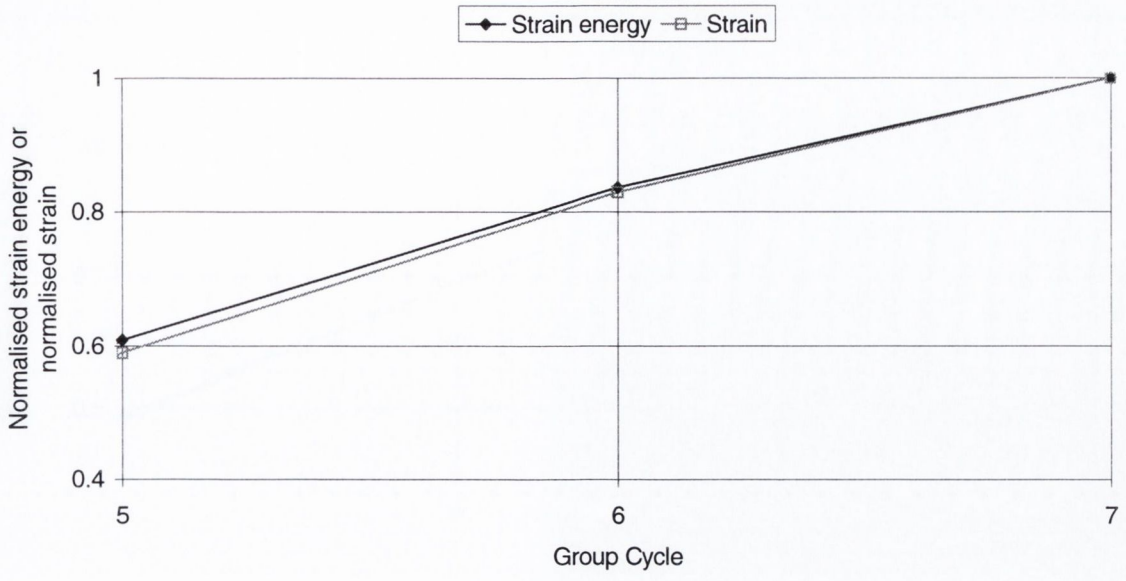

Figure E.5: C5.2(145,30): Normalised strain energy or normalised strain versus Group Cycle

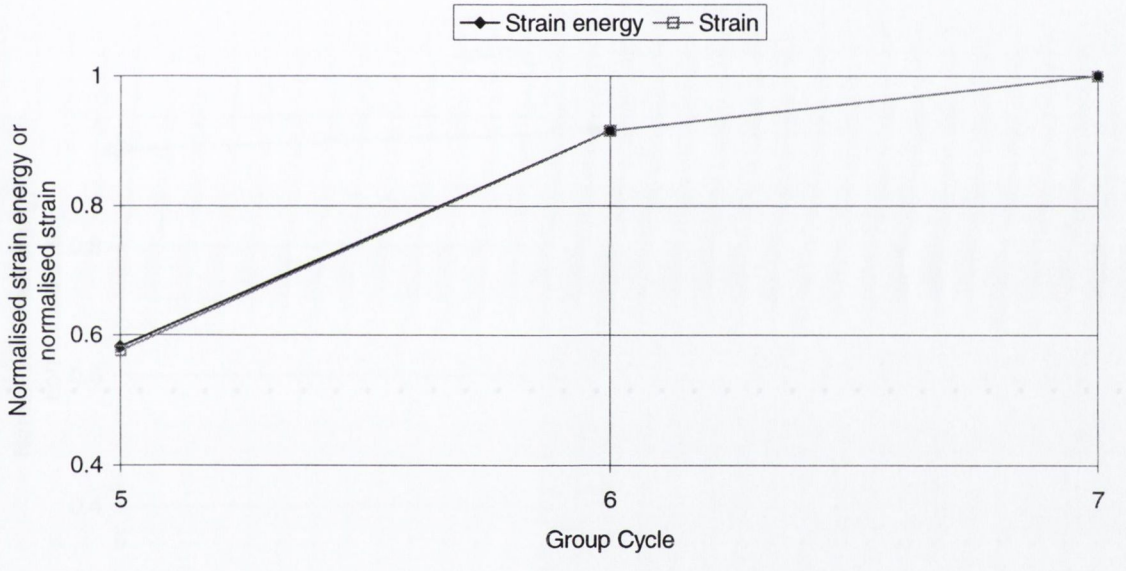

Figure E.6: C6.3(145,W,40): Normalised strain energy or normalised strain versus Group Cycle

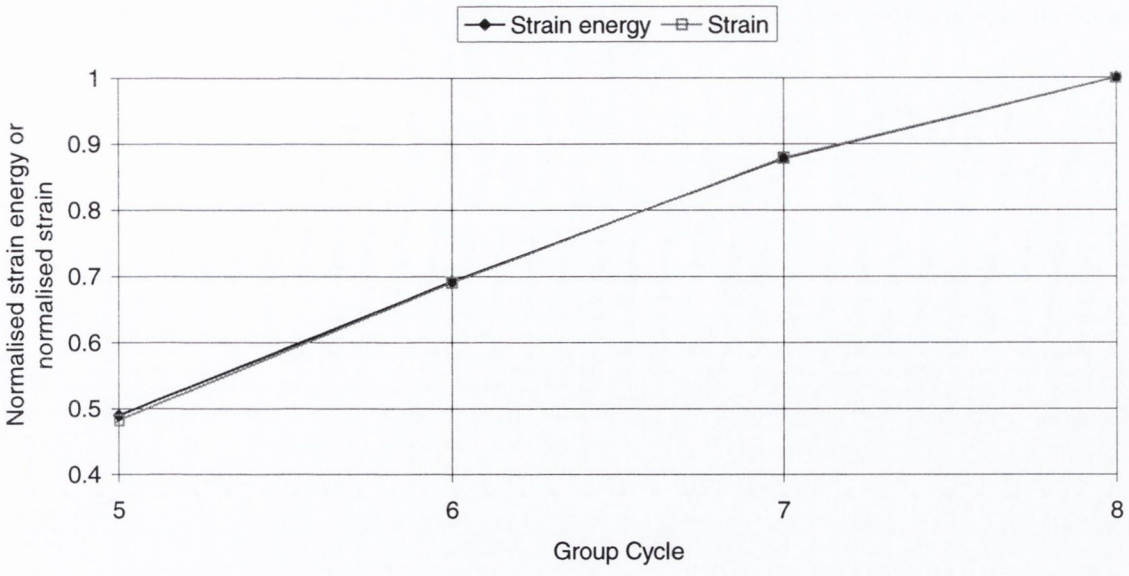

Figure E.7: C6.5(200,W,30): Normalised strain energy or normalised strain versus Group Cycle

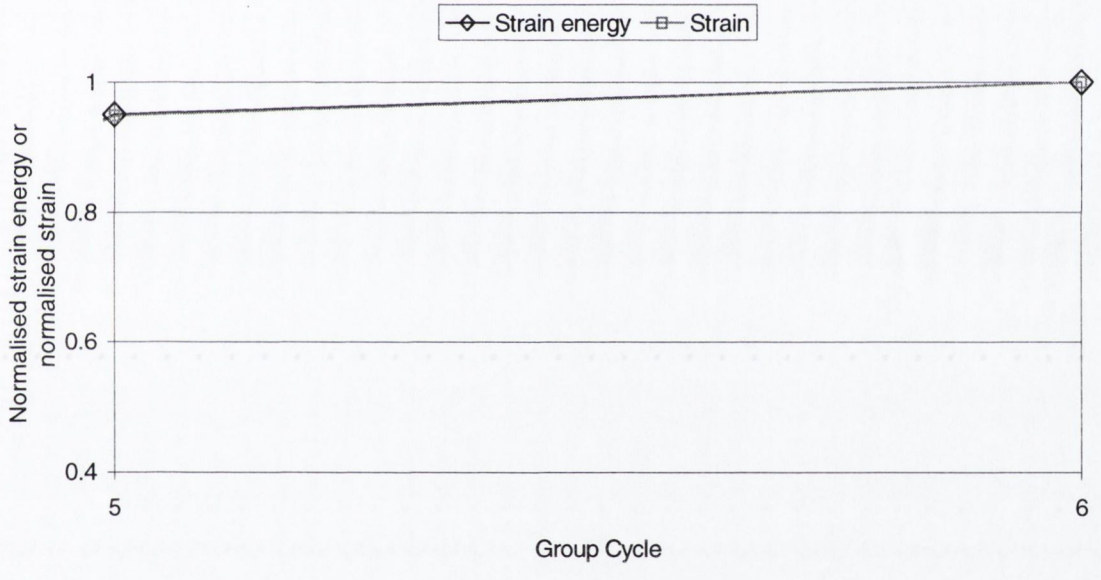

Figure E.8: C6.6(175,30): Normalised strain energy or normalised strain versus Group Cycle